# Reconstruction of the water mass circulation patterns in the Labrador Sea based on radiogenic isotopes and alkenone composition from the present day up to the Late Quaternary (35 kyrs).

DISSERTATION

ZUR ERLANGUNG DES DOKTORGRADES

DR. RER. NAT.

DER MATHEMATISCH-NATURWISSENSCHAFTLICHEN FAKULTÄT

DER CHRISTIAN-ALBRECHTS-UNIVERSITÄT ZU KIEL

VORGELEGT VON

ALEXANDRA FILIPPOVA

KIEL, 2016

1. Gutacher und Betreuer: Prof. Dr. Martin Frank

2. Gutachter: Prof. Dr. Markus Kienast

Eingereicht am:  8 November 2016

Datum der Disputation:

Zum Druck genehmigt:

**Erklärung**

Hiermit versichere ich an Eides statt, dass ich diese Dissertation selbständig und nur mit Hilfe der angegebenen Quellen und Hilfsmittel erstellt habe. Diese Arbeit ist unter Einhaltung der Regeln guter wissenschaftlicher Praxis der Deutschen Forschungsgemeinschaft entstanden und wurde weder ganz, noch in Teilen an anderer Stelle im Rahmen eines Prüfungsverfahrens eingereicht.

Teile dieser Arbeit sind bereits veröffentlicht oder sind in Vorbereitung eingereicht zu werden.

Kiel, den

# CONTENTS

## ABSTRACT.

The Labrador Sea plays a crucial role in influencing the strength of the Atlantic Meridional Overturning Circulation (AMOC), as it is one of the main deep water formation sites. Numerous studies have been carried out in the Labrador Sea, covering different aspects and time scales. This thesis presents an investigation of the complex processes that prevail in the Labrador Sea covering surface, intermediate and deep waters using a combination of organic (alkenone paleothermometry) and inorganic (radiogenic isotopes) geochemical proxies.

Over the past decades it has been debated, whether or not the alkenone unsaturation ratio can reliably be used as a paleo sea surface temperature proxy, especially in cold environments. Many studies have been published presenting contradicting results. In Chapter 4 an investigation of the proxy reliability was carried out based on available and newly obtained data from the western North Atlantic region. The results show that if certain conditions are met, such as appropriate age control of sediment samples, sufficient distance from the main ocean frontal systems characterized by high SST gradients, low risk of allochthonous input, alkenone-derived temperatures can be reliably used even in the cold regions of the North Atlantic.

These results were applied to reconstruct sea surface temperatures in the Labrador Sea over the last 35 kyrs based on alkenone unsaturation ratio of marine sediment samples from four cores (Chapter 5). The motivation of this study was to reconstruct the variability of sea surface conditions in the area and correlate it to presence or absence of cold/warm surface water currents. The sediment cores used in this study were recovered from around the Labrador Sea following the flow path of the main alongshore currents. Prior to 10 ka the record was only partially preserved and indicated significantly cold temperatures and negative $U_{37}^{K}$ values, suggesting that these data are unreliable. However, alkenone unsaturation ratios provided reliable sea surface temperature estimations over the Holocene. The study showed that the Holocene was a period of unstable climate in the Labrador Sea area, characterized by multiple temperature fluctuations that were caused by increased cold water input from the Arctic or fresh water inputs from land.

The investigation of the intermediate and deep waters in the Labrador Sea in this thesis was based on the Hf-Nd-Pb radiogenic isotope signatures of various archives such as sediment samples, foraminifera, detrital material and seawater. The named above isotopes have been used as a proxies for water mass mixing and weathering inputs over the past two decades and were shown to be a reliable tool in paleoceanography.

The Labrador Sea is a complex and dynamic region where the depth of the water formation varies from year to year. To be able to resolve these changes in the past more information is needed concerning mechanisms and processes crucial for the formation of the present day Hf-Nd isotope signatures of different water masses. In Chapter 3 new data were obtained from the Labrador Sea based on direct measurements of seawater. The results showed that all water masses present in the Labrador Sea have distinct hafnium and neodymium isotope signatures. However, some of the water masses such as the Irminger water and shallow and deep Labrador Sea Water are more distinctive in their hafnium isotope signatures compared to those of neodymium. This study suggests that εHf signatures of the main water masses in the Labrador Sea were most likely mainly formed due to weathering inputs from the surrounding terrains. Higher variability of εHf signatures suggests that its residence time is significantly shorter that previously assumed. The new data allow us to conclude that although tracing of large scale ocean mixing processes may not be possible based on Hf isotopes, there is clearly prospect for their application in other restricted basins with similar geological and hydrographic settings.

Based on the above understanding in Chapter 6 combined Hf, Nd and Pb isotopes were applied for the reconstruction of the intermediate and deep water mass circulation in the Labrador Sea over the last 35 kyrs. The results show that all three isotope proxies could be reliably extracted from marine sediments. The new data suggest an early inception of the Denmark Strait Overflow Water around 12 ka, based on εNd and εHf signatures of the leachates and detrital fraction. The εHf and εNd signatures of the detrital fraction suggest the establishment of the alongshore Labrador current around 12 ka. The modern day circulation patterns were most likely absent prior 8 ka. Combined Hf-Nd-Pb isotope signatures suggest that convection during the late Holocene in the Labrador Sea may have been more intensive and formation of the Labrador Sea Water reached significantly deeper than today to up to 2600 m. The position of the new data on εHf-εNd plots forms its own new trend termed “the Labrador Sea” array, which could be representative of the weathering of particular rocks in the source areas of the waters around the Labrador Sea.

# ZUSAMMENFASSUNG.

Die Labradorsee spielt eine entscheidende Rolle in der Atlantischen Meridionalen Umwälzzirkulation, da sie eines der Hauptgebiete für Tiefenwasserbildung ist. Zahlreiche Studien wurden in der Labradorsee durchgeführt, wobei verschiedene Aspekte und unterschiedliche Zeitskalen abgedeckt wurden. Jedoch setzte keine dieser Studien den Fokus auf mehr als nur einen Aspekt. Die vorliegende Arbeit umfasst eine umfangreiche Untersuchung der Oberflächen-, Zwischen- und Tiefenwässer der Labradorsee basierend auf einer Kombination aus organischen (Alkenon-Paläothermometrie) und anorganischen (radiogene Isotope) geochemischen Proxies.

In den vergangenen Jahrzehnten wurde diskutiert, ob das ungesättigte Alkenon-Verhältnis - insbesondere in kalten Umgebungen - zuverlässig als Proxy zur Bestimmung der Paläo-Oberflächenwassertemperaturen (sea surface temperature, SST) herangezogen werden kann. Viele veröffentlichte Studien präsentierten widersprüchliche Ergebnisse. In *Kapitel 4* der vorliegenden Arbeit wurde eine unabhängige Untersuchung der Proxy-Zuverlässigkeit basierend auf bereits publizierten und neuen eigenen Daten aus der westlichen Region des Nordatlantiks durchgeführt. Diese Studie zeigt, dass die aus den Alkenonen abgeleiteten Temperaturen selbst in kalten Regionen zuverlässig verwendet werden könnten wenn eine Reihe von Bedingungen erfüllt wird, darunter eine angemessene Alterskontrolle der Proben, eine Position abseits der primären Ozean-Frontalsysteme mit hohen SST-Gradienten, sowie geringe allochthone Einträge.

Diese Erkenntnisse wurden verwendet, um die Variabilität der Oberflächenwasserströme in der Labradorsee in den letzten 35 tausend Jahren zu untersuchen, wo SST anhand des ungesättigten Alkenon-Verhältnisses von marinen Sedimentproben aus vier Sedimentkernen rekonstruiert wurden (*Kapitel 5*). Ziel dieser Studie war es, die Variabilität der Meeresoberflächenbedingungen in der Region zu rekonstruieren und diese mit der An-/Abwesenheit von Kalt- oder Warmwasser-Oberflächenwasserströmen zu korrelieren. Sedimentkerne wurden dabei aus der gesamten Labradorsee entlang des Strömungspfades der küstenparallelen Ströme entnommen. Obwohl die Sedimentabfolge den Zeitraum vor zehn tausend Jahren nur zum Teil abdeckt, bietet das ungesättigte Alkenon-Verhältnis zuverlässige Schätzungen der SST für das Holozän. Die Studie charakterisiert das Holozän als eine Periode des instabilen Klimas, gekennzeichnet durch mehrere Temperaturschwankungen, die entweder durch die Erhöhung der Kaltwasserzufuhr aus der Arktis oder durch Frischwasserzufuhr vom Land verursacht wurden.

Die Untersuchung der Zwischen- und Tiefenwässer der Labradorsee basierte auf den radiogenen Hafnium- (Hf-), Neodym- (Nd-) und Blei- (Pb-) Isotopensignaturen aus verschiedenen Archiven, darunter Sedimentproben, Foraminiferen, detritischem Material und Meerwasser. Diese Isotopensysteme wurden seit Jahrzehnten als Proxy für Wassermassenmischungen und Verwitterungseinträge herangezogen, und wurden als zuverlässige Werkzeuge für paläozeanographische Untersuchungen befunden.

Die Labradorsee ist eine komplexe dynamische Region, in der die Tiefenwasserbildung von Jahr zu Jahr variiert. Um diese Änderungen in der Vergangenheit nachvollziehen zu können, ist das Verständnis der Mechanismen und Prozesse, die eine wichtige Rolle bei der Bildung der Hf- und Nd-Isotopensignaturen unterschiedlicher Wassermassen in der heutigen Zeit spielen, erforderlich. In Kapitel 3 wurden neue Daten aus der Labradorsee, basierend auf direkten Messungen von Meerwasser, herangezogen. Die Ergebnisse zeigten, dass Hf-Isotopensignaturen (repräsentiert durch εHf) eine bessere Auflösung einiger der Wassermassen, wie etwa Irminger Wasser und flaches und tiefes Labrador-Meerwasser erlauben, welche basierend auf Nd-Isotopensignaturen (repräsentiert durch εNd) nicht unterscheidbar sind obwohl alle Wassermassen in der Labradorsee deutliche Hf- und Nd-Isotopensignaturen aufweisen. Die Studie deutete darauf hin, dass die Hf-Isotopensignaturen der wichtigsten Wassermassen in der Labradorsee am wahrscheinlichsten durch Verwitterungseinträge aus den umliegenden Terrains gebildet wurden. Die höhere Variabilität der εHf-Signaturen legt nahe, dass die Verweilzeit von Hf um eine Größenordnung kleiner ist als bisher angenommen. Obwohl die Verfolgung von großflächigen Ozeanmischungsprozessen basierend auf Hf Isotopen nicht möglich erscheint, deuten die Daten auf ein klares Potential für die Anwendung von Hf Isotopen in anderen Randbecken mit ähnlichen geologischen und hydrographischen Konditionen.

Die kombinierten Hf-, Nd- und Pb- Isotopensysteme wurden mit Hilfe der oben genannten Erkenntnisse angewandt um die Zirkulation von Zwischen- und Tiefenwässern der Labradorsee für die letzten 35 tausend Jahre zu rekonstruieren (*Kapitel 6*). Die Ergebnisse zeigen, dass alle drei Isotopen-Proxies zuverlässig aus marinen Sedimenten extrahiert werden konnten und dass ihre Änderungen eng miteinander korrelieren. Basierend auf den angelösten und detritischen εHf- und εNd-Signaturen zeigen die neuen Daten, dass Überlaufwasser aus der Dänemarkstraße vor rund 12 tausend Jahren eintrat. Die εHf- und εNd-Signaturen der detritischen Fraktion zeigen die Etablierung des küstenparallelen Labradorstroms bei etwa 12 tausend Jahren vor heute. Die modernen Zirkulationsmuster waren allerdings höchstwahrscheinlich bis vor acht tausend Jahren noch nicht vorhanden. Die kombinierten Hf-Nd-Pb-Isotopensignaturen legen nahe, dass Konvektion in der Labradorsee während des späten Holozäns viel intensiver gewesen sein könnte, und dass die Bildung des Labrador Meerwassers viel tiefer war als heute. Die Lage der neuen Daten auf der εHf-εNd Abbildung bildet einen eigenen neuen Trend der hier als "Labradorsee-Array“ bezeichnet wird, welcher den Eintrag eines bestimmten Gesteinstyps aus den Quellbereichen rund um die Labradorsee repräsentieren könnte.

# 1. INTRODUCTION

## 1.1 THE THERMOHALINE CIRCULATION AND THE LABRADOR SEA

The ocean plays an important role in controlling regional and global climate. Short (decadal) and long term changes and fluctuations of the climate system in the past, in many instances, were predetermined by changes of the ocean circulation, which is driven by meridional heat and fresh water transport (cf. Dickson et al., 1988; Dommenget and Latif, 2002; Gulev et al., 2001). Understanding the mechanisms controlling the global ocean variability, and regular observations of the integral parts of the ocean systems, is therefore of great necessity not only for climatic modelling of the past but also for forecasting global climate dynamics in the future.

Heat exchange between the atmosphere and the ocean and heat transport from equatorial regions to high latitudes drives the so called Atlantic Meridional Overturning Circulation (AMOC). Understanding the dynamics and variability of the AMOC is crucial for climate change predictions. Variations in the processes of deep water convection and water mass formation in the past and in the modern time have been a focus of many studies (e.g. Dickson and Brown, 1994; Vellinga and Wood, 2002; Hall et al., 2006; Chen et al., 2012; Trouet et al., 2012; McCarthy et al., 2014).

One of the main deep water formation sites that plays a crucial role in influencing the AMOC strength and variability is the Labrador Sea. As the receiving basin of warm and saline waters from South Atlantic, which are brought there by the western branch of the North Atlantic current, and as one of the biggest sources of fresh and cold waters together with the polar regions, it significantly contributes to the formation of the deep and surface outflows to the Atlantic ocean (Yashayaev et al., 2015). The annual accumulation of cold and fresh water and its injection into the deeper layers makes the Labrador Sea the freshest and coldest basin of the Subpolar North Atlantic (SPNA) (Yashayaev et al., 2015). Wind driven convection, promoted by strong winter cooling, leads to the formation of Labrador Sea Water (LSW), which is being transported out of the Labrador Sea and is entrained in North Atlantic Deep Water (NADW) (Yashayaev and Clark, 2006; Yashayaev and Loder, 2009). Via surface and deep water mixing processes, dissolved atmospheric gases such as carbon dioxide, oxygen, nutrients and chlorofluorocarbons (CFCs) are added to LSW and are transported outside the Labrador Sea to intermediate depths of the North Atlantic ocean, thereby both ventilating the deeper parts of the Atlantic Ocean and removing atmospheric $CO_2$ (Lazier et al., 2002; Azetsu-Scott et al., 2003). The deep convection that takes place in the Labrador Sea is also crucial for AMOC dynamics given that it produces the densest water mass within the SPNA

(Yashayaev et al., 2015). Wind driven cooling that occurs in winter at the surface of the Labrador Sea is considered to be one of the main factors that control the size and strength of the subpolar gyre in the North Atlantic (Yashayaev et al., 2015).

Of particular importance for the water convection in the Labrador Sea are the upper 200 meters, which exert the largest and strongest control over the vertical stratification and mixing of the depth range of the upper 1000 m (Yashayaev et al., 2015). Accumulating fresh water from various internal sources throughout the year, such as continental runoff, precipitation, Arctic outflow waters, or ice melt, this layer captures important signals, which are subsequently spread in the surface and subsurface waters of SPNA and also injected into the deeper layers (Yashayaev et al., 2015). Increased fresh water inputs into the Labrador Sea lead to changes in surface and subsurface salinity thus intensifying vertical stratification and slowing down winter convection in the region, and at the same time increasing salinity and temperature of the deeper layers (Yashayaev et al., 2015).

The ability to trace and understand these processes is crucial for the reliability of our future climate predictions. Regular annual monitoring cruises in the Labrador Sea provided good quality climate records over the last few decades (Yashayaev and Clark, 2006; Yashayaev et al., 2008; Yashayaev et al., 2015). However to be able fully understand the ongoing processes and their role and significance in global climate change, records of the past ocean circulation are necessary. By means of applying innovative and established methods in paleoceanography we can obtain crucial information on the surface and deep water mass circulation patterns in the Labrador Sea that prevailed in the region in the past and compare it to the modern trends. The tools applied in this study are discussed in the following chapter.

## 1.2 ND-HF-PB ISOTOPE GEOCHEMISTRY

Long-lived radioactive systems are widely applied tools in paleoceanography to trace Earth system processes through geological time (Goldstein and Hemming, 2003). Some of the main parent-daughter systems used are Th-U-Pb, Sm-Nd and Lu-Hf. Long-lived systems are considered those that have a slow rate of decay comparable to the age of the solar system. Due to their very slow rate of decay, changes in the abundances of the stable daughter isotopes, referred to as “radiogenic” can be considered negligible on short millennial time scales and are denoted as a ratio to a primordial stable isotope of the same element that has not experienced ingrowth due to radioactive decay. The radiogenic isotope ratios of rocks are thus a function of the parent-daughter element ratios and the ages. Ideally, the element systems applied for the evaluation of present and past water mass mixing behave

conservatively in sea water and will only reflect mixing the source signatures of the water masses. Due to transport processes on the Earth surface, radiogenic isotope signatures in the weathering solutions represent mixtures of contributions from the different age terrains. Dissolved elements and their isotope ratio can be traced over their entire path in the ocean, as long as no additional inputs with different isotope ratios were added on the way (Goldstein and Hemming, 2003). There are three main ways of how dissolved elements can be introduced into the ocean, via rivers, from aeolian, or hydrothermal inputs (Frank, 2002). The importance of these sources for different isotope systems varies depending on the element mobility during weathering and erosional processes and chemical behavior. Below, the Sm-Nd, Lu-Hf and Th-U-Pb isotope systems are discussed in more detail.

### 1.2.1 SM-ND, LU-HF AND U-TH-PB ISOTOPE SYSTEMS

Sm is a rare earth element with seven naturally occurring isotopes, three of which are radioactive ($^{147}$Sm, $^{148}$Sm, $^{149}$Sm). The latter two have extremely long half-lives (> $10^{16}$) and therefore do not produce measurable amounts of the daughter isotopes $^{144}$Nd and $^{145}$Nd (Dickin, 2005). However, the half-life of $^{147}$Sm (14.99 % abundance) is short enough (106 Gyr) to produce small but measurable changes in the abundance of $^{143}$Nd over time.

Nd is also a rare earth element that has seven naturally occurring stable isotopes ($^{142}$Nd, $^{143}$Nd, $^{144}$Nd, $^{145}$Nd, $^{146}$Nd, $^{148}$Nd and $^{150}$Nd). $^{143}$Nd (abundance 12.18 %) is produced due to α-decay of $^{147}$Sm. The Sm/Nd ratio of the mantle is higher than that of the crust, and it follows that the $^{143}$Nd/$^{144}$Nd ratio is higher in the mantle than in the crust. Sm/Nd and $^{143}$Nd/$^{144}$Nd ratios of the bulk Earth are considered to be the same as of chondritic meteorites, which are believed to closely represent the composition of the bulk Earth prior to differentiation of mantle and crust (Frank, 2002; Goldstein and Hemming, 2003; Dicken, 2005). Due to the small differences in $^{143}$Nd/$^{144}$Nd ratios (four or fifth place after the decimal), Nd isotope ratios are expressed as εNd values:

$$\varepsilon Nd = \frac{(\frac{^{143}Nd}{^{144}Nd}sample) - (\frac{^{143}Nd}{^{144}Nd}CHUR)}{\frac{^{143}Nd}{^{144}Nd}CHUR} * 10000,$$

where CHUR represents the present-day chondritic $^{143}$Nd/$^{144}$Nd value of 0.512638 (Jacobssen and Wasserburg, 1980).

Lutetium is the heaviest of the rare earth elements (REEs) of the lanthanide series. It has two isotopes $^{175}$Lu and $^{176}$Lu with the first being most abundant (97.4 %) and the second 2.6% respectively. $^{176}$Lu decays into $^{176}$Hf by $\beta^-$ emission (Dicken, 2005) and is left in an excited state and then decays to the ground state by γ emission. This isotope is one of the six

stable Hf isotopes ($^{174}$Hf, $^{176}$Hf, $^{177}$Hf, $^{178}$Hf, $^{179}$Hf and $^{180}$Hf), and constitutes 5.2 % of total hafnium (Dicken, 2005). Hafnium as an element is not a REE but closely resembles Zr in its chemical behavior (Dicken, 2005).

The Hf system is in many aspects similar to Sm-Nd. Both elements are relatively immobile and refractory, and the bulk Earth's Lu/Hf ratio is assumed to be close to chondritic. The $^{176}$Hf/$^{177}$Hf ratio is lower in the crust in comparison to the mantle (White, 2000). $^{176}$Hf/$^{177}$Hf ratio is expressed as an εHf:

$$\varepsilon Hf = \frac{(\frac{^{176}Hf}{^{177}Hf}sample) - (\frac{^{176}Hf}{^{177}Hf}CHUR)}{\frac{^{176}Hf}{^{177}Hf}CHUR} * 10000,$$

where CHUR represents chondritic $^{176}$Hf/$^{177}$Hf value of 0.282785 (Nowell et al., 1988; Bouvier et al., 2008).

Lead has four stable isotopes $^{204}$Pb, $^{206}$Pb, $^{207}$Pb and $^{208}$Pb, only one of which, $^{204}$Pb, is non radiogenic. $^{206}$Pb, $^{207}$Pb and $^{208}$Pb are the final decay products of the uranium ($^{238}$U, $^{235}$U) and thorium ($^{232}$Th) decay series respectively, in which the intermediate members of the decay chain are relatively short-lived. The half-life of $^{238}$U is comparable to the age of the Earth whereas the half-life of $^{235}$U is much shorter, resulting in almost all primordial $^{235}$U having decayed to $^{207}$Pb. The half-life of $^{232}$Th is comparable to the age of the universe. The bulk Earth composition of U-Th-Pb system is less well defined than that of Sm-Nd and Lu-Hf. It is complicated by the volatility of Pb during nebular condensation and the high variability in depletion of volatile elements in the Earth (Goldstein and Hemming, 2003). Fractionation of the U-Th-Pb system between the crust and the mantle is less well defined and isotopic differences between them appear to be relatively small (Asmerom and Jacobsen, 1992).

### 1.2.2 CONTINENTAL WEATHERING EFFECTS AND THE SOURCES OF THE ELEMENTS IN THE OCEAN

The applicability of long-lived radiogenic isotope systems is based on their variability within the Earth and at its surface. This variability is a result of the gross chemical differentiation of the Earth associated with magmatic processes, as different isotope systems behave differently during magma formation. The behavior of the Sm-Nd system is similar to that of Lu-Hf in that Nd and Hf are less compatible than their parent isotopes during magma generation. As a result, Nd and Hf are more likely to enter the melts than Sm and Lu leading to a lower Sm/Nd and Lu/Hf ratios in the continental crust compared to the mantle. As time passes, this results in low $^{143}$Nd/$^{144}$Nd and $^{176}$Hf/$^{177}$Hf in the continental crust compared to the

mantle and bulk Earth (negative εNd and εHf). Consequently, young mantle derived rocks, such as mid-ocean ridge and ocean island basalts, have high $^{143}Nd/^{144}Nd$ and $^{176}Hf/^{177}Hf$ (positive εNd and εHf). With age, the distinction between continental and mantle isotope ratios increases. As the age of the continental crust is geographically variable, continents are isotopically heterogeneous, forming the basis for tracing the sources and transport. The similar fractionation behavior of Hf and Nd during the formation of the continental crust results in a strong positive correlation of radiogenic Nd and Hf isotopes in most terrestrial rocks, which has been defined as a "mantle-crust array" or "terrestrial array" (Fig. 1, $\varepsilon Hf = 1.55 * \varepsilon Nd + 1.21$, Vervoort et al., 2011).

However, unlike Sm and Nd, Lu and Hf undergo significant fractionation due to weathering and sediment transport (Dickin, 2005). In comparison to $^{147}Sm/^{144}Nd$, $^{176}Lu/^{177}Hf$ is strongly fractionated between sandstones and clays. Patchett et al. (1984) explained this effect by the affinity of Hf to be incorporated in zircons (~ 1% by weight), whereas at the same time zircons do not incorporate large amounts of Lu. Consequently, with time this results in less radiogenic signatures of zircons than the corresponding bulk rocks. Zircons are highly resistant to chemical and physical weathering and have low Lu/Hf and $^{176}Hf/^{177}Hf$ ratios. They are enriched in sand-grade sediments and Hf is depleted in the fine-clay fraction. Sorting of marine sediments during transport according to grain size leads to low Lu/Hf ratios of sand and turbidites on continental shelves and continental slopes, medium Lu/Hf ratios in shales and clays and very high ratios in red clays and Mn nodules in the deep ocean due to the absence of terrigenous sediments (van de Flierdt et al., 2002; Dickin, 2005; Carpentier et al., 2008). Hf released to the weathering solutions is consequently expected to be more radiogenic than the bulk rocks (van de Flierdt et al., 2002, 2007). The observed effect of Hf fractionation during weathering caused by zircons was termed as a "zircon effect" (van de Flierdt et al., 2007).

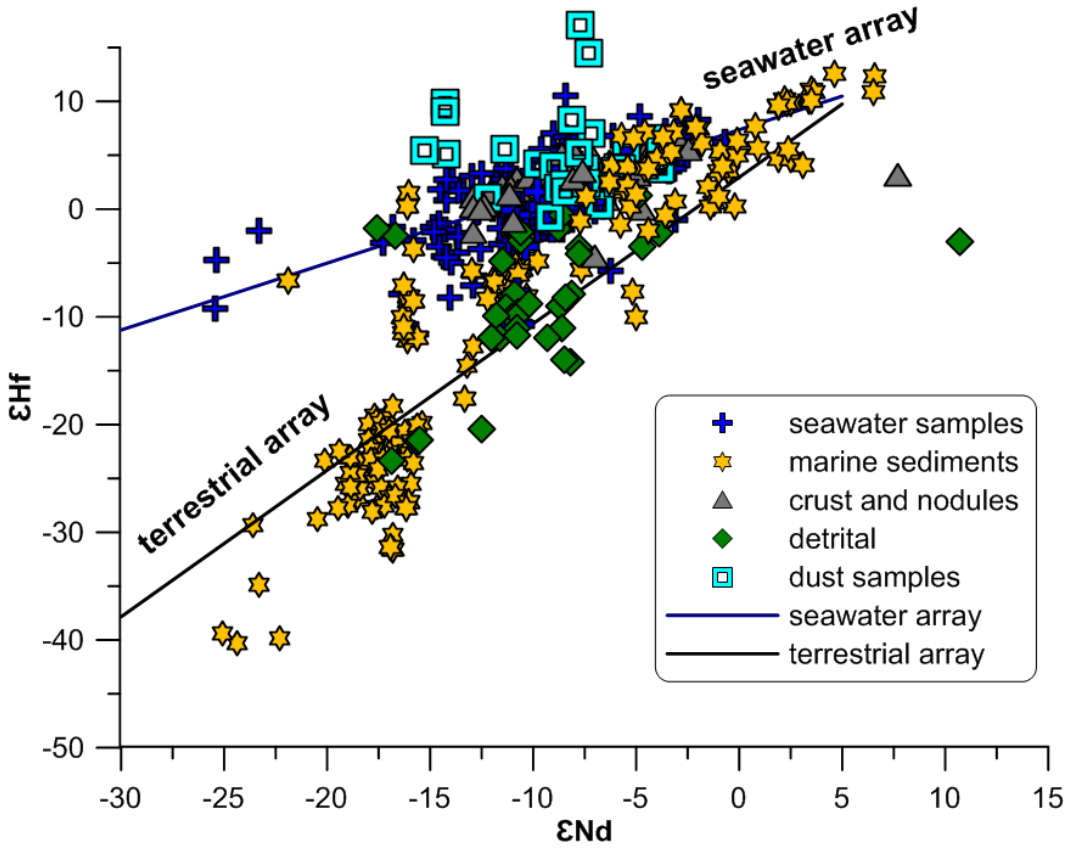


**Fig. 1** Hf-Nd isotope systematics of marine sediments, ferromanganese crusts and nodules, detrital fraction, atmospheric dust and seawater. Terrestrial array (εHf = 1.55 * εNd + 1.21, Vervoort et al., 2011) and seawater array (εHf = 0.62 * εNd + 7.38, Albarède et al., 1998; Godfrey et al., 1997; David et al., 2001) are shown on the plot. Data are taken from: marine sediments (Bayon et al., 2008; Vervoort et al., 2011; Chen et al., 2012; Garcon et al., 2013), ferromanganese crusts and nodules (Albarede et al., 1998; David et al., 2002), detrital fraction (Chen et al., 2012; Chen et al., 2013), seawater (Godfrey et al., 2009; Rickli et al., 2009, 2010, 2014; Stichel et al., 2012a,b; Zimmermann et al., 2009a,b; Filippova et al., 2016 submitted to GCA), dust samples (Chen et al., 2013).

Early studies of dissolved Hf-Nd isotope composition of seawater based on the ferromanganese nodules and crusts, which directly precipitate from seawater, showed the consequence of these fractionation processes and the fact that seawater forms a distinct and well defined correlation between Hf and Nd as well. For every given value of εNd, a more radiogenic value of εHf than expected from the bulk rock composition is observed (Fig. 1). This trend, which deviates from the "terrestrial array", is referred to as the "seawater array" (εHf = 0.62 * εNd + 7.38, Albarède et al., 1998; Godfrey et al., 1997; David et al., 2001). The direct measurements of seawater carried out over the last decade confirmed the existence of the seawater array. Initially, the formation of the seawater array was mainly ascribed to the

zircon effect (Bayon et al., 2006; Rickli et al., 2013). However, there was also the claim that an additional source of highly radiogenic Hf contributed to the offset formation, and suggested hydrothermal input as a potential contributor of highly radiogenic Hf (Bau et al., 2006). The similar behavior of Nd and Hf and the absence of hydrothermal contributions of Nd to seawater (Michard et al., 1983; German et al., 1990; Halliday et al., 1992) were used as an argument against significant inputs of highly radiogenic hafnium to the oceans. This, however, still remains to be proven by direct measurements of Hf in hydrothermal solutions (van de Flierdt et al., 2004a,b; Bau and Koschinsky, 2006; Firdaus et al., 2011). More recent studies, based on isotopic mass balance calculations, showed that the seawater offset cannot be explained by the zircon effect only (Chen et al., 2011). Instead, it has been proposed that preferential weathering of labile minerals with high Lu/Hf, such as apatite and sphene play an important role (Barford et al., 2003; Bayon et al., 2009; Godfrey et al., 2009; Chen et al., 2011). The role of aeolian input to the oceans as the source of radiogenic Hf has also been evaluated. Pettke et al., 2002a came to a conclusion, that dust bound Hf may have been a significant source of seawater Hf and seawater Nd. However it seems that this scenario is appropriate only at times when dust fluxes have been extremely high, such as in the North Pacific over the past few millions years (Pettke et al., 2002a). On the other hand, prior to the Pliocene dust bound Hf most likely had little or no effect (Pettke et al., 2002a,b). A recent study by Rickli et al. (2011), carried out on dust samples from the Saharan desert, showed that dust dissolution in seawater is a significant source for the marine REE budget. Hafnium, however, unlike Nd, is being released from the dust incongruently, most likely from more labile or secondary minerals, such as clays and possibly apatite. Consequently, the dissolved Hf isotopes do not reflect the bulk signal of the dust, and depending on the dust load isotopic composition of Saharan dust may be similar to seawater, making it hard to truly asses the significance of dust dissolution as a source of radiogenic Hf in seawater (Rickli et al., 2011).

Unlike Hf, Nd isotopes are generally not significantly influenced by fractionation during weathering processes (Goldstein et al., 1984). However, it has been proposed that minor fractionation effects may occur due to preferential release of unradiogenic Nd from minerals with low $^{143}Nd/^{144}Nd$ isotope ratios. This has been observed during weathering of glacial tills (Öhlander et al, 2000) and during erosion and partial dissolution of rocks that supply boreal rivers in northern Scandinavia (Andersson et al., 2001). Blanckenburg and Nägler (2001) came to the same conclusions based on their leaching experiments of Greenland river sediments. Hydrothermal input does not contribute to the dissolved seawater Nd budget due to high particle reactivity and immediate scavenging of Nd within

hydrothermal vents (German et al., 19990; Halliday et al., 1992). Numerous studies of the Nd budget showed that dust is an important source of dissolved Nd (Goldstein et a., 1984; Greaves et al., 1999; Rickli et al., 2011). One of the main sources of dissolved Nd to the global ocean is riverine input, a large fraction of which is being trapped in estuaries. However, up to 90% of Nd delivered to the ocean is being transported on colloids (Andersson et al., 2001). Lacan and Jeandel (2005) showed that there is an additional flux of Nd from the continental slope sediments, due to their leaching and mobilization, which leads to exchange and release of Nd to seawater. This process was termed "boundary exchange" and was also observed by other authors in later studies (Rickli et al., 2009; Wilson et al., 2012).

Lead isotope ratios do not display a strong correlation with Hf-Nd in continental rocks and oceanic basalts (Goldstein and Hemming, 2003), which usually express similar values for example in their $^{206}Pb/^{204}Pb$ ratios. In a graph of $^{206}Pb/^{204}Pb$ versus $^{207}Pb/^{204}Pb$, oceanic basalts normally fall below the continental rocks, which is a consequence of the short half-life of $^{235}U$ in comparison to $^{238}U$ and higher U/Pb ratio in the continental crust than in the mantle over the first half of Earth's history (Goldstein and Hemming, 2003), and continental crust derived lead can in most cases be distinguished from mantle derived lead. During weathering of continental rocks lead is fractionated, which is mainly caused by the radiation damage to the crystal lattice of the minerals during the radioactive decay of the parent isotopes. As a result the daughter isotopes are left loosely bound in the minerals, which causes their preferential mobilization at the grain boundaries (cf. Frank, 2002). As a consequence, radiogenic lead isotopes ($^{206}Pb$, $^{207}Pb$, $^{208}Pb$) are easier mobilized from rocks and minerals during weathering than nonradiogenic $^{204}Pb$. Thus, Pb isotope compositions of weathered solutions and dissolved Pb in seawater do not directly reflect the Pb isotope signature of the bulk source rocks (Blanckenburg and Nägler, 2001). The importance of the natural sources of lead in seawater is different from Nd and Hf. Besides riverine supply being the most important source of dissolved lead, hydrothermal inputs are at least of local importance (Barett et al., 1987). However on the global scale these inputs are considered to be relatively small (< 2%) (Chen et al., 1986). Dust inputs account for only 10-12 % of the preanthropogenic lead budget.

### 1.2.3 ND-HF-PB SIGNATURE IN THE GLOBAL OCEAN.

The first studies based on the long-lived radiogenic isotope systems were carried out on ferromanganese nodules and crusts and marine sediments, but with the advance of analytical techniques direct measurements of seawater became possible.

The first studies of the neodymium isotopic composition of the ocean were published in the late 70s (Richard et al., 1976; DePaolo and Wasserburg, 1976a; O'Nions et al., 1977). One of the first reports of Nd, along with Pb and Sr isotopes in manganese nodules and hydrothermal sediments was provided by O'Nions et al. (1978). These authors confirmed that the main source of neodymium is continents. However, they also inferred - incorrectly - that Nd is globally well mixed in the oceans and that its isotopic signature only covers a very narrow range. In the following years, studies carried out by Piepgras et al. (1978) and Goldstein and O'Nions (1981) showed distinct Nd isotopic signatures for the Pacific, Atlantic and Indian oceans. The Pacific is dominated by more radiogenic εNd values between 0 to -5, the Atlantic is unradiogenic (εNd between -10 to -14), and intermediate values between -7 to -10 characterize the Indian Ocean. Additionally, these authors found some systematic geographic variability within each ocean basin, which they attributed to the difference in age of the surrounding continental crust and potential addition of volcanically derived Nd in the case of Pacific Ocean.

The first direct measurements of seawater were carried by Piepgras et al., (1979) for 4 water samples from the Pacific Ocean and by Piepgras and Wasserburg, (1980) for water samples from the Atlantic. They showed a general agreement of Fe-Mn nodule and crust data with seawater for similar depths. Additionally they found a substantial vertical variability in Nd signature and suggested that North Atlantic Deep Water has a distinct Nd isotope signature, making Nd a potential tool in oceanography and paleoceanography. Since the late 70's, the neodymium isotope compositions of seawater have been widely measured, which results in a large data set of εNd signatures of different water masses in the global ocean ranging from -26.6 to +2.7 (Lacan et al., 2012; Grasse et al., 2012; Fröllje et al., 2016). These data confirm previous findings of well resolved εNd signatures for different water masses. The signals reflect weathering inputs from rocks of different ages and types ranging from old continental crust surrounding the Atlantic Ocean of Proterozoic or Archean age (εNd ~ -40) to young mantle derived material surrounding the Pacific Ocean characterized by highly radiogenic signatures of up to +20. The least radiogenic signatures were measured in Baffin Bay waters (-26, Stordal and Wasserburg, 1986). The admixture of water masses with distinct isotope signatures results in the modern day NADW signature of -13.5 (Lacan et al., 2012). The global average residence time of Nd in the ocean is considered to be on the order of 400 - 1000 years (Arsouze et al., 2009; Rempfer et al., 2011). Nd is generally depleted in the surface waters due to its particle reactivity and scavenging processes at the surface. With depth Nd concentration increases due to desorption/dissolution processes.

The first study of seawater Hf isotope compositions based on Fe-Mn nodules from Pacific, Atlantic and Indian Oceans was published in 1986 (White et al., 1986). Despite the coherent behavior of Nd and Hf, and high variability of Nd, hafnium was found to have homogeneous εHf values of around +2, with little variation outside analytical uncertainty. White et al. (1986) explained the homogenous signature of Hf in seawater by the equal admixture of two end members, crustal and mantle sources of dissolved Hf respectively. To achieve such a level of homogenization, however, the residence time of Hf would have to be at least on the order of or longer than the mean ocean mixing time of 1500 years. Due to analytical difficulties of measuring isotope ratios of Hf, the next study was published only 11 years later by Godfrey et al. (1997). Early studies on the behavior of Hf and its isotopic distribution in seawater were based on data of slowly accumulating ferromanganese crusts and nodules (Albarède et al., 1998; David et al., 2001; van de Flierdt et al., 2002, 2004a, 2004b; Bau and Koschinsky, 2006). The advance of MC-ICPMS based measurement techniques allowed the direct measurements of the Hf isotope composition in seawater. However, due to low concentrations of Hf in seawater (0.04 - 1.47 pmol $kg^{-1}$) (Godfrey et al., 1996; McKelvey and Orians, 1998) in comparison to Nd (15 - 45 pmol $kg^{-1}$) (Goldstein and Hemming, 2003) these measurements are analytically challenging and data are still scarce. Isotopic compositions of Hf in seawater are now available for the Atlantic Ocean (Rickli et al., 2009, 2010; Godfrey et al., 2009), the Southern Ocean (Stichel et al., 2012 a,b; Rickli et al., 2014), the Pacific Ocean (Zimmermann et al., 2009b), the Arctic Ocean (Zimmermann et al., 2009 a), and the central Baltic Sea (Chen et al., 2013). Available global open ocean εHf signatures range from -5.7 to +10 (Godfrey et al., 2009 and Rickli et al., 2010). The available data on Hf isotope signatures and Hf concentrations in the global ocean gave rise to controversial discussions on its oceanic residence time. A narrow range of Hf isotope signatures through the oceans implies very long residence time, on the order of 2000 years allowing its homogenization in the global ocean. On the other hand, unlike Nd, Hf concentrations do not increase along the deep ocean conveyor implying a much shorter residence time, on the order of just few hundred years (Rickli et al., 2009).

The interest in oceanic Pb isotope distributions started with attempts to date the age of the Earth by Pb/Pb method (Dickin, 2005). Chow and Patterson (1962) investigated the Pb isotope composition of pelagic sediments, which allowed some considerations about the lead distribution in the oceanic system. Concentration profiles of lead in the water column showed increased surface values, mainly attributed to anthropogenic inputs and depletion at depth (Schaule and Patterson, 1981). Due to high particle reactivity of lead (Schaule and Patterson,

1981; Cochran et al., 1990) its residence time in the ocean is considered to be much shorter than that of Nd or Hf and has been estimated at 200-400 years in the Pacific and only about 50 years in the Atlantic (Chow and Patterson, 1962; Craig et al., 1973; Henderson and Maier-Reimer, 2002). The main mechanism of lead transfer to marine sediments is considered to be non reversible scavenging accompanied by release at depth due to remineralization and decomposition of particles. First attempts to measure lead directly in seawater led to the conclusion that it is completely overprinted by anthropogenic inputs as a result of nuclear fallouts and use of lead contained in petrol (Chow and Johnstone, 1965; Chow et al., 1970). Although it restricted the application of lead to trace its natural isotope composition in seawater, it gave raise to numerous studies on the sources of anthropogenic lead in the ocean (Chow et al., 1970; Sturges and Barrie, 1987; Rosman et al., 1993). Information on the preathropogenic levels of dissolved lead in seawater can only be derived from the records preserved in marine authigenic sediments, such as ferromanganese crusts and nodules (Chow and Patterson, 1959, 1962). Chow and Patterson showed that based on the analysis of Mn nodules from the Atlantic ocean the lead signature is consistent with the continents being the main source , whereas in the Pacific Ocean submarine volcanic activity may be a significant source as well. A study by Abouchami and Goldstein (1995) based on circumpolar Mn nodules showed evidence of the importance of mixing between different water masses for the dissolved Pb isotope distribution. A study by Blanckenburg et al. (1996) based on Mn nodules revealed that within the Atlantic, Pacific and Indian Oceans the Pb signature is more homogenous, than in the circumpolar ocean. More recent studies, however, showed isotopic provinciality of Mn nodules in the deep oceans, where the Pb signature is strongly influenced by mixing between different bodies of water (Jones et al., 2000; Vlastelic et al., 2001). The available data on Pb isotope signatures shows $^{206}Pb/^{204}Pb$ values of around 19.3 for present NADW and around 18.5-18.8 for the deep Pacific water (Frank, 2002) clearly demonstrating the incongruent weathering release of Pb from the Archean and Proterozoic rocks ($^{206}Pb/^{204}Pb$ signatures of ~13-17) around the North Atlantic. The Indian and Southern oceans are generally intermediate between these values. However, important to notice that the age of the ferromanganese crust surfaces normally integrate tens to hundreds of thousands of years, and may not be representative of the preanthropogenic deep-water Pb signature for shorter periods of time.

### 1.2.4 CHANGES OF ND-HF-PB ISOTOPE SIGNATURES THROUGH THE LATE QUATERNARY

Initially, reconstructions of the past ocean Nd-Hf-Pb isotope signatures were mainly based on the analysis of ferromanganese crusts and nodules (e.g. Frank, 2002). These precipitate directly from ambient seawater and record the isotopic signal of deep waters in the past, which has been confirmed by numerous studies for Nd (O'Nions et al., 1978; Piepgras et al., 1979; Albaredè and Goldstein, 1992; von Blanckenburg et al., 1996 a,b; David et al., 2001;), Hf (Lee et al., 1999; Piotrowski et al., 2000; Pettke et al., 2002), and Pb (Burton et al., 1997; Frank and O'Nions, 1998; von Blanckenburg and O'Nions, 1999). Due to extremely slow growth rate, Fe-Mn crusts integrate the signal over long periods of time, from $10^4$ up to $10^5$ years. This precludes their application for studies of shorter term changes, such as on glacial-interglacial or even shorter time scales, which resulted in the quest for new archives capable of the reconstruction of short term variations in Nd-Hf-Pb isotope signatures of the past ocean.

One of the potential tools to reconstruct Nd isotope signatures were considered foraminifera, which are widely distributed and can yield high resolution profiles, due to their high sedimentation rates (Dickin, 2005). Foraminiferal shells are coated by a layer of ferromanganese oxihydroxides after their deposition on the sea floor, in which Nd concentrations are much higher than those in the foraminiferal carbonate themselves. Attempts to remove these coatings in order to obtain a surface water Nd isotope composition were presented by Vance and Burton (1999), who applied leaching with a strong reducing agent. The validity of the method was confirmed in 2000 by Burton and Vance, based on analyses of foraminiferal shells from a sediment core from the Indian Ocean. However, some important questions concerning the Nd isotope signature extraction from reductively cleaned foraminifera remain not fully answered. It is still debated which water depth the Nd isotope compositions extracted from the cleaned foraminifera reflect, and the consensus tends to be that they mainly reflect deep water signals (Robert et al., 2012, Pena et al., 2013; Kraft et al., 2013). Laboratory tests showed that no significant amounts of Hf are incorporated into foraminiferal shells (T. Chen, personal communication).

Over the last decade, an additional archive allowing the reconstruction of seawater Nd-Pb-Hf isotope fluctuations was explored. Amorphous authigenic Fe-Mn oxihydroxide coatings of bulk sediments or of foraminiferal shells formed at the sediment water interface are potentially preserving high resolution record of past ocean isotope variability of Nd (e.g. Rutberg et al., 2000; Bayon et al., 2002; Piotrowski et al., 2005; Gutjahr et al., 2008, 2010; Jang et al., 2013; Hillaire-Marcel et al., 2013) and of Pb (Fagel et al., 2004; Gutjahr et al., 2009; Crocket et al., 2013). However, caution must be taken during the leaching procedure as

the reliability of the results may be in question in some geographical areas due to potential contamination by preformed oxides and/or by the detrital fractions, such as volcanic material, which is easily dissolvable (e.g., Elmore et al., 2011; Wilson et al., 2013). Therefore, the leaching procedure needs to be validated for each location (foram analysis, core-top calibration). The modified procedure for Nd and Pb extraction from ferromanganese coatings of marine sediments has also been successfully transferred for Hf isotopes (Chen et al., 2012; Gutjahr et al., 2014).

## 1.3 RARE EARTH ELEMENTS

The rare earth elements consist of 17 transition metals starting from scandium (Sc), yttrium (Y) and the lanthanides. However, traditionally Sc is not included in the REEs due to its small ionic radius. The group of rare earth elements is thus represented by lanthanum (La), cerium (Ce), neodymium (Nd), samarium (Sm), europium (Eu), gadolinium (Gd), terbium (Tb), dysprosium (Dy), holmium (Ho), erbium (Er), thulium (Tm), ytterbium (Yb), lutetium (Lu), and yttrium (Y). REEs are divided into groups based on their atomic number. Low atomic number elements are termed light REE (LREEs) from La to Eu, and heavy REE (HREEs) from Gd to Lu. Y is normally included with HREEs due to its ionic radius, which is nearly identical to Ho (Fig. 2). Some authors divide REEs into three groups, including mid-REE for intermediate members of the series (Chakhmouradian and Wall, 2012).

The distinct differences in the abundances of even numbered elements relative to their odd numbered neighbors define a saw tooth distribution pattern of REEs in terrestrial and extraterrestrial material (Chakhmouradian and Wall, 2012). This saw tooth pattern makes distinction between data difficult and thus normalization of the REEs concentrations to a reference material is widely applied. The material used for normalization is chosen based on the practical and scientific task. For the comparison to the upper continental crust and seawater normally well-homogenized shales are used, in particular Post Archean Australian shale (Fig. 3, Taylor and Mclennan, 1999). Normalized concentrations are plotted on the logarithmic scale.

Fractionation of REEs between melts and crystals is defined by "lanthanide contraction" (Goldschmidt, 1925), a significant reduction in ionic radius from La to Lu, due to increasing attraction of the nuclei and 6s electron of the lanthanides. The Earth's upper mantle exhibits a depletion in normalized LREEs, whereas the continental crust is enriched in these elements. In the environment REEs are mainly present in an oxidation state of +3. The exceptions are, however, Ce and Eu, which can occur in +2 and +4 oxidation states. Y and Ho

express different partitioning behavior in aqueous solutions, which has been attributed to differences in metal-ligand bonding (Choppin, 2002) or to stereochemical changes during the transition from a solute to a solid (Tanaka et al., 2008). Fractionation of REEs in natural systems is driven by these difference's (radii, ligand bonding and oxidation state).

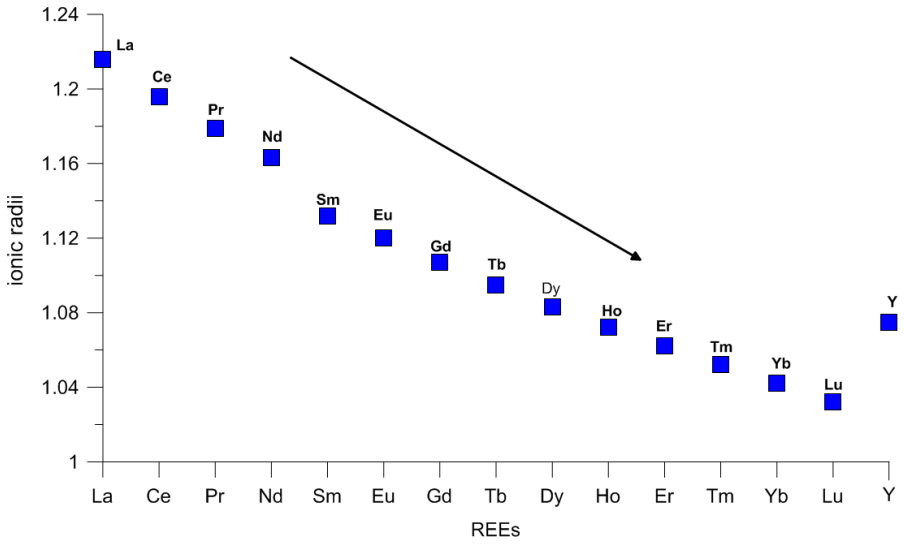


**Fig. 2** Ionic radii of the rare earth elements. Yttrium has almost the same ionic radii as Ho, and is normally included in heavy rare earth element group.

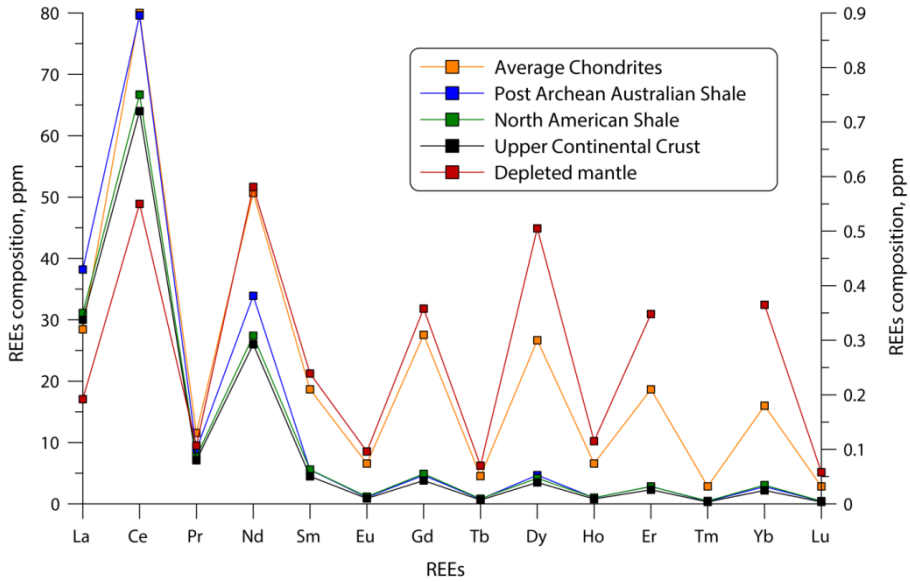


**Fig. 3** Composition of Rare Earth Elements in different rock standards: average chondrites values, plotted against second Y-axis on the right (Schmidt et al., 1963), Post Archean Australian Shale values (McLennan, 2001), North American Shale values (Gromet et al., 1984), Upper Continental Crust values (Wedepohl, 1969-1978; Rudnick and Gao, 2003; McLennan, 1989).

In seawater, REEs are mainly introduced through atmospheric inputs (Ederfield and Greaves, 1982; De Baar et al., 1983; Scholkovitz et al., 1993; Tachikawa et al., 1999) and via rivers (Goldstein et al., 1984; Frost et al., 1986; Byrne and Scholkovitz, 1996). The relatively stable trivalent oxidation state of REEs allows them to be appropriate tracers of suspended particulate matter of different origins (Censi et al., 2004), such as authigenic fractions formed by in situ processes (carbonates, silica, organic matter, ferromanganese oxihydroxides) and lithogenic fractions of terrigenous material (clay minerals, volcanic fallouts, residual minerals). Over the last decade a lot of research has been done on anthropogenic alterations, mainly close to densely populated areas such as for example a positive Gd anomaly caused by its use as a contrast reagent during medical examinations (Bau and Dulski, 1996; Bau, et al., 2006; Kulaksiz and Bau, 2007; Kulaksiz and Bau, 2011; Merschel et al., 2015).

On a global scale, shale normalized river water REE patterns exhibit significant enrichments in light, middle and heavy REEs in the range of up to the three orders of magnitude (Scholkovitz et al., 1989; Elderfield et al., 1990; Scholkovitz et al., 1992b). Shale normalized seawater REE patterns on the other hand are similar worldwide with some distinct common patterns, such as an overall depletion of LREEs in comparison to HREEs, positive La and Gd anomalies, a negative Ce anomaly, elevated Y/Ho ratio, and positive Lu anomaly. Marine REE patterns are clearly distinguishable from the smooth shale normalized patterns of rocks and detrital sediments. Expected concentration of one of the elements can be extrapolated from the ratios of the neighboring elements (Lawrence and Kambel, 2006). Anomalous behavior of Y is identified by the deviation of measured Y/Ho from the shale normalized value.

In seawater, REEs are generally depleted at the surface and enriched at depth (Elderfield, 1988; Bertram and Elderfield, 1993; Goldstein and Hemming, 2003; Lacan et al., 2012), typically with higher concentrations in the deep Pacific than in the deep Atlantic Ocean (Goldstein and Hemming, 2003), implying that particle scavenging and particle dissolution together with exchange at depth and the age of deep water masses control the oceanic distribution of REEs (Elderfield et al., 1988; Bertram and Elderfield, 1993; Scholkovitz et al., 1994). Studies of the behavior of REEs showed that fractionation and preferential removal of the light REEs over heavy REEs in estuaries play a significant role in the formation of the seawater pattern (Hoyle et al., 1984; Scholkovitz et al., 1995; Nozaki et al., 2000a; Rousseau et al., 2015). Besides inorganic complexation of REEs fractionation as a consequence of organic complexation has also been shown to be important (Hoyle et al., 1984; Scholkovitz et al., 1995; Tang and Johannessoon, 2003; Davranche et. al., 2004, 2005). Together with the Nd

isotope composition of seawater, REE concentrations and their shale normalized patterns are used as additional source of information to trace water mass transport and mixing (Lacan and Jeandel, 2005; Stichel et al., 2012; Molina-Kesher et al., 2014).

## 1.4 ALKENONE PALEOTHERMOMETRY

The presence of long-chain alkenones in marine sediments was unknown until the late 1970s when the advances in gas chromatography allowed to extract the alkenone signature through the use of long GC columns, capable of sustaining high temperatures at which long-chain alkenones are eluting (Herbert, 2003). Produced by haptophyte algae, the abundance of unsaturated alkenones was found to be correlated to sea surface temperature in which the organisms grew (Brassell et al., 1986; Prahl and Wakeham, 1987). The index of alkenone unsaturation is expressed as $U_{37}^{K}$ (Brassell et al., 1986; Prahl and Wakeham, 1987):

$$U_{37}^{K} = \frac{[C_{37:2}] - [C_{37:4}]}{[C_{37:2}] + [C_{37:3}] + [C_{37:4}]}$$

where C37:2, C37:3 and C37:4 denote the di-, tri-, and tetra-unsaturated C37 alkenone molecule, respectively.

Until today, the role of alkenones in the lifecycle of *E. huxleyi* is not fully understood, but it has been proposed that in analogy to many plants, alkenones might help to regulate membrane fluidity at different temperatures (Marlowe et al., 1984a; Brassell et al., 1986b). It is clear, however, that two species of coccolithophorides, *Emiliania huxleyi* and *Gephyrocapsa oceanica*, are the main producers of alkenones (Conte et al., 1994a; Volkmann et al., 1995).

*Emiliania huxleyi* is one of the most abundant coccolithophoride haptophyte algae, (Okada and Honjo, 1973; Winter et al., 1994). It may compose up to 80% of the coccolithophorid assemblages and can tolerate large changes in the marine environment such as temperature, salinity, nutrient levels, and light availability (Winter et al., 1994). Consequently, *E. huxleyi* is almost universally distributed in waters of nearly all temperatures, with the exception of polar oceans and highly saline waters. *G. oceanica* on the other hand is limited in its distribution by surface temperature and does not occur in waters colder than 12 °C (Okada and McIntyre, 1979). Most commonly, it is found in tropical and subtropical waters, in particular of the eastern Pacific and the Arabian Sea (Houghton and Uphta, 1991; Roth, 1994). In environments that favor diatom growth, such as polar Arctic waters and the opal belt of the Southern Ocean, or regions of high silicate availability such as the main

upwelling regions, coccolithophorids are generally limited in their abundance (Brand, 1991, 1994). Nevertheless, their generally universal distribution throughout the entire global ocean gave rise to the development of alkenone paleothermometry.

The detailed history of alkenone paleothermometry and some aspects, such as the low temperature end offset, potential sources of bias, and comparison to other temperature proxies are presented and discussed in more detail in chapter 4.

### 1.4.1 GENETIC VARIATIONS

One of the questions that is important for the alkenone SST proxy is whether or not a universal response to changes in temperature can be expected from different haptophyte producers. Brand (1982) showed that strains from cold environments are more adapted to cold temperatures than those from warm waters. This author also found differences in salinity tolerance in oceanic and coastal genotypes. However, genetic variability not always results in geographical separation. More recent studies support a strong genetic similarity of all marine producers. Medlin et al. (1996) found little genetic variation in rRNA from three geographically different types of A and B clones. Bollman (1997) studied a set of 70 globally distributed Holocene sediment assemblages and found a strong environmental control on the morphotypes. This author also found gradations in morphotypes and proposed six major morphotypes to be associated with different species. However, he did not have evidence to support or dismiss the assumption that these six morphotypes represent six different biological species or only one species with morphological differences and assumed the latter to be the case. Fujiwara et al. (2001) found a series of genetic similarities between *Emiliania*, *Isochrysis*, *Gephyrocapsa* and *Chrysotila*, which remains to be further supported.

### 1.4.2 ALKENONE ALTERATION IN THE WATER COLUMN AND SEDIMENTS.

In the last decade the possibility of alkenone alteration during metabolic processes has been extensively studied. Some results indicated that the alkenone unsaturation ratio can be affected during the transition of algae cells from the exponential to the stationary growth phase (Shifrin and Chisholm, 1981; Bell and Pond, 1996). Elgroth et al. (2005) observed that lipids biosynthetically related to long chain alkenones increase in abundance under nutrient limitation but disappear under prolonged darkness. This supported the assumption of a metabolic role of alkenones in *E. huxleyi* cells (Epstein et al., 2001). These authors proposed that a decrease in alkenone concentration observed during incubation under dark conditions is attributable to metabolic consumption of alkenones that serve as an additional energy source

when photosynthesis is not possible (Epstein et al., 2001; Prahl et al., 2003b; Pan and Sun, 2011).

Laboratory studies showed a variable degree of selectivity of alkenone consumption during the incubation of different strains of *E. huxleyi*, which may have resulted from the storage of alkenones in different parts of the cell (membranes or lipid bodies). However, as in these studies non-axanic strains of *E. huxleyi* were used, differences in consumption may be explained by the presence of bacteria in these cultures (Rontani et al., 2013). This is supported by the lack of variation in alkenone unsaturation ratios during incubation experiments of axenic strain of *E. huxleyi* (Pan and Sun, 2011) and isolation of bacteria, which are able to preferentially consume different alkenones from cells of E. huxleyi (Rontani et al., 2008; Zabeti et al., 2010).

Only a few studies were carried out on the effect of processing of alkenones by invertebrates (Volkmann et al., 1980b; Grice et al., 1998a). These studies were mainly focused on arthropods, which unlike ciliates and protists are not the main consumers of nannoplankton (coccolithophorides) (Olson and Strom, 2002; Antia et al., 2008). Few studies have addressed how benthic macrofauna affected specific biomarkers degradation in marine sediments. Ding and Sun (2006) observed in their microcosm experiment that fatty acids are more efficiently degraded than alkenones in the presence of the grass shrimp *Palaemonetes pugio*, but no preferential degradation of disaturated over trisaturated alkenones was observed.

Studies on the selective degradation of different unsaturated ketones by bacteria has so far shown positive results (Rontani et al., 2005; Rontani et al., 2008; Zabneti et al., 2010). Under oxygen-free conditions alkenones are most likely non-selectively degraded during methanogenic, sulfate reducing and denitrifying conditions (Treece et al., 1998; Rontani et al., 2005). Photodegradation and partial sulfurization do not seem to affect the alkenone unsaturation ratio in the sediments, however, auto oxidation and stereomutation have a potential to significantly affect the alkenone unsaturation ratio values (Rontani et al., 2013).

## 1.5 MOTIVATION AND RESEARCH QUESTIONS

CHAPTER 3. HF AS A WATER MASS TRACER.

The Labrador Sea is a key region for the deep water masses formation, which directly contribute to the NADW and as follows influence the global thermohaline circulation. Understanding of the mechanisms that control the water masses formation are thus crucial for deciphering the paleorecords. For decades, neodymium isotopes have been used as a tracer for

water mass mixing. and data on Nd isotope signature of different water masses are widely available. Hafnium data, on the other hand, are scarce, as its analysis is analytically challenging due to its low concentration in seawater. Lack of direct seawater measurements thus limits our understanding of Hf as a water mass proxy. Over the last decade, it has been debated if Hf could be applied as a proxy for global water mass mixing, or if it rather reflects the basin–wide scale processes. This study investigates in details the dissolved Hf and Nd distribution in the Labrador Sea, to assess the applicability of Hf isotopes for tracing the water mass mixing on the global scale and expand the understanding of the mechanisms controlling the Hf seawater signature formation. This study also trying to understand what processes control the Hf and Nd isotope composition of water masses in the Labrador Sea.

## CHAPTER 4. UNSATURATED KETONES AS A PROXY FOR SST.

Unsaturated ketones were used as a proxy for sea surface temperature reconstruction over the last 30 year. They have been applied for a wide range of temperatures and marine settings. However, the comparison with modern temperatures obtained from insitu measurements showed a high degree of offset, particularly in the cold regions, bringing into question the reliability of the proxy. Many studies were devoted to find the possible sources of bias, however, up until now many questions remain unanswered. This study assess the reliability of alkenone paleothermometry as a proxy for SST reconstruction in cold regions based on the compilation of the available data for the Western North Atlantic together with new data. Additionally, this study provides a list of potential and most likely sources for the offset in the region of North Atlantic, together with a set of conditions that need to be met to achieve a reliable SST reconstruction.

## CHAPTER 5. CLIMATE FLUCTUATIONS IN THE WESTERN NORTH ATLANTIC

Alkenone paleothermometry has widely been applied for SST reconstruction in the past. However, not a lot of studies have been done in the Labrador Sea, as cold regions have proven to be challenging. This study provides a detailed record of SST from the region from four marine sedimentary cores, improving our understanding of the climatic conditions over the period of the last 35 kyrs. Combination of alkenone down core data with Hf-Nd-Pb isotope data obtained from the same cores will help to determine the strength of the link between the atmosphere-ocean system, and asses the feedback mechanisms of this system.

## CHAPTER 5 AND 6. THE LABRADOR SEA WATER MASS CIRCULATION PATTERNS IN THE PAST.

Global climate change is one of the most important problems of the 21st century. Better understanding of the prerequisites of the climate change is crucial for more precise climate predictions in the future. Detailed studies of marine sedimentary records from key regions of the deep water mass formation such as the Labrador Sea may shed light onto the mechanisms that control climate change and help to improve the modern modelling studies. High resolution studies of Hf-Nd-Pb isotopes of the Labrador Sea sediments will help to reconstruct changes in the North Atlantic circulation as well as alteration of the weathering inputs in the area. This study will also allow to define when the modern circulation patterns were established.

## OUTLINE OF THE THESIS AND DECLARATION OF MY CONTRIBUTION TO THE FOLLOWING CHAPTERS

**Chapter 1** introduces the systematics of the Hf-Nd-Pb isotope systems and Rare Earth Elements, their behavior in marine sediments, crustal rocks and seawater, development of the proxy and its application in paleoceanography. Additionally, this chapter describes the main principals of alkenone paleothermometry and its application.

**Chapter 2** describes the methodology of the chemical procedures used to extract Nd-Hf-Pb isotope signals from marine sediments (leachates and detrital fraction), seawater and foraminifera, Rare Earth Elements concentrations from seawater samples, and unsaturated ketones from marine sediments. Details of mass spectrometric measurements of Hf, Nd and Pb and gas chromatographic measurements of unsaturated ketones are also described in detail.

The following chapters (3, 4, 5, 6) address the questions discussed in section 1.5 following different approaches.

**Chapter 3** *(Submitted to GCA)* suggests that tracing of large scale ocean mixing processes may not be possible based on Hf isotopes. However, there is clearly a prospect for their application in other restricted basins with similar geological and hydrographic settings based on the obtained Hf-Nd isotope data obtained from the seawater samples from the Labrador Sea.

**Chapter 3 Declaration:** Martin Frank proposed the study area. I have chosen the stations, where the water samples were collected. I collected the samples, carried out the analyses, interpreted the data, and wrote the manuscript. All co-authors and external reviewers helped improving and revising the manuscript.

**Chapter 4** *(published in G-cubed, 17 (4), 1370-1382, DOI: 10.1002/2015GC006106)* suggests that unsaturated ketones can be used for SST reconstruction in cold regions if a set of conditions are met and possible sources of bias can be kept small.

**Chapter 4 Declaration:** Markus Kienast proposed the study. Markus Kienast and Ralph Schneider provided surface sediment samples for the analysis. I analyzed the samples, interpreted the data, and wrote the manuscript. All co-authors and external reviewers helped improving and revising the manuscript.

**Chapter 5** *(to be submitted)* focuses on Sea Surface Temperature data reconstructed from the ketone unsaturation ratios obtained from four sediment cores studied in chapter 5 and 6.

**Chapter 5 Declaration:** Martin Frank, Claude Hallaire-Marcel and I discussed the possible cores to work on. I collected the samples, analyzed all the samples, interpreted the data, and wrote the chapter. Markus Kienast and Martin Frank helped improving the chapter.

**Chapter 6** *(to be submitted)* focuses on the Hf-Nd-Pb isotope data of Fe-Mn coatings of marine sediments and of the detrital fractions recovered from four sediment cores. The studied period covers the last 33 kyrs. The new data provide information about the establishment of the modern circulation patterns in the Labrador Sea and additionally suggest the most likely sources for the input material delivered to the Site locations.

**Chapter 6 Declaration:** Martin Frank, Claude Hallaire-Marcel and I discussed the possible cores to work on. I collected the samples, analyzed all the samples, interpreted the data, and wrote the chapter. Martin Frank and Markus Kienast helped improving the chapter.

## 1.6 REFERENCE LIST


Abouchami W., Goldstein S.L. (1995) A lead isotopic study of circum-antarctic manganese nodules. Geochim. Cosmochim. Acta 59 (9), 1809-1820.

Albarède, F., Simonetti, A., Vervoort, J.D., Blichert-Toft, J., Abouchami, W. (1998) A Hf-Nd isotopic correlation in ferromanganese nodules. Geophys. Res. Lett. 25 (20), 3895-3898.

Andersson, P., R. Dahlqvist, J. Ingri, and Ö. Gustafsson (2001) The isotopic composition of Nd in boreal river: A reflection of selective weathering and colloidal transport, 2001. Geochim, Cosmochim. Acta, 65, 521-527.

Antia A.N., Suffrian K., Holste L., Müller M.N., Nejestgaard J.C., Simonelli P., Carotenuto Y., Putzeys S. (2008). Dissolution of coccolithophorids calcite by microzooplankton and copepod grazing. Biogeosciences Discuss., 5, 1-23

Arsouze T., Dutay J.-C., Lacan F. and Jeandel C. (2009) Reconstructing the Nd oceanic cycle using a coupled dynamical biogeochemical model. *Biogeosciences* **6**(12), 2829–2846.

Asmerom, Y., Jacobsen, S.B., Knoll, A.H., Butterfield, N.J., Swett, K. (1991) Strontium isotopic

variations of Neoproterozoic seawater: Implications for crustal evolution. Geochimica et Cosmochimica Acta 55, 2883-2894.

Azetsu-Scott K., Jones E.P., Yashayaev I. (2003) Time series study of CFC concentrations in the Labrador Sea during deep and shallow convection regimes (1991-2000). Journal of Geophysical Research, vol. 108, no. C11, 3354, doi:10.1029/2002JC001317.

Barfod G.H., Otero O., Albarede F. (2003) Phosphate Lu-Hf geochronology. Chemical Geology 200, 241-253.

Barett T.J., Taylor P.N., Lugowski J. (1987). Metalliferous sediments from DSDP Leg 92: The East Pacific Rise transect, Geochim. Cosmochim. Acta, 51, 2241-2253.

Bayon G., German C.R., Boella R.M., Milton J.A., Taylor R.N., Nesbitt R.W. (2002). An improved method for extracting marine sediment fractions and its application to Sr and Nd isotopic analysis. Chemical Geology 187, 3-4, 179-199.

Bayon G., Vigier N., Burton K.W., Brenot A., Carignan J. and Etoubleau J. (2006) The control of weathering processes on riverine and seawater hafnium isotope ratios. Geology 34, 433-436.

Bau, M., Dulski, P. (1996) Anthropogenic origin of positive gadolinium anomalies in river waters. Earth and Planetary Science Letters 143, 245-255.

Bau, M., Knappe, A., Dulski, P. (2006) Anthropogenic gadolinium as a micropollutant in river waters in Pennsylvania and in Lake Erie, northeastern United States. Chemie der Erde - Geochemistry 66, 143-152.

Bau M. and Koshinsky A. (2006) Hafnium and neodymium isotopes in seawater and in ferromanganese crusts: The “element perspective”. Earth Planet. Sci. Lett. 241, 952-961.

Bell, M.V., Pond, D. (1996) Lipid composition during growth of motile and coccolith forms of Emiliania huxleyi. Phytochemistry 41, 465-471.

Elderfield, H., Bertram, C.J., Erez, J. (1996) A biomineralization model for the incorporation of trace elements into foraminiferal calcium carbonate. Earth and Planetary Science Letters 142, 409-423.

Bollman J. (1997) Morphology and biogeography of Gephyrocapsa coccoliths in Holocene sediments. Mar. Micropaleontol.29, 319–350.

Bouvier A., Vervoort J.D., Patchett P.J. (2008) The Lu-Hf and Sm-Nd isotopic composition of CHUR: Constraints from unequilibrated chondrites and implications for the bulk composition of terrestrial planets. Earth Planet. Sci. Lett. 273, 48-57, doi:10.1016/j.epsl.2008.06.010.

Brand L. E. (1982) Genetic variability and spatial patterns of genetic differentiation in the reproductive rates of the marine coccolithophores Emiliania huxleyi and Gephyrocapsa oceanica. Limmnol. Oceanogr. 27, 236–245.

Brand L. E. (1984) The salinity tolerance of forty-six marine phytoplankton isolates. Estuar. Coast. Shelf Sci. 18, 543–556.

Brand L. E. (1991) Minimum iron requirements of marine phytoplankton and the implications for the biogeochemical control of new production. Limnol. Oceanogr. 36,1756–1771.

Brassell, S.C., G. Eglinton, I.T. Marlowe, U. Pflaumann, Sarnthein M. (1986), Molecular stratigraphy a new tool for climatic assessment, Nature, 320, 129-133.

Elderfield, H., Bertram, C.J., Erez, J. (1996) A biomineralization model for the incorporation of trace elements into foraminiferal calcium carbonate. Earth and Planetary Science Letters 142, 409-423.

Burton, K.W., Ling, H.-F. and O'Nions, R. K. (1997). Closure of the Central American Isthmus and its effect on deep-water formation in the North Atlantic. *Nature* **386**, 382–5.

Burton, K. W. and Vance, D. (2000) Glacial-interglacial variations in the neodymium isotope composition of seawater in the Bay of Bengal recorded by planktonic foraminifera. *Earth and Planetary Science Letters* **176**, 425-441.

Carpentier, M., Chauvel, C., Maury, R. C., and Mattielli, N. (2009) The "zircon effect" as recorded by the chemical and Hf isotopic compositions of Lesser Antilles forearc sediments. *Earth and Planetary Science Letters* **287**, 86-99.

Chakhmouradian, A. R. & Wall, F. (2012). Rare earth elements: minerals, mines, magnets, (and more). Elements, 8(5), 333-340. Retrieved from http://elements.geoscienceworld.org/content/8/5/333.ful

Chen, CHIH-MING, T. K. Misra, S. Silver, and Rosen B. P. (1986) "Nucleotide sequence of the structural genes for an anion pump. The plasmid-encoded arsenical resistance operon." *Journal of Biological Chemistry* 261, no. 32: 15030-15038.

Chen T.Y., Ling H.F., Frank M., Zhao K.D., Jiang S.Y. (2011) Zircon effect alone insufficient to generate seawater Nd-Hf isotope relationships. $G^3$ 12, 5, Q05003, doi:10.1029/2010GC003363, ISSN:1525-2027.

Chen T.Y., Frank M., Brian A.H., Gutjahr M., Spielhagen R.F. (2012) Variations of North Atlantic inflow to the central Arctic Ocean over the last 14 million years inferred from hafnium and neodymium isotopes. Earth and Planetary Science Letters 353-354, 82-92.

Chen, T.-Y., Stumpf R., Frank M., Beldowski J., and Staubwasser M. (2013) Constraining geochemical cycling of hafnium and neodymium in the central Baltic Sea. Geochimica et Cosmochimica Acta 123, 166-180, doi:10.1016/j.gca.2013.09.011

Choppin, G. R., Liljenzin, J.-O., Rydberg J. (2002) *Radiochemistry and nuclear chemistry*. Butterworth-Heinemann

Chow, T. J. (1970) "Lead accumulation in roadside soil and grass." *Nature* 225, 295-296.

Chow, T. J., Patterson C. C. (1959) "Lead isotopes in manganese nodules." *Geochimica et Cosmochimica Acta* 17.1, 21-31.

Chow, Tsaihwa J., and Patterson C. C. (1962) "The occurrence and significance of lead isotopes in pelagic sediments." *Geochimica et Cosmochimica Acta* 26.2, 263-308.

Censi, P. A. O. L. O., et al. (2006) "Heavy metals in coastal water systems. A case study from the northwestern Gulf of Thailand." *Chemosphere* 64.7, 1167-1176.

Cochran, J.K., McKibbin-Vaughan, T., Dornblaser, M.M., Hirschberg, D., Livingston, H.D., Buesseler, K.O. (1990) 210Pb scavenging in the North Atlantic and North Pacific Oceans. Earth and Planetary Science Letters 97, 332-352.

Conte, M.H., Thompson, A., Eglinton, G. (1994) Primary production of lipid biomarker compounds by Emiliania huxleyi. Results from an experimental mesocosm study in fjords of southwestern Norway. Sarsia 79, 319-331.

Crocket, K.C., Foster, G.L., Vance, D., Richards, D.A., Tranter, M. (2013) A Pb isotope tracer of ocean-ice sheet interaction: the record from the NE Atlantic during the Last Glacial/Interglacial cycle. Quaternary Science Reviews 82, 133-144.

David, K., Frank, M., O'Nions, R. K., Belshaw, N. S., and Arden, J. W. (2001) The Hf isotope composition of global seawater and the evolution of Hf isotopes in the deep Pacific Ocean from Fe-Mn crusts. *Chemical Geology* **178**, 23-42. Davranche et. al., 2004, 2005

De Baar, H.J.W., Bacon, M.P., Brewer, P.G. (1983) Rare-earth distributions with a positive Ce anomaly in the Western North Atlantic Ocean. Nature 301, 324-327.

DePaolo, D. J. and Wasserburg, G. J. (1976), Inferences about magma sources and mantle structure from variations of $^{143}Nd/^{144}Nd$. Geophys. Res. Lett., 3: 743–746. doi:10.1029/GL003i012p00743

Dickin, Alan P. (2005) *Radiogenic isotope geology*. Cambridge University Press.

Dickson R.R., Meincke J., Malmberg S.-A., Lee A.J. (1988) The „Great Salinity Anomaly“ in the northern North Atlantic 1968-1982. Progress in Oceanography, 20, 10-31.

Dommemget D., Latif M. (2002) Analysis of observed and simulated SST spectra in the midlatitudes. Climate Dynamics, 19, 277-288.

Elderfield, H., Greaves, M.J. (1982) The rare earth elements in seawater. Nature 296, 214-219.

Elgroth, M.L., Watwood, R.L., Wolfe, G.V. (2005) Production and cellular localization of neutral long-chain lipids in the haptophyte algae Isochrysis galbana and Emiliania huxleyi. Journal of Phycology 41, 1000-1009.

Elderfield, H., M. Whitfield, J. D. Burton, M. P. Bacon, P. S. Liss (1988) The Oceanic Chemistry of the Rare-Earth Elements [and Discussion] Phil. Trans. R. Soc. Lond. A 1988 325 105-126; DOI: 10.1098/rsta.1988.0046

Elderfield, H., Kastner, M. and Martin, J.B. (1990). Compositions and sources of fluids in sediments of the Peru subduction zone. *Journal of Geophysical Research 95: doi: 10.1029/89JB03548. issn: 0148-0227.*

Elmore, A. C., Piotrowski, A. M., Wright, J. D., and Scrivner, A. E. (2011) Testing the extraction of past seawater Nd isotopic composition from North Atlantic deep sea sediments and foraminifera. *Geochemistry Geophysics Geosystems* **12**, Q09008, doi: 10.1029/2011gc003741.

Epstein, B.L., D'Hondt, S., Hargraves, P.E. (2001) The possible metabolic role of $C_{37}$ alkenones in Emiliania huxleyi. Organic Geochemistry, vol. 32, is. 6, pp. 867-875.

Fagel N., Hillaire-Marcel C., Humbelt M., Brasseur R., Weis D., Stevenson R. (2004) Nd and Pb isotope signatures of the clay-size fraction of Labrador Sea sediments during the Holocene: Implications for the inception of the modern deep circulation pattern. Paleoceanography, 9, doi:10.1029/2003PA000993

Firdaus, M. L., Minami, T., Norisuye, K., and Sohrin, Y. (2011) Strong elemental fractionation of Zr-Hf and Nb-Ta across the Pacific Ocean. *Nature Geoscience* **4**, 227-230.

Frank, M. (2002) Radiogenic isotopes: Tracers of past ocean circulation and erosional input. *Review of Geophysics* **40**, 1001, doi: 10.1029/2000RG000094

Frank, M., O'Nions, R. K., Hein, J. R. and Banakar,V.K. (1999). 60 Myr records of major elements and Pb–Nd isotopes from hydrogenous ferromanganese crusts: reconstruction of seawater paleochemistry. *Geochim. Cosmochim. Acta* **63**, 1689–708.

Fröllje, H., Pahnke, K., Schnetger, B., Brumsack, H.-J., Dulai, H., Fitzsimmons, J.N., 2016. Hawaiian imprint on dissolved Nd and Ra isotopes and rare earth elements in the central North Pacific: Local survey and seasonal variability. Geochimica et Cosmochimica Acta 189, 110-131.

Fujiwara S., Tsuzuki M., Kawchi M., Minaka N., and Inouye I. (2001) Molecular phylogeny of the Haptophyta based on the rbcL gene and sequence variation in the spacer region of the rubisco operon. J. Phycol. 37, 121–129.

German, C. R., Klinkhammer, G. P., Edmond, J. M., Mitra, A., and Elderfield, H. (1990) Hydrothermal Scavenging of Rare-Earth Elements in the Ocean. *Nature* **345**, 516-518.

Godfrey L.V., White W.M. and Salters V.J.M. (1996) Dissolved zirconium and hafnium distributions across a shelf break in the northeastern Atlantic Ocean. Geochim. Cosmochim. Acta 60, 3995-4006, doi:10.1016/S0016-7037(96)00246-3.

Godfrey L.V., Lee D.C., Sangrey W.F., Halliday A.N., Salters V.J.M., Hein J.R. and White W.M. (1997) The Hf isotopic composition of ferromanganese nodules and crusts and hydrothermal manganese deposits: implications for seawater Hf. Earth Planet. Sci. Lett. 151 (1-2), 91-105.

Godfrey L.V., Zimmermann B., Lee D.C., King R.L., Vervoort J.D., Sherrell R.M., Halliday A.N. (2009) Hafnium and neodymium isotope variations in NE Atlantic seawater. Geochem. Geophys. Geosys. 10, Q08015. http://dx.doi.org/10.1029/2009gc002508.

Goldstein S.L. and O'Nions R.K. (1981) Nd and Sr isotopic relationships in pelagic clays and ferromanganese deposits. *Nature* 292, 324 - 327 (23 July 1981); doi:10.1038/292324a0

Goldstein S.L., O'Nions R.K. and P.J. Hamilton (1984) A Sm-Nd isotopic study of atmospheric dust and particulates from major river systems. Earth Planet. Sci. Lett. 70, 221-236.

Goldstein S.L. and Hemming S.R. (2003) Long-lived Isotopic Tracers in Oceanography, Paleoceanography and Ice-sheet Dynamics. Book, Chapter 6.17.

Grasse, P., Stichel, T., Stumpf, R., Stramma, L., Frank, M. (2012) The distribution of neodymium isotopes and concentrations in the Eastern Equatorial Pacific: Water mass advection versus particle exchange. Earth and Planetary Science Letters 353–354, 198-207.

Greaves, M. J., H. Elderfield and. Sholkovitz E. R (1999) Aeolian sources of rare earth elements to the Western Pacific Ocean, *Mar. Chem.*, *68*, 31–38

Grice K., Klein Breteler W. C. M., Schoten S., Grossi V., de Leeuw J. W., and Sinninge Damste J. S. (1998) Effects of zooplankton herbivory on biomarker proxy records. Paleoceanography 13, 686–693.

Gulev S., Latif M., Keenlyside N., Park W., Koltermann K.P. (2013) North Atlantic Ocean control on surface heat flux on multidecadal timescales. Nature, 499, 464-467, http://dx.doi.org/10.108/nature12268.

Gutjahr, M., Frank, M., Stirling, C.H., Klemm, V., Van de Flierdt, T., Halliday, A.N. (2007) Reliable extraction of a deepwater trace metal isotope signal from Fe–Mn oxyhydroxide coatings of marine sediments. Chemical Geology 242, 351-370.

Gutjahr, M., Frank, M., Stirling, C. H., Keigwin, L. D., and Halliday, A. N., 2008. Tracing the Nd isotope evolution of North Atlantic deep and intermediate waters in the Western North Atlantic since the Last Glacial Maximum from Blake Ridge sediments. Earth and Planetary Science Letters 266, 61-77.

Gutjahr, M., Frank, M., Halliday, A.N., Keigwin, L.D. (2009) Retreat of the Laurentide ice sheet tracked by the isotopic composition of Pb in western North Atlantic seawater during termination 1. Earth and Planetary Science Letters 286, 546-555.

Gutjahr, M., Hoogakker, B.A., Frank, M., McCave, I.N. (2010) Changes in North Atlantic Deep Water strength and bottom water masses during Marine Isotope Stage 3 (45–35kaBP). Quaternary Science Reviews 29, 2451-2461.

Halliday, A. N., Davidson, J. P., Holden, P., Owen, R. M., and Olivarez, A. M. (1992) Metalliferous Sediments and the Scavenging Residence Time of Nd near Hydrothermal Vents. *Geophysical Research Letters* **19**, 761-764.

Hillaire-Marcel, C., Maccali, J., Not, C., Poirier, A. (**2013**) Geochemical and isotopic tracers of Arctic sea ice sources and export with special attention to the Younger Dryas interval, QUATERNARY SCIENCE REVIEWS. Houghton and Uphta, 1991

Jacobsen S.B., Wasserburg G.J. (1980) Sm-Nd isotopic evolution of chrondrites. Earth Planet. Sci. Lett. 50, 139-155.

Jones, C. E., A. N. Halliday, D. K. Rea, and R. M. Owen, (2000) Eolian inputs of lead into the North Pacific, *Geochim. Cosmochim. Acta*, *64*, 1405–1416.

Kraft, S., Frank, M., Hathorne, E. C., and Weldeab, S. (2013) Assessment of seawater Nd isotope signatures extracted from foraminiferal shells and authigenic phases of Gulf of Guinea sediments. *Geochimica et Cosmochimica Acta* **121**, 414-435.

Kulaksız, S., Bau, M., 2007. Contrasting behaviour of anthropogenic gadolinium and natural rare earth elements in estuaries and the gadolinium input into the North Sea. Earth Planet. Sci. Lett. 260, 361–371.

Lacan F. and Jeandel C. (2005) Acquisition of the neodymium isotopic composition of the North Atlantic Deep Water. $G^3$, 6, 12, Q12008, doi:10.1029/2005GC000956, ISSN:1525-2027.

Lacan F., Tachikawa K, Jeandel C. (2012) Neodymium isotopic composition of the oceans: a compilation of seawater data. Chemical Geology 300-301, 177-184, doi:10.1016/j.chemgeo.2012.01.019.

Lazier J., Hendry R., Clarke A., Yashayaev I., Rhines P., 2002. Convection and restratification in the Labrador Sea, 1990-2000. Deep-Sea Research I, 49, 1819-1835

Lawrence, M.G., Jupiter, S.D., Kamber, B.S., 2006. Aquatic geochemistry of the rare earth elements and yttrium in the Pioneer River catchment, Australia. Mar. Freshwater Res. 57, 725–736.

Lee, D. C., Halliday, A. N., Hein, J. R., Burton, K. W., Christensen, J. N., and Gunther, D. (1999) Hafnium isotope stratigraphy of ferromanganese crusts. *Science* **285**, 1052-1054.

Marlowe I. T., Green J. C., Neal A. C., Brassell S. C., Eglinton G., and Course P. A. (1984a) Long chain (n-C37–C39) alkenones in the prymnesiophyceae: distribution of alkenones and other lipids and their taxonomic significance. British Phycol. J. 19, 203–216.

McKelvey B.A. and Orians K.J. (1998) The determination of dissolved zirconium and hafnium from seawater using isotope dilution coupled plasma mass spectrometry. Mar. Chem. 60, 245-255.

Medlin, L. K., Kooistra, W. H. C. F., Gersonde, R. & Wellbrock, U. (1996). Evolution of the diatoms (Bacillariophyta). II. Nuclear- encoded small-subunit rRNA sequence comparisons conÆrm a paraphyletic origin for the centric diatoms. Mol Biol Evol 13 ,67±75

Merschel, G. and Bau, M.: Rare earth elements in the aragonitic shell of freshwater mussel Corbicula fluminea and the bioavail ability of anthropogenic lanthanum, samarium and gadolinium in river water, Sci. Total Environ., 533, 91–101, 2015

Michard, A., Albar`ede, F., Michard, G., Minster, J. F. and Charlou, J. L. (1983). Rare-earth elements and uranium in hightemperature solutions from East Pacific Rise hydrothermal vent field (13 ◦N). *Nature* **303**, 795–7.

Molina-Kescher, M., M. Frank, and E. C. Hathorne (2014), Nd and Sr isotope compositions of different phases of surface sediments in the South Pacific: Extraction of seawater signatures, boundary exchange, anddetrital/dust provenance, Geochem.Geophys. Geosyst. ,15 , 3502–3520, doi:10.1002/2014GC005443

Nowell G.M., Kempton P.D., Noble S.R., Fitton J.G., Saunders A.D., Mahoney J.J., Taylor R.N. (1998) High precision Hf isotope measurements of MORB and OIB by thermal ionization mass spectrometry: insights into the depleted mantle. Chem. Geol. 149, 211-233.

Okada H. and Honjo S. (1973) The distribution of oceanic coccolithophorids in the Pacific. Deep-Sea Res. 26, 355–374.

Okada H. and McIntyre A. (1979) Seasonal distribution of modern coccolithophores in the western North Atlantic Ocean. Mar. Biol. 54, 319–328.

O'Nions, R. K., Hamilton, P. J. and Evensen, N. M. (1977). Variation in 143Nd/144Nd and 87Sr/86Sr in oceanic basalts. *Earth Planet. Sci. Lett.* **34**, 13–22.

O'Nions, R. K., Carter, S. R., Cohen, R. S., Evensen, N. M. and Hamilton, P. J. (1978). Pb, Nd and Sr isotopes in oceanic ferromanganese deposits and ocean floor basalts. *Nature* **273**, 435–8.

Öhlander B., Ingri J., Land M., and Schöberg H. (2000) Change of Sm-Nd isotope composition during weathering of till. Geochim. Cosmochim Acta 64, 813-820.

Pan, H., Sun, M.-Y., 2011. Variations of alkenone based paleotempearature index ($U_{37}^{K'}$) during Emiliania huxleyi cell growth, respiration (auto-metabolism) and microbial degradation. Organic Geochemistry, 42, pp. 678-687.

Patchett P.J., White W.M., Feldman H., Kielinczuk S., Hofmann A.W. (1984) Hafnium Rare-Earth element fractionation in the sedimentary system and crystal recycling into the earth's mantle. Earth Planet. Sci. Lett. 69, 365-378

Pena, L. D., Goldstein, S. L., Hemming, S. R., Jones, K. M., Calvo, E., Pelejero, C., and Cacho, I. (2013) Rapid changes in meridional advection of Southern Ocean intermediate waters to the tropical Pacific during the last 30 kyr. *Earth and Planetary Science Letters* **368**, 20-32.

Pettke T.D., Lee D.C., Halliday A.N., rea D.K. (2002a) Radiogenic Hf isotopic compositions of continental eolian dust from Asia, tis variability and its implications for seawater Hf. Earth Planet. Lett. 202, 453-464, doi:10.1016/S0012-821X(02)00778-1.

Pettke, T., A. N. Halliday, and D. K. Rea (2002b), Cenozoic evolution of Asian climate and sources of Pacific seawater Pb and Nd derived from eolian dust of sediment core LL44-GPC3, *Paleoceanography*, *17*(3), doi: 10.1029/2001PA000673.

Piepgras, D. J., and G. J. Wasserburg, Rare earth transport in the western North Atlantic inferred from isotopic observations, *Geochim. Cosmochim. Acta*, *51*, 1257–1271, 1987.

Piepgras D. J., Wasserburg G. J., and Dasch E. J. (1979) The isotopic composition of Nd in different ocean masses. EarthPlanet. Sci. Lett. 45, 223–236

Piepgras D.J. and Wasserburg G.J. (1987) Rare-earth element transport in the western North Atlantic inferred from Nd isotopic observations. Geochim. Cosmochim. Acta 51, 1257-1271, doi:10.1016/j.epsl.2006.11.027.

Piotrowski, A. M., Lee, D. C., Christensen, J. N., Burton, K. W., Halliday, A. N., Hein, J. R., and Gunther, D. (2000) Changes in erosion and ocean circulation recorded in the Hf isotopic compositions of North Atlantic and Indian Ocean ferromanganese crusts. *Earth and Planetary Science Letters* **181**, 315-325.

Piotrowski A.M., Goldstein S.L., Hemming S.R., Fairbanks R.G. (2005) Temporal Relationships of carbon Cycling and Ocean Circulation at Glacial Boundaries. Science 307, 1933-1938, doi:10.1126/science.1104883

Prahl, F.G., Wakeham, S.G., 1987. Calibration of unsaturation patterns in long chain ketone compositions for paleotemperature assessments. Nature 330, 367-369.

Prahl, F.G., Wolfe, G.V., Sparrow, M.A., 2003b. Physiological impacts on alkenone paleotermometry. Paleoceanography 18, http://dy.doi.org/10.1029/2002PA000803

Rempfer J., Stocker T. F., Joos F., Dutay J.-C. and Sidall M. (2011) Modeling Nd-isotopes with a coarse resolution ocean circulation model: Sensitivities to model parameters and source/sink distributions. *Geochim. Cosmochim. Acta* **75**, 5927-5950

Richard P., Shimizu N., and Alle(c)gre C. J. (1976) 143Nd/146Nd, a natural tracer: an application to oceanic basalts. Earth Planet. Sci. Lett. 31, 269–278.

Rickli J., Frank M., Halliday A.N. (2009) The hafnium-neodymium isotopic composition of Atlantic seawater. Earth and Planetary Scince Letters 280, pp. 118-127.

Rickli J., Frank M., Baker A.R., Aciego S., de Souza G., Georg R.B., Halliday A.N. (2010) Hafnium and neodymium isotopes in surface waters of the eastern Atlantic Ocean: Implications for sources and inputs of trace metals to the ocean. Geochimica et Cosmochimica Acta 74, 540-557.

Rickli J., Frank M., Stichel T., Georg R.B., Vance D., Halliday A.N. (2013) Controls on the incongruent release of hafnium during weathering of metamorphic and sedimentary catchments. Geochim. et Cosmochim. Acta 101, 263-284, doi:10.1016/j.gca.2012.10.019.

Rickli J., Gutjahr M., Vance D., Fisher-Gödde M., Hillenbrand C.-D., Kuhn G. (2014) Neodymium and hafnium boundary contributions to seawater along the West Antarctic continental margin. Earth Planet. Sci. Lett. 394, 99-110.

Roberts, N. L., Piotrowski, A. M., Elderfield, H., Eglinton, T. I., and Lomas, M. W. (2012) Rare earth element association with foraminifera. *Geochimica et Cosmochimica Acta* **94**, 57-71. Rontani et al., 2005

Rontani, J.-F. , Harji, R., Guasco, Prahl S. F.P., Volkman J.K., Bonin P. (2008) Degradation of alkenones by aerobic heterotrophic bacteria: selective or not? Organic Geochemistry, 39, pp. 34–51

Rontani, J.F., Volkman, J.K., Prahl, F.G., Wakeham, S.G., (2013) Biotic and abiotic degradation of alkenones and implications for paleoproxy applications: A review. Organic Geochemistry 59, 95-113.Roth, 1994

Rutberg, R. L., Hemming, S. R., and Goldstein, S. L. (2000) Reduced North Atlantic Deep Water flux to the glacial Southern Ocean inferred from neodymium isotope ratios. *Nature* **405**, 935-938.

Schaule, B. K., and C. C. Patterson, Lead concentrations in the north Pacific: Evidence for global anthropogenic perturbations, *Earth Planet. Sci. Lett.*, *54*, 97–116, 1981.

Sholkovitz, E.R., Shaw, T.J., Schneider, D.L., 1992. The geochemistry of rare earth elements in the seasonally anoxic water column and porewaters of Chesapeake Bay. Geochim. et Cosmochim. Acta 56 (9), 3389–3402.

Sholkovitz, E.R., 1993. The geochemistry of rare earth elements in the Amazon River estuary. Geochim. et Cosmochim. Acta 57 (10), 2181–2190.

Sholkovitz, E. R., Landing, W. M. and Lewis, B. L. (1994). Ocean particle chemistry: The fractionation of rare earth elements between suspended particles and seawater. Geochimica et Cosmochimica Acta, 58, 1567–1579.

Sholkovitz, E.R., 1995. The aquatic chemistry of rare earth elements in rivers and estuaries. Aquat. Geochem. V1 (1), 1–34.

Shifrin, N. S. and Chisholm, S. W. (1981), PHYTOPLANKTON LIPIDS: INTERSPECIFIC DIFFERENCES AND EFFECTS OF NITRATE, SILICATE AND LIGHT-DARK CYCLES. Journal of Phycology, 17: 374–384.

Stichel T., Frank M., Rickli J., Hathorne E.C., Haley B., Jeandel C., Pradoux C. (2012a) Sources and input mechanisms of hafnium and neodymium in surface waters of the Atlantic sector of the Southern Ocean. Geochimica et Cosmochimica Acta 94, 23-37.

Stichel T., Frank M., Rickli J., Haley B. (2012b) The hafnium and neodymium isotope composition of seawater in the Atlantic sector of the Southern Ocean. Earth and Planetary Science Letters 317-318, 282-294.

Stordal M.C. and Wasserburg G.J. (1986) Neodymium isotopic study of Baffin Bay water sources of REE from very old terranes. Earth Planet. Sci. Lett. 77, 259-272.

Sturges W.T., Barrie L. (1987) Lead 206/207 Isotope Ratios in the Atmosphere of North America as Tracers of US and Canadian Emissions. *Nature* **329**, 144 - 146 ; doi:10.1038/329144a0

Tanaka T., Togashi S., Kamioka H., Amakawa H., Kagami H., Hamamoto T., Yuhura M., Orihashi, Y., Yoneda, S., Shimizu, H., Kunimaru, T., Takahashi, K., Yanagi, T., Nakano, T., Fujimaki, H., Shinjo, R., Asahara, Y., Tanimizu, M., Dragusanu, C. (2000) JNdi-1: a neodymium isotopic reference in consistency with LaJolla neodymium. Chem. Geol. 168 (3–4), 279–281.

Tang, J., Johannesson, K.H., 2003. Speciation of rare earth elements in natural terrestrial waters: assessing the role of dissolved organic matter from the modeling approach. Geochimica et Cosmochimica Acta 67, 2321-2339.

Tachikawa, K., Jeandel, C., Vangriesheim, A., Dupré, B., 1999. Distribution of rare earth elements and neodymium isotopes in suspended particles of the tropical Atlantic Ocean (EUMELI site). Deep Sea Research Part I: Oceanographic Research Papers 46, 733-755.

Taylor, S.R., McLennan, S.M., 1985. The Continental Crust, Its Composition and Evolution: An Examination of the Geochemical Record Preserved in Sedimentary Rocks. Blackwell Scientific, Oxford.

van de Flierdt T., Frank M., Lee D.-C., Haliday A.N. (2002) Glacial weathering and the hafnium isotope composition of seawater. Earth Planet. Sci. Lett. 198, 167-175. Republished with corrections: Earth Planet. Sci. Lett. 201, 639-647.

van de Flierdt T., Frank M., Lee D.C., Halliday A.N., Reynolds B.C., Hein J.R. (2004a) New constraints on the sources and behavior of neodymium and hafnium in seawater from Pacific Ocean ferromanganese crusts. Geochim. Cosmochim. Acta 68, 3827-3843.

van de Flierdt T., Frank M., Halliday A.N., Hein J.R., Hattendorf B., Gunther D., Kubik P.W. (2004b) Tracing the history of submarine hydrothermal inputs and the significance of hydrothermal hafnium for the seawater budget- a combined Pb-Hf-Nd isotope approach. Earth and Planetary Science Letters 222, 259-273.van de Flierdt et al., 2007

Vance, D. and Burton, K. (1999) Neodymium isotopes in planktonic foraminifera: a record of the response of continental weathering and ocean circulation rates to climate change. *Earth and Planetary Science Letters* **173**, 365-379.

Versteegh G. J. M., Riegman R., de Leew J. W., and Jansen J. H. F. (2001) U37 k0 values for Isochrysis galbana as a function of culture temperature, light intensity and nutrient concentrations. Org. Geochem. 32, 785–794.

Volkman, J.K., Eglinton, G., Corner, E.D.S., Sargent, R., 1980. Novel unsaturated straight-chain $C_{37}$-$C_{39}$ methyl and ethyl ketones in marine sediments and coccolithophore Emiliania huxleyi. Advances in Organic Geochemistry, pp. 219-227.

Volkman J. K., Jeffer S. W., Nichols P. D., Rogers G. I., and Garland C. D. (1989) Fatty acid and lipid composition of 10 species of microalgae used in mariculture. J. Exp. Mar. Biol. Ecol. 128, 219–240.

Volkman, J.K., Barrett, S.M., Blackburn, S.I., Sikes, E., 1995. Alkenones in Gephyrocapsa oceanica: Implications for studies of paleoclimate. Geochimica et Cosmochimica Acta, vol. 59, no. 3, pp. 513-520.

von Blanckenburg, F., R. K. O'Nions, and J. R. Hein, Distribution and sources of pre-anthropogenic lead isotopes in deep ocean water from Fe-Mn crusts, *Geochim. Cosmochim. Acta*, *60*, 4957–4936, 1996b.

von Blanckenburg, F. and Nägler, T. F., 2001. Weathering versus circulation-controlled changes in radiogenic isotope tracer composition of the Labrador Sea and North Atlantic Deep Water. Paleoceanography 16, 424-434.

von Blanckenburg, F., and R. K. O'Nions, Response of beryllium and radiogenic isotope ratios in Northern Atlantic Deep Water to the onset of northern hemisphere glaciation, *Earth Planet. Sci. Lett.*, *167*, 175–182, 1999.

Vervoort J.D., Plank T., Prytulak J. (2011) The Hf-Nd isotopic composition of marine sediments. Geochim. et Cosmocim. Acta 75, 20, 5903-5926, doi:10.1016/j.gca.2011.07.046.Vlastelic et al., 2001

White, W. M., P. J. Patchett, and D. Ben Othman, Hf isotope ratios of marine sediments and Mn nodules: Evidence for a mantle source of Hf in seawater, *Earth Planet. Sci. Lett.*, *79*, 46–54, 1986.

White, W.M., Albarède, F., Télouk, P., 2000. High-precision analysis of Pb isotope ratios by multi-collector ICP-MS. Chemical Geology 167, 257-270.

Wilson, D. J., Piotrowski, A. M., Galy, A., and McCave, I. N. (2012) A boundary exchange influence on deglacial neodymium isotope records from the deep western Indian Ocean. *Earth and Planetary Science Letters* **341–344**, 35-47.

Wilson, D. J., Piotrowski, A. M., Galy, A., and Clegg, J. A. (2013) Reactivity of neodymium carriers in deep sea sediments: Implications for boundary exchange and paleoceanography. *Geochimica et Cosmochimica Acta* **109**, 197-221.

Winter A., Jordan R., and Roth P. (1994) Biogeography of living coccolithophores in ocean waters. In Coccolithophores (eds. A. Winter and W. G. Siesser). Cambridge University Press, Cambridge, UK, pp. 161–177.

Yashayaev I., Holliday N.P., Bersch M., van Aken H.M. (2008) The History of the Labrador Sea Water: Production, Spreading, Transformation and Loss. In book: Arctic–Subarctic Ocean Fluxes, Defining the Role of the Northern Seas in Climate, Chapter: Chapter 24: The History of the Labrador Sea Water: Production, Spreading, Transformation and Loss, Publisher: Springer, Editors: Bob Dickson, Jens Meincke, Peter Rhines, pp.569–612

Yashayaev I. and Clark A. (2006) Recent warming of the Labrador Sea. AZMP Bulletin PMZA 5:12-20.

Yashayaev I. and Loder J.W., 2009. Replenishment of Labrador Sea Water to the ocean conveyor belt in 2008. Bio Sci. in partnership.

Yashayaev I., Seidov D., Demirov E., 2015. A new collective view of oceanography of the Actic and North Atlantic basins. Progress in Oceanography, 12, 1-21, doi:10.1016/j.pocean.2014.12.012.

Zimmermann B., Porcelli D., Frank M., Andersson P.S., Baskaran M., Lee D.C., Halliday A.N. (2009a) Hafnium isotopes in Arctic Ocean water. Geochim. Cosmochim. Acta 73, 32118-3233.

Zimmermann B., Porcelli D., Frank M., Rickli J., Lee D.C., Halliday A.N. (2009b) The hafnium isotope composition of Pacific Ocean water. Geochim. Cosmochim. Acta 73, 91-101.

# CHAPTER 2

# METHODS

# 2. METHODS

## 2.1 ISOTOPIC COMPOSITION AND REE CONCENTRATION ANALYSIS OF SEAWATER SAMPLES

### 2.1.1 SAMPLING AND PRECONCENTRATION PROCEDURE

Seawater samples were collected in the Labrador Sea along the AR7W transect, along the Belle Isle line and the Extended Halifax line during Fisheries and Oceans Canada's (DFO's) annual survey as part of its Atlantic Zone Off-shelf Monitoring Program (AZOMP; http://www.bio.gc.ca/science/monitoring-monitorage/azomp-pmzao/azomp-pmzao-en.php) in May, 2013. Full water depth profiles were collected from four deep stations, four surface water samples from four shallow stations and two deep water samples from two deep stations. For each sample, 20 L of seawater were directly filtered through 0.45 µl acetate filters into a pre-cleaned cubitainers from a standard rosette equipped with a 10 L Niskin bottle. After filtration on board every sample was acidified to a pH ≈ 2 using distilled concentrated HCl. One liter aliquot was kept from every sample in separate PE bottles for isotope dilution measurements. After the cruise, all samples were transferred to the laboratory facilities at Dallhousie University, Halifax, Canada for subsequent preparation (Rickli et al., 2009; Stichel et al., 2012). In the laboratory, about 0.5 ml of pre-cleaned Fe-solution was added to every sample and left to settle for at least 24 hours. To induce precipitation of dissolved metals, suprapure ammonia (25 %) was added to every sample to raise the pH up to 7.5 - 8. After that, samples were left untouched to form the precipitates and to settle down for at least 2 days. After co-precipitation of iron bound metal complexes the excess of "empty seawater" was siphoned off with a water jet vacuum pump and dumped. The remaining one liter of seawater with iron bound precipitates was transferred into one liter PE bottles and sent to the clean laboratory facilities at GEOMAR, Kiel, Germany for further preparation.

### 2.1.2 PREPARATION FOR SEPARATION AND COLUMN CHROMATOGRAPHY

Back in the clean laboratory at GEOMAR, Kiel the excess of water from one liter samples was siphoned off with a water jet vacuum pump and decanted. The precipitates were transferred into pre-cleaned 50 ml centrifuge tubes and centrifuged three times for 10 minutes at 3500 rpm. Between every centrifugation, the precipitates were rinsed with Deionised 18.2 Ω MilliQ. After the last centrifugation, excess water was removed and precipitates were dissolved in 3 ml of 6 M HCl. After complete dissolution of iron precipitates, the solution was transferred into 60 ml Teflon vials and dried on the hotplate under 100 °C. Subsequently 4 ml of aqua regia mixture (3 ml of HCl + 1 ml of $HNO_3$) were added to every sample and left to

reflux over night under 120 °C. Afterwards all samples were dried down on the hotplate and redissolved in 4 ml of 6 M HCl and subsequently refluxed.

To remove the excess of iron in the samples after co-precipitation, a pre-cleaned solution of 3 ml of di-ethyl ether was added. The cleaning step is based on the density difference between the sample and ether, which allows the separation of the mixture in to two phases. Iron is bound to the upper phase with di-ethyl ether, all trace metals in the sample stay in the acidic lower phase. The upper phase with iron is pipetted off and discarded. The step is repeated three times, until the sample is pale yellow. After the last cleaning all samples are evaporated to dryness on the hotplate.

To prepare the samples for ion chromatography, each sample is redissolved in 2 ml of 1 M HCl, transferred into 7 ml Teflon vials and dried again. Subsequently, all samples are redissolved in a mixture of 0.5 ml of 1 M HCl/0.05 M HF (to keep Hf in solution) and refluxed over night. Before loading onto the cation columns, all samples were centrifuged. If after centrifugation a jelly-like residue was observed on the bottom of the samples, the clear solution was pipetted off and kept in a separate 7 ml Teflon vials. The jelly-like residue was redissolved in 2 M HF and refluxed until it is totally dissolved (at least over night) and then evaporated to dryness on the hotplate. Afterwards, it was redissolved in 1 M HCL/0.05 M HF mixture and combined with the rest of the sample. The total sample was centrifuged again and then loaded onto the cation columns. Hafnium and REE separation from other trace metals matrix followed the steps presented in the table 1 (Münker et al., 2001)..

| Volume | Acid | Stage |
|---|---|---|
| 8 ml | 6MHNO$_3$/0.5 M HF | Pre-clean |
| 2*1 ml | MQ | Change the acid |
| 0.5 ml | 1MHCl/0.05 HF | Pre-clean |
| 1 ml | 1MHCl/0.05 HF | Pre condition |
| 0.5 ml | 1MHCl/0.05 HF | **Load and directly collect Hf** |
| 2 ml | 1MHCl/0.05 HF | **Collect Hf** |
| 5 ml | 3M HCl | Elute Fe |
| 2*1ml | MQ | Change the acid |
| 10 ml | 2M HNO$_3$ | Elute Ba |
| 6.5 ml | 6M HNO$_3$ | **Collect Ac/REE** |
| 2 ml | 6M HNO$_3$/ 0.5M HF | Clean |
| 2*1ml | MQ | Change the acid |
| 8ml | 6M HCl | Clean |
| 2*3ml | MQ | Pass/store |

**Table 1** Cation columns chemistry procedure, AG50W-X8 resin, dry mesh 200-400.

After cation columns two cuts were collected, one for REEs and one for Hf. The cut for REEs (Nd) was dried down and redissolved in 0.5 ml of concentrated HCl and dried down

again on the hotplate. The step was repeated twice. Afterwards samples were redissolved in 0.1 M HCl and refluxed before loading on the next set of columns for Nd separation from REEs. Neodymium separation from REEs followed the procedure presented in table.2 (Pin and Zalduegui, 1997).

| Volume | Acid | Stage |
|---|---|---|
| 8 ml | 6M HCl | Pre-clean |
| 0.5 ml | 0.1 M HCl | Pre condition |
| 1 ml | 0.1 M HCl | Pre condition |
| 0.5 ml | 0.1 M HCl | **Load the sample** |
| 0.5 ml | 0.1 M HCl | Wash and elute Ba |
| 8 ml | 0.25 M HCl | Elute LREE |
| 6.5 ml | 0.25 MHCl | **Collect Nd** |
| 8 ml | 6M HCl | Clean |
| 1 ml | MQ | Pass |
| 1 ml | MQ | Store |

**Table 2** Eichrom LN-Spec columns for Nd separation from REEs. The resin volume is 2 ml, bead size 50-100 µm.

The cut collected for Hf was dried down and redissolved in 0.5 ml of concentrated HCl and subsequently evaporated to dryness. The step was repeated two times. Finally, it was redissolved in 4 ml of 3 M HCL and refluxed before loading onto Eichrom LN-Spec columns with resin volume of 1 ml and bead size 100-150 µm. Before loading the samples onto the columns 0.4 M ascorbic acid dissolved in 0.8 ml of MQ was added to every sample to reduce the iron content. Hafnium separation from REEs matrix and other trace metals followed the procedure described in the table 3.

| Volume | Acid | Stage |
|---|---|---|
| 15ml | 6M HCl | Pre clean |
| 15 ml | 2M HF | Pre clean |
| 2 ml | MQ | Wash HF |
| 2*3 ml | 3M HCl | Pre condition |
| 4ml+0.8ml | 3M HCl+0.4M ascorbic acid | **Load the samples (a.a in every sample)** |
| 50 ml | 6MHCl | Elute matrix, REE |
| 2*3ml | MQ | Change acid |
| 30 ml | 4.5M $HNO_3$/0.09M citric/1wt%$H_2O_2$ | Elute Ti, W |
| 2*3 ml | MQ | Change acid |
| 5 ml | 2M HCl/0.1M HF | Elute Zr |
| 6ml | 3MHCl/0.2M HF | **Collect Hf** |
| 25 ml | 6M HCl | Clean |
| 25ml | 2M HF | Clean |

**Table 3** Eichrom LN-Spec columns for Hf separation from REEs. The resin volume is 1 ml, bead size 100-150.

Collected Hf and Nd cuts were dried down on the hotplate and redissolved in the mixture of 100 µl $H_2O_2$ + 100 µl $HNO_3$, to get rid of any organics leftovers and evaporated to dryness. Subsequently to get ready for mass spectrometry measurements Hf cut was redissolved in 1 ml of 0.5 M HNO3/0.1 M HF mixture and Nd cuts was redissolved in 1 ml of 2 % $HNO_3$.

### 2.1.3 ISOTOPE DILUTION MEASUREMENTS

For isotope dilution (ID) analysis, one liter aliquot from every sample was kept in a separate pre-cleaned PE-bottles (Rickli et al., 2009; Stichel et al., 2012). Weighted amount of spike solution enriched in $^{178}$Hf, $^{149}$Sm and $^{150}$Nd, respectively, was added to every sample gravimetrically. After spike addition, all samples were left for 4-5 days for homogenization prior to further analysis. Afterwards, about 25 µl of $FeCl_3$ solution was added to every sample and left for another day to homogenize. To induce the co-precipitation of iron bounded trace metal complexes suprapure ammonia (25 %) was added to every sample to raise the pH to around 7.5 - 8, shook and left to precipitate at least over night. Afterwards, the "empty seawater" was siphoned off with water jet pump and decanted. Precipitates were transferred into 50 ml centrifuge vials and centrifuged at 3500 rpm for 10 min. The first clear solution was kept as a seawater matrix for rare earth elements measurements. The following step was repeated three times with MilliQ rinse in between each step. The MilliQ after every rinse was decanted. Subsequently, all precipitates were dissolved in 1 ml of concentrated HCl and transferred into 7 ml vials and evaporated to dryness on the hotplate under 100 °C. Afterwards 400 µl of aqua regia (300 µl of HCl + 100 µl of $HNO_3$) was added to every sample and left to reflux over night under 120 °C, followed by drying. Before loading onto the columns, all samples were redissolved again in 1 ml of 1 M HCl and evaporated to dryness again and redissolved in loading solution of 0.5 ml of 1 M HCl/0.05 M HF. Only one set of columns (cation) was used to extract all trace metals for ID measurements.

## 2.2 Sediment samples preparation and column chromatography

### 2.2.1 LEACHING OF MARINE SEDIMENT SAMPLES

For the extraction of Hf and Nd isotope signal from the authigenic fraction of ferromanganese coatings of marine sediments, approximately 2 grams of freeze-dried sediments were used per sample. The leaching process was following the standard procedure

from Gutjahr et al., (2007). As it was recently discovered that the decarbonation of the sediment with acetic acid-Na acetat (40 %) mixture can lead to alteration of the true seawater Nd signal in some sediments, a test run of 12 samples and their duplicates was carried out, with and without decarbonation step.

First, all sediment samples were rinsed with 20 ml of de-ionised MilliQ (Ω = 18.2) water, shaken for 30 min in the shaker at 125 rpm and centrifuged for 20 minutes at 4500 rpm. The MilliQ was subsequently decanted and the step repeated twice. First test run of 12 samples was decarbonated with acetic acid-Na acetate mixture for two and a half hours on the shaker and then centrifuged for 30 min, the solution was decanted. Subsequently, the first set of samples was shaken over night in a mixture of 10 ml of MilliQ with 10 ml acetic acid-Na acetate, centrifuged for 30 minutes and the supernatant decanted. Afterwards all samples were rinsed with MilliQ, repeated twice. For the second test run, the decarbonation step was omitted. In the next step, all samples were leached with a mixture of 10 % hydroxylamin leach solution. As hafnium tends to readsorb during the leaching procedure, instead of MilliQ a solution of 0.03 M EDTA was used. All samples were leached in 22.5 ml of EDTA mixed with 2.5 ml of leaching solution (0.005 M hydroxylamin hydrochloride, 1.5 % acetic acid, 0.03 M EDTA-Na) buffered to a pH = 4 with NaOH and shook for one hour at 125 rpm, then centrifuged for 30 minutes at 4500rpm. The supernatants were pipetted off into 30 ml teflon vials and evaporated to dryness in the clean laboratory on the hotplates under 100 °C. Sediments were rinsed with MilliQ as in the step 1 and stored for further total dissolution procedure. The final analysis showed that in the Labrador Sea decarbanation step could lead to Nd isotope signature alteration and was omitted from the following analysis.

### 2.2.2 TOTAL DISSOLUTION PROCEDURE OF THE DETRITAL FRACTION

Prior to the total dissolution procedure, sediment samples after leaching were additionally leached for 6.5 hours with 10 % hydroxylamin leaching solution to make sure that all ferromanganese coatings have been removed. After the second leaching step, samples were rinsed with de-ionised MilliQ (twice), centrifuged and excess water was decanted. Afterwards samples were freeze-dried and ground in a mortar. About 100 - 150 mg of the freeze-dried sediment was used for every sample. The procedure was done following steps presented in table 4 (Bayon et al., 2002).

| Step | Remarks |
|---|---|
| 2 ml $H_2O_2$ (30 %)<br>10 ml MQ<br>loose vials, over the weekend<br>dry down at 100 °C | To destroy any organics present in the sediment samples |
| 3 ml conc. HCl<br>1ml conc. $HNO_3$<br>reflux overnight at 140 °C<br>dry down at 140 °C | To destroy any organics present in the sediment samples |
| 1 ml conc. $HNO_3$<br>2 ml conc. HF<br>Reflux over night at 140 °C<br>Dry down at 140 °C | To dissolve the silicates<br><br><br>To remove the silicates |
| 2 ml conc. $HNO_3$<br>1 ml conc. HF<br>0.5 ml $HClO_4$<br>Reflux over night at 140 °C<br>Dry down over night 180-190 °C | To destroy the refractory minerals and organics |
| 2 ml conc. $HNO_3$<br>4 ml conc. HF<br>High pressure digestion bombs over 4-5 nights<br>Dry down at 140 °C | Dissolve refractory minerals |
| 1 ml $HClO_4$<br>2 ml $HNO_3$<br>Dry down at 180-190 °C | Destroy fluorides<br><br>Remove perchloric acid |
| 2 ml conc. $HNO_3$<br>Dry down at 180-190 °C | Remove perchloric acid |
| 0.5 ml of $HClO_4$<br>Dry down at 180-190 °C<br>Repeat till all perchloric acid is gone (no fumes) | Remove the perchloric acid |
| 1 ml conc. HCl<br>Dry down at 100 °C | Change to $Cl^-$ form |
| Reflux in loading solution over night | |

**Table 4** Total dissolution procedure of the bulk sediment samples.

### 2.2.3 COLUMN CHROMATOGRAPHY

After the supernatant collected from the leaching procedure was dried down on the hotplate it was redissolved in 2 ml of concentrated $HNO_3$ and evaporated to dryness again, this step was repeated twice. Afterwards samples were transferred into $Cl^-$ form by redissolving in 2 ml of concentrated HCl. To make sure that no traces of organic were left in the samples, 100 µl of $H_2O_2$ was added to every sample and dried down. If the sample turned black, additional 100 µl of $H_2O_2$ was added to the sample. If the samples were still turning

black during the addition of peroxide, they were additionally treated with 1.5 ml of aqua regia and left to reflux over night on the hotplate at 120 °C and subsequently dried down, followed by redissolution in 1 ml of concentrated HCl and evaporation to dryness. Finally, samples were dissolved in 2 ml of loading solution 1 M HCl/0.05 M HF and refluxed for at least a few hours. After that sample solution was transferred into 1.5 ml safe-lock tubes and centrifuged at 14000 U/min before loading onto cation columns filled with AG50W-8 resin, mesh size 200-400 µm. The Hf and REEs separation for sediment samples followed the same procedure as in table 1 for seawater samples. Hf and Nd separation and purification procedure with Eichrom LN-Spec columns were following the same steps as in the table 2 and table 3, respectively. For lead chemistry, a 300 µl aliquot from each sample was kept prior the cation column chemistry, dried down on the hotplate, redissolved and subsequently dried down three times in 500 µl of 2M HBr. Before lead column chemistry, a set of solutions was prepared fresh each time. Solution A, consisting of the mixture of 10 ml of 1 M $HNO_3$ + 2 ml of 2M HBr + 8 ml of MQ; solution B, consisting of the mixture of 10 ml of 1 M $HNO_3$ + 0.30 ml of 2 M HBr + 9.7 ml of MQ, and fresh mixture of 0.25 M $HNO_3$. The day lead column chemistry was carried out, dried samples were redissolved in freshly prepared 300 µl of solution A and refluxed before the column for at least half an hour. The column chemistry followed the steps presented in table 5.

| Volume | Acid | Stage |
|---|---|---|
| Fill reservoir | 1 M $HNO_3$ | Clean the columns |
| Fill reservoir | MQ | Clean the columns |
| 1 ml | 0.25 M $HNO_3$ | Add immediately 100 µl of the resin |
| 1 ml | 0.25 M $HNO_3$ | Clean the resin |
| 1 ml | 0.25 M $HNO_3$ | Clean the resin |
| 100 µl | Solution A | Condition the resin |
| 100 µl | Solution A | Condition the resin |
| 300 µl | Solution A | Load the sample |
| 100 µl | Solution A | Elute the matrix |
| 100 µl | Solution A | Elute the matrix |
| 250 µl | Solution A | Elute the matrix |
| **200 µl** | **Solution B** | **Collect Pb** |
| **200 µl** | **Solution B** | **Collect Pb** |
| **300 µl** | **Solution B** | **Collect Pb** |
| **300 µl** | **Solution B** | **Collect Pb** |
| Backwash | MQ | Used resin to waste |
| Clean to waste | MQ | Clean columns to waste |
| store | 1 M HCl | Store the columns |

**Table 5** Lead column chemistry. AG1-X8 resin, dry mesh 100 - 200.

To prepare the samples for isotope composition measurements after the column separation, collected Hf, Nd and Pb cuts were dried down on the hotplate, redissolved in the mixture of 100 µl $H_2O_2$ + 100 µl $HNO_3$ and evaporated to dryness. Subsequently, the Hf cut was redissolved in 1 ml of 0.5 M $HNO_3$/0.1 M HF mixture and Nd and Pb cuts were redissolved in 1 ml of 2 % $HNO_3$.

## 2.3 FORAMINIFERA ANALYSIS

In order to establish whether the Nd isotope signature extracted from the ferromanganese coatings of marine sediments truly reflects the seawater signal, these data were compared with Nd isotope signature from reductively cleaned planktonic foraminifera.

The bulk freeze-dried sediment samples were washed out through a sieve (< 64 µm) and what was left on the sieve collected into the ceramic jar and dried in the oven over night. After the samples were dried, all planktonic and benthic foraminifera presented in the samples were picked for Nd isotope analysis. The foraminifera were crushed between two glass plates until all chambers are opened. Crushed samples were transferred into 1.5 ml safe-lock tubes and ultrasonicated twice with 1 ml MilliQ, one time with 1 ml of ethanol and three times with 1 ml MilliQ, after each sonication the rinsed solution was decanted. To dissolve all the shells in the sample, 500 µl MilliQ was added to every sample and mixed with 1 M acetic acid (suprapure) in 100 µl aliquots, added only after the reaction was complete. For complete dissolution of all foraminifera shells in the samples, on average 300-400 µl of 1 M acetic acid were used. After the dissolution, samples were centrifuged at 14000 U/min and transferred into 7 ml Teflon vials and dried down under 110 °C on the hotplate. Subsequently, they were redissolved in 0.5 ml of 6 M HCl and dried down again. This step was repeated twice. Afterward, all samples were redissolved in 0.5 ml of 1 M HCl for cation column chemistry. Cation columns procedure followed the steps presented in table 6.

| Volume | Acid | Stage |
|---|---|---|
| 8 ml | 6 M HCl | Pre-clean |
| 0.5 ml | 1 M HCl | Pre-condition |
| 1 ml | 1 M HCl | Pre-condition |
| **0.5 ml** | **1 M HCl** | **Load the sample** |
| 3*0.6 ml | 1 M HCl | Wash in |
| 10 ml | 3 M HCl | Elute Ca and Sr |
| 2*1 ml | MQ | Change acid |
| 8 ml | 2.5 M HNO3 | Elute Ba |
| **6 ml** | **6 M HNO3** | **Collect REE** |
| 6 ml | 6 M HNO3 | Clean |
| 2*1 ml | MQ | Change acid |
| 1 ml | 1 M HCl | store |

**Table 6** Cation column chemistry for separation of REE and Sr in foraminifera samples. AG50W-X12 resin, volume 0.8 ml, dry mesh 200-400.

After the REE cuts were collected, all samples were dried down on the hotplate and redissolved in 0.5 ml of 6 M HCl, followed by evaporation to dryness. The step was repeated two times. Afterwards, all samples were dissolved in 0.5 ml of 0.1 M HCl and refluxed before loading onto Eichrom LN-Spec columns for Nd separation. Nd separation procedure followed the steps presented in table 7.

| Volume | Acid | Stage |
|---|---|---|
| 8 ml | 6 M HCl | Pre-clean |
| 0.5 ml | 0.1 M HCl | Pre-condition |
| 1 ml | 0.1 M HCl | Pre-condition |
| **0.5 ml** | **0.1 M HCl** | **Load the sample** |
| 0.5 ml | 0.1 M HCl | Wash in |
| 10 ml | 0.25 M HCl | Elute LREE |
| 2 | 0.3 M HCl | Elute |
| **6 ml** | **0.3 M HCl** | **Collect Nd** |
| 8 ml | 6 M HCl | Clean |
| 1 + 1 ml | 0.3 M HCl | Pass and store |

**Table 7** Eichrom LN-Spec column chemistry for Nd separation, resin volume 3.14 ml, bead size 50 - 100 µm.

To prepare the samples for isotope composition measurements after the column separation Nd cuts were dried down on the hotplate and redissolved in the mixture of 100 µl $H_2O_2$ + 100 µl $HNO_3$ and evaporated to dryness. Subsequently all samples were redissolved in 1 ml of 2 % $HNO_3$.

## 2.4 MASS SPECTROMETRY MEASUREMENT

### 2.4.1 ISOTOPIC COMPOSITION MEASUREMENTS

Seawater samples for Nd, Nd isotope composition of foraminifera were measured on a Thermo Finnigan Neptune Plus MC-ICP-MS at the Max Planck Research Group for Marine Isotope Geochemistry in Oldenburg, Germany. The details of the measurement procedure of seawater samples are described in chapter 3. The measurement procedure of Nd isotope composition of foraminifera was carried out similarly to the seawater samples using the same settings and similar concentrations. Seawater Hf was measured on a Thermo Neptune Plus MC-ICP-MS at ETH Zurich yielding total Hf ion beams of ≥ 1.1 V/ppb ($10^{11}$ Ω resistor). The procedure is described in more detail in chapter 3.

Hf, Nd and Pb isotope ratios in marine sediment samples were carried out on the MC-ICP-MS at GEOMAR, Kiel. Prior to isotope composition measurements, the concentrations of all samples were tested and calculated accordingly, to bring all samples and standards to similar beam intensities to more stable measurements. Column chemistry separation allowed to get from 400 to 1300 ng/g Nd in sediment samples. Samples were run at concentration of 60 ppb and 100 ppb, bracketed by a set of JNdi-1 and SPEX standards after each three samples. Neodymium isotopic compositions were corrected for instrumental mass bias to $^{146}Nd/^{144}Nd = 0.7219$, applying an exponential mass fractionation law. All $^{143}Nd/^{144}Nd$ ratios were normalized to the accepted JNdi-1 standard value of 0.512115 (Tanaka et al., 2000). The external reproducibility varied from 0.2 to 0.5, with one exception were 2 S.D = 0.8 (one run). The average long term reproducibility was 2 S.D. = 0.41 over the course of three years. All blanks (n = 5) measured were less than 1 ng/g and considered negligible.

After column chemistry, the average concentration of Hf in sediment samples was low, between 5 ng/g and 80 ng/g, most likely as a consequence of omitting the decarbonation step. Hf isotope composition measurements of sediment samples with concentrations higher than 20 ppb were carried out on the MC-ICP-MS at GEOMAR, Kiel. All samples with concentrations lower than 20 ppb were measured on Thermo Finnigan Neptune Plus MC-ICP-MS at GEOMAR, Kiel. During the measurements on ICP-MC-MS, samples were run at concentrations of 30 ppb and 50 ppb (TD), bracketed by a set of JMC475 and Certipur standards after each three samples. External reproducibility varied between 0.3 and 0.7, with one exception during one run 2 S.D. = 1.8. Long term external reproducibility is 2 S.D. = 0.7 over the course of three years. Measured Hf isotope compositions were corrected for instrumental mass bias to $^{179}Hf/^{177}Hf$ of 0.7325 applying an exponential mass fractionation law. All $^{176}Hf/^{177}Hf$ ratios were normalized to the accepted JMC475 standard value of 0.28216 (Nowell et al., 1998). Procedural blanks were less than 1 ng/g (n = 4), with exception of one which was 5 ng/g and were considered negligible. On the Neptune Plus MC-ICP-MS Hf samples were generally run at concentrations of 10 ppb, bracketed by a pair of JMC475 and Certipur standards after each three samples. The external reproducibility was 2 S.D. = 0.3 based on Certipur standards.

Lead isotope composition measurements were carried on ICP-MC MS at GEOMAR, Kiel. The average concentration of Pb in the samples varied between 100 ng/g in total dissolution samples up to 1200 ng/g in some of the sediment samples. All samples were run at concentrations of 50 ppb. As lead has no stable isotopes to estimate the stability and reproducibility of the measurements each sample was bracketed by a pair of NBS981 and

SCP standards. All Pb ratios were normalized to the accepted values of NBS981 of 36.7219; 15.4963; 16.9405; 2.1677; 0.9147 for $^{208}Pb/^{204}Pb$, $^{207}Pb/^{204}Pb$, $^{206}Pb/^{204}Pb$, $^{208}Pb/^{206}Pb$ and $^{207}Pb/^{206}Pb$ ratios respectively. Blanks were on average less than 1 ng/g, with the exception of one = 28 ng/g, and considered negligible.

With each batch of samples, a reference material was analyzed (homogenized sediment sample), 2 S.D for Nd was ~ 0.3 (n = 4), and 2 S.D. (n = 4) for Pb was between 0.3 and 0.1 for different isotope ratios.

### 2.4.2 ISOTOPE DILUTION MEASUREMENTS

Isotope dilution measurements of Hf and Nd concentrations were carried out on the Nu Plasma MC-ICP-MS at GEOMAR, Kiel. The main principles, error estimations and calculations are presented in details in a publication by Stichel et al., (2010) and will only be discussed briefly here.

During the measurements, the external reproducibility was monitored based on the set of standards JNdi-1 as international standard, and SPEX as a laboratory standard of similar beam intensities to the samples, that are generally measured after each three samples. For Nd measurements, a Sm beam is substracted from the beam of $^{144}Nd$ and a mass fractionation law is subsequently applied using $^{146}Nd/^{144}Nd= 0.7219$ to calculate $^{143}Nd/^{144}Nd$. To estimate matrix effect, $^{138}Ba$ is closely monitored through each run. As all samples are only roughly corrected for $^{147}Sm$ interference, its presence in the sample most be as minimum as possible. $^{143}Nd/^{144}Nd$ were normalized to JNdi-1 = 0.512115 (Tanaka et al., 2000).

Hafnium isotope dilution measurements were corrected for mass fractionation based on $^{179}Hf/^{177}Hf= 0.7325$. $^{176}Yb$ beam was calculated based on the beam intensities of $^{172}Yb$ applying the mass fractionation law. During each run a set of international laboratory standards JMC475 and internal laboratory standard CertiPur were run in between each three samples. $^{176}Hf/^{177}Hf$ were normalized to JMC475 = 0.282160 (Nowell et al., 1998).

### 2.4.3 REE CONCENTRATION MEASUREMENTS

Rare Earth Element (REE) concentrations were measured on 8ml aliquots of filtered and acidified seawater, which was kept prior to the addition of $FeCl_3$ solution, using an online preconcentration technique (OP) ICP-MS at GEOMAR in combination with an automated "SeaFast" system (Elemental Scientific Inc.) coupled to an Agilent 7500ce ICP-MS (Hathorne et al., 2012). During the measurements, samples are pumped with a peristaltic pump through a column with ethylenediaminetriacetic acid and iminodiacetic acid resin (volume 200 µl), in

order to preconcentrate REEs and other metals and wash out alkali and alkaline cations. The actual volume of the sample loop is about 4.2 ml, so to make sure the whole column is filled with acidified and filtered seawater about 8 ml of sample is used. During the pre-cleaning, the column is sustained at pH ≈ 9 by a continuous flow of ammonium acetate buffer solution. As the sample is loaded onto the column it is flushed for 10 minutes with buffer solution to get rid of alkali and alkaline earth elements. After the matrix has been removed, the pre-concentrated seawater sample is eluted into the ICP-MS for measurements. To check that the elution procedure worked properly, an indium (In) spike was added prior the measurements to every sample in a known concentration. During the measurements, a set of standards (BATS, 15m; BATS, 2000m) was used to track the reproducibility of the data. "Empty seawater", from which all the REEs had been removed by Fe-co-precipitation, was used as a procedural blank, which was subtracted from the data. The values were normalized to Post Archean Australian Shale (PAAS; McLennan, 2001) and BATS, 15 m (van de Flierdt et al., 2012).

## 2.5 ALKENONE UNSATURATION RATIO ANALYSIS

### 2.5.1 ALKENONE EXTRACTION AND SEPARATION.

About 2 grams of freeze-dried sediment material was used for every sample. Before the alkenone extraction all samples were gently ground in an agrar mortar for homogenization and then placed into metal cells and covered to the top with pre-cleaned sand. Prior to the extraction 50 µl of internal standard (hexatriacontane of know concentration 12.3 $mg.l^{-1}$) was added to every sample to trace the recovery through the whole procedure. As a procedural blank, a sample of only pre-cleaned sand was used, which was treated as a sample with each batch. The procedural blanks were low and considered negligible. Additionally, a homogenized sediment sample was run with each batch as a reference material.

A mixture of methylene chloride and methanol (9:1v/v) was used as an extraction solution. All samples were loaded into an automated solvent extraction system (ASE), which was run over 24 hour period at 1000 psi pressure and 100 °C with five 5 minute static phases. After the procedure, the extracted solutions were dried down in a Turbo-vap system to get rid of excess solvent, and redissolved in 0.5 M KOH:MeOH mixture and placed on the hotplate under 80 degrees for 2 hours, then the amount of the solvent was decreased to 5% of the total volume. Alkenones were extracted from the solvent 3 times with hexane and dried down before column separation. Dry samples were transferred with hexane to a liquid state and alkenone fraction was isolated by silica gel chromatography and eluted with DCM:Hexane

(2:1) mixture, the second fraction was isolated with methanol. Finally, samples were dried down under a nitrogen gas stream and redissolved in 50 µl of hexane for measurements.

### 2.5.2 GC MEASUREMENTS.

To be able to measure the alkenone concentration in marine sediments, a gas chromatographer is used, coupled to one of the several detectors, which allow the separation of alkenones from their lipid matrix. Alkenones have high molecular weights and high boiling points, which defines the necessity of long chromatographic columns and slow temperature programs to be used during the measurements. Alkenone measurements in this study were carried out on GC with Flame Ionization Detector (FID), Agilent, model 6890 with CP-Sil 5CBH column 60 meters long. Liquid hydrogen was used as a carrier gas.

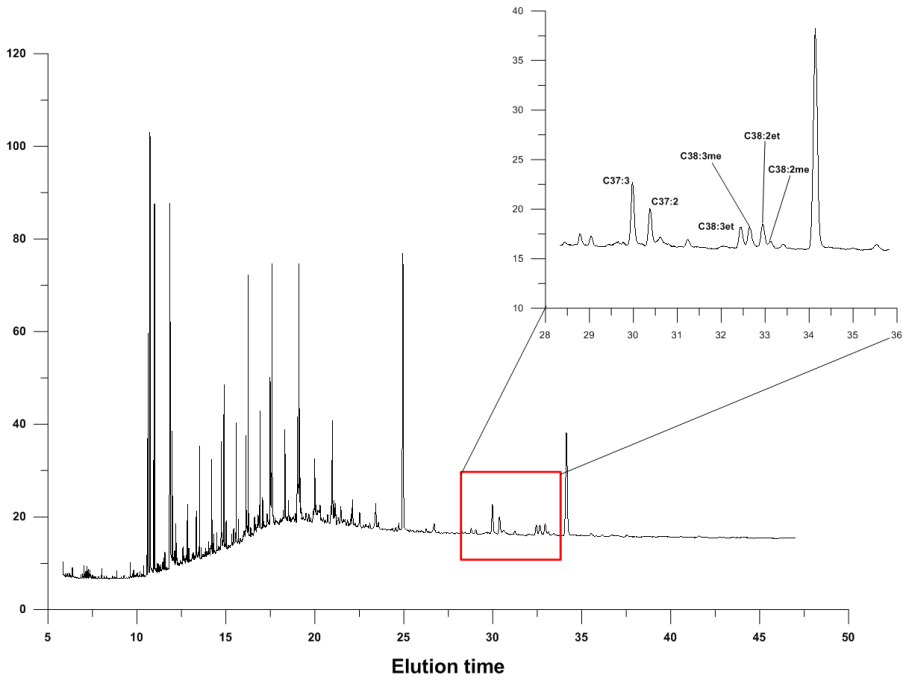


**Fig. 4** Example of Gas Chromatogram from one of the samples (HU84-045-021_1 cm).

Alkenones are identified by FID based on their elution times. As the compounds that elute at the same time as alkenones cannot be separated from the signals of interest, the high quality of chromatographic separation is of great importance. Internal standards and a strain of E. huxleyi CCMP1742 were run together with all samples for recovery rate assessment and for precise retention times, respectively. During the measurements, peak areas of $C_{37:2}$; $C_{37:3}$; $C_{37:4}$ and $C_{38:2Me}$; $C_{38:Et}$; $C_{38:3Et}$; $C_{38:Me}$; $C_{38:3ee}$ were defined. After the measurements, all samples were dried down under the nitrogen flow and stored in a freezer.

## REFERENCE LIST


Bayon, G., German, C. R., Boella, R. M., Milton, J. A., Taylor, R. N., and Nesbitt, R. W. (2002) An improved method for extracting marine sediment fractions and its application to Sr and Nd isotopic analysis. *Chemical Geology* **187**, 179-199.

Münker, C., Weyer, S., Scherer, E., and Mezger, K. (2001) Separation of high field strength elements (Nb, Ta, Zr, Hf) and Lu from rock samples for MC-ICPMS measurements. *Geochemistry Geophysics Geosystems* **2**, doi: 10.1029/2001GC000183.

Nowell, G. M., Kempton, P. D., Noble, S. R., Fitton, J. G., Saunders, A. D., Mahoney, J. J., and Taylor, R. N. (1998) High precision Hf isotope measurements of MORB and OIB by thermal ionisation mass spectrometry: insights into the depleted mantle. *Chemical Geology* **149**, 211-233.

Pin, C. and Zalduegui, J. F. S. (1997) Sequential separation of light rare-earth elements, thorium and uranium by miniaturized extraction chromatography: Application to isotopic analyses of silicate rocks. *Anal Chim Acta* **339**, 79-89.

Rickli, J., Frank, M., and Halliday, A. N. (2009) The hafnium-neodymium isotopic composition of Atlantic seawater. *Earth and Planetary Science Letters* **280**, 118-127.

Spielhagen, R. F., Bonani, G., Eisenhauer, A., Frank, M., Frederichs, T., Kassens, H., Kubik, P. W., Mangini, A., NorgaardPedersen, N., Nowaczyk, N. R., Schaper, S., Stein, R., Thiede, J., Tiedemann, R., and Wahsner, M. (1997) Arctic Ocean evidence for late Quaternary initiation of northern Eurasian ice sheets. *Geology* **25**, 783-786.

Stichel, T. (2010) Tracing water masses and continental weathering by neodymium and hafnium isotopes in the Atlantic sector of the Southern Ocean, University of Kiel.

Tanaka, T., Togashi, S., Kamioka, H., Amakawa, H., Kagami, H., Hamamoto, T., Yuhara, M., Orihashi, Y., Yoneda, S., Shimizu, H., Kunimaru, T., Takahashi, K., Yanagi, T., Nakano, T., Fujimaki, H., Shinjo, R., Asahara, Y., Tanimizu, M., and Dragusanu, C. (2000) JNdi-1: a neodymium isotopic reference in consistency with LaJolla neodymium. *Chemical Geology* **168**, 279-281.

# CHAPTER 3.

# WATER MASS CIRCULATION AND WEATHERING INPUTS IN THE LABRADOR SEA BASED ON COUPLED HF-ND ISOTOPE COMPOSITIONS AND RARE EARTH ELEMENT DISTRIBUTIONS.

Submitted as: Filippova A., Frank M., Kienast M., Rickli J., Hathorne E., Yashayaev I.M., Pahnke K. (2016) Water mass circulation and weathering inputs in the Labrador Sea based on coupled Hf-Nd isotope compositions and rare earth element distributions. Geochimica et Cosmochimica Acta.

## ABSTRACT.

The Labrador Sea is one of the key areas for deep water formation driving the Atlantic thermohaline circulation and thus plays an important role in Northern Hemisphere climatic fluctuations. In order to better constrain the overturning processes and the origins of the distinct water masses, combined dissolved Hf-Nd isotopic compositions and Rare Earth Element (REE) distribution patterns were obtained from four water depth profiles along a section across the Labrador Sea. These were complemented by one surface sample off the southern tip of Greenland, three shallow water samples off the coast of Newfoundland, and two deep water samples off Nova Scotia.

Although light REEs are markedly enriched in the surface waters off the coast of Newfoundland compared to north Atlantic waters, the REE concentration profiles are essentially invariant throughout the water column across the Labrador Sea. The hafnium concentrations of surface waters exhibit a narrow range between 0.6 and 1 pmol/kg but are not significantly higher than at depth.

Neodymium isotope signatures (εNd) vary from unradiogenic values between -16.8 and -14.9 at the surface to more radiogenic values near -11.0 at the bottom of the Labrador Sea mainly reflecting the advection of the Denmark Strait Overflow Water and North East Atlantic Deep Water, the signatures of which are influenced by weathering contributions from Icelandic basalts. Unlike Nd, water column radiogenic Hf isotope signatures (εHf) are more variable representing diverse weathering inputs from the surrounding landmasses. The least radiogenic seawater εHf signatures (up to -11.7) are found in surface waters close to Greenland and near the Canadian margin. This reflects the influence of recirculating Irminger current waters, which are affected by highly unradiogenic inputs from Greenland. A three to four εHf unit difference is observed between Denmark Strait Overflow Water (εHf ~ -4) and North East Atlantic Deep Water (εHf ~ -0.1), although their source waters have essentially the same εNd signature. This most likely reflects different weathering signals of hafnium delivered to Denmark Strait Overflow Water and North East Atlantic Deep Water (incongruent weathering of old rocks from Greenland versus basaltic rocks from Iceland). In addition, the εHf data resolve two layers within the main body of Labrador Sea Water not visible in the εNd distribution, which are shallow Labrador Sea Water (εHf ~ -2) and deep Labrador Sea Water (εHf ~ -4.5). The latter layer was formed between the late 1980's and mid 1990's during the last cold state of the Labrador Sea and underwent substantial modification since its formation through the admixture of Irminger Water, Iceland Slope Water and North East Atlantic Deep Water, which is reflected in its less radiogenic εHf signature. The overall

behavior of Hf in the water column suggests its higher sensitivity to local changes in weathering inputs on annual to decadal timescales. Although application of Hf isotopes as a tracer for global water mass mixing is complicated by their susceptibility to incongruent weathering inputs they are a promising tracer of local processes in restricted basins such as the Labrador Sea.

## 3.2 INTRODUCTION

Combined radiogenic Hf and Nd isotope compositions are a powerful tool to trace present and past ocean circulation and changes in weathering inputs (Bayon et al., 2006, 2008; Godfrey et al., 2009; Rickli et al., 2009, 2010; Chen et al., 2012; Stichel et al., 2012 a,b) but the exact mechanisms controlling their behavior and distribution in seawater, in particular those of Hf isotopes, are still not well constrained. Due to very small differences in the abundance of the radiogenic isotopes ($^{176}$Hf, $^{143}$Nd), the hafnium and neodymium isotope ratios of interest ($^{176}$Hf/$^{177}$Hf or $^{143}$Nd/$^{144}$Nd) are normally expressed in epsilon units as deviations from the Chondritic Uniform Reservoir corresponding to 0.512638 for Nd (Jacobsen and Wasserburg, 1980) and 0.282785 for Hf (Bouvier et al., 2008).

$$\varepsilon Hf \text{ or } \varepsilon Nd = [R_{SAMPLE}/R_{CHUR}-1]*10000,$$

where R reflects $^{176}$Hf/$^{177}$Hf and $^{143}$Nd/$^{144}$Nd, respectively.

The neodymium isotope composition in seawater has been studied for many decades (since the late 70's) resulting in a large data set of εNd signatures of different water masses in the global ocean ranging from -26.6 to +2.7 (Lacan et al., 2012, Grasse et al., 2012; Fröllje et al., 2016). Clear and well resolved εNd signatures of different water masses in the ocean reflect weathering inputs from rocks different in age and type in their source areas. The average residence time of Nd is on the order of 400 - 1000 years (Arsouze et al., 2009; Rempfer et al., 2011). Given that the Nd isotope signatures generally covary with salinity and nutrient content of deep waters in the modern ocean, they have also been used as a tracer for past water mass mixing and ocean circulation based on seawater-derived Nd isotope signatures extracted from sediments (cf. Frank, 2002; Goldstein and Hemming, 2003; Piotrowski et al., 2005). Neodymium isotopes are generally not influenced by fractionation during weathering processes (Goldstein et al., 1984) with evidence for limited incongruent weathering of Nd isotopes in some high latitude glacial weathering environments (Öhlander et al, 2000; Andersson et al., 2001).

In contrast, the applicability of Hf isotopes for the reconstruction of water mass mixing is complicated by a strong incongruent weathering effect on Hf isotopes resulting in a

relatively low variability between different water masses (van de Flierdt et al., 2007; Rickli et al., 2009; Stichel et al., 2012 a,b). However, seawater Hf isotopic compositions appear to be sensitive to changing continental weathering conditions implying that they are a valuable tool to monitor such changes (van de Flierdt et al., 2002). Early studies on the behavior of Hf and its isotopic distribution in seawater were based on data of slowly accumulating ferromanganese crusts and nodules (Albarède et al., 1998; David et al., 2001; van de Flierdt et al., 2002, 2004a, 2004b; Bau and Koschinsky, 2006). Direct measurements of the Hf isotope composition in seawater are, however, still scarce. Low concentrations of Hf (0.04 - 1.47 pmol $kg^{-1}$) (Godfrey et al., 1996; McKelvey and Orians, 1998) in comparison to Nd (15 - 45 pmol $kg^{-1}$) (Goldstein and Hemming, 2003) make these measurements analytically challenging. Isotopic compositions of Hf in seawater are available for the Atlantic Ocean (Rickli et al., 2009, 2010; Godfrey et al., 2009), the Southern Ocean (Stichel et al., 2012 a,b; Rickli et al., 2014), the Pacific Ocean (Zimmermann et al., 2009b), the Arctic Ocean (Zimmermann et al., 2009 a), and the central Baltic Sea (Chen et al., 2013). Global open ocean εHf signatures range from -5.7 to +10 (Chen et al., 2013; Godfrey et al., 2009; Rickli et al., 2009, 2010, 2014; Stichel et al., 2012 a,b; Zimmermann et al., 2009a,b) ; all εHf values are given relative to the new CHUR value of 0.282785 from Bouvier et al., 2008).

Hafnium and Nd isotope compositions are closely correlated in continental rocks and oceanic basalts, which is a consequence of their similar behavior during magmatic processes. This results in a well-constrained linear trend in a plot of εHf against εNd known as the "mantle-crust array" or "terrestrial array" (εHf = 1.55 * εNd + 1.21, Vervoort et al., 2011). Studies on ferromanganese crusts already suggested that seawater samples form a separate well-defined trend, which deviates from the terrestrial array and is referred to as the "seawater array" (εHf = 0.62 * εNd + 7.38, Albarède et al., 1998; Godfrey et al., 1997; David et al., 2001). For a given εNd the εHf values are more radiogenic than the terrestrial array. The direct measurements of seawater carried out over the last decade confirmed the existence of the offset seawater array. One of the possible explanations for this offset is the difference in the behavior of Nd and Hf isotopes during continental weathering. Large fractions of the rock-hosted unradiogenic Hf are trapped in zircons highly resistant to weathering. During weathering this leads to preferential release of highly radiogenic Hf from the non-zircon portion of the rocks to river waters and eventually to the ocean (Bayon et al., 2006; Rickli et al., 2013), which is referred to as the "zircon effect" (Patchett et al., 1984). However, isotopic mass balance calculations show that the seawater offset cannot be solely explained by the zircon effect (Chen et al., 2011). Instead, it has been proposed that weathering of minerals

with high Lu/Hf such as garnet, apatite and sphene also play an important role (Barford et al., 2003; Bayon et al., 2009; Godfrey et al., 2009; Chen et al., 2011).

Similar to Nd, the contribution of hydrothermal Hf to seawater is thought to be negligible based on the currently available data. This, however, still remains to be proven by direct measurements of Hf in hydrothermal solutions (van de Flierdt et al., 2004a,b; Bau and Koschinsky, 2006; Firdaus et al., 2011). Pettke et al., (2002) evaluated the role of aeolian inputs as a source of radiogenic Hf to seawater and found it to be of minor importance. Later Rickli et al., (2010) observed significant release of Hf from Saharan dust to surface waters of the Eastern Atlantic Ocean. Once dissolved in seawater, the estimates of the residence time of Hf show a large range between a few hundred and several thousand years (Godfrey et al., 1996; Firdaus et al., 2008; Rickli et al., 2009), which reflects the different approaches of estimation and our still limited understanding of Hf behavior in seawater.

Here we present the first systematic study of combined dissolved Hf and Nd isotope compositions and REE distribution patterns in the Labrador Sea. The aim of this study is to trace the mechanisms by which deep water masses obtain their radiogenic isotope signature and to evaluate the applicability of Hf isotopes as a tracer for water mass mixing on relatively short time and length scales in the light of the new data.

## 3.3 MATERIALS AND METHODS

### 3.3.1 SEAWATER

Twenty-six 20 L seawater samples were collected during an expedition in May 2013 on board of CCGS Hudson (Fig. 1, Table 1). Four full water depth profiles were collected across the Labrador Sea along the AR7W transect. Station 8.5 is the station closest to the coast with a water depth of 1702 m, located over the Labrador Sea slope and sampling the waters of the Labrador Current (LC, Table 2). The depth of the station is not sufficient to sample North East Atlantic Deep Water (NEADW) and Denmark Strait Overflow Water (DSOW). Stations 13.6 and 15.5 are located on the Labrador slope at a depth of about 3560 m, which is deep enough to sample all water masses present in the Labrador Sea. Station 17.5 is the deepest station sampled (~ 3620 m), located in the central part of the Labrador Sea. Each station was sampled at five different depths, covering the main water masses in the Labrador Sea. Station 28, located at the southern tip of Greenland, is a shallow station (~ 100 m). The station samples waters coming from the Arctic and waters of Irminger Sea origin. Shallow stations BIL02, BIL04 and BIL06 (depth less than 300 m) were sampled along the Belle Isle line, in close proximity to the coast of Newfoundland. Additionally, two deep water

samples HL11 and HL08, representing lower North Atlantic Deep Water (NADW), were collected along the extended Halifax line on the way out of the Labrador Sea, off the coast of Nova Scotia, above the Nova Scotian slope.

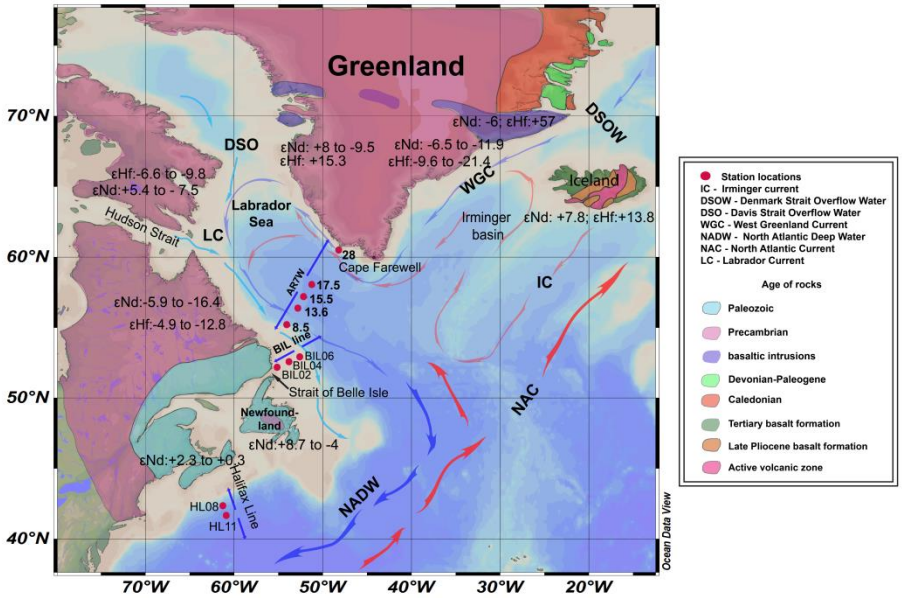


**Fig. 1** Schematic map of the study area. Blue arrows represent cold deep currents and red arrows denote warm surface currents. Red dots indicate the positions of the stations occupied during CCGS Hudson Cruise 2013. A schematic representation of the geology of the surrounding landmasses is shown and includes average εHf and εNd values of the rocks. For full ranges of the values, please\\ refer to original publications (Gerasimovsky et al., 1975; Zindler et al., 1982; Swinden et al., 1990; Stern et al., 1994; Camire et al., 1995; Skulski et al., 1996; La Fleche et al., 1998; Maclachlan et al., 1998; Nowell et al., 1998; Salter et al., 1998; Blichert-Toft et al., 1999; Minifie et al., 1999; Fitton et al., 2000; Goodenough et al., 2002; Stracke et al., 2003; West et al., 2004; Gaffney et al., 2007; Kitagawa et al., 2008; Tappe et al., 2008; Peate et al., 2008; Hoffmann et al., 2010; Jackson et al., 2010; Chekolt et al., 2011; Koornneef et al., 2012; Szilas et al., 2012;Rizo et al., 2013; Manning et al., 2014 ).

| Station | Depth of station [m] | Latitude [N] | Longitude [W] | Device | Depth [m] | Water mass | Salinity | T [°C] | σ [kg/m$^3$] | O2 [ml/l] | 143Nd/144Nd | εNd | Internal error 2 S.E.M. | External error 2 S.D. | 143Nd/144Nd | Second run εNd | External error 2 S.D. | Nd [pmol/kg] | 176Hf/177Hf | εHf | Internal error 2 S.E.M. | External error 2 S.D. | Hf [pmol/kg] |
|---|---|---|---|---|---|---|---|---|---|---|---|---|---|---|---|---|---|---|---|---|---|---|---|
| 8.5 | | 55.19 | -54.06 | CTD | 150 | Surface | 34.66 | 3.35 | 27.58 | 7.09 | 0.511811 ± 6 | -15.8 | 0.3 | 0.4 | | | | 20.2 | 0.282704 ± 16 | -2.9 | 0.6 | 0.5 | 0.70 |
| 8.5 | | 55.19 | -54.06 | CTD | 400 | IW | 34.89 | 3.94 | 27.71 | 6.50 | 0.511891 ± 18 | -14.0 | 0.3 | 0.4 | | | | 18.0 | 0.282551 ± 13 | -8.3 | 0.5 | 0.5 | 0.79 |
| 8.5 | 1702 | 55.19 | -54.06 | CTD | 750 | SLSW | 34.85 | 3.48 | 27.72 | 6.61 | 0.511885 ± 12 | -14.3 | 0.3 | 0.4 | | | | 18.6 | 0.282662 ± 11 | -4.3 | 0.4 | 0.5 | 0.67 |
| 8.5 | | 55.19 | -54.06 | CTD | 1050 | DLSW | 34.90 | 3.65 | 27.74 | 6.26 | 0.511908 ± 18 | -13.7 | 0.3 | 0.4 | | | | 18.0 | 0.282670 ± 18 | -4.1 | 0.6 | 0.6 | 0.83 |
| 8.5 | | 55.19 | -54.06 | CTD | 1500 | DLSW | 34.91 | 3.56 | 27.76 | 6.17 | 0.511911 ± 12 | -13.7 | 0.3 | 0.4 | | | | 18.0 | 0.282723 ± 19 | -2.2 | 0.7 | 0.6 | 1.03 |
| 13.6 | | 56.37 | -52.85 | CTD | 100 | Surface | 34.67 | 3.25 | 27.59 | 6.97 | 0.511775 ± 8 | -16.4 | 0.3 | 0.4 | | | | 19.6 | 0.282564 ± 11 | -7.8 | 0.4 | 0.6 | 1.02 |
| 13.6 | | 56.37 | -52.85 | CTD | 1000 | SLSW | 34.86 | 3.54 | 27.72 | 6.62 | 0.511850 ± 6 | -14.6 | 0.3 | 0.4 | | | | 18.4 | 0.282688 ± 12 | -3.4 | 0.4 | 0.6 | 0.73 |
| 13.6 | 3560 | 56.37 | -52.85 | CTD | 1700 | DLSW | 34.92 | 3.54 | 27.76 | 6.07 | 0.511889 ± 16 | -14.0 | 0.3 | 0.4 | | | | 18.0 | 0.282646 ± 13 | -4.9 | 0.5 | 0.6 | 0.80 |
| 13.6 | | 56.37 | -52.85 | CTD | 2400 | NEADW | 34.92 | 2.95 | 27.82 | 6.14 | 0.511965 ± 4 | -12.6 | 0.3 | 0.4 | | | | 16.7 | 0.282681 ± 16 | -3.7 | 0.6 | 0.6 | 1.13 |
| 13.6 | | 56.37 | -52.85 | CTD | 3360 | DSOW | 34.90 | 1.76 | 27.91 | 6.45 | 0.512044 ± 10 | -11.2 | 0.3 | 0.4 | | | | 18.5 | 0.282777 ± 21 | -0.3 | 0.7 | 0.6 | 0.96 |
| 15.5 | | 57.17 | -52.01 | CTD | 80 | Surface | 34.60 | 3.39 | 27.53 | 7.27 | 0.511803 ± 15 | -16.0 | 0.5 | 0.3 | 0.511639 ± 8 | -16.8* | 0.5 | 19.2 | 0.282737 ± 13 | -1.7 | 0.4 | 0.6 | 1.02 |
| 15.5 | | 57.17 | -52.01 | CTD | 1000 | SLSW | 34.87 | 3.60 | 27.72 | 6.48 | 0.511879 ± 20 | -14.3 | 0.4 | 0.4 | | | | 18.5 | 0.282731 ± 18 | -1.9 | 0.6 | 0.6 | 1.64 |
| 15.5 | 3574 | 57.17 | -52.01 | CTD | 1700 | DLSW | 34.92 | 3.48 | 27.77 | 6.08 | 0.511924 ± 8 | -13.7 | 0.3 | 0.4 | | | | 19.3 | 0.282711 ± 17 | -2.6 | 0.6 | 0.6 | 1.21 |
| 15.5 | | 57.17 | -52.01 | CTD | 2300 | NEADW | 34.92 | 3.00 | 27.82 | 6.14 | 0.511969 ± 12 | -12.7 | 0.3 | 0.4 | | | | 16.6 | 0.282779 ± 17 | -0.2 | 0.6 | 0.6 | 0.77 |
| 15.5 | | 57.17 | -52.01 | CTD | 3512 | DSOW | 34.90 | 1.49 | 27.93 | 6.57 | 0.512051 ± 20 | -11.0 | 0.4 | 0.4 | | | | 18.1 | 0.282653 ± 13 | -4.7 | 0.5 | 0.6 | 3.95 |
| 17.5 | | 58.01 | -51.10 | CTD | 80 | Surface | 34.79 | 3.96 | 27.62 | 7.15 | 0.511851 ± 26 | -14.9 | 0.5 | 0.4 | | | | 19.7 | 0.282738 ± 17 | -1.7 | 0.6 | 0.6 | 0.62 |
| 17.5 | | 58.01 | -51.10 | CTD | 1000 | SLSW | 34.85 | 3.48 | 27.71 | 6.61 | 0.511884 ± 13 | -14.4 | 0.5 | 0.3 | 0.511751 ± 9 | -14.5* | 0.5 | 18.6 | 0.282748 ± 15 | -1.3 | 0.5 | 0.6 | 0.73 |
| 17.5 | 3620 | 58.01 | -51.10 | CTD | 2000 | DLSW | 34.92 | 3.49 | 27.77 | 6.09 | 0.511886 ± 14 | -14.2 | 0.3 | 0.4 | | | | 19.7 | 0.282659 ± 18 | -4.5 | 0.6 | 0.6 | 0.79 |
| 17.5 | | 58.01 | -51.10 | CTD | 3000 | NEADW | 34.92 | 2.58 | 27.85 | 6.20 | 0.511996 ± 24 | -12.1 | 0.5 | 0.4 | | | | 15.2 | 0.282793 ± 13 | 0.3 | 0.4 | 0.6 | 0.73 |
| 17.5 | | 58.01 | -51.10 | CTD | 3670 | DSOW | 34.90 | 1.48 | 27.92 | 6.66 | 0.512024 ± 12 | -11.6 | 0.3 | 0.4 | | | | 16.8 | 0.282694 ± 16 | -3.2 | 0.6 | 0.6 | 0.83 |
| 28 | 107 | 60.59 | -48.23 | CTD | 100 | IW | 34.07 | 1.85 | 27.23 | 7.49 | 0.511839 ± 21 | -15.3 | 0.4 | 0.3 | 0.511699 ± 10 | -15.7* | 0.5 | 26.0 | 0.282455 ± 12 | -11.7 | 0.4 | 0.5 | 0.84 |
| BIL02 | 147 | 52.20 | -55.19 | CTD | 50 | Surface | 32.91 | -1.49 | 26.48 | 7.91 | 0.511311 ± 8 | -25.4 | 0.1 | 0.4 | 0.511177 ± 7 | -25.9 | 0.3 | 48.2 | 0.282524 ± 11 | -9.2 | 0.4 | 0.6 | 1.13 |
| BIL04 | 199 | 52.56 | -53.91 | CTD | 50 | Surface | 32.99 | -1.27 | 26.53 | 7.85 | 0.511317 ± 12 | -25.4 | 0.3 | 0.4 | 0.511214 ± 10 | -25.1 | 0.3 | 42.8 | 0.282652 ± 16 | -4.7 | 0.6 | 0.6 | 0.72 |
| BIL06 | 260 | 52.99 | -52.61 | CTD | 50 | Surface | 33.62 | 0.01 | 26.99 | 7.40 | 0.511426 ± 12 | -23.3 | 0.3 | 0.4 | 0.511287 ± 8 | -23.6 | 0.3 | 36.5 | 0.282729 ± 16 | -2.0 | 0.6 | 0.6 | 0.80 |
| HL08 | 3480 | 42.36 | -61.35 | CTD | 2500 | NEADW | 34.93 | 2.96 | 27.83 | 5.98 | 0.511971 ± 4 | -12.7 | 0.3 | 0.4 | | | | 19.1 | 0.282776 ± 11 | -0.3 | 0.4 | 0.6 | 0.84 |
| HL11 | 4515 | 41.78 | -60.91 | CTD | 3750 | DSOW | 34.89 | 1.99 | 27.89 | 6.03 | 0.511958 ± 6 | -12.9 | 0.3 | 0.4 | | | | 23.6 | 0.282609 ± 10 | -6.2 | 0.3 | 0.6 | 1.03 |

All $^{143}Nd/^{144}Nd$ ratios were normalized to the accepted JNdi-1 standard value of 0.512115 (Tanaka et al., 2000). All $^{176}Hf/^{177}Hf$ ratios were normalized to the accepted JMC475 standard value of 0.28216 (Nowell et al., 1998).

Hafnium and neodymium isotopic compositions are expressed in epsilon units as deviations from the Chrondritic Uniform Reservoir 0.512638 for Nd and 0.282785 for Hf ( Jacobsen and Wasserburg, 1980; Bouvier et al., 2008; respectively)

1. * indicates the samples, that were measured at GEOMAR, Kiel, Germany

**Table 1** Information about each station: longitude, latitude, temperature, salinity, oxygen and density, together with Hf and Nd isotope signatures and concentrations. Both internal and external errors of the measurements are shown.

### 3.3.2 HYDROGRAPHY

The Labrador Sea plays an important role in controlling the strength of the Atlantic thermohaline circulation (Azetsu-Scott et al., 2003). As one of the regions of deep water formation contributing to NADW and as the last recipient of warm saline waters advected from the tropical Atlantic, the Labrador Sea has had a significant impact on the global climate and its variability on seasonal to multi-millennial timescales (Yashayaev et al., 2015) and vice versa. Temperatures and salinities recorded in May 2013 in the Labrador Sea were higher than previously recorded between 1994 and 2008 suggesting that warming had already reached the deepest layers of the Labrador Sea (Yashayaev and Loder, 2008, 2016).

The Labrador Sea is characterized by a cyclonic circulation (Lazier and Wright, 1993) formed by the LC, the West Greenland Current (WGC) and its underlying current, extending to the Deep Western Boundary Current (DWBC) (Fig. 1) (Azetsu-Scott et al., 2003). This cyclonic circulation is bounded by the North Atlantic Current (NAC) on its southeastern margin (Azetsu-Scott et al., 2003; Yashayaev and Clark, 2006; Yashayaev et al., 2015).

Surface waters on the Labrador shelves and slopes down to a depth of about 200 m are relatively warm and fresh ($T > 2.8$ °C, $S < 34.8$) and are formed by mixing of WGC, LC, Irminger Current (IC), NAC and large fresh water inputs from land (Lazier et al., 2002). Spreading offshore, these waters create a distinct body between 100 and 200 m water depth (Lazier et al., 2002) and produce alongshore currents (Csanady, 1976, 1978; Smith and Schwing, 1990). The presence of LC waters, that can propagates up to depths of 1500 m (deep LC) on the southeastern Labrador shelf and slope was detected at the shallow stations (BIL02; BIL04; BIL06) along the Belle Isle line. The position of the stations lies in the pathway of cold and fresh waters, flowing from the Hudson Strait and Baffin Bay along the Canadian shelf, which is consistent with the cold temperatures and low salinities at stations BIL02, BIL04 ($T \sim -1.2$ °C to -1.4 °C; $S \sim 32.91$ to 32.99, Fig. 2). In addition, they may have been influenced by admixture of waters intruding from the coast through the Belle Isle Strait (Fig. 1). Waters sampled at station BIL06, located further offshore, are slightly warmer and saltier ($T \sim 0$ °C, $S \sim 33.62$).

The hydrographic properties of the water collected at station 28 on the Greenland shelf from a depth of 107 m (7.5 ml/l oxygen, 1.85 °C and a relatively low salinity of 34.07) are consistent with waters of polar origin transported by the WGC (continuation of the East Greenland current). However, temperature and salinity increase with depth at station 28, indicating the presence of waters originating from the Irminger Current (IC, Fig. 1), which flows in from the Irminger Sea and propagate as a tongue of saltier, warmer waters into the

Labrador Sea at depths of 300 - 800 m (Reynaud et al., 1995, Fogelqvist et al., 2003). Its deeper parts contain Iceland Slope Waters (ISW) (Yashayaev et al., 2008). The temperature and salinity signal of this current is also detectable at the northern and southern margin of the Labrador Sea but is more pronounced on the Greenland side because eddy formation and recirculation dilute these waters along their pathway around the Labrador Sea (Yashayaev and Clarke, 2006). At the southern margin of the Labrador Sea these waters have been sampled in the upper few hundred meters at station 8.5, at densities between 27.69 and 27.71 kg/m$^3$ (normalized to zero pressure at surface layer) (Fig. 2 B, D).

The penetration depths of newly formed Labrador Sea Water (LSW) (from 900 up to 2400 m) depend on the intensity of cold, northwesterly winds blowing from Canada over the surface of the Labrador Sea and on the severity of winters in previous years (Yashayaev and Clark, 2006). In addition, stratification of the affected water column before and at the time of each convective event also plays a role. The 2012/2013 wintertime convection of the Labrador Sea was moderately strong producing mixed layer depths varying between 1300 and 1500 m that were not uniformly distributed across the Labrador Sea. The presence of shallow LSW (SLSW) at all stations is clearly marked by salinities of 34.85 - 34.87 and temperatures around 3.6 °C (Fig. 2B), covering the density range from 27.71 to up to 27.725 kg/m$^3$. Oxygen concentrations of these waters are relatively high at 6.5 - 6.6 ml/l (Fig. 2D).

A gradual increase in salinities to up to 34.91 - 34.92 at all stations (Fig. 2B) reaching densities near 27.75 kg/m$^3$ (Fig. 2D) likely indicates the presence of old deep LSW (DLSW) produced between 1987 and 1994 during the most recent cold state of the Labrador Sea when deep convection reached down to 2400 m. In subsequent years, convection only reached to shallower depths, and this layer of higher density, salinity and temperature formed through admixture with IW and ISW, became isolated and by the time of sampling in 2013 had lost most of its volume (Yashayaev et al., 2008).

The relatively salty water mass below LSW reaching a density of 27.8 kg/m$^3$ recorded at stations 13.6, 15.5 and 17.5 is the North East Atlantic Deep Water (NEADW), the core of which is associated with a deep salinity maximum at 2500 - 3000 meters (S ~ 34.92, $\sigma$ ~ 27.85 - 27.87, oxygen concentrations of ~ 6.2 ml/l, Fig 2. B,D) (Yashayev, 2007). The sample from 2500 m water depth along the Halifax line (st. HL08) has temperature characteristics (T ~ 2.96 °C) similar to NEADW across the Labrador Sea, but a slightly higher salinity of 34.92 (Fig. 2 B,D).

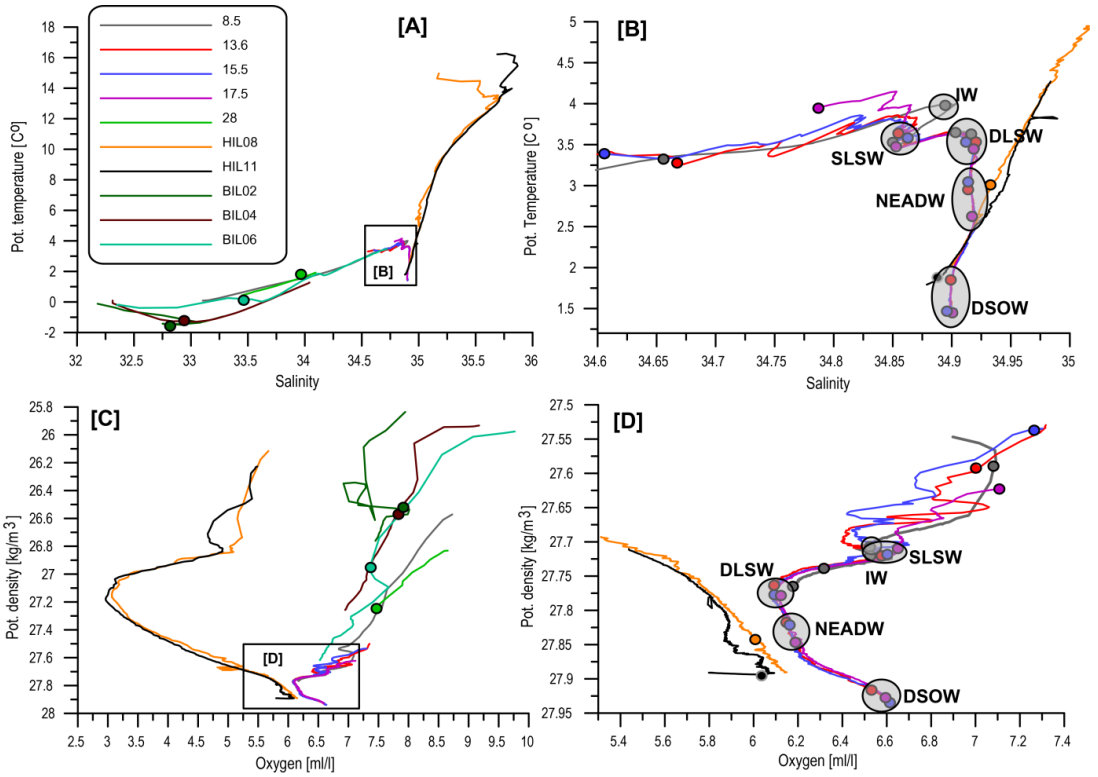


**Fig. 2** CTD data for all stations. A. Salinity vs. Temperature. B. Enlarged version of A for deep waters. C. Density vs. Oxygen concentration. D. Enlarged version of C for deep waters. Light grey circles denote the major prevailing water masses.

Denmark Strait Overflow Water (DSOW) is the densest water mass found in the Labrador Sea. It is noticeably colder, fresher and more oxygenated than NEADW (Yashayaev and Dickson, 2008). Its presence below NEADW is identified at stations 15.5 and 17.5 based on maximum oxygen concentrations ~ 6.7 ml/l at the bottom. These waters are denser than 27.9 kg/m$^3$, salinities range between 34.89 and 34.90 and the potential temperature is near 1.48 °C. The bottom sample at station 13.6 although falling within the same density and salinity range, has slightly higher potential temperature and lower oxygen concentration, suggesting that this sample does not represent pure DSOW. Similar characteristics are recorded along the Halifax line at st. HL11, where salinity is ~ 34.89 similar to an average value of 34.90 for DSOW along the AR7W transect (Fig. 2B) and temperature of ~ 1.99 °C, which is, however, warmer than in the Labrador Sea (1.48 °C).

The mixture of the deep water masses described above results in the formation of the core of NADW, which leaves the Labrador Sea in a southerly direction, ultimately occupying water depths between 1000 and 4000 meters (Schmitz, 1996).

### 3.3.3 METHODS

Seawater samples were collected in 10 L Niskin bottles attached to a CTD rosette and directly filtered through Acropac 0.45 µm filter cartridges into 20 L pre-cleaned cubitainers. Subsequently, all samples were acidified with distilled concentrated HCl to pH ≈ 2. A one liter aliquot from every sample was kept separate in polyethylene bottles after acidification for precise Nd and Hf concentration measurements by isotope dilution (Stichel et al., 2012a). The remaining water was further processed in the clean laboratory following established methods (Rickli et al., 2009; Stichel et al., 2012a). The trace metals were pre-concentrated by co-precipitation with a pre-cleaned Fe chloride solution. An ethyl ether step was applied to remove most of this iron in preparation for column chemistry. To separate Hf and Nd from the seawater matrix, three sets of ion exchange columns were used: cation columns with AG 50W-X8 resin (200 - 400 dry mesh), columns loaded with Eichrom Ln-Spec resin with a bead size of 50 - 100 µm for Nd purification and a third set of columns loaded with Eichrom Ln-Spec resin with a bead size of 100 - 150 µm for Hf purification (Pin and Zalduegui, 1997; Münker et al., 2001).

Most Nd isotope measurements were carried out on a Thermo Finnigan Neptune Plus MC-ICP-MS at the Max Planck Research Group for Marine Isotope Geochemistry in Oldenburg, Germany. Only samples with Nd concentrations higher than 40 ng in the resulting 1 ml solution after purification were measured on the Nu Plasma MC-ICP-MS at GEOMAR. Neodymium isotopic compositions were corrected for instrumental mass bias to $^{146}Nd/^{144}Nd$ = 0.7219 applying an exponential mass fractionation law. All $^{143}Nd/^{144}Nd$ ratios were normalized to the accepted JNdi-1 standard value of 0.512115 (Tanaka et al., 2000). The repeated measurement of one of the samples (n = 3) gave a 2 S.D. = 0.29. The external reproducibility on both instruments was between 0.3 and 0.4 (2 S.D.) based on repeated measurement of the JNdi-1 standard (n = 23) and an internal laboratory standard (n = 10) run at 30 ppb and 10 ppb at the GEOMAR and in Oldenburg, respectively. Internal measurement errors were smaller than the external errors for all samples with the exception of st. 17.5, 3000 m and st. 17.5, 80 m (0.5 εNd, 2 S.E.M.). The procedural blanks (for laboratory analysis) for Nd were below 2 % of the sample Nd content (~ 300 pg) and are considered negligible. Replicates measured on both mass spectrometers gave the same results within analytical errors (Table 2).

Given that 20 L of water were available for Hf isotopic analysis, sample amounts corresponded to 1.6 to 4.3 ng of Hf only. Hafnium isotope compositions were measured on a Thermo Neptune Plus MC-ICP-MS at ETH Zurich yielding total Hf ion beams of ≥ 1.1 V/ppb ($10^{11}$ Ω resistor). Measured Hf isotope compositions were corrected for instrumental mass

bias to $^{179}Hf/^{177}Hf$ of 0.7325 applying an exponential mass fractionation law. External reproducibility was estimated from repeated measurements of the JMC475 standard at a concentration of 5 ppb and corresponded to 0.6 εHf (2 S.D., n = 12, 20 and 22). Internal errors and beam sizes of the sample measurements were in most cases similar to the run standards (internal errors ranging between 0.4 and 0.6, 2 S.E.M.) indicating that the error estimate from standard measurements is applicable for most samples (Table 1). Procedural blanks were less than 3 % of the sample Hf contents (less than 28 pg) and are considered negligible.

Isotope dilution measurements of Hf and Nd concentrations were carried out on the Nu Plasma MC-ICP-MS at GEOMAR. Hafnium and Nd spike solutions, enriched in $^{178}Hf$, $^{149}Sm$ and $^{150}Nd$, were added to every sample gravimetrically. Neodymium and Hf preconcentration based on iron co-precipitation was applied and purification was achieved by a single step column separation (AG50W-X8, 200 - 400 dry mesh). A detailed description of the method and uncertainties is presented in Stichel et al. (2012a).

Rare Earth Element (REE) concentrations were measured on an 8 ml sample loop using an online preconcentration technique (OP) ICP-MS at GEOMAR employing an automated "SeaFast" system (Elemental Scientific Inc.) coupled to an Agilent 7500ce ICP-MS (Hathorne et al., 2012). During the measurements, reference seawater from the Bermuda Atlantic Time Series (BATS, 15 m; BATS, 2000 m, van de Flierdt et al., 2012) was used to track the reproducibility and accuracy of the data (Table 3.3). "Empty seawater", from which all the REEs had been removed by Fe-coprecipitation, was used as a procedural blank, which was subtracted from the data.

Neodymium concentrations were measured by OP-ICP-MS as well as isotope dilution. The paired t-test for dependent variables showed no difference between these two methods ($t(25) = 4.76$, $p = 0.0001$), as has been demonstrated previously (Hathorne et al., 2012). Further discussion of Nd concentrations in the context of Nd isotopes will utilize the more precise isotope dilution data.

| **Abbreviation** | **Full name** | Description |
|---|---|---|
| **NADW** | North Atlantic Deep Water | Represents the mixture of intermediate and deep waters formed within Arctic and subarctic |
| **WGC** | Western Greenland Current | Flows northward along the coast carrying water from Denmark Strait |
| **LC** | Labrador Current | Fresh-water-laden current that flows south along the Labrador coast, formed due to admixture of outflows from Hudson Strait , Davis Strait and the waters of Western Greenland Current |

| | | |
|---|---|---|
| **NAC** | North Atlantic Current | Originates in the Gulf Stream, flows north along the east side of Grand Banks, where it turns east and flows across the ocean |
| **IW/IC** | Irminger Current or Irminger Water | Counterclockwise flow of warm and salty water around the rim of the Labrador Sea, which originates in the Irminger Sea |
| **LSW** | Labrador Sea Water | Formed due to the admixture of warmer saltier water of tropical origin (North Atlantic Current, Irminger Water) with polar outflows and admixtures from the shelf and upper slope (Western Greenland Current and Labrador Current) |
| **DWBC** | Deep Western Boundary Current | Continuation of Deep North Boundary Current, formed due to admixture of Iceland Scotland Overflow Water and Denmark Strait Overflow Water, flowing southward to the Southern Ocean and incorporating the deep waters from the Labrador Sea |
| **SLSW** | Labrador Sea Water 2008 | Formed after 1994, when the convection was weaker |
| **DLSW** | Labrador Sea Water 1987-1994 | Remnants of the old Labrador Sea Water produced between 1987 and 1994 |
| **NEADW** | North Eastern Atlantic Deep Water | Formed by the admixture of Iceland Scotland Overflow Water, modified North Atlantic Water, Labrador Sea Water and Eastern Lower Deep Water |
| **ISOW** | Iceland Scotland Overflow Water | Dense water overflow coming from Norwegian Seas through the Faroe Bank Channel, admixed with Modified North Atlantic Water and Labrador Sea Water |
| **ISW** | Iceland Slope Waters | Formed through a mixing of the original ISOW with Atlantic thermocline water near the Faroes. Flows along the slopes of Iceland and Reykjanes Ridge, until it enters Irminger Sea. |
| **MNAW** | Modified North Atlantic Water | Originates from the North Atlantic Current |
| **ELDW** | Eastern Lower Deep Water | Derived from Antarctic Bottom Water and flows through the entire Atlantic Ocean until it enters the Subpolar North Atlantic region from the East within Deep Eastern Boundary Current off the European coast |
| **DSOW** | Denmark Strait Overflow Water | Enters the Labrador Sea at the base of the continental slope off Cape Farewell, Greenland as a part of Deep Western Boundary Current |
| **SPMW** | SubPolar Mode Waters | Formed due to mixing of the water masses in the Northern North Atlantic of subtropical and polar origin, occupies the upper 1000 m of the North Atlantic Subpolar Gyre |

Water mass definitions are based on: Kearns and Rossby, 1998; Lacan and Jeandel, 2004a,b; Lacan and Jeandel, 2005; Yashayaev and Clark, 2006; Straneo et al., 2008.

**Table 2** List of the abbreviations used in the text.

## 3.4 RESULTS

### 3.4.1 REE AND HF CONCENTRATIONS IN SEAWATER

The REE concentrations (OP-ICP-MS) in the surface waters of the Labrador Sea along the AR7W transect exhibit little variability but are slightly enriched in the light REEs (La - Nd) compared to the deeper waters (Fig. 3). Below the surface, rare earth element concentrations are invariable with depth with only two exceptions (Fig. 3). A marked increase in Gd concentration from 4.76 pmol/kg to 19.81 pmol/kg is observed in the deepest sample of st. 15.5 coincident with an increase of Yb from 5.16 pmol/kg up to 6.61 pmol/kg. Neodymium concentrations (ID) (Fig. 4A) in surface waters across the Labrador Sea (AR7W transect, Fig. 1) range from 19.2 pmol/kg at st. 15.5 to 20.2 pmol/kg at st. 8.5. Hafnium concentrations vary between 0.62 pmol/kg at st. 17.5 and 1.02 pmol/kg at st. 15.5 and st. 13.6 (Fig. 4B). Station 13.6 in general shows higher LREE concentration than other stations along the transect at corresponding depths. The surface water samples along the Belle Isle line from 50 meters depth collected north of Newfoundland (BIL02; BIL04; BIL06) have light and middle REE concentrations up to an order of magnitude higher than the surface waters across the Labrador Sea (AR7W transect, Fig. 3). Neodymium concentrations are about twice as high as in the open Labrador Sea ranging from 36 to 48 pmol/kg, whereas Hf concentrations are not elevated and range from 0.72 to 1.13 pmol/kg. At these stations, the Nd concentrations systematically decrease with distance from the shore (Fig. 4A) but no such trend is observed for the Hf concentrations (Fig. 4B). The surface sample collected in close proximity of the southern tip of Greenland (st. 28) exhibits lower REE concentrations than the surface samples collected north of Newfoundland, but still 10 to 60% higher than those collected along the AR7W transect for some of the REEs. Hafnium concentrations are similar in all surface samples. The deep water sample collected from the Halifax line off the coast of Nova Scotia (HL08, 2500 m) has REE and Nd (19.06 pmol/kg) concentrations similar to the corresponding depths along the AR7W transect. However, st. HL11, 3750 m has higher REE and Nd (23.63 pmol/kg) concentrations than observed at similar depths along the AR7W transect. Hafnium concentrations are similar to those along the transect at both stations.

| Station | Depth [m] | La [pmol/kg] | Ce [pmol/kg] | Pr [pmol/kg] | Nd [pmol/kg] | Nd (ID) [pmol/kg] | Sm [pmol/kg] | Eu [pmol/kg] | Gd [pmol/kg] | Tb [pmol/kg] | Dy [pmol/kg] | Ho [pmol/kg] | Er [pmol/kg] | Tm [pmol/kg] | Yb [pmol/kg] | Lu [pmol/kg] | La/Yb[a] | Ce/Ce*[b] |
|---|---|---|---|---|---|---|---|---|---|---|---|---|---|---|---|---|---|---|
| 8.5 | 150 | 29.7 | 11.3 | 5.42 | 22.7 | 20.2 | 4.17 | 0.96 | 5.90 | 0.85 | 6.04 | 1.64 | 5.11 | 0.72 | 4.96 | 0.83 | 0.35 | 0.20 |
| 8.5 | 400 | 26.3 | 6.44 | 4.53 | 18.4 | 18.0 | 3.79 | 0.92 | 4.71 | 0.84 | 5.82 | 1.53 | 4.92 | 0.82 | 4.78 | 0.81 | 0.33 | 0.13 |
| 8.5 | 750 | 27.7 | 6.91 | 4.40 | 19.9 | 18.6 | 3.71 | 0.77 | 4.92 | 0.84 | 6.01 | 1.59 | 5.52 | 0.77 | 4.41 | 0.80 | 0.37 | 0.14 |
| 8.5 | 1050 | 27.3 | 6.61 | 4.72 | 21.3 | 18.0 | 3.20 | 0.91 | 4.99 | 0.78 | 6.20 | 1.54 | 5.17 | 0.76 | 4.99 | 0.78 | 0.32 | 0.13 |
| 8.5 | 1500 | 25.7 | 5.28 | 4.35 | 19.2 | 18.0 | 3.56 | 0.91 | 4.28 | 0.77 | 5.74 | 1.60 | 5.23 | 0.77 | 4.81 | 0.82 | 0.32 | 0.11 |
| 13.6 | 100 | 32.8 | 12.6 | 5.69 | 23.0 | 19.6 | 4.00 | 0.95 | 5.71 | 0.88 | 6.20 | 1.64 | 5.69 | 0.84 | 4.74 | 0.89 | 0.41 | 0.21 |
| 13.6 | 1000 | 27.1 | 6.76 | 4.51 | 19.7 | 18.4 | 3.16 | 0.84 | 4.77 | 0.81 | 5.77 | 1.53 | 4.95 | 0.75 | 4.58 | 0.74 | 0.35 | 0.14 |
| 13.6 | 1700 | 26.6 | 6.21 | 4.64 | 18.4 | 18.0 | 3.88 | 0.88 | 5.21 | 0.76 | 6.11 | 1.60 | 5.48 | 0.84 | 4.75 | 0.80 | 0.33 | 0.13 |
| 13.6 | 2400 | 24.4 | 5.47 | 4.27 | 16.9 | 16.7 | 3.97 | 0.92 | 5.19 | 0.79 | 5.85 | 1.62 | 5.01 | 0.75 | 4.71 | 0.85 | 0.31 | 0.12 |
| 13.6 | 3360 | 26.2 | 7.22 | 4.63 | 20.0 | 18.5 | 4.01 | 0.89 | 5.89 | 0.84 | 5.76 | 1.58 | 5.09 | 0.77 | 4.81 | 0.81 | 0.32 | 0.15 |
| 15.5 | 80 | 29.5 | 10.8 | 5.12 | 20.9 | 19.2 | 3.78 | 0.88 | 4.77 | 0.73 | 5.55 | 1.42 | 4.94 | 0.75 | 4.31 | 0.70 | 0.41 | 0.20 |
| 15.5 | 1000 | 26.5 | 6.20 | 4.41 | 18.4 | 18.5 | 3.11 | 0.86 | 4.88 | 0.84 | 5.86 | 1.49 | 5.00 | 0.80 | 4.56 | 0.77 | 0.34 | 0.13 |
| 15.5 | 1700 | 24.6 | 4.79 | 4.30 | 18.6 | 19.3 | 3.49 | 0.81 | 4.74 | 0.75 | 5.99 | 1.72 | 5.24 | 0.83 | 4.82 | 0.80 | 0.30 | 0.11 |
| 15.5 | 2300 | 24.8 | 6.10 | 4.43 | 18.8 | 16.6 | 3.96 | 0.94 | 4.76 | 0.86 | 5.98 | 1.47 | 5.46 | 0.77 | 5.16 | 0.82 | 0.28 | 0.13 |
| 15.5 | 3512 | 26.3 | 6.50 | 4.43 | 19.4 | 18.1 | 3.97 | 1.04 | 19.8 | 0.74 | 6.55 | 1.65 | 5.30 | 0.79 | 6.61 | 0.86 | 0.24 | 0.14 |
| 17.5 | 80 | 26.7 | 10.6 | 4.76 | 19.5 | 19.7 | 3.36 | 0.82 | 4.48 | 0.81 | 5.87 | 1.51 | 4.71 | 0.75 | 4.34 | 0.77 | 0.36 | 0.21 |
| 17.5 | 1000 | 28.0 | 7.58 | 4.94 | 20.2 | 18.6 | 3.54 | 0.81 | 5.11 | 0.90 | 5.95 | 1.62 | 5.34 | 0.69 | 4.87 | 0.78 | 0.34 | 0.15 |
| 17.5 | 2000 | 27.2 | 8.45 | 4.49 | 19.1 | 19.7 | 3.52 | 0.78 | 5.04 | 0.80 | 5.94 | 1.62 | 5.30 | 0.75 | 5.00 | 0.82 | 0.32 | 0.17 |
| 17.5 | 3000 | 23.5 | 5.36 | 3.85 | 16.4 | 15.2 | 3.07 | 0.78 | 3.98 | 0.72 | 5.81 | 1.41 | 4.69 | 0.67 | 4.51 | 0.76 | 0.31 | 0.13 |
| 17.5 | 3670 | 25.2 | 6.22 | 3.98 | 17.4 | 16.8 | 3.16 | 0.72 | 4.92 | 0.78 | 5.01 | 1.56 | 4.70 | 0.69 | 4.75 | 0.78 | 0.31 | 0.14 |
| 28 | 100 | 36.3 | 18.6 | 6.23 | 24.9 | 26.0 | 5.00 | 1.21 | 6.21 | 0.97 | 6.80 | 1.65 | 6.01 | 0.87 | 5.17 | 0.86 | 0.42 | 0.28 |
| BIL02 | 50 | 82.9 | 40.0 | 12.8 | 52.6 | 48.2 | 7.08 | 1.64 | 8.70 | 1.35 | 9.12 | 2.25 | 6.84 | 1.03 | 6.52 | 1.13 | 0.75 | 0.26 |
| BIL04 | 50 | 77.1 | 35.1 | 11.5 | 44.9 | 42.8 | 6.95 | 1.41 | 8.58 | 1.21 | 7.86 | 1.99 | 6.79 | 1.01 | 6.25 | 0.91 | 0.73 | 0.27 |
| BIL06 | 50 | 63.3 | 28.2 | 10.1 | 40.6 | 36.5 | 6.65 | 1.34 | 7.68 | 1.19 | 8.59 | 2.12 | 6.26 | 0.92 | 6.36 | 1.12 | 0.59 | 0.25 |
| HL08 | 2500 | 26.9 | 6.89 | 4.64 | 20.1 | 19.1 | 3.83 | 0.99 | 4.84 | 0.88 | 5.96 | 1.64 | 5.19 | 0.78 | 4.81 | 0.83 | 0.33 | 0.14 |
| HL11 | 3750 | 34.5 | 9.58 | 5.93 | 25.1 | 23.6 | 5.23 | 1.16 | 6.04 | 0.95 | 6.44 | 1.77 | 5.82 | 0.83 | 5.61 | 0.87 | 0.36 | 0.15 |
| 2 S.D.*[e] | | 0.76 | 0.56 | 0.25 | 0.73 | | 0.38 | 0.06 | 0.5 | 0.12 | 0.43 | 0.14 | 0.34 | 0.09 | 0.38 | 0.08 | | |
| GEOTRACES BATS intercalibration | | | | | | | | | | | | | | | | | | |
| [e]BATS 15 m | | | | | | | | | | | | | | | | | | |
| average | n = 7 | 14.9 | 10.8 | 3.2 | 15.1 | | 3.29 | 0.79 | 4.72 | 0.82 | 5.98 | 1.56 | 4.99 | 0.68 | 4.10 | 0.67 | | |
| 2σ | | 0.76 | 0.56 | 0.25 | 0.73 | | 0.38 | 0.06 | 0.50 | 0.12 | 0.43 | 0.14 | 0.34 | 0.09 | 0.38 | 0.08 | | |
| [e]BATS 2000 m | | | | | | | | | | | | | | | | | | |
| average | n = 3 | 24.1 | 4.16 | 4.1 | 18.0 | | 3.09 | 0.87 | 4.79 | 0.79 | 5.72 | 1.54 | 5.10 | 0.76 | 4.75 | 0.84 | | |
| 2σ | | 0.41 | 0.08 | 0.17 | 1.34 | | 0.89 | 0.08 | 0.53 | 0.07 | 0.29 | 0.09 | 0.43 | 0.08 | 0.24 | 0.03 | | |
| [c]BATS 15 m | | | | | | | | | | | | | | | | | | |
| average | n = 17 | 14.7 | 12.0 | 3.12 | 14.1 | | 3.21 | 0.89 | 4.83 | 0.79 | 5.90 | 1.49 | 4.80 | 0.70 | 4.16 | 0.67 | | |
| 2σ | | 2.21 | 2.74 | 0.37 | 1.24 | | 0.36 | 0.11 | 0.55 | 0.08 | 0.52 | 0.13 | 0.42 | 0.07 | 0.51 | 0.09 | | |
| [d]BATS 2000 m | | | | | | | | | | | | | | | | | | |
| average | n = 17 | 23.6 | 5.12 | 4.03 | 17.3 | | 3.45 | 0.91 | 4.84 | 0.79 | 5.80 | 1.52 | 5.04 | 0.74 | 4.76 | 0.81 | | |
| 2σ | | 2.79 | 2.27 | 0.35 | 1.22 | | 0.34 | 0.10 | 0.53 | 0.08 | 0.38 | 0.09 | 0.25 | 0.05 | 0.25 | 0.04 | | |

a. Ce/Ce*=Ce/((La+Pr)/2), values used are normalized to PAAS
b. La/Yb=La/Yb, values used are normalized to PAAS
c. Uncertainties and average values from the study by van de Flierdt et al., 2012 for BATS 15 m
d. Uncertainties and average values from the study by van de Flierdt et al., 2012 for BATS 2000 m
e. Uncertainties of the REE measurement by OP-ICP MS based on the repeated measurement of BATS 15m, n=7 (van de Flierdt et al., 2012)

**Table 3** REE concentrations obtained by OP ICP-MS (pmol/kg) and Nd concentrations obtained via the isotope dilution method (pmol/kg). La/Yb ratio and Ce anomaly are also shown. Additionally, GEOTRACES BATS intercalibration results are included (van de Flierdt et al., 2012).

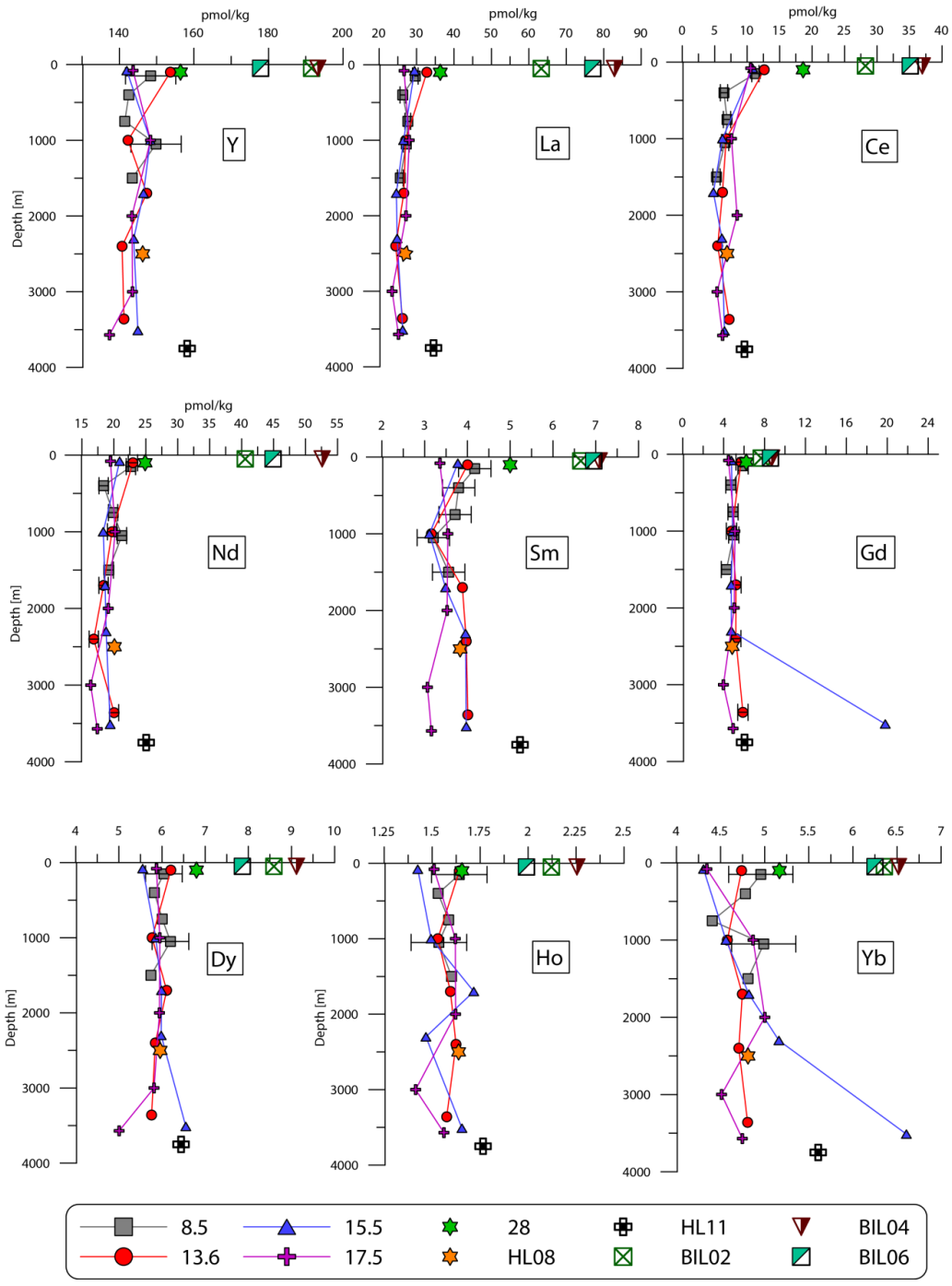


**Fig. 3.** Concentrations of individual Rare Earth Elements versus water depth based on OP-ICP-MS analysis. The error bars shown on the plots for one profile denote the 2S.D. reproducibility of all data.

### 3.4.2 ND ISOTOPE COMPOSITIONS

The Nd isotope compositions of the four water depth profiles along the AR7W line (Fig. 4C) range from -16.8 (st. 15.5, 80 m) to -11 (st. 15.5, 3512 m). The εNd signatures at stations 13.6 and 15.5 become continuously more radiogenic with depth. At station 17.5, two samples collected from the upper 2000 m of the water column yield an average εNd signature

of ~ -14 being identical within analytical uncertainty. Below a depth of 2000 m, the εNd signature becomes more radiogenic, reaching -11.6 near the bottom at 3670 m. The most radiogenic εNd value of -11 is observed in the lowermost sample of station 15.5, 3512 m. At the shallower station 8.5 (water depth of 1702 m), the εNd signature of the profile shows uniform values throughout the water column (average εNd = -13.9) with the exception of the less radiogenic surface sample (εNd = -15.8). The two deep water samples collected along the Halifax line (HL11, 3750 m and HL08, 2500 m) show virtually identical εNd signature with an average of -12.8. These results are consistent with previous εNd observations at neighboring sites in the Labrador Sea (Hudson 83-036, station 9, 2550 m and station 11, 2500 - 3850 m) (Piepgras and Wasserburg, 1987).

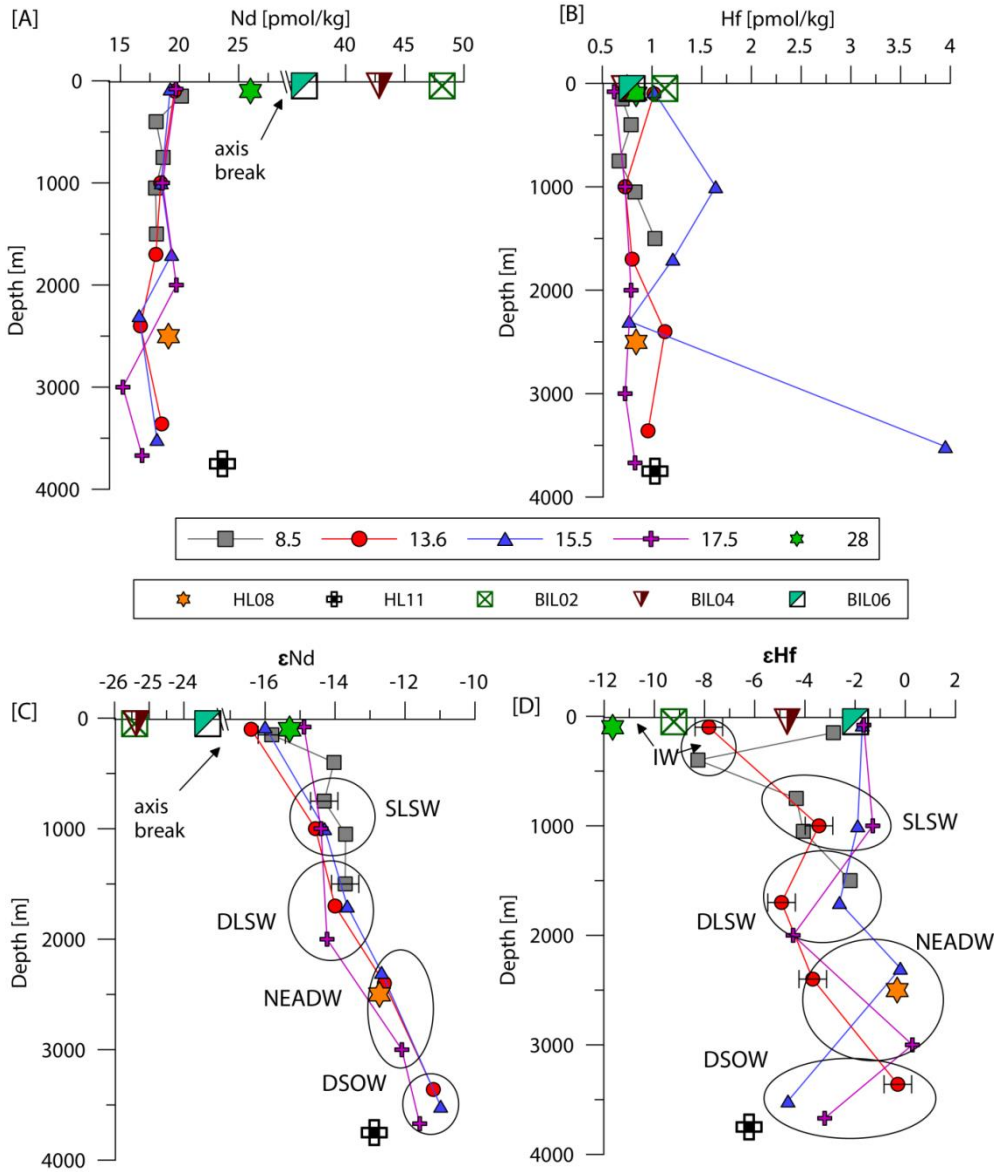


**Fig. 4.** Depth distributions of εHf and εNd signatures and Hf and Nd concentrations (isotope dilution method). A. Nd concentrations in pmol/kg. B. Hf concentrations in pmol/kg.

C. εNd signature. D. εHf signature. Black circles denote samples representing the same water masses.

Near surface waters along the AR7W transect have less radiogenic values than the deep samples, ranging between -16.8 (st. 15.5, 80 m) and -14.9 (st. 17.5, 80 m). A similarly low Nd isotope composition is also observed at shallow depth close to the southern tip of Greenland (st. 28, 100 m, εNd = -15.7). Surface samples collected along the Belle Isle line show the most unradiogenic values of this study ranging from -25.4 (st. BIL02, st. BIL04, both 50 m) to -23.3 (st. BIL06, 50 m), clearly documenting terrestrial input from the Precambrian terrains of the Canadian Shield. With distance from shore the εNd signature becomes slightly more radiogenic.

### 3.4.3 HF ISOTOPE COMPOSITIONS

Hafnium isotope signatures range from +0.3 (st. 17.5, 3000 m) to -11.7 (st. 28, 100 m), which is the least radiogenic εHf value for seawater measured globally so far (Fig. 4D). Surface samples along the Belle Isle line off Newfoundland range from -9.2 at BIL02 to -2 at BIL06, with εHf signatures becoming systematically more radiogenic with distance from the coast. Surface seawater signatures from the four water depth profiles are generally invariant (average εHf = -2) with the exception of the sample at st. 13.6 (100 m, εHf = -7.8).

Unlike εNd, the εHf signatures of the four water depth profiles along the AR7W transect show a high degree of variability in the water column, with stations 15.5 and 17.5 showing similar distributions. Two samples from the upper 1000 meters yield an average εHf signature of -1.7 (Fig. 4D, Table. 2) whereas below the εHf signature is less radiogenic at depths of 1700 - 2000 m and more radiogenic again between 2300 and 3000 m. At the bottom the signature changes to less radiogenic values again, which includes the sample with the anomalously high Gd and Yb concentrations of st. 15.5. The Hf isotope composition at st. 8.5 is most radiogenic near the bottom at 1500 m (εHf = -2.2) and shows a distinct unradiogenic peak below the surface at 400 m (εHf = -8.3). At st. 13.6 the εHf signature becomes more radiogenic with depth below 1700 m.

The deep sample collected along the Halifax line at st. HL08, 2500 m has an εHf signature of -0.3, which is similar to the observation at st.15.5, 2300 m (εHf = -0.2) and st.17.5, 3000 m (εHf = +0.3). The sample from st. HL11, 3750 m, in contrast, shows a highly unradiogenic εHf signature of -6.2, which is about 2 εHf units less radiogenic, than at the corresponding depth along the AR7W transect (st. 17.5, 3670 m εHf ~ -3.2 and st. 15.5, 3512 m εHf ~ -4.7).

## 3.5 DISCUSSION

### 3.5.1 REE DISTRIBUTION AND PATTERNS AND HF CONCENTRATION

The lack of variability in most of the REE and Hf concentrations with water depth in the Labrador Sea (AR7W transect), and essentially identical REE patterns normalized to Post-Archean Average Australian Sedimentary Rock (PAAS; McLennan, 2001) for different water masses (Fig. 3, Fig 5) suggest efficient vertical mixing in the region. However, at the same time we observe variability in εHf and a systematic gradual change in εNd towards more radiogenic signatures with water depth (Fig. 4). These opposing observations can be reconciled if waters advected into the Labrador Sea are characterized by minor differences in their REE, Hf, and Nd concentrations. Previously published studies by Lacan and Jeandel (2004 a,b, 2005) and Lambelet et al. (2015) show that rare earth element patterns and concentrations delivered to the Labrador Sea through the Denmark Strait via ISOW and IW are essentially uniform. Unfortunately, no Hf concentration data are available to infer similar preformed concentrations for Hf. Another potential source with distinct REE signature are Baffin Bay waters and waters from the Hudson Strait, which are highly enriched in Nd and REE (Stordal and Wasserburg, 1986; Goldstein and Jacobsen, 1988). Admixture of these waters into the Labrador Sea should result in variations of REE concentrations but these waters are not dense enough to directly contribute to the deep water mass formation in the region, which restricts their influence to the LC flowing at the surface along the coast (Lacan and Jeandel, 2005). This could explain why some of the REE concentrations (La, Ce, Nd, Sm, Gd, Ho and Dy) at stations 13.6 and 8.5 in general are slightly higher in surface waters than at corresponding depths of two other stations (Fig. 3). This suggests that the uniform signal supplied to the Labrador Sea together with restricted influence of the coastal waters are responsible for the homogenous distribution of the REEs throughout the water column rather than intensive vertical mixing involved in other oceanographic regions (Hathorne et al., 2015; Nozaki and Aibo, 2003; Sholkovitz and Schneider, 1991).

The small changes in Hf concentrations between some of the stations at a given depth appear to be unsystematic. Although vertical Hf concentration profiles are flat, spatial variability in Hf concentrations at different stations within the same water masses may be explained by a combination of factors such as Hf being influenced to a large extent by local terrestrial inputs and the difference in time it takes DSOW and NEADW within the Labrador Sea to record the change in LSW formation (Yashayaev et al., 2008, more details in section 4.2). This would result in different Hf concentrations, as the waters move around the Labrador Sea, reflecting the signal of temporally changing inputs. In addition, the differences in Nd

concentrations in comparison to data from Lacan and Jeandel (2005) at neighboring sites from July 1999 suggest annual or seasonal variability. The intermediate waters (~ 1600 m) sampled in 2013 have 1 pmol/kg higher Nd concentrations than the waters sampled from corresponding depths in 1999 while deep waters (> 2500 m) sampled in 2013 have lower (3 to 5 pmol/kg) Nd concentrations than waters sampled in 1999. This may be caused by the annual variability in LSW production. However, samples of deep waters in the study by Lacan and Jeandel, (2005) were not filtered, which also could have resulted in higher Nd concentrations. One surface sample, where filtration technique was used showed identical results, which is, however, not sufficient enough to establish whether or not filtration has a significant effect on Nd concentrations, especially for deep waters. Concentrations of both elements, therefore, could depend on the intensity of the winter convection, which, however, would need to be confirmed by repeated measurements of Hf and Nd at the same stations. The local maximum in Hf concentration observed at st. 15.5, 3512 m most likely originates from partial dissolution of suspended sediment in an extended nepheloid layer.

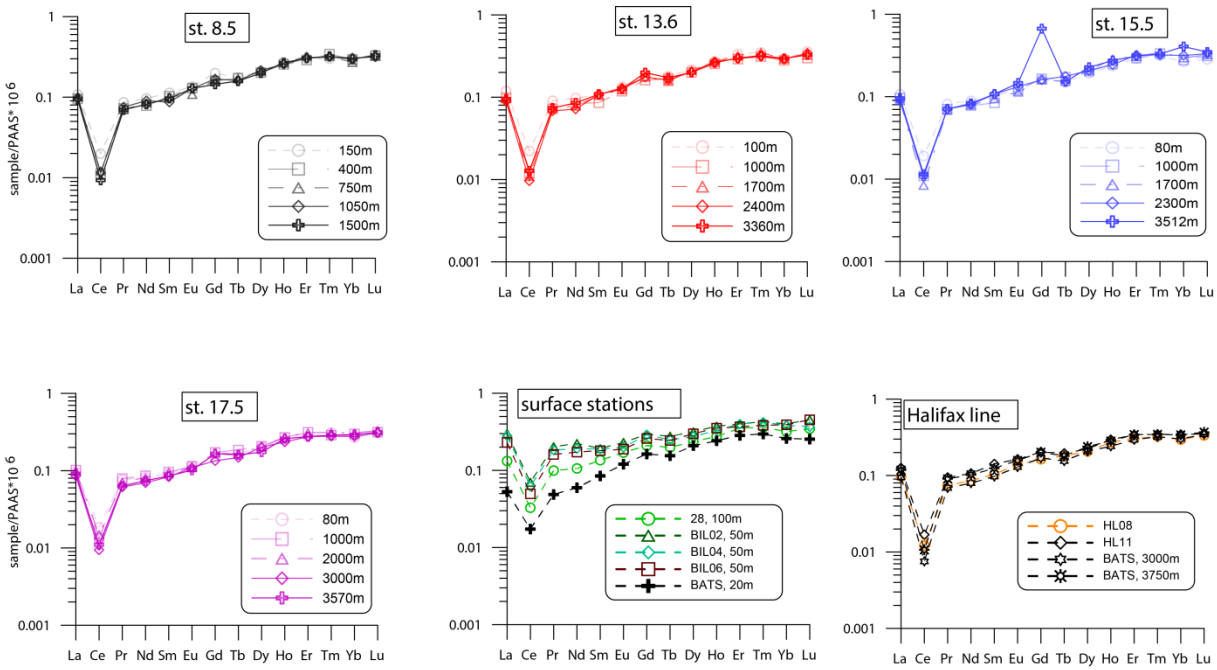


**Fig. 5** Rare Earth Element patterns normalized to Post-Archean Australian Sedimentary rocks (PAAS) (McLennan, 2001), additionally BATS 20 m, BATS 3000 m and BATS 3750 m normalized to PAAS are shown for comparison (Pahnke et al., 2012).

Comparison of the coastal samples collected from both sides of the Labrador Sea, shows a clear distinction in signal of the terrestrial inputs coming from Canada and Greenland. Samples collected from stations BIL02, BIL04, and BIL06 along the Belle Isle line have elevated REE concentrations with a distinct LREE enrichment compared to station 28. This enrichment can still be clearly seen in the REE patterns normalized to 15 m depth

Bermuda Atlantic Time series waters (BATS, Fig. 6), which represent the waters coming from the south, indicating that Canadian terrains are a major contributor of REEs to the surface waters of the Labrador Sea. Although the fresh waters supplied to these sites are not dense enough to be vertically mixed within the Labrador Sea, which is similar to observations in the Arctic Ocean (Porcelli et al., 2009), the LREE signal appears to be transported into deeper waters as it is observed in the NADW (Fig. 6, Halifax Line, this study, and BATS 3000 m and 3750 m, Pahnke et al., 2012). This may be explained by release of REE's from the dissolution of suspended particles (Rousseau et al., 2015) transported from the Hudson Bay estuary within the surface waters of the LC.

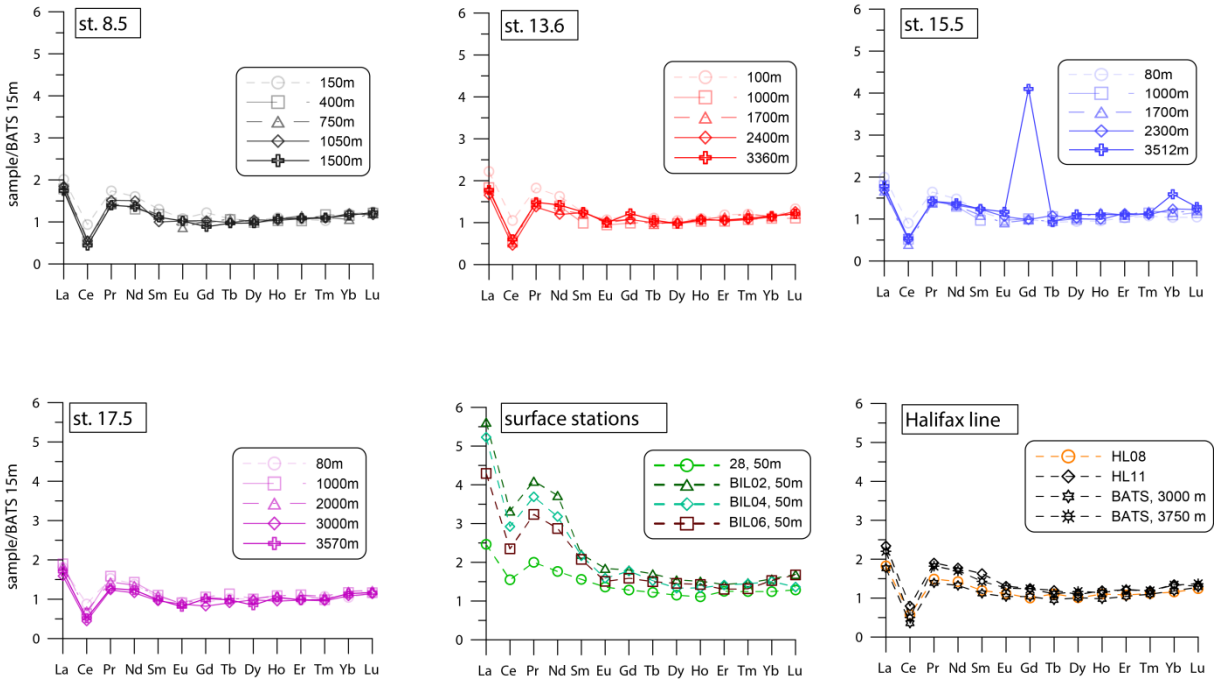


**Fig. 6** Rare Earth Element patterns normalized to Bermuda Atlantic Time Series data values from 15 m from van de Flierdt et al., (2012).

## 3.5.2 ISOTOPIC SIGNATURE OF DIFFERENT WATER MASSES

### 3.5.2.1 DSOW

Denmark Strait Overflow Water is the densest water mass in the Labrador Sea with potential densities above 27.90 kg/m$^3$, which corresponds to the bottom samples collected from stations 17.5, 3670 m, 15.5, 3512 m and 13.6, 3360 m. These waters have a uniform εNd signature of ~ -11.3 and a broader range of εHf between -0.3 (st. 13.6, 3360 m) and -4.7 (st. 15.5, 3512 m). The most radiogenic εHf value of -0.3 could be explained by the admixture of overlying NEADW, which has a more radiogenic εHf signature (Fig. 4D, Fig. 7). This is

supported by a higher temperature (+0.3 °C) and lower oxygen content (-0.2 ml/l, Fig. 2) recorded for this sample.

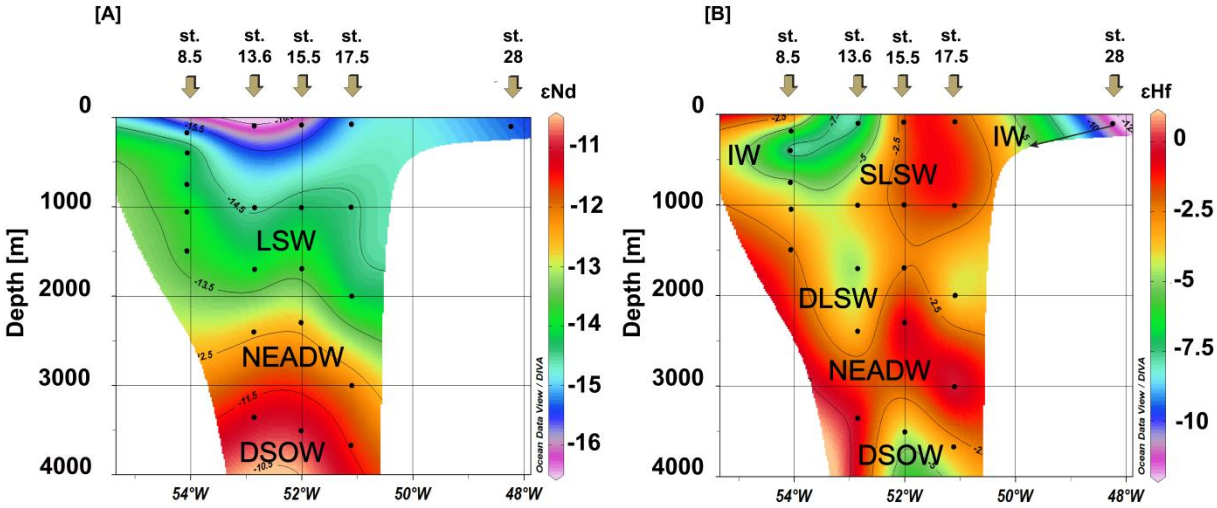


**Fig. 7** Water mass distribution versus depth in the Labrador Sea based on their εNd (A) and εHf (B) signatures.

The εNd signature of DSOW between -11 and -11.6 is in a good agreement with previously published data from nearby locations (Lacan and Jeandel, 2005; Lambelet et al., 2015). The acquired εNd signature is also consistent with the mixing of the source waters contributing to DSOW in the Labrador Sea (Schmitz, 1996), a significant fraction of which is NEADW (εNd ~ -12.5) integrating contributions from unradiogenic LSW (εNd ~ -14.1) and Subpolar Mode Waters (SPMW) (on average -13 to -14) and mixing with the more radiogenic original DSOW before its entrainment into the Labrador Sea (-10 to -7) (Lacan and Jeandel, 2005). The Nd isotope signatures, however, only show subtle differences between DSOW and NEADW at any of the stations below 3000 m (Fig. 4D, Fig. 7). This is explained by the lack of significant differences in the source waters forming these water masses, which would also imply similar signatures for εHf. Although overall ranges of DSOW and NEADW εHf signatures largely overlap, the εHf values within each station exhibit a clear distinction between DSOW and NEADW of up to 4 εHf units. Less radiogenic values of DSOW might reflect the influence of highly unradiogenic IW, the signal of which was recorded at st. 28, 100 m (εHf = -11.7). An influence of highly unradiogenic terrestrial inputs from Greenland into DSOW is also possible. This is supported by higher Nd (> 2 pmol/kg) and Hf (> 0.2 pmol/kg) concentrations of the bottom samples at stations 13.6 and 15.5 than at st. 17.5, 3670 m, and higher Nd and Hf concentrations at st. 13.6, 3360 m than in average NEADW accompanied by higher concentrations of some light and middle REEs including La, Ce, Pr

and Gd (Fig. 3). In addition, there is an εHf shift to less radiogenic values at st. 13.6, 1700 m (εHf = -4.9) and 13.6, 2400 m (εHf = -3.7) compared to the corresponding depths at stations 17.5 (εHf = -1.3, 1700 m) and 15.5 (εHf = -2.6 and -0.2, respectively).

The higher variability in εHf than in εNd may reflect the differences in the timing of DSOW and NEADW production and advection, which results in a higher sensitivity of DSOW to decadal changes. DSOW requires about 1 year to travel to the Labrador Sea, while NEADW only reaches the Labrador basin 5 to 8 years after formation (Yashayaev and Clark, 2006; Yashayev et al., 2008). The εHf signature may then reflect decadal changes in local weathering inputs and distinct Hf isotope signatures of rocks along the different flow paths of DSOW and NEADW. To preserve such variability, the Hf residence time needs to be on the order of the mixing time of the water masses in the Labrador Sea. The almost complete absence of information on Hf fluxes from shelves and rivers limits our ability to quantitatively constrainour the seawater residence time of Hf. The more homogeneous Hf signal outside of the Labrador Sea most likely reflects the remoteness from the marginal input fluxes along the water mass pathways. An overall shorter residence time of Hf than that of Nd could result from the different chemical speciations of these elements in seawater where Nd is dominated by carbonate complexes and Hf is mainly present as a hydroxide (Bruland, 1983). Variable Hf isotope compositions in the Labrador Sea are thus a function of the short residence times of the water masses and the degree of incongruent weathering inputs from the surrounding landmasses and their distinct εHf signatures, which can also explain the relatively high variability in Hf concentrations across the Labrador Sea.

The two deep samples from the Halifax line off the coast of Nova Scotia show a similar εNd signature near -12.8. In contrast, εHf differs by almost 6 units (st. HL11, 3750 m, -6.2 and st. HL08, 2500 m, -0.3). At station HL08, 2500 m, the εHf and εNd signatures are consistent with a NEADW origin, which is also indicated in hydrographic properties (Fig. 2). Station HL11, 3750 m, however, received significant contributions from a source other than DSOW, given that both εHf and εNd are significantly less radiogenic than DSOW (εNd ~ -11.3, εHf between -0.3 and -4.7) along the AR7W transect in the Labrador Sea. The hydrographic data indicate that these waters are less dense (< 27.9 kg/m$^3$) and depleted in oxygen in comparison to DSOW. These waters are thus similar in hydrographic characteristics to st. 13.6, 3360 m but slightly warmer by 0.26 °C and slightly less saline by 0.01. This may indicate that this sample represents the advection of a mixture of upper NEADW with DSOW below. However, the signal recorded at st. HL11, 3750 m is still too unradiogenic in Hf in comparison to DSOW in the Labrador Sea. Unfortunately, the absence

of Hf and Nd isotope data from the full water depth profiles along the Halifax line does not allow an unambiguous identification of the source of this shift and we can thus only speculate on its origin. One possible explanation is the intrusion of particle-loaded waters coming from land through the Gulf of Maine carrying highly unradiogenic values for both Nd and Hf isotopes as indicated by stations BIL02, BIL04, and BIL06 along the Belle Isle line (εNd between -25.9 to -23.3, εHf between -11.7 to -4.7) (Fig. 4 C,D).

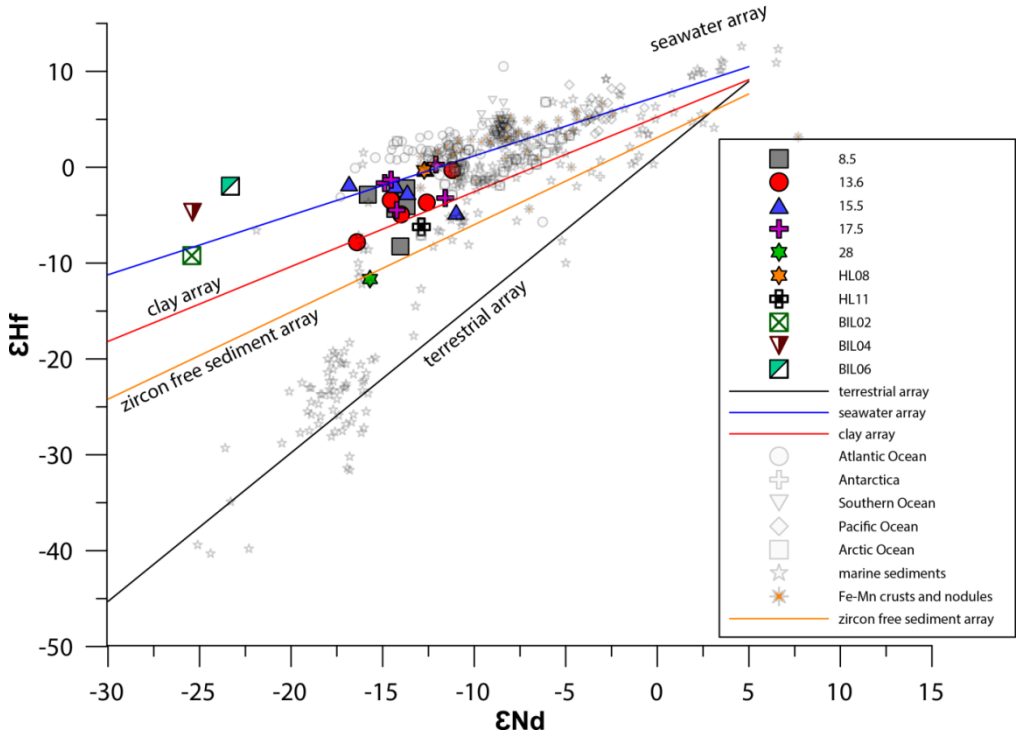


**Fig. 8**. εHf versus εNd of the seawater data of this study together with terrestrial array (Vervoort et al., 2011), seawater array (David et al., 2001), clay array (Bayon et al., 2016), and zircon free sediment array (Bayon et al., 2009). Data for seawater samples are compiled from Godfrey et al., (2009), Rickli et al., (2009, 2010, 2014), Stichel et al., (2012a,b), Zimmermann et al., (2009a,b). Data for sediments are from Bayon et al., (2009), Chen et al., (2012), Garcon et al., (2013). Data for Fe-Mn crusts are from Albarède et al., (1998); David et al., (2001).

The other more likely explanation of the less radiogenic εHf signature at st. HL11 is exchange with resuspended sediments moving down the slope. This has previously been documented to be the cause for shifts in εNd without changing concentrations ("boundary exchange") (Lacan and Jeandel, 2005; Wilson et al., 2012) and has also been suggested to influence seawater Hf isotope composition (Rickli et al., 2009; Zimmermann et al., 2009a). The movement of the resuspended sediment load down the slope may cause release and exchange with the particles through desorption/adsorption or partial dissolution of the particles. Additionally, assuming that the suspended loads mainly consist of sediments

derived from the Precambrian Canadian terrain, one would expect highly unradiogenic Hf and Nd values. The shift in εHf and to a lesser extent of εNd to less radiogenic values than of DSOW recorded in the Labrador Sea, which is accompanied by elevated REE, Nd and Hf concentrations along the Halifax line at st. HL11, 3750 m in comparison to DSOW in the Labrador Sea, suggests dissolution and terrestrial input rather than any kind of "boundary exchange" process, which is also supported by the fact that this sample plots close to the zircon free sediment bearing array in εHf - εNd space, suggesting a more congruent weathering signal (Fig.8).

#### 3.5.2.2 NEADW

North Eastern Atlantic Deep Water was encountered at three stations between densities of 27.80-27.88 kg/m$^3$. The new Nd isotope data are consistent with previously published values (Lacan and Jeandel, 2005; Lambelet et al., 2015). The εNd signature of NEADW is in the range between -12.1 and -12.7. The εHf signature of NEADW ranges between -0.2 to +0.3. However, the sample collected within the NEADW density range from st. 13.6 at 2400 m shows a less radiogenic signature of -3.7, which is most likely explained by admixture with water from the upper layer of DLSW which is not seen , however, in hydrographic data. The more radiogenic εHf signature of NEADW in comparison to DSOW may reflect weathering of Icelandic basalts and dissolution of volcanic glasses, which are highly radiogenic and easily leachable (Pearce et al., 2013). Also, these waters have potentially spent more time in contact with basaltic rocks, due to longer travelling time of NEADW into the Labrador Sea (Yashayaev and Clark, 2006; Yashayev et al., 2008), while DSOW is more likely to be under the influence of terrestrial inputs coming from Greenland.

The advection of NEADW outside of the Labrador Sea is traceable at st. HL08, 2500 m, where Hf (-0.3) and Nd (-12.7) isotope signatures are consistent with the average NEADW values. Salinity, temperature and density profiles clearly document NEADW presence, although with slightly lower oxygen concentrations (~ 0.2 ml/l) (Fig. 2).

#### 3.5.2.3 LSW AND IW

The depth of LSW formation is highly variable from year to year depending on the atmospheric conditions of the previous winter, such that colder conditions lead to more intense convection (Yashayaev and Clark, 2006; Yashayaev et al., 2008). As outlined in section 2.2, a distinction can be made between SLSW (27.70 and 27.725 kg/m$^3$) and DLSW (27.75 and 27.79 kg/m$^3$) representing the remnants of the LSW that formed during the last

cold state of the Labrador Sea between the late 1980's and the early 90's. This layer was also detected in 2008 as a layer of higher density and salinity below SLSW (Fig. 2, Fig. 9) (Yashayaev et al., 2008).

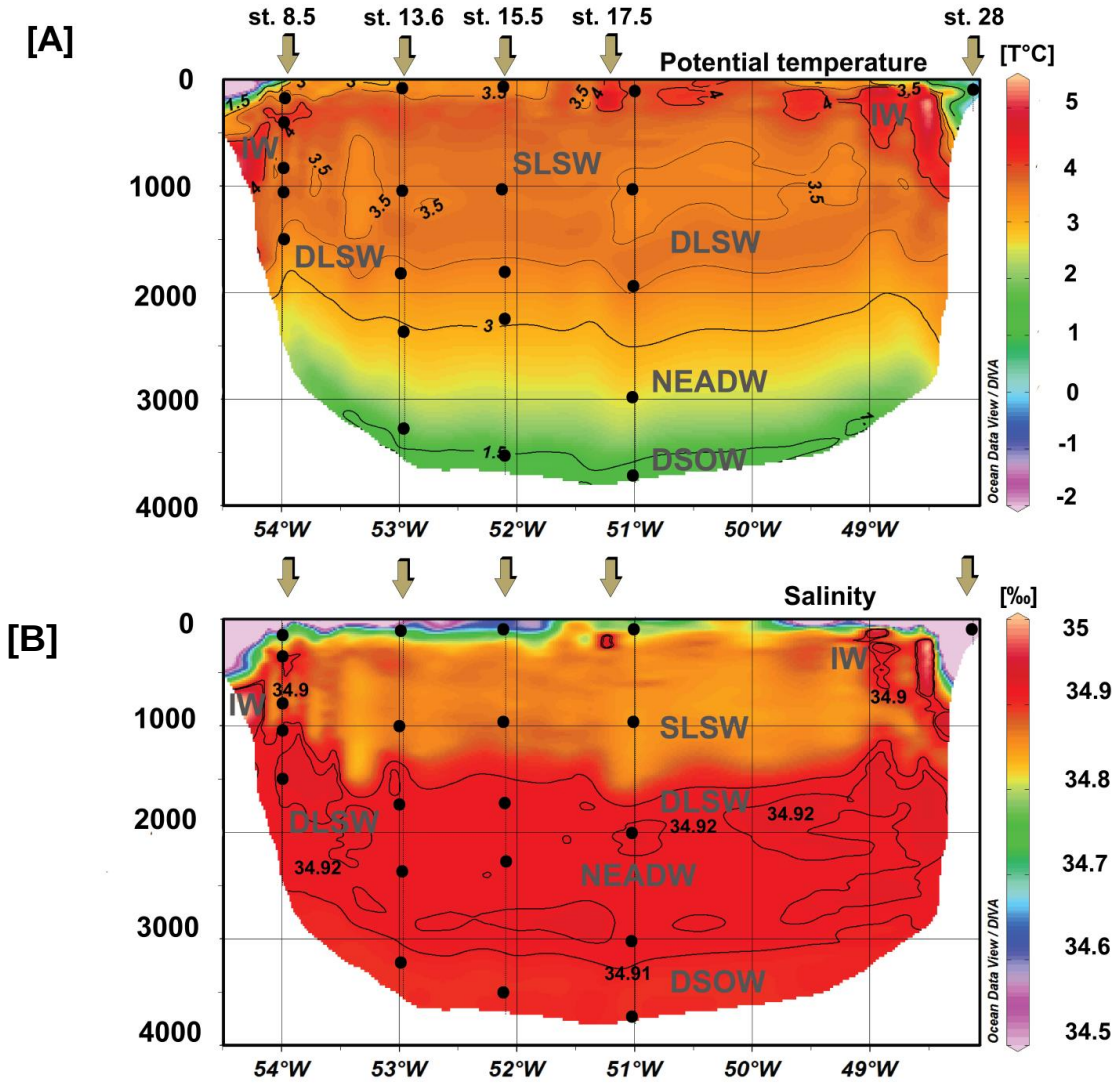


**Fig. 9** Potential temperature (A) and salinity (B) versus depth across the AR7W transect in May, 2013. Contours denote potential temperatures and salinities of different water masses. Black dots represent the depths, from which water samples were taken at each station.

The εNd signatures of SLSW and DLSW in our study are consistent with previously published data (Lacan and Jeandel, 2005; Lambelet et al., 2015) and reveal an average value of -14.1. There has only been one previous study reporting εHf signatures of two samples collected in the Labrador Sea (Rickli et al., 2009). The sample from a depth corresponding to SLSW (1000 m, εHf = -2.1) is within the range of values of SLSW along our transect (εHf ranges between -1.3 and -4.3). Unlike εNd, the εHf between 1700 and 2000 m is distinct from the upper water column, allowing DLSW and SLSW to be distinguished at each station. Deep

LSW sampled at densities between 27.76 and 27.77 kg/m$^3$ at st. 17.5, 2000 m and st. 13.6, 1700 m, st. 15.5, 1700 m and st. 8.5, 1500 m has εHf signatures between -2.2 and -4.9. Less radiogenic values of DLSW at some stations in comparison to SLSW can be explained by a larger influence of IW, which has highly negative εHf values as recorded at st. 28 (εHf = -11.7) (Fig 4, Fig. 7). More radiogenic εHf signatures at st. 15.5, 1700 m and st. 8.5, 1500 m show values closer to the one recorded by SLSW, but the samples are lower in oxygen and more salty, which indicates the presence of DLSW and implies mixing between the two water masses. This is also explainable by the fact that this layer formed between 1980 and 1994 lost much of its distinct signature via mixing and most likely was not evenly distributed across the Labrador Sea (Yashayaev et al., 2008).

The more radiogenic εHf signatures in the upper column of ~ -1.3 at st. 17.5, 1000 m and ~ -1.9 at st. 15.5, 1000 m may be explained by the intrusion of SPMW, which has a more positive εHf signature of -1.6 and is characterized by a less radiogenic εNd signatures of -14.8 (Rickli et al., 2009). Less radiogenic signatures of εHf at st. 13.6, 1000 m and st. 8.5, 1050 m and 750 m are best explained by the admixture of highly unradiogenic IW, which is consistent with much more radiogenic εHf signatures of surface waters at these stations (Fig. 7).

#### 3.5.2.4 UPPER WATER COLUMN

At st. 28, 100 m, the εHf signal is extremely unradiogenic at -11.7, which is the most negative value ever measured for Hf isotopes in seawater so far, while the εNd signature of -15.7 is the same within error as the surface waters across the Labrador Sea sampled at other stations. These waters are advected along the slope of the Labrador Sea. Their presence has not only been recorded in temperature, salinity and oxygen characteristics on the Canadian side of the Labrador Sea (Fig. 2, Fig. 9), but also in the Hf isotope signatures (Fig. 7). At st. 8.5, 400 m and even 13.6, 100 m, these waters are characterized by highly unradiogenic εHf signatures between -8.3 and -7.8, and εNd signatures ranging from -14.0 to -16.4. Admixture of these water masses causes εHf at stations 8.5 and 13.6 to be less radiogenic than εHf signatures prevailing at the corresponding depths at the central Labrador Sea stations. As we assume that this sample represents IW, its highly unradiogenic εHf and unradiogenic εNd signatures require discussion. Taking into account the origin and the flow path of IW and their potential close contact with basaltic rocks from Iceland, we would expect rather more radiogenic εHf and εNd signatures, likely similar to ISOW. This apparent conflict can be explained in a few ways: (i). the NAC waters are unradiogenic, which needs to be confirmed by direct measurements, (ii). there is no significant influence of the weathering of basaltic

rocks on IW, (iii.) there is a significant unradiogenic input from Greenland that shifts the signature. The latter explanation is favored due to higher REE and Nd concentration at st. 28 in comparison to the open Labrador Sea.

#### 3.5.2.5 EXTENDING THE ND/HF ISOTOPE SEAWATER ARRAY

On a plot of εHf against εNd, the seawater data of our study confirm the clear deviation from the terrestrial array, consistent with previous findings (e.g. Albarède et al., 1998; Godfrey et al., 1997; David et al., 2001; Rickli et al. 2009). In comparison to Fe-Mn crusts, the new data show a larger range and significantly extend the seawater array at the unradiogenic end (up to -11 for εHf). The εHf and εNd isotopic signatures of Fe-Mn crusts recovered in the Atlantic Ocean from different depths (Piotrowski et al., 2000, David et al., 2001) are consistent with the combined εHf and εNd signatures from LSW, NEADW and DSOW in the Labrador Sea, which form the NADW. In addition, the two crusts Hudson St 54 (~ 1829 m; εHf = +0.2, εNd = -12.9) and TR079 (~ 2000 m; εHf = 0, εNd = -12.5), as well as crust ALV 539 (~ 2700 m; εHf = -2.2, εNd = -12.9) (David et al., 2002) show the same trend observed along the Halifax line at st. HL08 and HL11, where these stations have an εNd like NADW, while with increasing depth εHf becomes less radiogenic.

Most of the new Labrador Sea data plot between the seawater and terrestrial arrays reflecting the degree of the incongruent weathering delivered to the source waters around the Labrador Sea (Fig. 8) (Bayon et al., 2006; Rickli et al., 2013). Most of the deep water and surface samples fall on the seawater array, suggesting that their signature reflects the true water mass signature of the dissolved hafnium fraction. However, samples representing LSW plot very close to the clay array recently derived by Bayon et al. (2016). This may suggest that intermediate waters in the Labrador Sea are largely controlled by Hf release from the dissolution of clay particles or the presence of very fine clay particles (< 0.45 µm) or clay associated colloids in the water samples.

Interestingly, the samples that are under the strongest influence of terrestrial inputs, such as shallow Canadian shelf samples BIL02, BIL04, and BIL06, plot directly on or slightly above the seawater array and therefore reflect the strongest incongruent weathering signal at the lower end of the seawater array. The rapid change in Hf isotope signatures when moving away from the shore, accompanied by a decrease in Hf concentration in samples BIL04 and BIL06, suggests a high particle reactivity of Hf and fast removal from the surface waters. Samples collected at stations 28, 100 m and st. 8.5, 400 m plot well along the zircon free sediment array (Bayon et al., 2009). This supports our assumption that these waters are

significantly influenced by terrestrial inputs from Greenland. Samples collected at st. HL11, characterized by a less radiogenic εHf signature, and at st. 15.5, 3512 m, also plot close to the zircon free sediment array, possibly indicating an input from resuspended sediments or an extensive nepheloid layer.

## 3.6 CONCLUSIONS

The first combined systematic investigation of the distributions of dissolved εNd and εHf signatures in the Labrador Sea in 2013 reveals distinct water mass signatures. The εHf signatures in the Labrador Sea allow distinction of particular water masses that do not differ in their Nd isotope compositions. This is the consequence of the large range of Hf isotope compositions of the weathering inputs from the adjacent continental landmasses combined with the likely shorter residence time of Hf than Nd in the Labrador Sea . The new data for intermediate waters fall along the new clay array, suggesting that these waters may be affected by dissolution of clay particles. Some of the samples fall along the zircon free sediment array, clearly supporting terrestrial input at these locations. The new data also significantly expand the unradiogenic end of the seawater array. The new data allow Hf isotopes to serve as a sensitive tracer of water mass mixing processes in the restricted Labrador Sea Basin and allows detection of changes in the source waters feeding Labrador Sea Water production on decadal time scales. While tracing of large scale ocean mixing processes may not be possible based on Hf isotopes, there is clearly prospect for their application in other restricted basins with similar geological and hydrographic settings.

## ACKNOWLEDGMENTS

Full-depth temperature, salinity and DO profiles and water samples, including Hf-Nd isotopes, on the AR7W (Atlantic Repeat Hydrography Line 7 West) line across the Labrador Sea and extended Halifax Line (XHL) were obtained during Fisheries and Oceans Canada's (DFO's) annual survey as part of its Atlantic Zone Off-shelf Monitoring Program (AZOMP; http://www.bio.gc.ca/science/monitoring-monitorage/azomp-pmzao/azomp-pmzao-en.php).

The Labrador Sea component of the AZOMP survey, generally conducted in spring shortly after the wintertime convection period, is a continuation of annual surveys of the AR7W line conducted by the Bedford Institute of Oceanography (BIO) since the start of the World Ocean Circulation Experiment (WOCE) in 1990 (e.g., Lazier et al., 2002; Yashayaev et al., 2015). Since 2004, the AR7W survey has been carried out in May occupied between the Labrador and Greenland Shelves.

A. Filippova was supported by a PhD fellowship of the Helmholtz Research School on Ocean System Science and Technology HOSST (www.hosst.org) at GEOMAR Helmholtz Centre for Ocean Research Kiel (VH-KO-601) and Kiel University. We thank Torben Stichel for discussions. We thank Philipp Böning for assistance with Nd measurements. We also would like to thank Tianyu Chen, Veit Dausmann, Jutta Heinze, Georgi Laukert, Anne Osborne, and Moritz Zieringer for their help in the laboratory. The crew of CCGS Hudson is thanked for their help during sampling on board. Financial support for the analyses in Oldenburg came from the ICBM, Oldenburg, and the Max Planck Institute for Marine Microbiology, Bremen.

## REFERENCES

Albarède F., Simonetti A., Vervoort J.D., Blichert-Toft J., Abouchami W. (1998) A Hf-Nd isotopic correlation in ferromanganese nodules. Geophys. Res. Lett. 25 (20), 3895-3898.

Andersson, P., Dahlqvist R., Ingri J., and Gustafsson Ö. (2001) The isotopic composition of Nd in boreal river: A reflection of selective weathering and colloidal transport, 2001. Geochim, Cosmochim. Acta, 65, 521-527.

Arsouze T., Dutay J.-C., Lacan F. and Jeandel C. (2009) Reconstructing the Nd oceanic cycle using a coupled dynamical biogeochemical model. *Biogeosciences* **6**(12), 2829–2846.

Azetsu-Scott K., Jones E.P., Yashayaev I. (2003) Time series study of CFC concentrations in the Labrador Sea during deep and shallow convection regimes (1991-2000). Journal of Geophysical Research, vol. 108, no. C11, 3354, doi:10.1029/2002JC001317.

Barfod G.H., Otero O., Albarède F. (2003) Phosphate Lu-Hf geochronology. Chemical Geology 200, 241-253.

Bayon G., Vigier N., Burton K.W., Brenot A., Carignan J. and Etoubleau J. (2006) The control of weathering processes on riverine and seawater hafnium isotope ratios. Geology 34, 433-436.

Bayon G., Burton K.W., Soulet G., Vigier N., Dennielou B., Etoubleau J., Ponzevera E., German C.R., Nesbitt R.W. (2009) Hf and Nd isotopes in marine sediments: constraints on global silicate weathering. Earth Planet. Sci. Lett. 277, 318-326.

Bayon G., Skonieczny C., Delvigne C., Toucanne S., Bermell S., Ponzevera E., André L. (2016) Environmental Hf–Nd isotopic decoupling in World river clays. Earth and Planetary Science Letters 438, 25-36.

Bau M. and Koshinsky A. (2006) Hafnium and neodymium isotopes in seawater and in ferromanganese crusts: The "element perspective". Earth Planet. Sci. Lett. 241, 952-961.

Blichert-Toft J., Arndt N. T. (1999) Hf isotope compositions of komatiites. Earth Planet. Sci. Lett. 171, 439-451, doi: 10.1016/S0012-821x(99)00151-X

Bouvier A., Vervoort J.D., Patchett P.J. (2008) The Lu-Hf and Sm-Nd isotopic composition of CHUR: Constraints from unequilibrated chondrites and implications for the bulk composition of terrestrial planets. Earth Planet. Sci. Lett. 273, 48-57, doi:10.1016/j.epsl.2008.06.010.

Bruland, K. W. (1983) Trace Elements in Sea Water. In J.P. Riley and R. Chester (Editors), Chemical Oceanography, 8, Academic Press, 157-220

Camire G. E., La Fleche M. R., Jenner G. A. (1995) Geochemistry of Pre-Taconian Mafic Volcanism in the humber zone of the Northern Appalachians, Quebec, Canada. Chem. Geol. 119, 55-77, doi: 10.1016/0009-2541(94)00104-G

Chen T.Y., Ling H.F., Frank M., Zhao K.D., Jiang S.Y. (2011) Zircon effect alone insufficient to generate seawater Nd-Hf isotope relationships. $G^3$ 12, 5, Q05003, doi:10.1029/2010GC003363, ISSN:1525-2027.

Chen T.Y., Frank M., Brian A.H., Gutjahr M., Spielhagen R.F. (2012) Variations of North Atlantic inflow to the central Arctic Ocean over the last 14 million years inferred from hafnium and neodymium isotopes. Earth and Planetary Science Letters 353-354, 82-92.

Chen, T.-Y., Stumpf R., Frank M., Beldowski J., and Staubwasser M. (2013) Constraining geochemical cycling of hafnium and neodymium in the central Baltic Sea. Geochimica et Cosmochimica Acta 123, 166-180, doi:10.1016/j.gca.2013.09.011

Chekol T. A., Kobayashi K., Yokoyama Tetsuya, Sakaguchi C., Nakamura E. (2011) Timescales Of Magma Differentiation From Basalt To Andesite Beneath Hekla Volcano, Iceland: Constraints From U-Series Disequilibria In Lavas From The Last Quarter-Millennium Flows. Geochim. Cosmochim. Acta, 75 , 256-283

Csanady G.T. (1976) Mean circulation in shallow seas. Journal of Geophysical Research 81, 5389-5399.

Csanady G.T. (1978) The arrested topographic wave. Journal of Physical Oceanography 8, 47-62.

David K., Frank M., O'Nions R.K., Belshaw N.S., Arden J.W., Hein J.R. (2001) The Hf isotope composition of global seawater and the evolution of Hf isotopes in the deep Pacific Ocean from Fe-Mn crusts. Chem. Geol. 178, 23-42.

Firdaus M.L., Norisuye K., Nakagawa Y., Nakatsuka S., Sohrin Y. (2008) Dissolved and labile particulate Zr, Hf, Nb, Ta, Mo and W in the western North Pacific Ocean. J. Oceanogr. 64, 247-257.

Firdaus M.L., Minami T., Norisuye K., Sohrin Y. (2011) Strong elemental fractionation of Zr-Hf and Nb-Ta across the Pacific Ocean. Nature Geoscience 4, 227-230, doi:10,1038/ngeo1114

Fitton J. G., Larsen L. M., Saunders A. D., Hardarson B. S., Kempton P. D.J. (2000) Paleogene continental to oceanic magmatism on the SE Greenland continental margin at 63° N: a review of the results of ocean drilling program legs 152 And 163. Petrol. 41, 951-966, doi: 10.1093/petrology/41.7.951

Fogelqvist E., Blindheim J., Tanhua T., Osterhus S., Buch E., Rey F. (2003) Greenland-Scotland overflow studied by hydro-chemical multivariate analysis. Deep-Sea Research I 50, 73-102.

Frank M. (2002) Radiogenic isotopes: Tracers of past ocean circulation and erosional input. Reviews of Geophys. 40, 1001, 1001, 10.1029/2000RG000094

Fröllje, H., Pahnke, K., Schnetger, B., Brumsack, H.-J., Dulai, H., Fitzsimmons, J.N., 2016. Hawaiian imprint on dissolved Nd and Ra isotopes and rare earth elements in the central North Pacific: Local survey and seasonal variability. Geochimica et Cosmochimica Acta 189, 110-131.

Gaffney A. M., Blichert-Toft J., Nelson B. K., Bizzarro M., Rosing M. T., Albarede F. (2007) Constraints on source-forming processes of West Greenland kimberlites inferred from Hf-Nd isotope systematics. Geochim. Cosmochim. Acta 71, 2820-2836, doi: 10.1016/j.gca.2007.03.009

Garcon M., Chauvel C., France-Lanord C., Huyghe P., Lave J. (2013) Continental sedimentary processes decouple Nd and Hf isotopes. Geochim. et Cosmochim. Acta 121, 177-195, doi:10.1016/j.gca.2013.07.027.

Gerasimovsky V. I., Laktionova N. V., Kovalenker V. G. (1975) Vanadium, Chromium, Nickel Cobalt And Copper In Iceland Lavas ; Geochem. Int., 12 (4), 160-171

Godfrey L.V., White W.M. and Salters V.J.M. (1996) Dissolved zirconium and hafnium distributions across a shelf break in the northeastern Atlantic Ocean. Geochim. Cosmochim. Acta 60, 3995-4006, doi:10.1016/S0016-7037(96)00246-3.

Godfrey L.V., Lee D.C., Sangrey W.F., Halliday A.N., Salters V.J.M., Hein J.R. and White W.M. (1997) The Hf isotopic composition of ferromanganese nodules and crusts and hydrothermal manganese deposits: implications for seawater Hf. Earth Planet. Sci. Lett. 151 (1-2), 91-105.

Godfrey L.V., Zimmermann B., Lee D.C., King R.L., Vervoort J.D., Sherrell R.M., Halliday A.N. (2009) Hafnium and neodymium isotope variations in NE Atlantic seawater. Geochem. Geophys. Geosys. 10, Q08015. http://dx.doi.org/10.1029/2009gc002508.

Goldstein S.L., O'Nions R.K. and P.J. Hamilton (1984) A Sm-Nd isotopic study of atmospheric dust and particulates from major river systems. Earth Planet. Sci. Lett. 70, 221-236.

Goldstein, S.J., Jacobsen, S.B. (1988) REE in the Great River estuary, northwest Quebec. Earth and Planetary Science Letters 88, pp. 241-252.

Goldstein S.L. and Hemming S.R. (2003) Long-lived Isotopic Tracers in Oceanography, Paleoceanography and Ice-sheet Dynamics. Book, Chapter 6.17.

Goodenough K. M., Upton B. G. J., Ellam R. M. J.(2002) Long-term memory of subduction processes in the lithospheric mantle: evidence from the geochemistry of basic dykes in the Gardar Province of south Greenland. Geol. Soc. London 159, 705-714, doi: 10.1144/0016-764901-154

Grasse, P., Stichel, T., Stumpf, R., Stramma, L., Frank, M., 2012. The distribution of neodymium isotopes and concentrations in the Eastern Equatorial Pacific: Water mass advection versus particle exchange. Earth and Planetary Science Letters 353–354, 198-207.

Hathorne E.C., Haley B., Stichel T., Grasse P., Zienger M., Frank M. (2012) Online preconcentration ICP-MS analysis of rare earth elements in seawater. $G^3$, 13, 1, Q01020, doi:10.1029/2011GC003907, ISSN:1525-2027.

Hathorne, E.C., Stichel, T., Brück, B., Frank, M. (2015) Rare earth element distribution in the Atlantic sector of the Southern Ocean: The balance between particle scavenging and vertical supply. Marine Chemistry 177, Part 1, 157-171.

Hoffmann J. E., Münker C., Polat A., König S., Mezger K., Rosing M. T. (2010) Highly Depleted Hadean Mantle Reservoirs In The Sources Of Early Archean Arc-Like Rocks, Isua Supracrustal Belt, Southern West Greenland. Geochim. Cosmochim. Acta 74, 7236-7260, doi: 10.1016/j.gca.2010.09.027

Jackson m. G., Carlson R. W., Kurz M. D., Kempton P. D., Francis D. M., Blusztajn J. (2010) Evidence for the survival of the oldest terrestrial mantle reservoir ; Nature 466, 853-856, doi: 10.1038/NATURE09287

Jacobsen S.B. and Wasserburg G.J. (1980) Sm-Nd isotopic evolution of chrondrites. Earth Planet. Sci. Lett. 50, 139-155.

Kearns E.J. and Rossby H.T. (1998) Historical position of the North Atlantic Current. Journal of Geoph. Res. 103, 15.509-15.524

Kitagawa H., Kobayashi K., Makishima A., Nakamura E. (2008) Multiple Pulses Of The Mantle Plume: Evidence From Tertiary Icelandic Lavas. J. Petrol., 49, 1365-1396

Koornneef J. M., Stracke A., Bourdon B., Meier M. A., Jochum K. P., Stoll B., Grönvold K. (2012) Melting Of A Two-Component Source Beneath Iceland. J. Petrol., 53, 127-157

La Fleche M. R., Camire G. E., Jenner G. A. (1998) Geochemistry of post-arcadian, carboniferous continental intraplate basalts from the Maritimes Basin, Magdalenen Islands, Quebec, Canada. Chem. Geol. 148, 115-136, doi: 10.1016/S0009-2541(98)00002-3

Lacan F. and Jeandel C. (2004a) Denmark Strait water circulation traced by heterogeneity in neodymium isotopic compositions. Deep-Sea Research Part I-Oceanographic Research Papers 51(1), 71-82, doi:10.1016/j.dsr.2003.09.006.

Lacan F. and Jeandel C. (2004b) Neodymium isotopic composition and rare earth element concentrations in the deep and intermediate Nordic Seas: Constraints on the Iceland Scotland Overflow Water signature, Geochemistry Geophysics Geosystems 5, doi:10.1029/2004GC000742.

Lacan F. and Jeandel C. (2005) Acquisition of the neodymium isotopic composition of the North Atlantic Deep Water. $G^3$, 6, 12, Q12008, doi:10.1029/2005GC000956, ISSN:1525-2027.

Lacan F., Tachikawa K, Jeandel C. (2012) Neodymium isotopic composition of the oceans: a compilation of seawater data. Chemical Geology 300-301, 177-184, doi:10.1016/j.chemgeo.2012.01.019.

Lambelet M., van de Flierdt T., Crocket K., Rehkämper M., Kreissig K., Coles B., Rijkenberg M.J.A., Gerringa L. J.A., de Baar H.J.W., Steinfeldt R. (2015) Neodymium isotopic composition and concentration in the western North Atlantic Ocean: results from the GEOTRACES GA02 section. Geochimica et Cosmochimica Acta 177, 1-29 doi:10.1016/j.gca.2015.12.019.

Lazier J.R.N. and Wright D.G. (1993) Annual velocity variations in the Labrador Current. J. Phys. Oceanogr. 23, 659-678.

Lazier J., Hendry R., Clarke A., Yashayaev I., Rhines P. (2002) Convection and restratification in the Labrador Sea, 1990-2000. Deep Sea Research Part I: Ocean. Research Papers 49, 10, 1819-1835, doi:19.1016/S0967-0637(02)00064-X.

Maclachlan K., Dunning G. R. (1998) 235-258 U-Pb ages and tectonomagmatic relationships of Early Ordovician Low-Ti Tholeiites, Boninites and related plutonic rocks in Central Newfoundland, Canada. Contrib. Mineral. Petrol. 133

Maclachlan K., Dunning G. R. Can. J. (1998) U-Pb ages and tectono-magmatic evolution of Middle Ordovician volcanic rocks of the Wild Bight Group, Newfoundland, Appalachians Earth Sci. 35, 998-1017, doi: 10.1139/cjes-35-9-998

Manning C. J., Thirlwall M. F. (2014) Isotopic Evidence For Interaction Between Öraefajökull Mantle And The Eastern Rift Zone, Iceland. Contrib. Mineral. Petrol., 167 (959)

McKelvey B.A. and Orians K.J. (1998) The determination of dissolved zirconium and hafnium from seawater using isotope dilution coupled plasma mass spectrometry. Mar. Chem. 60, 245-255.

McLennan S.M. (2001) Relationships between the Trace Element Composition of Sedimentary Rocks and Upper Continental Crust. Geochemistry Geophysics Geosystems 2, 4, 1-24, doi:10.1029/2000GC000109.

Minifie M. J., Kerr A. C., Ernst R. E., Hastie A. R., Ciborowski T. J. R., Desharnais G., Millar I. L. (2013) The Northern and Southern sections of the Western ca. 1880 Ma Circum-Superior Large Igneous Province, North America: The Pickle Crow Dyke Connection? Lithos 174, 217-235, doi: 10.1016/j.lithos.2012.03.017

Münker C., Weyer S., Scherer S., Mezger K. (2001) Separation of high field strength elements (Nb, Ta, Zr, Hf) and Lu from rock samples for MC-ICPMS measurements. Geochem. Geophys. Geosys. 2, 12, doi:10.1029/2001GC000183.

Nowell G.M., Kempton P.D., Noble S.R., Fitton J.G., Saunders A.D., Mahoney J.J., Taylor R.N. (1998) High precision Hf isotope measurements of MORB and OIB by thermal ionization mass spectrometry: insights into the depleted mantle. Chem. Geol. 149, 211-233. doi: 10.1016/S0009-2541(98)00036-9

Nozaki, Y., Alibo, D.S. (2003) Importance of vertical geochemical processes in controlling the oceanic profiles of dissolved rare earth elements in the northeastern Indian Ocean. Earth and Planetary Science Letters 205, 155-172.

Öhlander B., Ingri J., Land M., and Schöberg H. (2000) Change of Sm-Nd isotope composition during weathering of till. Geochim. Cosmochim Acta 64, 813-820.

Pahnke K., van de Flierdt T., Jones K.M., Lambelet M., Hemming S.R., Goldstein S.L. (2012) GEOTRACES intercalibration of neodymium isotopes and rare earth element concentrations in seawater and suspended particles. Part 2: Systematic tests and baseline profiles. Limnology and Oceanography: methods 10, 252-269.

Patchett P.J., White W.M., Feldman H., Kielinczuk S., Hofmann A.W. (1984) Hafnium Rare-Earth element fractionation in the sedimentary system and crystal recycling into the earth's mantle. Earth Planet. Sci. Lett. 69, 365-378.

Pearce, C.R., Jones M.T., Oelkers E.H., Pradoux C., Jeandel C. (2013) The effect of particulate dissolution on the neodymium (Nd) isotope and Rare Earth Element (REE) composition of seawater. Earth Planet. Sci. Lett. 369-370, 138-147. doi:10.1016/j.epsl.2013.03.023

Peate D. W., Breddam K., Baker J. A., Kurz M. D., Barker A. K., Prestvik T., Grassineau N., Skovgaard A. C. (2010) Compositional Characteristics And Spatial Distribution Of Enriched Icelandic Mantle Components. J. Petrol., 51, 1447-1475

Pettke T.D., Lee D.C., Halliday A.N., Rea D.K. (2002) Radiogenic Hf isotopic compositions of continental eolian dust from Asia, tis variability and its implications for seawater Hf. Earth Planet. Lett. 202, 453-464, doi:10.1016/S0012-821X(02)00778-1.

Piepgras D.J. and Wasserburg G.J. (1987) Rare-earth element transport in the western North Atlantic inferred from Nd isotopic observations. Geochim. Cosmochim. Acta 51, 1257-1271, doi:10.1016/j.epsl.2006.11.027.

Pin C., Zalduegui J.S. (1997) Sequential separation of light rare-earth elements, thorium and uranium by miniaturized extraction chromatography: application to isotopic analyses of silicate rocks. Anal. Chem. Acta 339, 79-89

Piotrowski A. M., Lee D.-C., Christensen J. N., Burton K. W., Halliday A. N., Hein J. R. and Gunther D. (2000) Changes in erosion and ocean circulation recorded in the Hf isotopic compositions of North Atlantic and Indian Ocean ferromanganese crusts. Earth Planet. Sci. Lett. 181, 315–325.

Piotrowski A.M., Goldstein S.L., Hemming S.R., Fairbanks R.G. (2005) Temporal Relationships of carbon Cycling and Ocean Circulation at Glacial Boundaries. Science 307, 1933-1938, doi:10.1126/science.1104883

Porcelli D., Andersson P.S., Baskaran M., Frank M., Björk G., Semiletov I. (2009) The distribution of neodymium isotopes in Arctic Ocean basins. Geochim et Cosmochim Acta 73, 2645-2659, doi:10.1016/j.gca.2008.11.046.

Rempfer J., Stocker T. F., Joos F., Dutay J.-C. and Sidall M. (2011) Modeling Nd-isotopes with a coarse resolution ocean circulation model: Sensitivities to model parameters and source/sink distributions. *Geochim. Cosmochim. Acta* **75**, 5927-5950

Reynaud T.H., Weaver A.J., Greatbach R.J. (1995) Summer mean circulation of the northwestern Atlantic Ocean. Journal of Geophysical Research 100, 779-816.

Rickli J., Frank M., Halliday A.N. (2009) The hafnium-neodymium isotopic composition of Atlantic seawater. Earth and Planetary Scince Letters 280, pp. 118-127.

Rickli J., Frank M., Baker A.R., Aciego S., de Souza G., Georg R.B., Halliday A.N. (2010) Hafnium and neodymium isotopes in surface waters of the eastern Atlantic Ocean: Implications for sources and inputs of trace metals to the ocean. Geochimica et Cosmochimica Acta 74, 540-557.

Rickli J., Frank M., Stichel T., Georg R.B., Vance D., Halliday A.N. (2013) Controls on the incongruent release of hafnium during weathering of metamorphic and sedimentary catchments. Geochim. et Cosmochim. Acta 101, 263-284, doi:10.1016/j.gca.2012.10.019.

Rickli J., Gutjahr M., Vance D., Fisher-Gödde M., Hillenbrand C.-D., Kuhn G. (2014) Neodymium and hafnium boundary contributions to seawater along the West Antarctic continental margin. Earth Planet. Sci. Lett. 394, 99-110.

Rousseau T.C.C., Sonke J.E., Chmeleff J., van Beek P., Souhaut M., Boaventura G., Seyler P., Jeandel C. (2015) Rapid neodymium release to marine waters from lithgenic ssediments in the Amazon estuary. Nature communications, doi:10.1038/ncomms8592

Salters V. J. M., White W. M. (1998) Hf Isotope Constraints On Mantle Evolution ; Chem. Geol., 145, 447-460

Schmitz W. (1996) On the World Ocean Circulation: Volume I. Some Global Features/ North Atlantic Circulation. Woods Hole Oceanographic Institution, Technical report, WHOI-96-03

Sholkovitz, E.R., Schneider, D.L. (1991) Cerium redox cycles and rare earth elements in the Sargasso Sea. Geochimica et Cosmochimica Acta 55, 2737-2743.

Skulski T., Percival J. A. (1996) Allochthonous 2.78 Ga Oceanic Plateau Slivers In A 2.72 Ga Continental Arc Sequence; Vizien Greenstone Belt, Northeastern Superior Province, Canada. Lithos 37, 163-179, doi: 10.1016/0024-4937(95)00035-6

Smith P.C. and Schwing F.B. (1990) Mean circulation and variability on the eastern Canadian continental shelf. Continental Shelf Research 11, 977-1012.

Stern R. A., Percival J. A., Mortensen J. K. (1994) Geochemical evolution of the Minto block: a 2.7 ga continental magmatic arc built on the Superior Proto-Craton. Prec. Research 65, 115-133, doi: 10.1016/0301-9268(94)90102-3

Stichel T., Frank M., Rickli J., Hathorne E.C., Haley B., Jeandel C., Pradoux C. (2012a) Sources and input mechanisms of hafnium and neodymium in surface waters of the Atlantic sector of the Southern Ocean. Geochimica et Cosmochimica Acta 94, 23-37.

Stichel T., Frank M., Rickli J., Haley B. (2012b) The hafnium and neodymium isotope composition of seawater in the Atlantic sector of the Southern Ocean. Earth and Planetary Science Letters 317-318, 282-294.

Stordal M.C. and Wasserburg G.J. (1986) Neodymium isotopic study of Baffin Bay water sources of REE from very old terranes. Earth Planet. Sci. Lett. 77, 259-272.

Stracke A., Zindler A., Salters V. J. M., Mckenzie D. M., Blichert-Toft J., Albarede F., Grönvold K. (2003) Theistareykir Revisited ; Geochemistry Geophysics Geosystems, 4

Straneo, F. and Saucier F. (2008) The outflow from Hudson Strait and its contribution to the Labrador Current. DEEP SEA RES. I, 55, 926-946.

Swinden H. S., Jenner G. A., Fryer B. J., Hertogen J., Roddick J. C. (1990) Petrogenesis and paleotectonic history of the Wild Bight Group, an ordovician rifted island arc in Central Newfoundland. Contrib. Mineral. Petrol. 105, 219-241, doi: 10.1007/BF00678987

Szilas K., Hoffmann J. E., Schersten A., Rosing M. T., Windley B. F., Kokfelt T. F., Keulen N., Van Hinsberg V., Naeraa T., Frei R., Münker C. (2012) Complex calc-alkaline volcanism recorded in mesoarchaean supracrustal belts north of Frederikshab Isblink, Southern West Greenland: implications for subduction zone processes in the early Earth. Prec. Research 208-211, 90-123, doi: 10.1016/j.precamres.2012.03.013

Szilas K., Hoffmann J. E., Schersten A., Kokfelt T. F., Münker C.(2013) Archaean andesite petrogenesis: insights from the Graedefjord Supracrustal Belt, Southern West Greenland. Prec. Research 236, 1-15, doi: 10.1016/j.precamres.2013.07.013

Tanaka T., Togashi S., Kamioka H., Amakawa H., Kagami H., Hamamoto T., Yuhura M., Orihashi, Y., Yoneda, S., Shimizu, H., Kunimaru, T., Takahashi, K., Yanagi, T., Nakano, T., Fujimaki, H., Shinjo, R., Asahara, Y., Tanimizu, M., Dragusanu, C. (2000) JNdi-1: a neodymium isotopic reference in consistency with LaJolla neodymium. Chem. Geol. 168 (3–4), 279–281.

Tappe S., Foley S. F., Kjarsgaard B. A., Romer R. L., Heaman L. M., Stracke A., Jenner G. A. (2008) Between carbonatite and lamproite-diamondiferous torngat ultramafic lamprophyres formed by carbonate-fluxed melting of cratonic marid-type metasomes. Geochim. Cosmochim. Acta 72, 3258-3286, doi: 10.1016/j.gca.2008.03.008

van de Flierdt T., Frank M., Lee D.-C., Halliday A.N. (2002) Glacial weathering and the hafnium isotope composition of seawater. Earth Planet. Sci. Lett. 198, 167-175. Republished with corrections: Earth Planet. Sci. Lett. 201, 639-647.

van de Flierdt T., Frank M., Lee D.C., Halliday A.N., Reynolds B.C., Hein J.R. (2004a) New constraints on the sources and behavior of neodymium and hafnium in seawater from Pacific Ocean ferromanganese crusts. Geochim. Cosmochim. Acta 68, 3827-3843.

van de Flierdt T., Frank M., Halliday A.N., Hein J.R., Hattendorf B., Gunther D., Kubik P.W. (2004b) Tracing the history of submarine hydrothermal inputs and the significance of hydrothermal hafnium for the seawater budget- a combined Pb-Hf-Nd isotope approach. Earth and Planetary Science Letters 222, 259-273.

van de Flierdt T., Goldstein S.L., Hemming S.R., Roy M., Frank M., Halliday A.N. (2007) Global neodymium-hafnium isotope systematics- revisited. Earth Planet. Sci. Lett. 259, 432-441.

van de Flierdt T. et al. (2012) GEOTRACES intercalibration of neodymium isotopes and rare earth element concentrations in seawater and suspended particles. Part 1: reproducibility of results for the international intercomparison. Limnol. Oceanogr. 10, 234–251.

Vervoort J.D., Plank T., Prytulak J. (2011) The Hf-Nd isotopic composition of marine sediments. Geochim. et Cosmocim. Acta 75, 20, 5903-5926, doi:10.1016/j.gca.2011.07.046.

West D. P.; Jr., Coish R. A., Tomascak P. B. (2004) Tectonic setting and regional correlation of ordovician metavolcanic rocks of the Casco Bay Group, Maine: evidence from trace element and isotope geochemistry. Geol. Mag. 141, 125-140, doi: 10.1017/S0016756803008562

Wilson D. J., Piotrowski A. M., Galy A., and McCave I. N. (2012) A boundary exchange influence on deglacial neodymium isotope records from the deep western Indian Ocean. *Earth and Planetary Science Letters* **341–344**, 35-47.

Yashayaev I. (2007) Hydrographic changes in the Labrador Sea, 1960-2005. Prog. Oceanogr. 73(3-4), 2442-276, doi:10.1016/j.pocean.2007.04.015

Yashayaev I. and Clark A. (2006) Recent warming of the Labrador Sea. AZMP Bulletin PMZA 5:12-20.

Yashayaev I., Dickson R.R. (2008) Transformation and fate of overflows in the northern North Atlantic, in Arctic-Subarctic Ocean Fluxes: Defining the Role of the Northern Seas in Climate, edited by R.R. Dickson, J. Meincke and P. Rhines, Chapter Arctic-Subarctic Ocean Fluxes 505-526, Springer, New York.

Yashayaev I., Loder J.W. (2009) Enhanced production of Labrador Sea Water in 2008, *Geophys. Res. Lett. 36*, L01606, doi:10.1029/2008GL036162, (published online November 2008).

Yashayaev I., Loder J.W. (2016) Recurrent Replenishment of Labrador Sea Water and Associated Decadal-Scale Variability. Journal of Geophysical Research - Oceans, Accepted manuscript, DOI: 10.1002/2016JC012046

Yashayaev I., Holliday N.P., Bersch M., van Aken H.M. (2008) The History of the Labrador Sea Water: Production, Spreading, Transformation and Loss. In book: Arctic–Subarctic Ocean Fluxes, Defining the Role of the Northern Seas in Climate, Chapter: Chapter 24: The History of the Labrador Sea Water: Production, Spreading, Transformation and Loss, Publisher: Springer, Editors: Bob Dickson, Jens Meincke, Peter Rhines, pp.569–612

Zimmermann B., Porcelli D., Frank M., Andersson P.S., Baskaran M., Lee D.C., Halliday A.N. (2009a) Hafnium isotopes in Arctic Ocean water. Geochim. Cosmochim. Acta 73, 32118-3233.

Zimmermann B., Porcelli D., Frank M., Rickli J., Lee D.C., Halliday A.N. (2009b) The hafnium isotope composition of Pacific Ocean water. Geochim. Cosmochim. Acta 73, 91-101.

Zindler A., Komatiites (Arndt, N. T.,E. G. Nisbet, E. G.) (1982) Nd And Sr isotopic studies of komatiites and related rocks, Allen & Unwin, 399-420

# CHAPTER 4.

# ALKENONE PALEOTHERMOMETRY IN THE NORTH ATLANTIC: A REVIEW AND SYNTHESIS OF SURFACE SEDIMENT DATA AND CALIBRATIONS

Published as: Filippova A., Kienast M., Frank M., Schneider, R., 2016. Alkenone paleothermometry in the North Atlantic: A review and synthesis of surface sediment data and calibrations. Geochemistry, Geophysics, Geosystems, 17 (4), 1370-1382, DOI: 10.1002/2015GC006106.

## 4.1 ABSTRACT.

Despite a clear correlation of alkenone unsaturation and sea surface temperatures (SST) throughout most parts of the ocean, scatter of the regression for various calibration equations has been shown to increase significantly at low SSTs. In this study we combine previously published ($n$ = 101) and new ($n$ = 51) surface sediment data from the northern North Atlantic to constrain uncertainties of alkenone paleothermometry at low SSTs and to discuss possible sources of the increased scatter in the regression. The correlation between alkenone unsaturation and SSTs is strongest, in particular at the cold end (SSTs <10°C), when $U^{K}_{37}$the tetra-unsaturated alkenones ($C_{37:4}$) are included in the unsaturation index (expressed as $U^{K}_{37}$) and regressed against spring-summer temperature. Surface ocean salinity and sea ice cover are not correlated with $U^{K}_{37}$ *per se*. However, samples located in regions of permanent winter sea ice cover exhibit a significant warm bias. Deviation from the linear regression is posited to be related to a number of additional non-exclusive factors, such as advection of allochthonous material, local temperature stratification, and uncertainty in the absolute age of surface sediment samples assumed to be equivalent to modern conditions. We conclude that alkenone unsaturation allows accurate reconstruction of SST records from many regions of the North Atlantic if the factors confounding alkenone paleothermometry detailed here can be excluded.

## 4.2 INTRODUCTION

The application of unsaturated ketones produced by prymnesiophytes as a paleotemperature proxy started with the first documentation of their presence in marine sediments by *Boon et al.* [1978] in a Deep Sea Drilling Project (DSDP) core from the Walvis Ridge in the eastern south Atlantic. In 1980 *Leeuw et al.* confirmed their structure as $C_{37}$ - $C_{39}$ methyl and ethyl ketones and in the same year, *Volkman et al.* [1980] proposed the coccolithophore species *Emiliania huxleyi* as the main producer of long chain alkenones. *Brassell et al*. [1986] then found that the molecular record of long chain alkenones ($C_{37}$ - $C_{39}$) displays a striking resemblance with the glacial-interglacial variability of the foraminiferal $\delta^{18}$O signatures in a sediment core from the eastern equatorial Atlantic highlighting a possibility for reconstruction of past sea surface temperatures. This finding started alkenone paleothermometry. Expressed as an index of alkenone unsaturation, these organic compounds have been used ever since as a proxy for sea surface temperature (SST) reconstruction [*Brassell et al.*, 1986].

$$U_{37}^{K} = \frac{[C_{37:2}] - [C_{37:4}]}{[C_{37:2}] + [C_{37:3}] + [C_{37:4}]}$$

Culture experiments with *E. huxleyi* carried out by *Prahl and Wakeham* [1987] confirmed the temperature dependence of ketone unsaturation: The linear dependence ($U_{37}^{K'} = 0.033T + 0.043$) accurately predicted unsaturation patterns in particulate material collected from seawater of known temperature the coccolith strains grew in, supporting the proposed use as paleotemperature proxy. Based on their experiments, *Prahl and Wakeham* [1987] introduced a simplified version of the ketone unsaturation index, omitting the tetra ketones from the relationship, as they are rarely detectable in marine sediments.

$$U_{37}^{K'} = \frac{[C_{37:2}]}{[C_{37:2}] + [C_{37:3}]}$$

Regionally very focused studies of surface ocean particulate matter [*Freeman and Wakeham,* 1992; *Conte et al.,* 1992; *Conte and Eglinton,* 1993; *Sikes and Volkman,* 1993] reported significant offsets from the original relationship between $U_{37}^{K'}$ and growth temperature introduced by *Prahl and Wakeham* [1987]. However, a calibration based on 370 surface sediment samples globally distributed between 60°S and 60°N [*Müller et al.,* 1998], was intriguingly similar to the calibration equation of *Prahl and Wakeham* [1987]. This field-based global calibration presented by *Müller et al.* [1998] was statistically indistinguishable from the one derived by *Prahl and Wakeham* [1987] based on culture experiments. In addition, *Müller et al.* [1998] compared the $U_{37}^{K'}$ index with Word Ocean Atlas (WOA) temperatures from the surface and subsurface. They showed that the strongest correlation between ketone unsaturation and atlas values is achieved for the upper 10 m. Comparison of $U_{37}^{K'}$ values to SSTs from the four seasons showed that in regions with low seasonal SST difference using only summer rather than mean annual temperatures has a minor effect on the $U_{37}^{K'}$ - SST relationship. However, *Müller et al.* [1998] excluded data from particularly challenging regions such as the Greenland and Norwegian Seas between 66° and 74° N from their calibration. They suggested that these may have been altered by ice rafting or bottom transport of fine-grained, organic-rich sediments, by not well constrained atlas values, or by different physiological response of phrymnesiophytes to very low water temperature. Even though the calibration was restricted to samples from latitudes between 60° N and 60° S covering a wide range in SSTs (0° to 29 °C), deviations from the regression between $U_{37}^{K'}$ and SST were observed at the cold and very warm ends of the data set. To address this problem, *Conte et al.* [2006] carried out a study based on a compilation of 742 coretop samples

covering a variety of marine settings and compared them to 629 samples of surface ocean suspended particulates. Most of this extended set of coretop data, has its best fit with ocean atlas values by a linear regression, statistically indistinguishable from the original calibration of *Müller et al.* [1998]. Alkenone unsaturation measured on surface ocean particulates, however, was shown to exhibit a non-linear relationship in parts of the ocean as in studies before [*Conte and Eglinton*, 1993*; Rosell-Mele*, 1998*; Grimalt et al.*, 2000*; Conte et al.*, 2001*; Sicre et al.*, 2002*; Bendle and Rosell-Mele*, 2004]. In addition, particularly the cold regions with low annual SSTs below 10 °C remained problematic, even with non-linear regression models accounting for some of the non-linearity at the low temperature extremes, [*Conte et al.*, 2006].

### 4.2.1 CALIBRATION AT THE LOW TEMPERATURE END IN THE NORTH ATLANTIC REGION

*Conte and Eglinton* [1993] analyzed suspended particulate matter collected primarily from the euphotic zone of the eastern North Atlantic ranging from cold (< 10 °C) nutrient-rich and highly productive subarctic waters of the Iceland Basin up to warm (> 25 °C) oligotrophic waters off the coast of Africa. Analysis of within class distributions of $C_{37,}$ $C_{38}$ and $C_{36}$ (percentage abundance to the sum total) showed no dependence on nutrient concentrations, bloom status, or other surface water properties. The unsaturation ratio of the alkenones in waters below 16 °C was not correlated with SST. In warm waters (> 16 °C) the alkenone unsaturation ratio increased linearly. *Conte and Eglinton* [1993] suggested that the difference in temperature trends between these two regions may be related to genetic differences between cold and warm water strains of *E. huxleyi* or related species (*Gephyrocapsa sp.*) and could account for the observed difference in temperature dependence of alkenone unsaturation in warm and cold regions. In addition, these authors suggested that multivariate temperature calibrations incorporating all major features of alkenone production would give a more precise temperature estimate over a wide range of paleoenviromental conditions compared to a calibration based on a single variable. In contrast to this analysis of suspended particulate alkenones, long chain alkenones and alkyl alkenoates in sediments from the Northeast Atlantic investigated by *Rosell-Mele and Eglinton* [1993] showed a linear correlation of both the degree of unsaturation and the relative abundance of alkenones and alkenoates with sea surface temperature (5° to 27 °C). In a follow-up study, *Rosell-Mele et al.* [1995] analyzed an extensive dataset of sediment samples from the northeastern Atlantic (2° S -75° N), covering a wide range of temperatures between 0° and 28 °C. They showed that sea surface

temperatures corresponding to winter and autumn months correlate best with alkenone unsaturation ratios, although summer and spring months had a high correlation coefficient as well. Even though they extended the dataset and constrained the sea surface temperatures to a certain production season, data at the cold end (< 5 °C) showed an increased scatter and deviated from linearity.

To constrain monthly variability and the potential influence of specific oceanographic features (eddies, upwelling zones), an extensive sediment trap study was carried out by *Rosell-Mele et al.* [2000]. The sediment trap station was located within the North Atlantic Transition Zone and was investigated as part of the Joint Global Ocean Flux Study (JGOFS) and the North Atlantic Bloom Experiment from April 1989 until March 1990. As the timing of the only bloom observed was not equivalent to the timing of the maxima of alkenone flux elsewhere in the ocean, they concluded that, based on their dataset, this does not justify the assumption of a world-wide uniform season of coccolithophoride blooms. This inference has been corroborated by a more recent synthesis of all available sediment trap time series of alkenone flux at 34 sites from all major ocean basins [*Rosell-Mele and Prahl*, 2013].

Based on samples of surface ocean suspended particulate matter covering a wide range of temperatures in the North Atlantic, including the Nordic Seas (4° - 20 °C), *Sicre et al.* [2002] found a linear correlation between $U_{37}^{K'}$ and temperature in cold surface waters, and a linear correlation of the relative abundance of tetra alkenones with temperature below 12 °C. This contrasts with results obtained by *Rosell-Mele* [1998] from the same area, that showed no correlation of $U_{37}^{K'}$ with SSTs for temperatures below 10 °C for sediment samples. In the latter publication it was found that the abundance of tetra-unsaturated alkenones in sediment samples relative to the total abundance of alkenones collected in the area of Nordic Seas does not correlate with SST at $C_{37:4}$ contents > 5 % of the total sum of $C_{37}$ alkenones, but a linear correlation with overlying sea surface temperature was observed for lower concentrations. Based on these results, *Rosell-Mele* [1998] proposed to use $C_{37:4}$ abundances exceeding 5 % to identify settings where $U_{37}^{K'}$ paleothermometry is unreliable. Additionally, *Rosell-Mele* [1998] proposed that variations in salinity may be responsible for changes in sedimentary records of tetra alkenone abundance and obtained a preliminary calibration for $C_{37:4}$ % = $f$(salinity), which was supported by the observation of a strong correlation between % $C_{37:4}$ and salinity in the data of *Sicre et al.* [2002]. However, a compilation study by *Sikes and Sicre* [2002] based on surface water and sediment trap samples carried out in the North and Equatorial Atlantic, the western Equatorial Pacific, and the Australian and Indian sectors of the Southern Ocean showed no salinity influence on $C_{37:4}$ in the open ocean or in cold waters.

According to *Sikes and Sicre* [2002], any correlation between tetra alkenone abundance and salinity (particularly in North Atlantic) could be an artifact of salinity and temperatures closely co-varying in this region.

In an attempt to clarify the importance of the tetra-unsaturated alkenones and to delimit the applicability of the $U_{37}^{K}$ and $U_{37}^{K'}$ indexes for SST estimation in the subpolar and polar regions of the North Atlantic, *Bendle and Rosell-Mele* [2004] compared sea surface POM data with previously reported sedimentary data from the same region, and suggested that $U_{37}^{K}$ correlates better with SSTs for POM from the Nordic Seas. However, due to the high abundance of tetra-unsaturated alkenones the application of $U_{37}^{K}$ can lead to negative values in some instances. To avoid this, *Bendle and Rosell-Mele* [2004] introduced an alternative index, $U_{37}^{K^*}$, to estimate SSTs for samples with significant concentrations of $C_{37:4}$, defined as

$$U_{37}^{K^*} = \frac{C_{37:2}}{C_{37:2} + C_{37:3} + C_{37:4}}$$

However, this index did not resolve the major discrepancies between POM and surface sedimentary data

Despite these uncertainties, however, a number of recent studies have successfully used alkenone unsaturation in the western North Atlantic as a proxy for SST reconstruction. For instance, *Sicre et al.* [2008] showed a record of decadal-scale SST variability off North Iceland during the last 2,000 years, in which differences between the Medieval Warm Period and the Little Ice Age are resolved. In a more recent study, *Sicre et al.* [2014] inferred Labrador Current variability over the last 2,000 years from $U_{37}^{K} -$ derived SST contrast between NE and SE Newfoundland. This is superimposed on a longer-term cooling trend during the Holocene inferred by *Sachs et al.* [2007]. At all these study sites, surface sediment alkenone unsaturation-index derived temperature estimates agree within analytical and calibration uncertainties with modern SSTs.

Here we synthesize published alkenone unsaturation data from surface sediments (n = 101) in the North Atlantic north of 30° N, which are complemented by 51 new data points, including data from previously undersampled regions of the SW Labrador Sea. Three different alkenone unsaturation indexes ($U_{37}^{K}$, $U_{37}^{K'}$, and $U_{37}^{K^*}$) are regressed against annual mean and mean spring-summer temperatures. Scatter of alkenone unsaturation versus SST around the global linear regression established by *Müller et al.* [1998], i.e. residuals, are discussed in the context of the possible input of allochthonous alkenones from other areas of the Atlantic, particularly from ocean frontal systems with large SST gradients, sea surface salinities and sea ice extent. The warm offset in the Nordic Seas is explained as a possible

result of water restratification and surface water warming. Furthermore, we compare the uncertainty of alkenone paleothermometry at the cold end of the regression to other geochemical SST proxies.

## 4.3 METHODS

### 4.3.1 ANALYTICAL METHODS

Details of sampling and laboratory procedures for previously published data can be found in the original publications by *Rosell-Mele* [1998], *Marmen* [2000], *Conte et al.* [2006] and *Rodrigo-Gamiz et al.* [2015]. The new data presented in this study are from the western coast of the Labrador Sea, the Gulf of Maine, off the coast of Nova Scotia, the Newfoundland Bank, the Flemish Cap, the Orphan Basin and the southeastern margin of Greenland (Fig. 1 A, Table A1). Alkenone extraction, purification and quantification were carried out at Dallhousie University, Halifax, Canada, following established protocols [*Dubois et al.*, 2011].

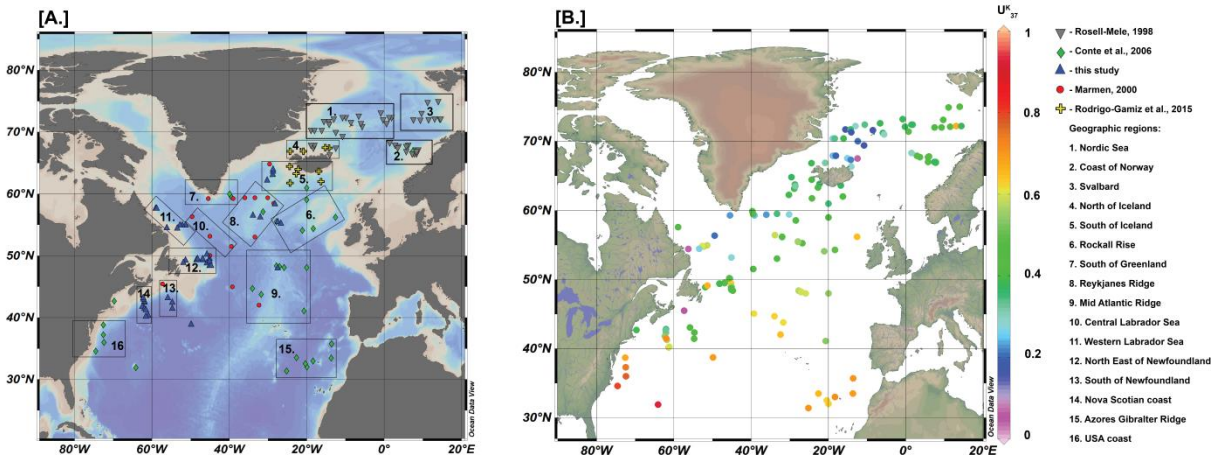


**Figure 1** Map of sample locations. A. Different geographical regions are marked by boxes, symbols represent different laboratories. Data from Rosell-Mele, 1998; Marmen, 2000; Conte et al., 2006; Rodrigo-Gamiz et al., 2015; this study. B. Map of alkenone unsaturation ratios, expressed as $U^{K}_{37}$ in N Atlantic surface sediments.

Briefly, two grams of freeze-dried, homogenized material were extracted using an automated solvent extraction system (Dionex ASE) at 1000 psi pressure and 100 °C with five minute static phases, using a mixture of methylene chloride and methanol (9:1 v/v). Prior to GC analysis, a standard solution of hexatriacontane was added to every sample. Samples were saponified for 2 hours at 80 °C prior to silica column separation into different fractions.

The extracts were analyzed by capillary gas chromatography with a flame ionization detector, Aglient, model 6890 equipped with a 60 meters long CP-Sil 5CBH column. During each run, a set of internal standards and the extract of a strain of *E. huxleyi* CCMP1742 were

measured. Peak areas of $C_{37:2}$; $C_{37:3}$; $C_{37:4}$ and $C_{38:2Me}$; $C_{38:Et}$; $C_{38:3Et}$; $C_{38:Me}$; $C_{38:3ee}$ were defined based on retention times of the *E. huxleyi* culture extract, with limit of quantification (LOQ) defined as 10 times background noise. The recovery calculated based on the internal standard added prior to the extraction was on average 75 %. Twenty-one samples were run twice and one sample was run 3 times to estimate the repeatability of the measurement. The average difference between the repeat runs was 0.07 $U_{37}^{K}$ values (2 S.D. = 0.13), resulting in 1.7 °C degree offset between the values on average. Five samples with really high differences between repeat runs, from 0.11 to 0.21, showed alkenone concentrations near detection limit. These five samples from the SW Labrador Sea also exhibit high residuals (from 7° to 12 °C). Exclusion of these samples leads to an average difference of 0.03 $U_{37}^{K}$ units (2 S.D. 0.05), resulting in an average difference of 1.05 degree C. By comparison, *Rosell-Mele et al.* [2001] showed interlaboratory comparability of $U_{37}^{K}$ determinations to be 1.6 °C.

A number of samples/data were excluded from the final data set analyzed below, including samples for which alkenones were not detectable (n = 14), as well as samples for which either or both the $C_{37:2}$ or $C_{37:3}$ ketone concentrations are below the limit of quantification (n = 36). Most of the samples with very low alkenone concentrations are found along the SW Labrador Sea margin. Finally, two samples with negative $U_{37}^{K}$ values due to particularly high tetra alkenone concentrations were removed from the final dataset, as they lead to unreasonably cold SSTs.

### 4.3.2 DATA SOURCES AND ANALYSIS

Sea ice data were collected from NSIDC Virtual Globes (http://nsidc.org/data/google_earth/) for the period from 1979 up to 2014 and presented as sea ice intensity index (number of times when sea ice was detected at this location over this period). Data are available for two months: March (maximum sea ice extent) and September (minimum sea ice extent) (NSIDC Virtual Globes). No ice was detected at any of the sample locations over this period for September.

Mean annual and monthly SST from March to September, and mean annual salinity were obtained from the World Ocean Atlas (WOA) 2013, based on 0.25 grid interpolation (http://www.nodc.noaa.gov/OC5/woa13/). Updated WOA 2013 annual and spring-summer temperatures were used for comparison to all alkenone unsaturation data, including previously published ones.

In the northern hemisphere, coccolithophoride blooms occur over spring and summer, with a minor peak in March and a major one in August [*Brown and Yoder,* 1994; *MODIS sub-*

*surface Chlorophyll-A concentration*]. We therefore compare alkenone unsaturation ratios to mean annual SSTs and to the mean SST of all potential production months (sp-su_SST or spring summer surface temperature).

Data from the different studies were analyzed separately, to account for any potential bias introduced from the synthesis into one dataset due to differences in the laboratory procedures in different laboratories. The full dataset was also divided into different geographical regions, (Fig. 1 A), and each region was analyzed separately.

### 4.3.3 AGE CONSTRAINTS

Very few direct age constraints are available to ascertain that surface sediment samples are actually "modern". Surface sediment alkenone unsaturation data presented by *Rosell-Mele* [1998] represent an averaged signal over hundreds up to a few thousands of years, according to the authors [*Rosell-Mele et al.*, 1995, *Rosell-Mele*, 1998].

Data collected by *Marmen* [2000] most likely represent surface sediment samples covering a few thousands of years (3-5kyrs), based on the available $^{14}C$ dates of surface samples [http://www.unites.uqam.ca/geotop/paleoceanographicDatabase].

No data on the age constraints of their surface sediment samples are presented in the original publications by *Rodrigo-Gamiz et al.* [2015] and *Conte et al*. [2006]. Likewise, none of the surface sediment samples presented here were dated directly.

## 4.4 RESULTS

To define the most suitable unsaturation index for alkenone paleothermometry in the North Atlantic and to establish the ocean temperature most accurately reflected by alkenone unsaturation, mean annual and sp_su SST were regressed against the three different indexes, $U_{37}^{K}$, $U_{37}^{K'}$ and $U_{37}^{K^*}$. Overall, all three indexes have a moderate positive correlation with both mean annual and sp-su SSTs, with $r^2$ coefficients between 0.42 and 0.52 (Table 1). RMSD values [°C] (or root mean square error, RMSE, i.e. the square root of the mean square error) are calculated based on the residuals (shown in Fig. 2), calculated as modern SST minus SST reconstructed from, $U_{37}^{K}$, $U_{37}^{K'}$ and $U_{37}^{K^*}$ based on the calibration of *Müller et al.* [1998]. The $r^2$ and RMSD for separate analyses of data from each individual laboratory are available in Table A2.

Comparison of the three alkenone unsaturation indexes suggests that including the tetra-unsaturated alkenones in the index improves the correlation measures for the entire data set (higher $r^2$ and lower RMSD, °C). Although $U_{37}^{K}$ and $U_{37}^{K^*}$ do not uniformly improve regression for all the samples where tetra-unsaturated alkenones were detected, these indexes

appear to be more representative of cold regions, with $U^{K}_{37}$ showing the best correlation of $r^2$ = 0.51 versus annual SST and 0.52 versus spring-summer SST and the closest agreement at low SSTs with the global calibration of *Müller et al* [1998], i.e. lowest RMSD (Fig. 2 A,B). However, no overall correlation between SST and the abundance of tetra-unsaturated alkenones is observed, suggesting that their presence might reflect the influence of yet unknown factors prevailing in cold settings. Analysis of the data from different laboratories shows that the best correlation between alkenone unsaturation and SSTs comes from *Conte et al.* [2006], *Marmen* [2000] and *Rodrigo-Gamiz* et al. [2015] (Table A2). Data presented in these studies have highest correlation ($r^2$ of around 0.8) and lowest RMSD (< 2.6 °C). Conversely, most of the scatter with lowest correlation comes from the new data presented in this study and the data from *Rosell-Mele* [1998]. Given that close-by samples analyzed in different laboratories agree with each other within less than 0.09 $U^{K}_{37}$ units (equivalent to less than 2 °C) along the Mid Atlantic Ridge, the Reykjanes Ridge or south of Iceland, offsets between different laboratories of up to 3-5 °C for close-by samples from NE of Newfoundland, North of Iceland, and off the coast of Norway are likely due to the overall distribution of uncertainty (residuals) of alkenone paleothermometry in the North Atlantic (see Fig. 3), rather than systematic offsets between individual laboratories.

Correlation coefficients are generally higher when alkenone unsaturation is regressed against spring-summer rather than mean annual SSTs, with the highest coefficients for $U^{K}_{37}$ ($r^2$ = 0.52); however the difference with the $r^2$ for annual_SST (0.51) is insignificant. Comparison of RMSD values for sp-su versus annual mean SSTs for the $U^{K}_{37}$ index also shows that spring-summer temperatures reflect the modern temperatures of alkenone production most accurately (Table 1).

Analysis of the data set separated by different geographical regions (21 in total, 16 with more than one sample; Table S4.3), supports these observations. In almost all geographical regions, $U^{K}_{37}$ gives lower RMSD for both SSTs (Fig. A1 A,B). This is particularly true in the cold regions. The best accuracy is achieved with $U^{K}_{37}$ regressed against sp_su_SST (Fig. 3C). Overall, the increased scatter at low temperatures is non-random, with deviations from the global regression highly weighted towards a warm bias (also evident from the overall lower slope of the regional regressions presented here compared to *Müller et al.*, 1998; Fig. 3 A,D, Fig. A2) and maximum deviations toward higher alkenone unsaturation indexes.

| Data analyzed | Data removed | Number of samples | | Ann_SST WOA 2013 | | | Sp_Su_SST WOA, 2013 | | |
|---|---|---|---|---|---|---|---|---|---|
| | | | | $U^{K}_{37}$ | $U^{K'}_{37}$ | $U^{K*}_{37}$ | $U^{K}_{37}$ | $U^{K'}_{37}$ | $U^{K*}_{37}$ |
| Rosell-Mele, 1998; Conte et al., 2006; Marmen, 2000; This study; Rodrigo-Gamiz et al., 2015 | Full data set | 152 | $r^2$ | 0.51 | 0.43 | 0.49 | 0.52 | 0.42 | 0.48 |
| | | | 2sdev | 7.94 | 8.31 | 7.9 | 8.03 | 8.58 | 8.09 |
| | | | RMSD | 5.01 | 6.01 | 5.65 | 4.84 | 5.85 | 5.46 |
| | | | SEM | 0.32 | 0.34 | 0.32 | 0.33 | 0.35 | 0.33 |
| Conte et al., 2006; Marmen, 2000; This study; Rodrigo-Gamiz et al., 2015 | Rosell-Mele, 1998 (removed) | 106 | $r^2$ | 0.3 | 0.32 | 0.34 | 0.28 | 0.31 | 0.34 |
| | | | 2sdev | 8.42 | 8.06 | 7.98 | 8.52 | 8.21 | 8 |
| | | | RMSD | 4.95 | 5.15 | 5.06 | 4.74 | 4.91 | 4.8 |
| | | | SEM | 0.41 | 0.39 | 0.39 | 0.41 | 0.4 | 0.39 |
| Rosell-Mele, 1998; Conte et al., 2006; Marmen, 2000; Rodrigo-Gamiz et al., 2015 | This study (removed) | 101 | $r^2$ | 0.71 | 0.61 | 0.67 | 0.71 | 0.61 | 0.68 |
| | | | 2sdev | 6.48 | 7.7 | 7.04 | 6.56 | 7.84 | 7.14 |
| | | | RMSD | 4.01 | 5.61 | 5.03 | 3.91 | 5.51 | 4.92 |
| | | | SEM | 0.32 | 0.38 | 0.35 | 0.33 | 0.39 | 0.36 |
| Conte et al., 2006; Marmen, 2000; Rodrigo-Gamiz et al., 2015 | This study; Rosell-Mele, 1998 (removed) | 55 | $r^2$ | 0.81 | 0.84 | 0.85 | 0.82 | 0.86 | 0.87 |
| | | | 2sdev | 5.11 | 5 | 4.74 | 5.12 | 4.82 | 4.59 |
| | | | RMSD | 2.7 | 3.01 | 2.79 | 2.6 | 2.74 | 2.54 |
| | | | SEM | 0.34 | 0.34 | 0.32 | 0.35 | 0.32 | 0.31 |
| Conte et al., 2006; Marmen, 2000 | This study; Rosell-Mele, 1998; Rodrigo-Gamiz et al., 2015 (removed) | 45 | $r^2$ | 0.82 | 0.81 | 0.83 | 0.82 | 0.83 | 0.85 |
| | | | 2sdev | 5.11 | 5.24 | 4.87 | 5.06 | 4.97 | 4.6 |
| | | | RMSD | 2.58 | 2.98 | 2.69 | 2.5 | 2.68 | 2.43 |
| | | | SEM | 0.38 | 0.39 | 0.36 | 0.38 | 0.37 | 0.35 |
| all other geographical regions | Western Labrador removed | 145 | $r^2$ | 0.58 | 0.5 | 0.55 | 0.58 | 0.49 | 0.55 |
| | | | 2sdev | 7.3 | 7.82 | 7.37 | 7.42 | 8.05 | 7.55 |
| | | | RMSD | 4.59 | 5.61 | 5.23 | 4.43 | 5.43 | 5.04 |
| | | | SEM | 0.3 | 0.32 | 0.31 | 0.31 | 0.33 | 0.31 |

**Table 1** Analysis of the complete dataset with removal of data sets from different laboratories.

Two main regions can be defined where negative residual temperatures are largest: the SW Labrador Sea and the Nordic Seas. In both regions, surface temperatures during bloom or spring-summer seasons rarely exceed 5 °C and intermediate and low salinities (<34.5 ‰) prevail year round.

Whereas the concentrations of individual alkenones do not correlate with salinity, the overall lowest temperature residuals are observed at salinities above 35 (Fig. 3 B,E, Fig. S4.3). However, even at lowest salinities, residuals are near zero in some locations, e.g., close to the Gulf of Maine.

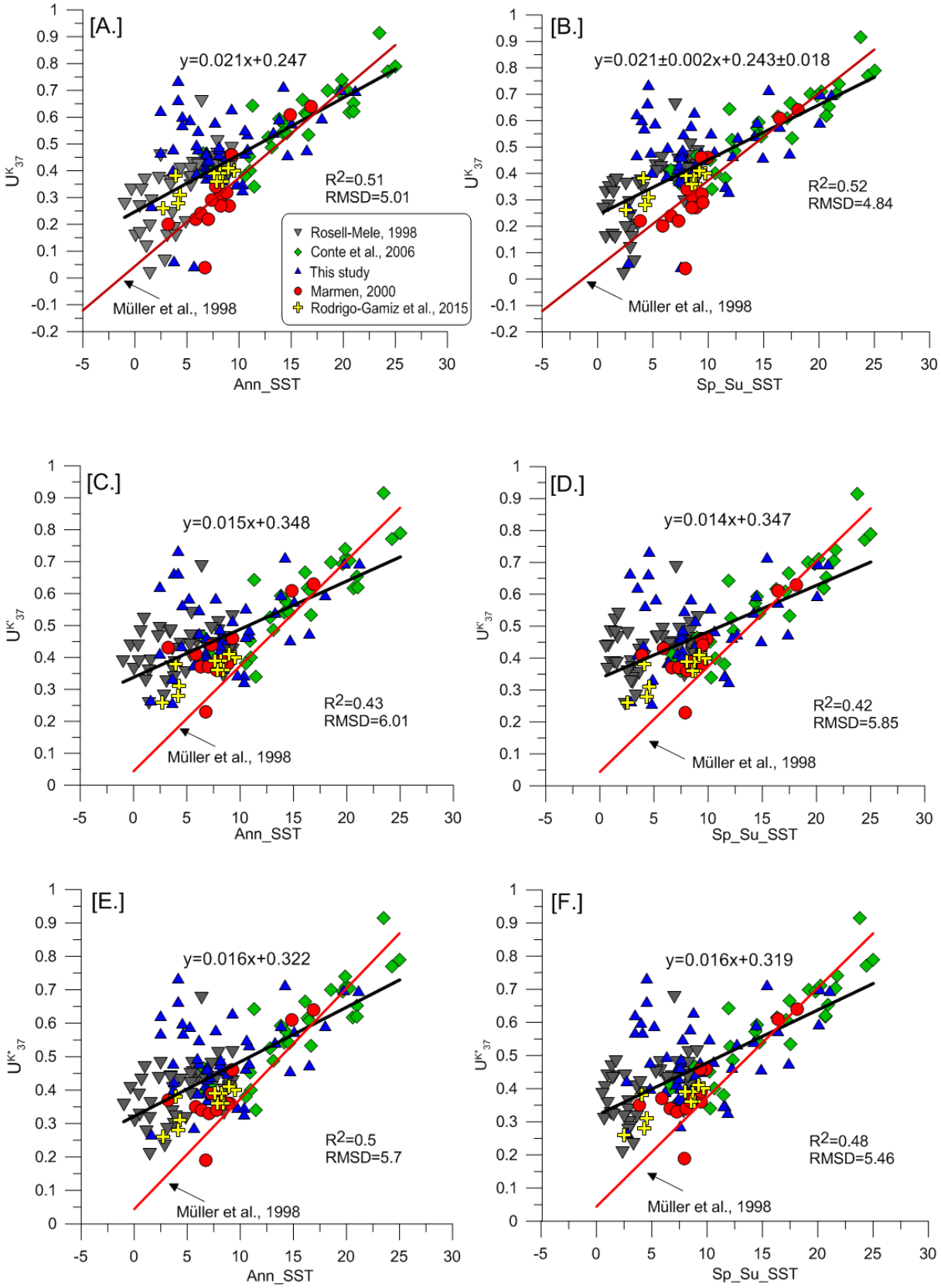


**Figure 2** Alkenone unsaturation ratios ($U_{37}^{K}, U_{37}^{K'}, U_{37}^{K^*}$) versus WOA SST. A. $U_{37}^{K}$ vs mean annual SST B. $U_{37}^{K}$ vs sp_su SST C. $U_{37}^{K'}$ vs mean annual SST D. $U_{37}^{K'}$ vs sp_su SST E. $U_{37}^{K^*}$ vs

annual SST F. $U_{37}^{K*}$ sp_su SST. Linear fits (black line) and corresponding equations are shown together with correlation coefficients ($r^2$). RMSD [°C] values are calculated versus the global linear regression equation of *Müller et al.*.[1998; red line; see text].

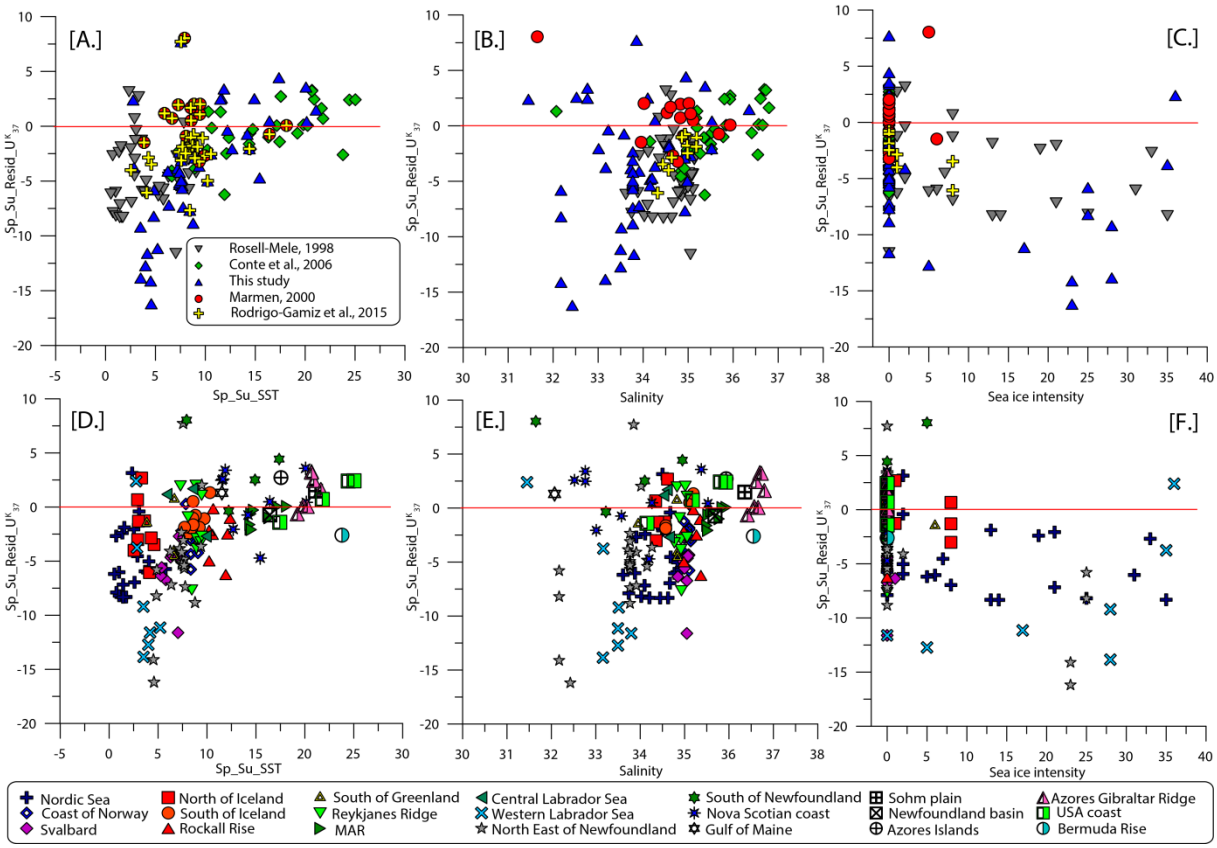


**Figure 3** $U_{37}^{K}$ Sp_Su residuals for different studies versus A. Sp_Su SST. B. Salinity. C. Sea ice intensity. $U_{37}^{K}$ Sp_Su residuals of different geographical regions versus D. Sp_Su SST E. Salinity F. Sea ice intensity. All data are provided in the supplementary material (Fig. A2, A3, A4).

Analysis of sea ice cover over a period of 35 years shows that there are two main areas exposed to annual winter sea ice conditions lasting to at least the end of March: the western coast of the Labrador Sea and northeastern side of Greenland. Overall, no correlation is observed between sea ice intensity and residual temperatures for all three indexes (Fig. 3C, Fig. A4). However, almost all sample sites with significant sea ice presence coincide with regions also characterized by large negative temperature residuals.

Comparison of the linear regression with highest correlation coefficient based on the compiled data ($U_{37}^{K}$ versus sp_su_SST; $U_{37}^{K}$ = 0.021T+0.243) with the two global calibration equations of *Müller et al.* [1998] and *Conte et al.* [2006] shows a significant difference in the slopes and intercept. This difference is not surprising, however, given that *Müller et al.* [1998]

explicitly excluded the North Atlantic samples deviating from the global calibration line, and *Conte et al.* [2006] excluded the Nordic Seas data as well. However, the regression versus SST of the North Atlantic alkenone unsaturation data synthesized here also differs from previously published calibrations for the NE Atlantic by *Rosell-Mele* [1995] and for the Atlantic Ocean by *Müller et al.* [1998].

## 4.5 DISCUSSION

Compared to the simple correlation coefficient $r^2$, RMSD (RMSE) is more informative, because it reflects the difference between the values predicted by a model and values observed in nature. Accordingly, the most accurate model for estimating SSTs from alkenone unsaturation in the (northern) North Atlantic is the $U^{K}_{37}$ index, which shows lowest RMSDs. Even though tetra alkenones are not detectable in all samples from the North Atlantic and the concentration of tetra-unsaturated alkenones does not correlate with SST, their inclusion in the equation helps to more accurately predict SSTs in cold regions (Table 1, Table A3). At sites where tetra alkenones are not detectable, $U^{K}_{37}$ values are identical to the $U^{K'}_{37}$ index, without introducing an additional error. In case the use of $U^{K}_{37}$ index leads to negative values of the unsaturation index, these samples should be discarded from the analysis (only two samples in this study).

Even though the North Atlantic $U^{K}_{37}$ correlate with SSTs, the absolute RMSD is a factor ~ 3 larger than the commonly accepted uncertainty of alkenone paleothermometry [1.2 °C, *Conte et al.*, 2006]. In the following we discuss a number of non-exclusive explanations of the large residual temperature at low SSTs, other than the presence of sea ice mentioned above.

### 4.5.1 INTRODUCTION OF ALLOCHTHONOUS ALKENONES AND LATERAL ADVECTION

The spatial distribution of the samples with high temperature residuals indicate that largest residuals coincide with areas of the ocean characterized by steep gradients and frontal systems, such as the western Labrador Sea and North East of Newfoundland. This is illustrated by a correlation of residual temperatures with SST gradient calculated in km (shortest distance over which a change in SST of 1 °C occurs, Fig. 4, Fig. A5, Fig. A.6). Most of the samples with residuals between 5 and 10 °C lie in areas of particularly steep temperature gradients. This is especially true for regions with overall low SSTs. On the other hand, samples from areas of low SST gradients, and even from regions of high gradients but overall warmer SSTs show small residuals, such as the Azores-Gibraltar Ridge, the MAR,

south of Iceland or off Nova Scotia and off the northeastern USA coast, respectively. This could imply that in strongly temperature stratified waters or highly dynamic ocean environments mean WOA temperature fields do not capture the highly dynamic SST variability, thereby introducing a bias. On the other hand, lateral transport of material by only a few kilometers during settling and depositions has the potential in regions characterized by steep SST gradients to introduce allochthonous alkenones not reflective of the immediate sea surface at the core site. In the regions off the coast of Nova Scotia and south of Newfoundland residuals range from 1° to 5 °C, which could similarly be explained by the advection of warm and saline waters by the North Atlantic current (NAC), which mix with cold and fresh waters, from the Gulf of St. Lawrence and from the Gulf of Maine (Fig. 5).

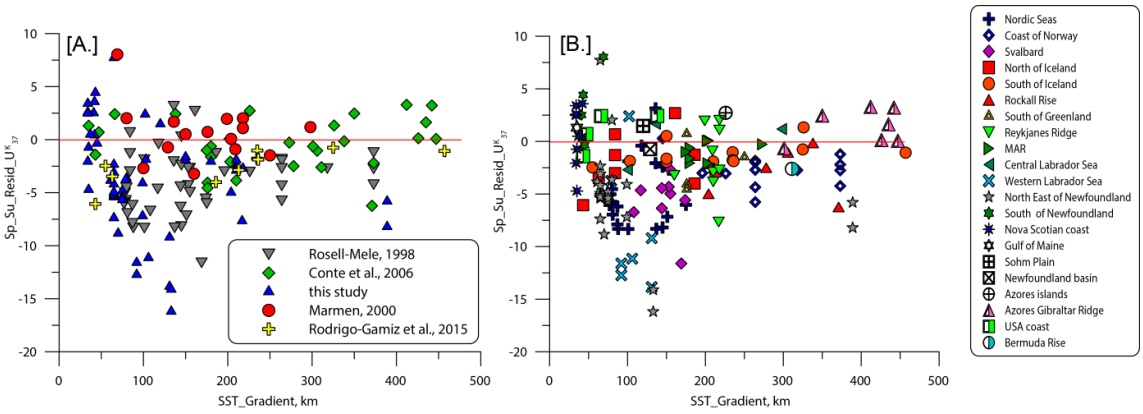


**Figure 4** Residuals versus SST_Gradient [km; see text]. A. $U^{K}_{37}$-Sp_Su residuals for data from different studies. B. $U^{K}_{37}$-Sp_Su residuals by geographical regions. (Complete figures for all annual and spring-summer residuals by laboratories and geographical regions are provided in supplementary materials Fig. A5 and A6, respectively).

The western coast of the Labrador Sea is the region of the highest RMSD values (> 10 °C; Table 3, sup. mat.). It is also a region of very low overall alkenone concentrations (see 2.1 above). It is conceivable that allochthonous alkenones from geologically warmer periods have been introduced to near-coastal sites or to sites with significant deposition of ice rafted detritus. *Mao et al.* [2014] speculate that alkenone-based SST estimates far exceeding possible surface ocean temperatures in the Labrador Sea are the result of glacial erosion on the continental shelf of Cretaceous and Paleogene highstand limestone and chalks, which contain abundant coccolithophores, and by inference also alkenones.

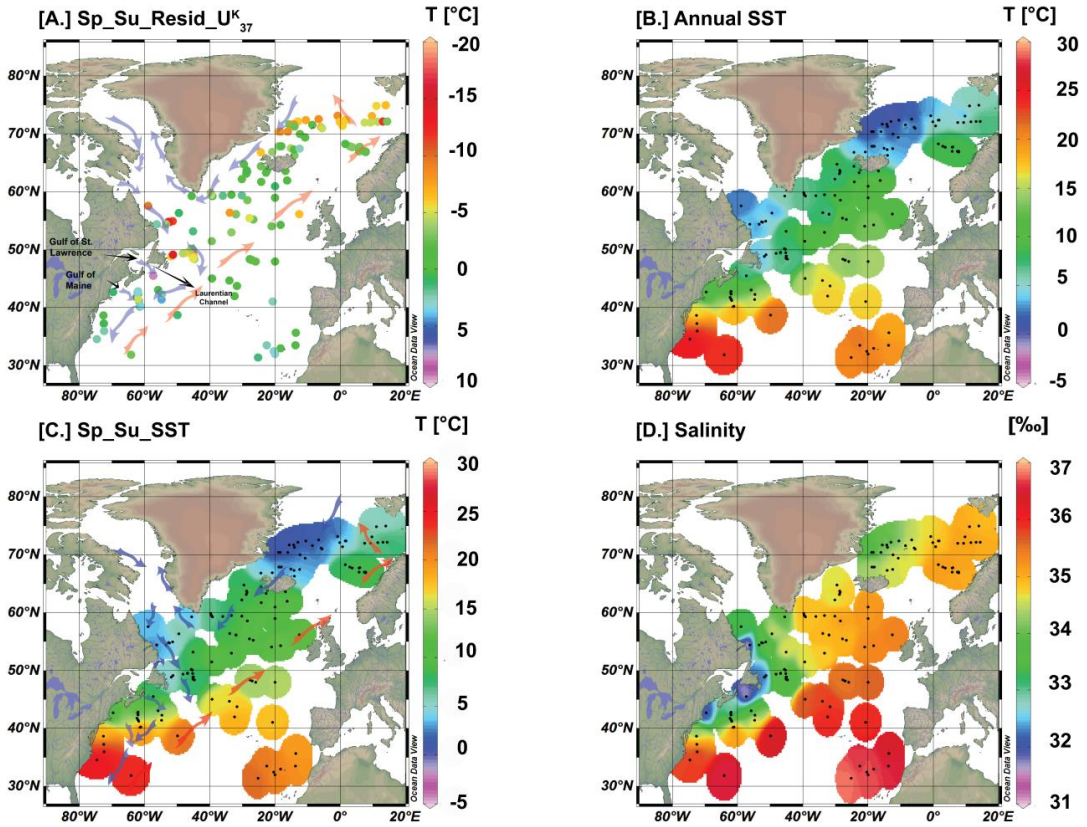


**Figure 5.** Maps of A. $U_{37}^{K}$-Sp_Su residuals compared with B. Annual SST C. Sp_Su SST D. Salinity.

### 4.5.2 TEMPERATURE STRATIFICATION IN THE NORDIC SEAS

It is plausible that local ocean restratification followed by changes in SST, not reflected in the modern surface temperature data sets like WOA, takes place in some of the regions of the North Atlantic Ocean prone to fresh water intrusions. In a series of sensitivity experiments *Kleinen et al.* [2009] showed that fresh water input to the North Atlantic can lead to enhanced warming of subsurface layers in the Nordic Seas. Using four different scenarios of freshwater discharge, their model runs indicate that freshwater discharge may cause a decrease of the subpolar gyre circulation, which leads to an increase of water mass transport into the GIN Sea (Greenland Scotland Iceland). Due to this change in subpolar gyre circulation, a warmer subsurface layer is transported below the surface of the GIN Sea. As convection starts, warm waters mix vertically in the water column resulting in a strong increase of SST and salinity. These experiments showed that in the center of GIN Seas surface temperature increases caused by this mechanism can reach up to 4 °C [*Kleinen et al.*, 2009], which is in quantitative agreement with the average warm bias of 3.5 for this region. In addition, their modelling results indicate areas where freshwater discharge will cause a

decrease in SST, which agree reasonably well with locations of those samples where cold offsets were recorded [Fig. 2 in *Kleinen et al.*, 2009].

Melt water inputs to the Nordic Seas from Greenland may also induce changes in salinity. These changes could push the prymnesiophytes out of their salt tolerance zone [*Shelford*, 1931], thus causing a change in their alkenone biosynthesis. This might also explain why in this particular region *Rosell-Mele et al.* [1998, 2002] observed a close relationship between salinity and changes in the concentration of $C_{37:4}$.

### 4.5.3 NON-MODERN CORE TOP SAMPLES

Almost all proxy calibration studies relying on surface sediments (tacitly) assume that core tops represent modern sedimentary material. This will not be the case at many sites, however. In particular, sediment dynamics along the SW Labrador Sea are notorious for leaving large swaths of the margin devoid of any sediment cover representing the accumulation of the last few thousands of years [*Wu and Hillarie-Marcel*, 1993]. Given the indications that early to mid Holocene SSTs were much warmer in parts of the North Atlantic [*Moros et al.*, 2004; *Leduc et al.*, 2010], it is conceivable that some of the warm biases are a reflection of SSTs of the early to mid Holocene rather than systematic residual temperatures. This could only be fully resolved by $^{14}C$ ages for all surface sediment samples.

A general analysis of the existing age models from different sites all over the North Atlantic indicates that a lot of regions in this study might represent older sediments, with a few exceptions. Based on the study from *Wu and Hillarie-Marcel* [1993] we can assume that most of the samples located over the slopes of the Labrador Sea represent much older sediment, possibly as old as early Holocene. However, in the Central Labrador Sea, where the topography is different, sediment samples should represent modern ages, not older than 1 kyr [*Wu and Hillarie-Marcel*, 1993]. On the other hand, samples collected off the coast of Africa, off the coast of the US and around the Mid Atlantic Ridge (MAR) are likely to represent modern ages, not older than 1 kyrs [*Chapman et al.*, 1996; *Bout-Rouzmazeilles et al.*, 1997; *Vogelsang et al.*, 2000; *Saenger et al.*, 2011].

### 4.5.4 COMPARISON OF UNCERTAINTY OF TEMPERATURE PROXIES AT THE COLD END

Regions of extreme temperature conditions have proven to be a challenge for almost all proxies used to reconstruct past surface sea water temperatures.

The sensitivity of the Mg/Ca proxy decreases with decreasing SSTs, because of the non-linearity of the relationship between temperature of precipitation and Mg/Ca. For instance, [*Meland et al.,* 2005] showed that Mg/Ca ratios in foraminifera are poorly correlated with calcification temperature, or with $\delta^{44/40}$ Ca signatures, in polar waters, where peak summer temperatures are below 3 °C [*Kozdon et al.,* 2009]. Samples, recovered from the Nordic Seas and around Iceland show a large offset ranging from 1 to 8 °C for both Mg/Ca and $\delta^{44/40}$ Ca [*Kozdon et al.,* 2009]. The average offset is 3 to 4 °C, which is similar to the RMSD of the alkenone data discussed here.

Similarly, $TEX_{86/}TEX^{L}_{86}$ in surface sediment samples from subpolar and polar regions [*Ling Ho et al.*, 2014] show a considerable scatter in the $TEX_{86}/TEX^{L}_{86}$ - SST relationship for samples collected from the temperature range between -2 to 17 °C, with large residuals of up to -15 to -20 °C for some of the samples, with RMSD of 3.91 °C and 4.92 °C, respectively. However, similar to $U^{K}_{37}$, some of the subpolar regions express a robust relationship between these indices and SST.

Dinocyst assemblages, in comparison to other geochemical proxies, have lower RMSDs for modern winter and summer SSTs (1.2 and 1.7 degrees C, respectively) [*de Vernal et al.,* 2011]. However, uncertainties of reconstructions in the past can increase significantly because of non-analog assemblages (ibid.).

Overall, the uncertainty of SST prediction from alkenone unsaturation (up to 5 °C) is therefore comparable to the uncertainties of other geochemical proxies in the North Atlantic region.

## 4.6 SUMMARY AND CONCLUSIONS

The synthesis of 101 previously published and 51 new alkenone unsaturation ratios obtained from surface sediments in the North Atlantic north of 30° N confirms that alkenone unsaturation is correlated with surface ocean temperatures. Even though $C_{37:4}$ concentrations are not correlated with SSTs themselves, the strongest correlation is obtained if unsaturation ratios including the tetra-unsaturated alkenones are regressed against spring-summer temperatures. The $U^{K^*}_{37}$ index proposed to best relate alkenone unsaturation to SSTs in the Nordic Seas [*Bendle and Rosell-Mele*, 2004] does not improve the regression for the North Atlantic overall.

In particular at cold temperatures, the unsaturation ratio is significantly higher at many sites than would be expected from SSTs, resulting in uncertainties, expressed as residual temperatures, much larger than observed from global calibrations [*Müller et al.,* 1998; *Conte*

*et al.*, 2006] of alkenone unsaturation ratios against SSTs. A number of possible non-exclusive sources of this warm bias are entertained. Even though residual temperatures do not correlate with sea ice intensity, almost all sites that are covered by sea ice during parts of the year show a warm bias. Regions of largest temperature residuals coincide with areas of the North Atlantic characterized by steep SST gradients and frontal systems. Analogous to similar offsets observed in oceanographically dynamic regions off Namibia [*Schneider et al.*, 1996] and off Peru [*Kienast et al*., 2012], this could imply that the $U_{37}^{K}$ ratio is biased if alkenones are produced in strongly temperature stratified waters or in environments affected by highly dynamic SST variability not captured by mean WOA temperature fields. Finally, allochthonous alkenones from Cretaceous and Paleogene carbonates that outcrop around the Labrador Sea are a possible source of the observed warm bias there.

Despite these uncertainties, alkenone unsaturation is shown to follow established global regression models of $U_{37}^{K}$ versus SST in parts of the northern North Atlantic, in particular in marginal environments not affected by highly dynamic surface ocean conditions and sedimentology, including south of Iceland, Greenland, and the western Atlantic continental margin. In other regions, however, including the southwestern Labrador Sea and the Nordic Seas, SSTs inferred from alkenones are much too warm at many sites. The overall uncertainty of prediction, however (up to 5 °C), is comparable to the uncertainty related to other geochemical SST proxies, Mg/Ca and $TEX_{86}$. A combination of compound-specific radiocarbon dating [e.g. *Ohkouchi et al.*, 2002; *Mollenhauer et al.*, 2005] and isotope tracking [e.g. from dD, *Engelbrecht et al.* 2005] in future studies will help test some of the causes entertained here of the large positive temperature residuals observed throughout the northern North Atlantic.

## ACKNOWLEDGEMENTS

This study was supported by a PhD fellowship to A.F. through the Helmholtz Research School on Ocean System Science and Technology (www.hosst.org) at GEOMAR Helmholtz Centre for Ocean Research Kiel (VH-KO-601) and Kiel University, and by the Discovery Grant program of the National Science and Engineering Research Council (NSERC) Canada (M.K.). We thank David Piper and Anne de Vernal for discussion, and Claire Normandeau for assistance during laboratory experiments. David Piper and the Bedford Institute of Oceanography kindly and generously provided surface sediment material. Dan Kelley provided help calculating SST gradients from WOA SST data. We gratefully acknowledge the thoughtful and constructive comments on an earlier iteration of this

contribution by two anonymous colleagues, which helped improve this manuscript. The additional graphs not included in the main text can be found in the supporting material.

## REFERENCE LIST


Bendle, J. and A. Rosell-Mele (2004), Distribution of $U_{37}^{K}$ and $U_{37}^{K'}$ in the surface waters and sediments of the Nordic Seas: Implications for paleoceanography, Geochemistry, Geophysics, Geosystems, 5, Q11013, doi:10.1029/2004GC000741.

Boon, J.J., F.W. Van Der Meer, P.J.W. Schuyl, J.W. De Leeuw, P.A. Schenk and A.L. Burlingame (1978), Organic geochemical analysis of cores from site 362 Walvis Ridge, DSDP leg 40, Initial report of DSDP, 40, 627-637.

Bout-Roumazeilles V., Debrabant P., Labeyrie L., Chanley H., Cortijo E., 1997. Latitudinal control of astronomical forcing parameters on the high-resolution clay mineral distribution in the 45° -60° N range in the North Atlantic Ocean during the past 300, 000 years. Paleoceanography, 12, 5, 671-686.

Brassell, S.C., G. Eglinton, I.T. Marlowe, U. Pflaumann, M. Sarnthein (1986), Molecular stratigraphy a new tool for climatic assessment, Nature, 320, 129-133.

Brown, C.W., J.A. Yoder (1994), Coccolithophoride blooms in the global ocean, Journal of Geophysical Research, 99, 7467-7482.

Chapman, M.R., N.J. Shackleton, M. Zhao, G. Eglinton (1996) Faunal and alkenone reconstructions of subtropical North Atlantic surface hydrography and paleotemperature over the last 28 kyr, Paleoceanography, 11, 3, 343-357.

Conte, M.H., G. Eglinton (1993), Alkenone and alkenoate distributions within the euphotic zone of the eastern North Atlantic: correlation with production temperature, Deep-Sea research I, 40, 1935-1961.

Conte, M.H., G. Eglinton, L.A.S. Madureira (1992), Long chain alkenones and alkyl alkenoates as paleotemperature indicators: their production, flux and early sedimentary diagenesis in the Eastern North Atlantic. Org. Geochem., 19, 287-298

Conte, M.H., J.C. Weber, L.L. King, S.G. Wakeham (2001), The alkenone temperature signal in western North Atlantic surface waters, Geochimica et Cosmochimica Acta, 65, 4275-4287.

Conte, M.H., M.-A. Sicre, C. Rühlemann, J.C. Weber, S. Schulte , D. Schulz-Bull, T. Blanz (2006), Global temperature calibration of the alkenone unsaturation index $U_{37}^{K'}$ in surface waters and comparison with surface sediments, Geochemistry, Geophysics, Geosystems, 7(2), Q0205, doi:10.1029/2005GC0011054.

De Leeuw, J.W., F.W. van Der Meerand, W.I.C. Rijpastra (1980), On the occurrence and structural identification of long chain unsaturated ketones and hydrocarbons in sediments, Advances in Organic Geochemistry 1979, A.G. Douglas and J.R. Maxwell, editors, pp. 211-217.

De Vernal, A., A. Rochon (2011) Dinocysts as tracers of sea-surface conditions and sea-ice cover in polar and subpolar environments, Earth and Env. Sci., 14, doi:10.1088/1755-1315/14/1/012007

Dubois, N., M. Kienast, S. Kienast, C. Normandeau, S.E. Calvert, T.D. Herbert, M. Alan, (2011) Millennial-scale variations in hydrography and biogeochemistry in the Eastern Equatorial Pacific over the last 100 kyr, Quat. Sci. Rev., 30, 210-223, doi:10.1016/j.quascirev.2010.10.012.

Engelbrecht, A.C., J.P. Sachs (2005), Determination of sediment provenance at drift sites using hydrogen isotopes and unsaturation ratio in alkenones, Geochimica et Cosmochimica Acta, 69, 4253-4265.

Freeman K.H and Wakeham S.G. (1992), Variations in the distiributions and isotopic compositions of alkenones in Black Sea particles and sediments. Org. Geochem., 19, 277-285.

Grimalt, J.O., J. Rullkötter, M.A. Sicre, R. Summons, J. Farrington, H.R. Harvey, M. Goni, K. Sawada (2000), Modifications of the $C_{37}$ alkenone and alkenoate composition in the water column and sediment: Possible implications for sea surface temperature estimates in paleoceanography, Geochemistry, Geophysics, Geosystems, 1, 2000GC000141, doi:10.1029/2000GC000053.

Kienast, M., G. MacIntyre, N. Dubois, S. Higginson, C. Normandeau, C. Chazen, T.D. Herbert (2012), Alkenone unsaturation in surface sediments from the eastern equatorial Pacific: Implications for SST reconstruction, Paleoceanography, 27, PA1210, doi:10.1029/2011PA002254.

Kleinen, T., T.J. Osborn, K.R. Briffa (2009), Sensitivity of climate response to variations in freshwater hosing location, Ocean Dyn., 59, 509-521.

Kozdon, R., A. Eisenhauer, M. Weinelt, M.Y. Meland, D. Nürnberg (2009), Reassessing Mg/Ca temperature calibrations of Neogloboquadrina pachyderma (sinistrial) using paired $\delta^{44/40}$Ca and Mg/Ca measurements, Geochemistry, Geophysics, Geosystems, 10, Q03005 doi:10.1029/2008GC002169.

Leduc, G., R. Schneider, J.-H. Kim, G. Lohmann (2010), Holocene and Eemian sea surface temperature by alkenones and Mg/Ca paleothermometry , Quaternary Science Reviews, 29, 7-8, 989-1004, doi:10.1016/j.quascirev.2010.01.004

Ling Ho, S., G. Mollenhauer, S. Fietz, A. Martinez-Garcia, F. Lamy, G. Rueda, K. Schipper, M. Meheust, A. Rosell-Mele, R. Stein, R. Tiedemann (2014), Appraisal of $TEX_{86}$ and $TEX^{L}_{86}$ thermometries in subpolar and polar regions, Geochimica et Cosmochimica Acta, 131, 213-226, doi:10.1016/j.gca.2014.01.001

Lisitzin, A.P. (1995), The marginal filter of the ocean, Oceanology, 34, 671-682.

Marmen, S. (2000), Analyse des Alke`nones dans les se`diments de L'Atlantique Nord aux fins de reconstitution des pale`otempe`ratures et des pale`oproductivite`s, Me`moire Pre`sente` Comme Exigence Partielle De La Maitrise Chimie, Universite` Du Que`bec A` Montre`al, MARS 2000.

Mao, L., D.J.W. Piper, F. Saint-Ange, J.T. Andrewsa, M. Kienast (2014), Provenance of sediment in the Labrador Current: a record of hinterland glaciation over the past 125ka, Journal of Quaternary Science, 29, 650-660.

Meland, M.Y., E. Jansen , H. Elderfield (2005), Constraints on SST estimates for the northern North Atlantic/Nordic Seas during the LGM, Quaternary Science Reviews, 24, 835-852.

Mollenhauer G., M. Kienast, F. Lamy, H. Meggers, R.R. Schneider, J.M., Hayes, T.I., Eglinton (2005), An evaluation of $^{14}$C age relationships between co-occurring foraminifera, alkenones, and total organic carbon in continental margin sediments, Paleoceanography, 20, 1, doi:10.1029/2004PA001103

Moros M., K. Emeis, B. Risenbrobakken, I. Snowball, A. Kuijpers, J. McManus, E. Jansen (2004), Sea surface temperature and ice rafting in the Holocene North Atlantic: climate influences on northern Europe and Greenland, Quaternary Science Reviews, 23, 2113-2126.

Müller, P.J., G. Kirst, G. Ruhland, I. von Storch, A. Rosell-Mele (1998), Calibration of alkenone paleotemperature index $U^{K'}_{37}$ based on core-tops from the eastern South Atlantic and the global ocean (60°N-60°S), Geochimica et Cosmochimica Acta, 62, 1757-1772.

NASA Goddard Space Flight Center, Ocean Ecology Laboratory, Ocean Biology Processing Group; (2014): MODIS-Terra Ocean Color Data; NASA Goddard Space Flight Center, Ocean Ecology Laboratory, Ocean Biology Processing Group. http://dx.doi.org/10.5067/TERRA/MODIS_OC.2014.0

National Snow and Ice Data Center. September Sea Ice Extent, 1979-2012. http://nsidc.org/data/google_earth/

National Snow and Ice Data Center. March Sea Ice Extent, 1979-2012. http://nsidc.org/data/google_earth/

Ohkouchi, N., T.I. Eglinton, L.D., Keigwin, J.M., Hayes (2002), Spatial and temporal offsets between proxy records in a sediment drift, Science, 298, 1224-1227.

Rodrigo-Gamiz, M., S.W. Rampen, H. de Haas, M. Baas, S. Schouten, J.S. S. Damste (2015), Constraints on the applicability of the organic temperature proxies $U^{K'}_{37}$, $TEX_{86}$ and LDI in the subpolar region around Iceland, Biogeosciences, 12, 6573-6590, doi:10.5194/bg-12-6573-2015.

Rosell-Mele, A., J. Carter, G. Eglinton (1993), Distributions of long-chain alkenones and alkyl alkenoates in marine surface sediments from the North East Atlantic, Organic Geochemistry, 22, 501-509.

Rosell-Mele, G. Eglinton , U. Pflaumann, M. Sarnthein (1995), Atlantic core-top calibration of the $U^{K}_{37}$ index as a sea-surface paleotemperature indicator, Geochimica et Cosmochimica Acta, 59, 3099-3107.

Rosell-Mele, A. (1998), Interhemispheric appraisal of the value of alkenone indices as temperature and salinity proxies in high-latitude locations, Paleoceanography, 13, 694-703.

Rosell-Mele, A., P. Comes, P.J. Müller, P. Ziveri (2000), Alkenone fluxes and anomalous $U^{K'}_{37}$ values during 1989-1990 in the Northeast Atlantic (48°N, 21° W), Marine Chemistry, 71, 251-264.

Rosell-Mele A., et al (2001), Precision of the current methods to measure the alkenone proxy $U^{K'}_{37}$ and absolute alkenone abundance in sediments: Results of an interlaboratory comparison study, Gechem. Geophys. Geosys., 2, 1525-2027, doi:10.1029/2000GC000141.

Rosell-Mele, A., E. Jansen, M. Weinelt (2002), Appraisal of a molecular approach to infer variations in surface ocean freshwater inputs into the North Atlantic during the last glacial, Global and Planetary Change, 34, 143-152.

Rosell-Mele A., F.G. Prahl (2013) Seasonality of $U^{K'}_{37}$ temperature estimates as inferred from sediment trap data, Quaternary Sci. Rev., 72, 128-136, doi:10.1016/j.quascirev.2013.04.017

Pan, H., M.-Y. Sun (2011), Variations of alkenone based paleotemperature index ($U^{K'}_{37}$) during Emiliania huxleyi cell growth, respiration (auto-metabolism) and microbial degradation, Organic Geochemistry, 42, 678-687.

Prahl, F.G., S.G. Wakeham (1987), Calibration of unsaturation patterns in long chain ketone compositions for paleotemperature assessments, Nature, 330, 367-369.

Prahl, F.G., L.A. Muehlhausen and D.L. Zahnle (1988), Further evaluation of long-chain alkenones as indicators of paleoceanographic conditions, Geochimica et Cosmochimica Acta, 52, 2303-2310.

Sachs, J.P. (2007), Cooling of Northwest Atlantic slope waters during the Holocene, Geophysical Research Letters, 34, L03609, doi:10.1029/2006GL028495.

Saenger C., R.E. Came, D.W. Oppo, L.D. Keigwin, A.L. Cohen (2011), Regional climate in the western subtropical North Atlantic during the past two millennia, Paleoceanography, 26, PA2206, doi:10.1029/2010PA002038

Schneider, R., P.J. Müller, G. Ruhland, G. Meinecke, H. Schmidt, G. Wefer (1996), Late Quaternary Surface Temperatures and Productivity in the East-Equatorial South Atlantic: Response to Changes in

Trade/Monsoon Wind Forcing and Surface Water Advection in the South Atlantic, Present and Past circulation, edited by G. Wefer et al., 527-551, Springer, Berlin.

Shelford, V.E. (1931), Some concepts of Bioecology, Ecology, 12(3), 455-467.

Sicre, M.-A., E. Bard, U. Ezat, F. Rostek (2002), Alkenone distributions in the North Atlantic and Nordic sea surface waters, Geochemistry, Geophysics, Geosystems, 3(2), 1013, doi:10.1029/2001GC000159.

Sicre, M.-A., J. Jacob, U. Ezat, S. Rousse, C. Kissel, P. Yiou, J. Eiriksson, K.L. Knudsen, E. Jansen, J.L. Turon (2008), Decadal variability of sea surface temperatures off North Iceland over the last 2000 years, Earth and Planetary Letters, 268, 137-142.

Sicre, M.-A., K. Weckström, M.-S. Seidenkrantz, A. Kujipers, M. Benetti, G. Masse, U. Ezat, S. Schmidt, I. Bouloubassi, J. Olse, M. Khodri, J. Mignot (2014), Labrador current variability over the last 2000 years, Earth and Planetary Science Letters, 400, 26-32.

Sikes E.L., J.K. Volkman (1993), Calibration of alkenone unsaturation ratios ( $U_{37}^{K'}$) for paleotemperature estimation in cold polar waters. Geochim Cosmochim. Acta, 57,1883-1889

Sikes, E.L., M.-A. Sicre (2002), Relationship of the tetra-unsaturated $C_{37}$ alkenone to salinity and temperature: Implications for paleoproxy applications, Geochemistry, Geophysics, Geosystems, 3, 1063, doi:10.1029/2002GC000345.

Vogelsang E., M. Sarnthein, U. Pflaumann (2000), $\delta^{18}O$- Stratigraphy, Chronology and Sea Surface Temperatures of Atlantic Sediment Records, Berichte – Reports Institure für Geowissenschften Christian-Albrechts Universität zu Kiel, 13, 11 S., 1 Abb., 1 Tab., 244 Anhang-S., Kiel, (Jan.) 2001, ISSN 0175-9302

Volkman, J.K., G. Eglinton, E.D.S. Corner, R. Sargent (1980), Novel unsaturated straight-chain $C_{37}$-$C_{39}$ methyl and ethyl ketones in marine sediments and coccolithophore Emiliania huxleyi, Advances in Organic Geochemistry 1979, A.G. Douglas and J.R. Maxwell, editors, 219-227.

World Ocean Atlas, (2013). www.nodc.noaa.gov

Wu G., C. Hillaire-Marcel (1993), Accelerator mass spectrometry radiocarbon stratigraphies in deep Labrador Sea cores: paleoceanographic implications, Canadian Journal of Earth Science, doi:10.1139/e94-005

# CHAPTER 5

# LABRADOR SEA SURFACE WATER CIRCULATION OVER THE LAST 35 KYRS INFERRED FROM ALKENONE PALEOTHERMOMETRY.

to be submitted as: Filippova A., Kienast M., Frank M., Hillaire-Marcel C., (2017) Labrador Sea surface water circulation over the last 35 kyrs inferred from alkenone paleothermometry.

## Abstract.

The latest monitoring cruises in the Labrador Sea recorded a warming trend that already have reached the deepest layer of the Labrador Sea. These changes could be a part of the cyclic evolution of the Labrador Sea linked to the production and dissipation of the Labrador Sea Water. To evaluate and improve the understanding of the processes and mechanisms of the LSW formation and their role in controlling atmospheric temperature fluctuations, it is important to know how sea surface temperatures in the upper water column have changed in this region in the past. Here we present records of alkenone unsaturation from the Labrador Sea from four marine sediment cores covering the last 35 kyrs and discuss them in terms of SST estimates. The record before the Holocene was only partially preserved in all cores and expressed sea surface temperatures well below zero. The $U_{37}^{K'}$ and $U_{37}^{K^*}$-derived Sea Surface Temperatures show much warmer SST (higher than the present day SST in the Labrador Sea) during the LGM than $U_{37}^{K}$- derived SST. Although $U_{37}^{K}$- derived SST's support the notion that the Holocene period was a time of climatic instability characterized by multiple temperature fluctuations while $U_{37}^{K'}$ and $U_{37}^{K^*}$- derived SST's in contrast show the Holocene as a period of a relatively stable climate. The youngest part of the record suggests universally warm temperatures over the Labrador Sea, ranging from 16 to 12°C, consistent with dissipating signal of the Irminger Waters moving around the Labrador Sea. Current study provides new insight into the processes of the deep water formation and ocean-climate feedback mechanisms, while additionally providing a record of the NAC behavior.

## 5.2 INTRODUCTION.

The global ocean is significantly warmer today than it has been in the mid-20$^{th}$ century (Levitus et al., 2009). This warming trend seems to be a persistent feature that could be carried into the future. The observed warming is up to date the most pronounced in the northern North Atlantic and high latitudes (Levitus et al., 2005, 2009, 2012; Domingues et al., 2008). One of the places in the North Atlantic, where this warming has been recently recorded is the Labrador Sea. Regular monitoring cruises and observations carried out in the Labrador Sea have provided hydrographic information that goes back to the 1930's (Yashayaev and Clark, 2006). The data show that over the last decades the Labrador Sea experienced several warm (1960 – 1971, 1977- 1983 and from 1995 until now) and cold (1984 – 1994) states (Yashayaev and Clark, 2006). The last coldest state of the Labrador Sea of the record was observed in 1994. Since 1995 the Labrador Sea has been in a state of warming (Yashayaev et al., 2008; Filippova et al., submitted). Potential temperatures of different water masses

recorded in the Labrador Sea have been rising every year (Yashayaev and Clark, 2006, Yashayaev et al., 2008; Filippova et al., submitted) and have now come close to the highest values ever recorded (Yashayaev and Clark, 2006). It has been suggested that these changes are part of a cyclic evolution of the Labrador Sea linked to the production and dissipation of the Labrador Sea Water (LSW) (Yashayaev and Clark, 2006). Surface waters in the Labrador Sea occupy the upper 200 m of the water column (Lazier and Wright, 1993). Their formation is defined by mixing of waters such as the West Greenland Current (WGC) and warm waters of Irminger Sea or Irminger Current (IC) originated from the north, the North Atlantic Current (NAC) from the south, and cold waters advected from the Baffin Bay through the Davis Strait and through the Hudson Strait together forming the Labrador Current (LC). In addition, cold and fresh waters are supplied from land (Azetsu-Scott et al., 2003; Yashayaev and Clark, 2006; Yashayaev et al., 2015). To evaluate and improve the understanding of the processes and mechanisms of the LSW formation and their role in controlling atmospheric temperature fluctuations, it is important to know how sea surface temperatures (SST's) in the upper water column have changed in this region in the past.

Alkenone paleothermometry has been widely applied for reconstructions of past SSTs. Although there are still unresolved questions concerning its exact calibration, in particular in the northern North Atlantic (Rosell-Mele et al., 1995; Sicre et al., 2002; Bendle and Rosell-Mele, 2004; Conte et al., 2006), it has proven to be a robust proxy for SST reconstruction in a wide variety of regions (e.g., Müller et al., 1998; Conte et al., 2006; Filippova et al., 2016). Expressed as an index of the degree of ketone unsaturation ($U_{37}^{K}$), it is correlated to the water temperature in which the biolipids (alkenones $C_{37:4}$, $C_{37:3}$ and $C_{37:2}$) were produced (Brassell et al., 1986; Prahl and Wakeham, 1987; Müller et al., 1998). Although tetra alkenones are not present everywhere, their inclusion into the empirical temperature equation appears to improve SST estimation in cold regions (Rosell-Mele, 1995; Rosell-Mele, 1998; Bendle and Rosell-Mele, 2004; Filippova et al., 2016).

$$U_{37}^{K} = \frac{[C_{37:2}] - [C_{37:4}]}{[C_{37:2}] + [C_{37:3}] + [C_{37:4}]}$$

Here we present records of alkenone unsaturation from the Labrador Sea from four marine sediment cores covering the last 35 kyrs and discuss them in terms of SST estimates. The records show large gaps (absence of alkenones) at times coincident with cold periods including Heinrich Stadial 2 (HS2) and Heinrich Stadial 1 (HS1), the Last Glacial Maximum

(LGM), and the Younger Dryas (YD), whereas a well preserved, mostly undisrupted record is available for the Holocene at all four locations.

### 5.2.1 STUDY AREA

Numerous paleotemperature studies applying different proxies have focused on North Atlantic SST reconstructions, including from the Labrador Sea, but showed conflicting results.

Based on a study of alkenone unsaturation ratios in sediments from the North West Atlantic slope, Sachs (2007) showed that despite previous indications of the Holocene as a period of climatic stability, it was characterized by large secular changes. These records suggest a 4 to 10 °C cooling during the Holocene from temperatures of around 14 - 16 °C on the Scotian Margin and Laurentian Fan during the early Holocene to about 8 °C during the late Holocene. Sicre et al. (2014) showed similar results for the late Holocene off NE and SE Newfoundland, where SST's ranged between 4 - 6 °C based on the $U_{37}^{K}$ ratio. More generally, a compilation of available data by Leduc et al. (2010) showed decreasing Holocene SSTs to be a common feature in most of the mid to high-latitude alkenone-derived SST records from the Atlantic, while Mg/Ca records showed either no trend or a slight warming over the Holocene.

Going further back in time, the CLIMAP project was one of the first coordinated attempts to reconstruct temperatures at the time of the LGM (19 - 23 ka) based on a transfer function of $^{18}\delta$ O values (CLIMAP, 1976). This SST reconstruction showed a maximum temperature difference of -18 to -12 °C compared to the modern in the Western North Atlantic between 40 °N and 50 °N. The steep temperature gradients were interpreted as a consequence of the absence of strong warm and salty inflow from the south as part of the NAC, the IC or the Norwegian current (CLIMAP, 1976).

The overall cooling during the LGM is in agreement with a comparison of SST's derived from alkenones, coccoliths and foraminiferal assemblages south of Iceland over the past 120 kyrs (Weaver et al., 1999). Foraminiferal SST data showed low temperatures between 70 and 22 kyrs, which declined even further at 18 ka prior to the onset of the deglaciation. Based on these data, the overall glacial to interglacial temperature increase reached 9 °C. Sea surface temperatures inferred from alkenone unsaturation ratios at the same site also show colder temperatures at the LGM (10 °C) and a warming trend during the Holocene, when SST's reached 15 °C, consistent with Mg/Ca data from Leduc et al. (2010).

Following in the footsteps of CLIMAP, the GLAMAP 2000 project (Pflaumann et al., 2003) reconstructed SST's in the North Atlantic based on census counts of planktic foraminifera using the Maximum Similarity technique with 947 modern analog samples and 119 dated cores. This study revealed SST's around 0 ° degrees in the Labrador Sea and Nordic Seas during the LGM winters, whereas warmer temperatures south of Iceland prevailed (~ 2 - 3 °C), which is much lower than those inferred by Weaver et al., (1999). The LGM summer temperatures in the Labrador Sea and Nordic Seas were several degrees warmer, around 3 - 4 °C and around 4 - 7 °C south of Iceland, respectively. Comparison with the CLIMAP reconstruction showed that most of the differences were observed for the Northern Summer off southern Greenland (~ 2 - 3 °C) and west of Ireland (up to 4 °C). Winter temperature reconstructions showed consistent results.

Similar results were achieved by Meland et al., (2005) for the Nordic Seas. They constrained SST's, derived from $\delta^{18}O$ of planktic foraminifera, to 0 to 2 °C during the LGM. However, unlike CLIMAP, their results showed warmer temperatures south east of Iceland reaching 7 °C off the coast of England, suggesting that some element of meridional heat transport was maintained.

A compilation by de Vernal et al. (2006) based on different proxies reconstructed the SST's in the northern North Atlantic during the LGM. Significant differences were observed for different proxies. Planktonic foraminifera indicated temperatures much colder than today, with SST < 2 °C for the LGM. Dinoflagellate cyst data suggest distinct regional patterns, with much colder conditions along the Canadian margin reaching -2 °C, and around 2 to 6 °C south of Greenland and in the Irminger Sea. Temperatures off the coast of Newfoundland only reached 0 to 2 °C. At the same time, alkenone based reconstructions suggested warmer conditions in the Irminger basin and the Labrador Sea around 10 to 12 °C, and even warmer off the coast of Newfoundland reaching 14 - 16 °C. Planktonic foraminifera and alkenone based SST's indicated particularly warm temperatures off the coast of Europe during LGM between 15 – 22 °C.

The international MARGO project (MARGO project members, 2009) presented a global synthesis of all available SST reconstructions for the LGM. In broad agreement with CLIMAP, they showed that the largest cooling in comparison to the present occurred in the mid-latitude North Atlantic Ocean. Furthermore, the data compiled by MARGO suggested ice-free Nordic Seas, consistent with the study by Meland et al. (2005).

Although the reconstructed SST's at different locations differ between these studies, the overall SST trends during the LGM obtained from different proxies (Mg/Ca, foraminifera,

and dinoflagellate cyst) gave comparable results ranging from 0 to 4 °C in the Nordic and Labrador Seas throughout the year, and around 0 to 6 °C south of Greenland. The exception, however, are reconstructions based on alkenones, which show significantly higher temperatures for the LGM reaching up to 15 °C at some locations. The Holocene was not a period of climatic stability and was characterized by multiple SST changes.

## 5.3 SAMPLE MATERIAL AND METHODS.

### 5.3.1 SAMPLE MATERIAL.

Core MD99-2227, hereafter 2227 (58°55.26 N, 048°22.38 W), was collected from a water depth of 3460 m at the southwest Greenland Rise on board of research vessel *Marion Dufresne* in 1999 (Fig. 1). This study focused on the first 6.5 m of the 42.96 m long core, which cover the period of the Holocene, the YD, HS1 and the inception of the Northern Hemisphere deglaciation from 20.3 ka to 0.8 ka. The age model is linearly interpolated between AMS $^{14}$C ages and was previously published by Fagel et al., (2004) (Fig. 2). The core was sampled every 15 to 30 cm, depending on availability of material and with a higher resolution of 10 cm near the 8.2 ka event, the YD and HS1. At the beginning of the Holocene, the sedimentation rate increased from ~ 19 cm/kyr to 61 cm/kyr and then decreased again to 39 cm/kyr during the middle and late Holocene.

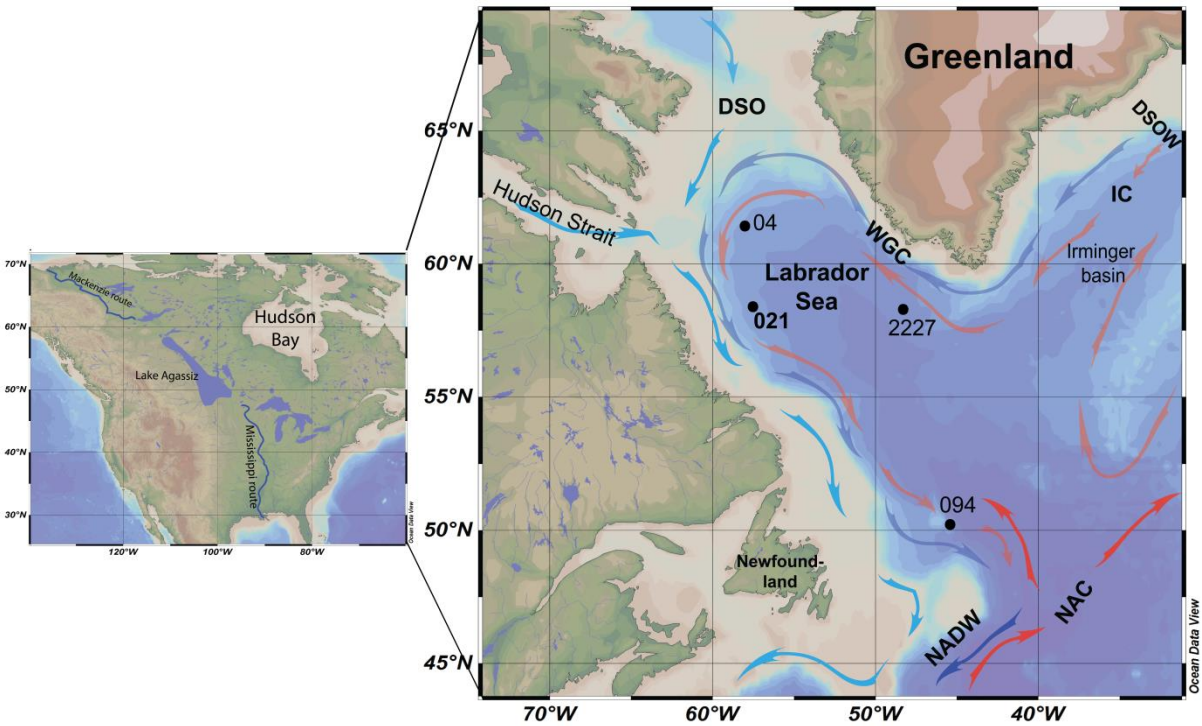


**Fig. 1** Map of the study area. Black dots show the core locations. Red arrows denote warm water currents, blue arrows cold water currents (adopted from Yashayaev and Clark,

2006). Abbreviations stand for: Davis Strait Water (DSO), Denmark Strait Overflow Water (DSOW), Irminger Current (IC), North Atlantic Current (NAC), North Atlantic Deep Water (NADW), Western Greenland Current (WGC). Additionally, the most likely locations of postglacial Lake Agassiz (Murton et al., 2010), and of the Mackenzie and Mississippi rivers are shown.

Core HU08-029-0004, hereafter 04 (61°2749 N, 58°0211 W), was obtained off the southern Baffin Island shelf in the northern Labrador Sea on board the Canadian Coast Guard (CCGS) research vessel *Hudson* in 2008, from a water depth of 2674 m (Fig. 1). This study covers the entire length of the core of 895 cm. The age model was previously published by Gibb et al. (2014). The sedimentation rate increases from values of ~ 27 cm/kyr prior to the LGM to higher sedimentation rates during HS1 (44 cm/kyr) and the YD (102 cm/kyr). During the Holocene, the sedimentation rate gradually decreases to values as low as ~ 10 cm/kyr at the end of the Holocene.

Core HU84-030-021, hereafter called 021 (58°22600 N, 57°30.42 W), was collected from the continental slope of the western Labrador Sea from a water depth of 2853 m (Fig. 1). This study focuses on the upper 8 m. The age model was previously published by Hillaire-Marcel and de Vernal (1989) and was linearly interpolated between available AMS $^{14}$C ages. The sedimentation rate over the period from 27 to 17 ka was 27 - 28 cm/kyr. A slight increase is observed at the time of the YD reaching sedimentation rates around 39 cm/kyr, followed by a decrease to lower sedimentation rates of 16 cm/kyrs during the late Holocene.

Core HU91-045-094, hereafter called 094 (50°12.26 N, 45°41.14 W), was recovered from the western part of the Labrador Sea at Orphan Knoll, on board *CCGS Hudson* in 1991, from a depth of 3448 m. The total length of the core is 24 m, but this study focuses on the uppermost 4.5 m only. The age model is based on the previously published data by Hillaire-Marcel et al. (1994) and was linearly interpolated between available AMS $^{14}$C ages. Lower sedimentation rates observed prior the LGM, the YD and the middle to late Holocene range between 10 and 13 cm/kyr. High sedimentation rates between 35 and 39 cm/kyr were recorded from the LGM to HS1.

Between 22 and 59 samples per core were analyzed for their alkenone unsaturation ratios (Table A4).

### 5.3.2 METHODS.

The detailed methods of alkenone extraction and analysis are described elsewhere (Filippova et al., 2016) and only briefly presented here. One to two grams of freeze-dried,

homogenized material were used for alkenone extraction in an automated solvent extraction system (ASE) under 1000 psi pressure and 100 °C temperature with five 5 minutes static phases. A mixture of methylene chloride and methanol (9:1v/v) was used to extract the lipid fraction from the sediment. Prior to analysis, a standard solution of hexatriacontane with a concentration of 12.3 $mg.l^{-1}$ was added to every sample. Triple hexane extraction of alkenones from the solution was followed by silica gel chromatography. The alkenone fraction was eluted with a DCM:Hexane (2:1 v/v) mixture whereas the methyl fraction was isolated with methanol. The extracts were analyzed by capillary gas chromatography with a flame ionization detector, Agilent, model 6890 equipped with a 60 m long CP-Sil 5CBH column. Hydrogen was used as a carrier. During each run, a set of internal standards and a strain of *E. huxleyi* CCMP1742 were measured. Peak areas of $C_{37:2}$; $C_{37:3}$; $C_{37:4}$ and $C_{38:2Me}$; $C_{38:Et}$; $C_{38:3Et}$; $C_{38:Me}$; $C_{38:3ee}$ were defined based on retention times in repeat runs of an extract of the *E.hux* culture. The recovery rate based on the internal standard added to every sample prior the analysis at a known concentration was on average 75 %. The detection limit was based on 10 times background noise for individual alkenones. Samples below the detection limits were not considered in the analysis. The SST estimations are primarily based on the $U_{37}^{K}$ following the results of Filippova et al. (2016). Samples with negative $U_{37}^{K}$ values were considered unreliable.

## 5.4 RESULTS.

### 5.4.1 ALKENONE CONCENTRATION.

The alkenone record of the four sedimentary records covers the last 28 - 33 kyr with one shorter record of only 18 kyrs (core 2227). In general, all four cores are characterized by a well preserved record over the Holocene. Prior to 11 kyr, however, multiple gaps are observed in the data, where alkenones are not detectable, in general between 28 and 24, as well as between 20 and 11 kyr.

The total concentration of alkenones (sum of all alkenones) show high variability with depth in each core (Fig. 2). In general, the highest abundance (%) of tetra alkenones was detected during the LGM and early Holocene (Fig. 2) with additional peak during YD in core 2227, 28 ka and between 15 and 13 ka in core 04, and YD and middle Holocene in core 021. The overall abundance of tetra alkenones range from 8 to 35 % in cores 2227 and 094, with higher abundance in cores 021 and 04 (up to 54 %). In general, tetra alkenones are absent during the middle and late Holocene. The peaks in tetra alkenone abundances appear randomly at different time periods in each core. Total concentrations of alkenones are

particularly high during the early Holocene and at around 6 ka in core 2227, during the LGM, between 14 and 13 ka, at around 12 ka and 9 ka in core 04, at the beginning of the Holocene, and during late Holocene at around 1 ka and 500 years in core 021, and around 28 ka, 10 ka and during the late Holocene in core 094. Overall, the total concentration of alkenones in all cores seems to be higher during the early Holocene,. In core 021, total concentration of alkenones was similar from 28 ka up to the middle Holocene, whereas during the late Holocene the total concentration of alkenones increases. The $C_{38}$ methyl and ethyl groups follow similar trends.

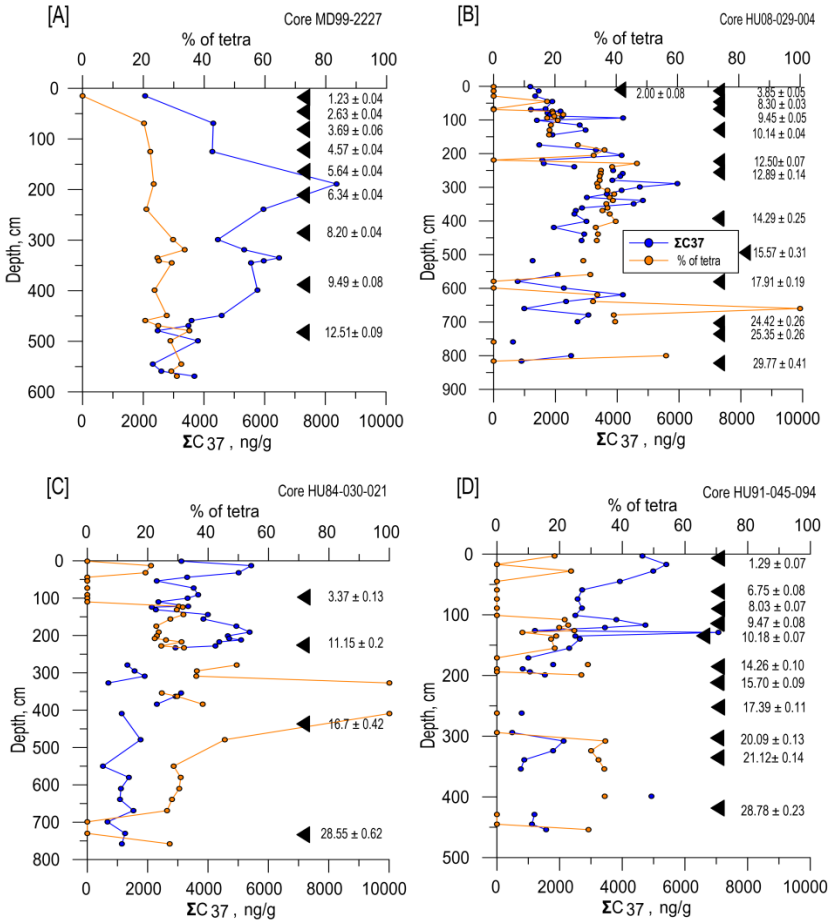


**Fig. 2** Total concentration, in ng/g sediment, of all alkenones together with % abundance of tetra alkenones versus depth in cm. Breaks in the line indicate sample depths with alkenone concentrations below detection limits. Black triangles denote depths, for which $^{14}C$ ages were obtained (Gibb et al., 2914; Fagel et al., 2004; Hillaire-Marcel and de Vernal, 1989; Hillaire-Marcel et al., 1994). A. Core MD-2227 B. Core HU08-029-004 C. Core HU84-030-021 D. Core HU91-045-094.

### 5.4.2 ALKENONE UNSATURATION RATIO

Although our study focuses only on $U_{37}^{K}$ values, $U_{37}^{K'}$ and $U_{37}^{K^*}$ data are also presented, where

$$U_{37}^{K'} = \frac{C_{37:2}}{(C_{37:2} + C_{37:3})}$$

and

$$U_{37}^{K^*} = \frac{C_{37:2}}{(C_{37:4} + C_{37:2} + C_{37:3})}$$

$U_{37}^{K}$ values range from -0.08 (~ 8.09 ka) to 0.57 (~ 1.1 ka) in core 2227, from -0.37 (~ 13 ka) to 0.55 (~ 18 ka) in core 04, from -0.50 (~ 18 ka, peak of tetra concentration) to 0.50 (27 ka) in core 021 and from -0.11 (~ 20.6 ka) to 0.58 (~ 30 ka) in core 094. Negative $U_{37}^{K}$ values observed in all cores are the result of high concentration of tetra alkenones. Negative $U_{37}^{K}$ values in core 04 from 29 up to 12 kyr lead to the unreasonably cold SST estimates far below zero. $U_{37}^{K'}$ and $U_{37}^{K^*}$ -based SST estimates show much more reasonable values. Based on the study of alkenone unsaturation in northern North Altantic surface sediments, Filippova et al. (2016) suggested the $U_{37}^{K}$ index to be more reliable for SST reconstructions in cold regions. Here we present all three indices and compare the results to test the validity and applicability of the $U_{37}^{K}$ index for SST reconstructions in the Labrador Sea covering the last 33 kyrs. Any sample with negative $U_{37}^{K}$ values or negative temperatures is considered unreliable and "SST" estimates are not going to be interpreted further, however all data are shown in Fig. 4, with "SST's" below zero marked in red. Possible reasons for these unreasonable SST estimates prior the Holocene will be discussed.

### 5.4.3 SEA SURFACE TEMPERATURES.

Comparison of the youngest samples from each core with the modern day bloom SST's obtained from World Ocean Atlas 2013 shows about 8 to 9 degree C difference for core 04 (~ 1 ka) and 2227 (~ 0.1 ka), located in the northern Labrador Sea and off the southern tip of Greenland, respectively (Fig. 3). The residuals (reconstructed SST minus the actual SST) are lower for core 021 (only 3 °C for $U_{37}^{K}$ inferred SST, ~ 0.03 ka) and core 094 (less than 2 °C for $U_{37}^{K}$ inferred SST, ~ 1.5 ka). The lowest residual for core 094 is observed for $U_{37}^{K^*}$- derived SST and is less than 0.3 °C (Fig. 3). No tetra alkenones are detected in the youngest samples of cores 2227, 04 and 021, resulting in identical SST's for all three indices in these three cores.

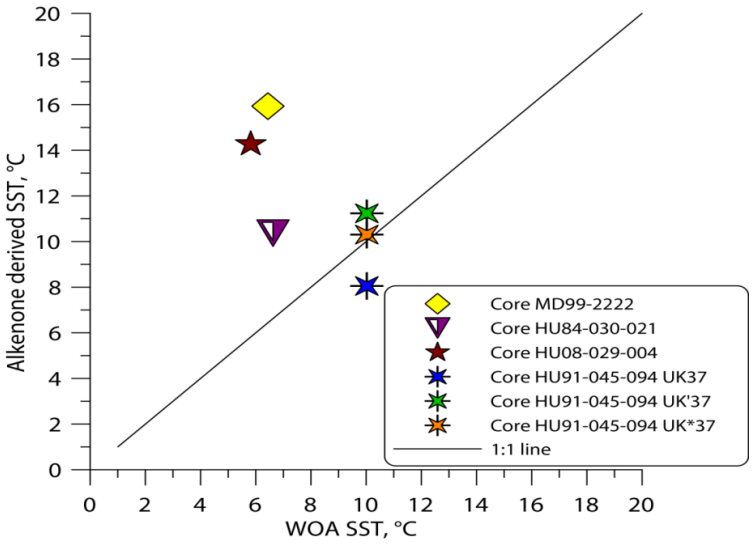


**Fig. 3** Comparison of alkenone-derived SST's (using the global calibration of Müller et al., 1998) from the youngest samples with SST's obtained from World Ocean Atlas 2013. Black line denotes 1 to 1 relationship. $U_{37}^{K'}$ and $U_{37}^{K^*}$ -derived SST's for core 094 are also shown. $U_{37}^{K'}$ and $U_{37}^{K^*}$ -derived SST's for cores 2227, 021 and 04 are the same as $U_{37}^{K}$-derived SST, as no tetra alkenones were present in these samples.

In general, there are large gaps in the records of all cores due to the absence of alkenones prior the Holocene (Fig. 4). The available data, however, show that around 33 ka (core 094) SST's were relatively cold (~ 5 °C, $U_{37}^{K}$- derived SST ), followed by a warming trend reaching up to 16 °C (for all three indices) for the 2 - 2.5 kyr period coincident with Heinrich Stadial 3 (HS3) (Fig. 4). A similar temperature increase is observed in core 021 from 6 ($U_{37}^{K}$- derived SST ) up to 14 degrees C (for all three indices) between 28 and 27 ka. The Heinrich Stadial 2 shows $U_{37}^{K}$- derived SST's below zero in all cores. However, data from before HS2 in core 021 show $U_{37}^{K}$- derived SST's around 4 degrees C followed by a decrease prior the LGM, where SST's dropped to around 2 degrees C. Neither LGM nor HS1 were recorded in any of the data. The time after HS1, however, suggest cold $U_{37}^{K}$- derived SST's based on signal one data point from cores 2227 (~ 3 °C, ~ 16 ka), core 04 (~ 1 °C, ~ 15 ka), core 021 (0 - 2 °C, ~ 14 ka) and SST's decreased prior to the YD in core 094 from 8 °C (~ 14.5 ka) to 5 °C (~ 13 ka). The $U_{37}^{K'}$ and $U_{37}^{K^*}$ -derived SST's follow the same trends as $U_{37}^{K}$-derived SST, however, they show much warmer SST's all the way up to the beginning of the Holocene (Fig. 4). The biggest SST differences between the three indices is observed for the time of HS1 in cores 04 (> 20 °C, $U_{37}^{K'}$- derived SST) and 094 (> 15 °C, $U_{37}^{K'}$- derived SST) and the LGM for all three cores (~ 16 °C).

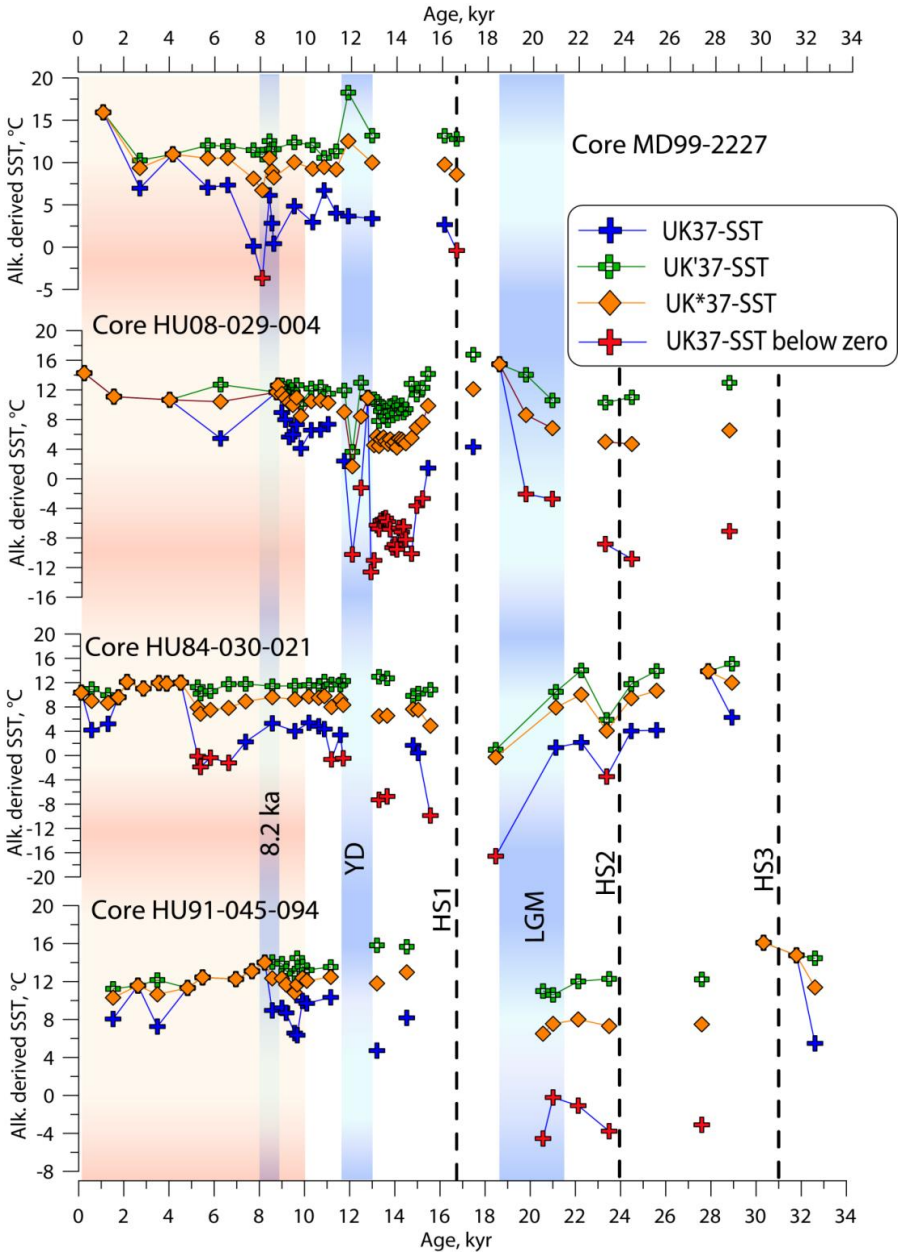


**Fig. 4** Alkenone-derived SST's from the 4 sediment cores. SST's are shown for $U_{37}^{K}$, $U_{37}^{K'}$ and $U_{37}^{K*}$. Vertical bars denote times of the major events: Heinrich Stadials (HS3, HS2 and HS1); Last Glacial Maximum (LGM), Younger Dryas (YD), 8.2 ka event or Lake Agassiz outbreak, Holocene. Red symbols denote unreasonable $U_{37}^{K}$ - derived SST below zero degrees C.

The most pronounced drop in $U_{37}^{K}$derived SST's on the order of almost 6 degrees C occurred at the beginning of the Holocene, as recorded in core 2227 and was followed by a temperature increase up to 6 degrees C. Around 8 ka in core 2227, however, $U_{37}^{K}$- derived SST dropped below zero, followed by a prominent SST increase through the middle Holocene of almost 11 degrees C. The time period between 7 and 4 ka was characterized by stable $U_{37}^{K}$-derived SST's between 13 and 11 °C in core 094 and a significant cooling up to 5 °C at 6 ka

in core 04 , while in cores 021 $U_{37}^{K}$- derived SST's felt below zero between 6.5 ka and 4 ka. The youngest samples of the late Holocene are characterized by a relatively small range of warm $U_{37}^{K}$- derived SST's in cores 2227, 021 and 04, between 16 and 12 °C, with higher temperatures south of Greenland and lower on the western side of the Labrador Sea. Interestingly, in core 094 two drops in $U_{37}^{K}$- derived SST's on the order of 5 to 6 degrees C are observed around 3 ka (~ 7 °C) and 1 ka (~ 8 °C). These cold events also coincide with an SST minimum in core 2227 around 3 ka and a SST decrease in core 021 around 1 ka. The $U_{37}^{K'}$ and $U_{37}^{K^*}$ - derived SST's on the other hand show relatively stable warm conditions over the Labrador Sea in all four sediment cores all the way up to the late Holocene, with SST's between 10 and 14 degrees C.

## 5.5 DISCUSSION.

This study of four sedimentary cores provides a well-preserved record throughout the Holocene and partially also for the YD period. Time intervals coincident with events like HS2 and HS1, LGM, were not preserved in all cores and are generally characterized by a complete absence of alkenones, or their presence below the detection limit.

### 5.5.1 PERIOD FROM 33 KA TO 11 KA.

A comprehensive study published by Filippova et al. (2016) came to conclusion that the $U_{37}^{K}$ index is most reliably related to SST's in cold regions. Based on that observation, the analysis here will be mainly focused on $U_{37}^{K}$-derived SST, however other indices are also presented and their results will be compared with $U_{37}^{K}$-derived SST. The down core records show that prior to the Holocene most $U_{37}^{K}$-derived SST's in all cores fall below zero, suggesting that between 33 ka and 11 ka alkenone paleothermometry fails to provide reliable SST's for a number of reasons. The $U_{37}^{K'}$ and $U_{37}^{K^*}$- derived SST's on the other hand show particularly warm temperatures, up to 13 deg C higher than observed in the present day in the Labrador Sea (Filippova et al., submitted).

The preserved alkenones over the time period between 33 ka and 11 ka and particularly warm $U_{37}^{K'}$ and $U_{37}^{K^*}$- derived SST on one hand could be the result of allochthonous input, advected from the south with warmer currents, such as the NAC. This signal could have been produced in the warmer environments and delivered to the sites, or it could have been a signal of pre-formed alkenones produced during a warmer geological periods, introduced via the Mississippi river system and through the Gulf of Mexico into the NAC (Fig. 1, Rosell-Mele et al., 1997; Mao et al., 2014).

On the other hand, we also speculate that melting of the icebergs may have led to local water restratification and increased SST's in some areas, which has been shown in model simulations (Kleinen et al., 2009). In that case, localized temperature increases may have followed the massive fresh water inputs, causing a change in the circulation patterns. However, in their study local SST increase did not exceed 5 degrees C (Kleinen et al., 2009). High water input might have resulted in an increase of seasonality in the ice free zones, which was proposed before for times before the YD cold interval (between 17.5 and 14.5 ka) (Williams et al., 2012). However, more data are needed to substantiate any of these hypotheses.

Extremely low $U_{37}^{K}$-derived SST's recorded during the LGM in some of the cores are accompanied and caused by the high concentrations of tetra alkenones (Fig. 2). The occurrence of tetra alkenones in each core coincident with the time of the LGM is consistent with previous suggestions that they are mainly produced during cold temperatures. High abundances of tetra alkenones may be an indicator of a yet unknown factor from this time period, such as iceberg discharge signatures or a function of increased salinity due to brine rejection during the formation of sea ice. However, no obvious relation is seen in the data with Heinrich Stadials, suggesting the armada of icebergs launched into the Labrador Sea most likely was not the source of tetra alkenones, or cause of their increased concentrations.

However our record preserved through the LGM based on $U_{37}^{K}$-derived SST's suggests cold temperatures below zero (~ -4 to -5 °C) unlike significantly warmer $U_{37}^{K'}$ and $U_{37}^{K^*}$-derived SST's. Similar results were obtained in other studies based on different proxies (Weaver et al., 1999; Pflaumann et al., 2003; Meland et al., 2005; Vernal et al., 2006). Cold $U_{37}^{K}$-derived SST's would be consistent with conclusions made by the CLIMAP, 1976 project members based on $^{18}\delta$ O data, inferred as absence of warm salty inflow of NAC, IW or the Norwegian current into the area. Warmer glacial sea surface temperature estimates based on $U_{37}^{K'}$, however, appear to imply glacial temperatures, including during the LGM, that are consistent with the MARGO compilation and other studies using this particular index to estimate SST's.

The absence of alkenones during such events as HS2, HS1 and the YD seem to be a feature in all four cores. Significantly colder SST's together with freshening and ice coverage at the time of the Heinrich stadials (Keigwin and Lehman, 1994) likely prevented the production of any biolipids. Where conditions still allowed the production of alkenones, for example due to local SST increases caused by water restratification or due to extreme

seasonality, an armada of icebergs launched through the Hudson Strait into the Labrador Sea could have resulted in advection of suspended in seawater material further down.

### 5.5.2 HOLOCENE.

The Greenland ice core records suggested that the Holocene was a time of relatively stable climate (Dansgaard, et al., 1993), which has been revised based on different records (Alley et al., 1997; Bond et al., 1997; Nesje et al., 2000; Anderssen et al., 2004).

The beginning of the Holocene period is characterized by a narrow range of $U_{37}^{K}$-derived SST's between 5 - 7 °C in cores 2227, 04, and 021, and slightly warmer SST of around 10 °C in core 094 recorded over the Labrador Sea, which agrees with other studies (Andersen et al., 2004). The period of the early Holocene is characterized in our records by multiple large-amplitude $U_{37}^{K}$-derived SST fluctuations, while $U_{37}^{K'}$ and $U_{37}^{K^*}$- derived SST's show 3 to 4 degrees C warmer but relatively constant temperatures over the early Holocene period in all four cores. The cooling trend observed in cores 2227, 04 and 094 between 11 ka and 10 ka was replaced by positive excursion towards warmer $U_{37}^{K}$-derived SST's between 10 ka and 8 ka in two of four locations (04 and 094), reaching similar values between 13 and 14 °C, consistent with the data presented by Andersen et al. (2004). In core 2227 on the other hand, a prominent SST drop down to zero degrees C based on $U_{37}^{K}$-derived SST's was observed prior to 8 ka, while in core 021 over the first 2 kyr of the early Holocene SST's were relatively constant (~ 4 °C, $U_{37}^{K}$-derived SST's). The near zero $U_{37}^{K}$-derived SST observed in core 2227 (~ 8 ka) coincident with the time of the Lake Agassiz outbreak is also accompanied by high abundances of tetra alkenones, while no tetra alkenones were detected in cores 04 and 094 at the same time. The warm signal recorded in cores 04 and 094 could be an indication of warm water input into the Labrador Sea by the IC, which is a branch of NAC that moves around the Labrador Sea and brings warm and salty water into the Labrador Sea (Yashayaev and Clark, 2006). Colder $U_{37}^{K}$-derived SST's off the southern tip of Greenland could reflect increased input of cold Arctic waters through the Denmark Strait. A $U_{37}^{K}$-derived SST drop in core 2227 and to a lesser extent in core 094 due to the admixture of cold and fresh waters within the water column in the Labrador Sea could have potentially resulted in a slowdown of the AMOC and a reduction of NAC inflow (Ellison et al., 2006; Kleiven et al., 2008; Hoogakker et al., 2011). Cold $U_{37}^{K}$-derived SST's in core 04 (~ 4 °C) around 6 ka and below zero temperatures in core 021 during the middle Holocene could be a reflection of much larger input of cold water from the Canadian Arctic as a result of wider channels due to

isostatic depression based on study by Williams et al. (1995). None of these SST changes were recorded in $U_{37}^{K'}$ or $U_{37}^{K^*}$- derived SST's, where temperature fluctuations during the middle Holocene did not exceed the analytical uncertainty of 1.7 ° C (Filippova et al., 2016). The Sea surface temperature decrease around that time is also consistent with cold interval recorded in core DS97-02P south of Iceland (~ 5.6 ka) (Moros et al., 2012).

The end of the middle Holocene was characterized by similar $U_{37}^{K}$, $U_{37}^{K'}$ or $U_{37}^{K^*}$- derived SST's in cores 021 and 2227 (~ 12 °C) as in cores 094 and 04 during the early Holocene. Such warm temperatures most likely reflect the increasing influence of IW, which agrees with striking resemblance of SST record of core 094 with the core LO09-04, located over the western flank of the Reykjanes Ridge south of Iceland under the influence of IW (Andersen et al., 2004). This also strongly suggests that core 094 is a perfect location for long term studies of NAC variability.

During the late Holocene we observed two $U_{37}^{K}$- derived SST drops in core 094 over a period of only 2 kyrs not reflected in $U_{37}^{K'}$ or $U_{37}^{K^*}$- derived SST's. The down core record shows that similar $U_{37}^{K}$- derived SST decrease was observed in core 2227 at 3 ka and in core 021 at 1 ka. A $U_{37}^{K}$- derived SST decrease at around 3 ka is possibly coincident with the 2.7 ka cooling event detected in numerous records in the North Atlantic (Alley et al., 1999; Andrews and Giraudeau, 2003; Bakke et al., 2008), which then was followed by an overall warming at 2 ka, linked to a "Roman Warm Period", a widely recorded feature in the northern North Atlantic region (Moros et al., 2012). Oppo et al. (2003) connected this 2.7 ka event with surface cooling and subsequent possible slowdown of AMOC. Our data of bottom water εNd signature from core 094 suggests an increased input of Denmark Strait Overflow Water around 3 ka, indicating a higher inflow of waters from the Arctic through the Denmark Strait, which could explain the surface cooling and $U_{37}^{K}$- derived SST decrease at sites 2227 and 094. The overall cold $U_{37}^{K}$- derived SST intervals recorded in our study (~ 6 ka; 3 ka; 1 ka) are consistent with data by Moros et. al (2012) and fit well with the proposed mechanism of a long-term link of NAC fluctuations with the Subpolar Gyre dynamics (Thornalley et al. 2009).

The youngest part of the Holocene record is characterized by overall warm temperatures identical for all three indices in cores 2227, 04 and 021 with SSTs being warmer south of Greenland (16 °C, 2227) and colder on the western side of the Labrador Sea (~ 10 °C, 021). Decreasing SSTs around the Labrador Sea are consistent with dissipation of the IW

signal, moving around the Labrador basin, which is weaker on the Canadian side of the Sea (Yashayaev and Clark, et al., 2006).

In general, the $U_{37}^{K}$- derived SST records indicate highly unstable climatic conditions during most of the Holocene, unlike $U_{37}^{K'}$ and $U_{37}^{K^*}$- derived SST's, which show warmer but stable SST conditions. The positions of the cores around the Labrador basin allow monitoring the behavior of the NAC, and its changes due to the fresh water inflow into the Labrador basin. The consistency of the Holocene records between the different cores reflects the intensity of the surface circulation in the region.

## 5.6 CONCLUSIONS.

The sea surface temperature records recovered from four sediment cores provide new information on sea surface conditions, as well as inputs and circulation changes over the past 33 kyr. The record before the Holocene was only partially preserved in all cores and expressed sea surface temperatures well below zero. Climatic events such as Heinrich Stadials and Younger Dryas are characterized by an absence of alkenones in all the cores, most likely due to either cold sea surface temperatures or fresh water preventing alkenone production. The $U_{37}^{K'}$ and $U_{37}^{K^*}$- derived SST's show much warmer SST (higher than the present day SST in the Labrador Sea) during the LGM than $U_{37}^{K}$- derived SST, suggesting that these values also need to be treated with caution.

Our records support the notion that the Holocene period was a time of climatic instability characterized by multiple temperature fluctuations based on $U_{37}^{K}$- derived SST's. In core 094, SST changed around 3 ka consistent with an increased inflow of Arctic water through the Denmark Strait. The overall cold temperature spells centered around 6 ka, 3 ka and 1 ka support a previously proposed link between NAC fluctuations and dynamics of the Subpolar Gyre. The $U_{37}^{K'}$ and $U_{37}^{K^*}$- derived SST's in contrast show the Holocene as a period of a relatively stable climate. The youngest part of the record suggests universally warm temperatures over the Labrador Sea, ranging from 16 to 12°C, consistent with dissipating signal of the Irminger Waters moving around the Labrador Sea.

Consistency of the $U_{37}^{K}$- derived SST's estimates between different cores and with data from other proxies suggests that the records presented in this study reliably reflect the overall temperature trends in the Labrador Sea over the past 10 kyr extending the conclusions of Filippova et al. (2016) for at least the Holocene period. Taking into account the position of the cores along the flow path of the main water currents around the Labrador Sea contributing to

the mixture of the surface waters in the basin, this information provides new insight into the processes of the deep water formation and ocean-climate feedback mechanisms, while additionally providing a record of the NAC behavior.

## ACKNOWLEDGMENT.

This study was supported by a PhD fellowship to A.F. through the Helmholtz Research School on Ocean System Science and Technology (www.hosst.org) at GEOMAR Helmholtz Centre for Ocean Research Kiel (VH-KO-601) and Kiel University, and by the Discovery Grant program of the National Science and Engineering Research Council (NSERC) Canada (M.K.). We thank Claire Normandeau for assistance during laboratory experiments.

## REFERENCE LIST.

Alley, R.B., Mayewski, P.A., Sowers, T., Stuiver, M., Taylor, K.C. and Clark, P.U., 1997. Holocene climatic instability: A prominent, widespread event 8200 yr ago. *Geology*, *25*(6), pp.483-486.;

Andersen, Christine, et al. "Nonuniform response of the major surface currents in the Nordic Seas to insolation forcing: implications for the Holocene climate variability." *Paleoceanography* 19.2 (2004).

Azetsu-Scott K., Jones E.P., Yashayaev I. (2003) Time series study of CFC concentrations in the Labrador Sea during deep and shallow convection regimes (1991-2000). Journal of Geophysical Research, vol. 108, no. C11, 3354, doi:10.1029/2002JC001317.

Bond, G., Broecker, W., Johnsen, S., McManus, J., Labeyrie, L., Jouzel, J., Bonani, G., 1993. Correlations between climate records from North Atlantic sediments and Greenland ice. Nature 365, 143-147.Brassell, S.C., G. Eglinton, I.T. Marlowe, U. Pflaumann, M. Sarnthein (1986), Molecular stratigraphy a new tool for climatic assessment, Nature, 320, 129-133.

CLIMAP (1976) The surface of the Ice-age earth. Science 191, 1131–1137.

Conte, M.H., M.-A. Sicre, C. Rühlemann, J.C. Weber, S. Schulte , D. Schulz-Bull, T. Blanz (2006), Global temperature calibration of the alkenone unsaturation index $U_{37}^{K'}$ in surface waters and comparison with surface sediments, Geochemistry, Geophysics, Geosystems, 7(2), Q0205, doi:10.1029/2005GC0011054.

Dansgaard, W., White, J.W.C., Johnsen, S.J., 1989. The abrupt termination of the Younger Dryas climate event. Nature 339, 532-534.

de Vernal, A. , Rosell-Mele, A., Kucera, M., Hillaire-Marcel, C., Eynaud, F., Weinelt, M., Dokken, T., Kageyama, M., **2006**. Comparing proxies for the reconstruction of LGM sea-surface conditions in the northern North Atlantic, *Quaternary Science Reviews*, 25, 2820-2834. GEOTOP publication n° 2006-0008

Ellison, C.R.W., Chapman, M.R., Hall, I.R., 2006. Surface and Deep Ocean Interactions During the Cold Climate Event 8200 Years Ago. Science 312, 1929.

Fagel, N., C. Hillaire-Marcel, M. Humblet, R. Brasseur, D. Weis, *and* R. Stevenson *(*2004*)*, Nd and Pb isotope signatures of the clay-size fraction of Labrador Sea sediments during the Holocene: Implications for the inception of the modern deep circulation pattern, Paleoceanography, 19, *PA3002*, *doi:*10.1029/2003PA000993.

Filippova A., Kienast M., Frank M., Schneider, R., 2016. Alkenone paleothermometry in the North Atlantic: A review and synthesis of surface sediment data and calibrations. Geochemistry, Geophysics, Geosystems, 17 (4), 1370-1382, DOI: 10.1002/2015GC006106.

Filippova A., Frank M., Kienast M., Rickli J., Hathorne E., Yashayaev I.M., Pahnke K. (2016) Water mass circulation and weathering inputs in the Labrador Sea based on coupled Hf-Nd isotope compositions and rare earth element distributions. Geochimica et Cosmochimica Acta.

Gibb, Olivia T., Claude Hillaire-Marcel, and Anne de Vernal. "Oceanographic regimes in the northwest Labrador Sea since Marine Isotope Stage 3 based on dinocyst and stable isotope proxy records." *Quaternary Science Reviews* 92 (2014): 269-279.

Grousset, F. E., et al. "Patterns of ice-rafted detritus in the glacial North Atlantic (40–55 N)." *Paleoceanography* 8.2 (1993): 175-192.

Gwiazda, R. H., S. R. Hemming, and W. S. Broecker. "Provenance of icebergs during Heinrich event 3 and the contrast to their sources during other Heinrich episodes." *Paleoceanography* 11.4 (1996): 371-378.

Hemming, Sidney R. "Heinrich events: Massive late Pleistocene detritus layers of the North Atlantic and their global climate imprint." *Reviews of Geophysics* 42.1 (2004).

Hillaire-Marcel, C., et al. "High-resolution isotopic and micropaleontological studies of upper Pleistocene sediments at ODP Site 645, Baffin Bay." *Proceedings of the Ocean Drilling Program B* 105 (1989): 599-616.

Hillaire-Marcel, C., et al. "Isotope stratigraphy, sedimentation rates, deep circulation, and carbonate events in the Labrador Sea during the last~ 200 ka." *Canadian Journal of Earth Sciences* 31.1 (1994): 63-89.

Hoogakker, Babette AA, et al. "Dynamics of North Atlantic deep water masses during the Holocene." *Paleoceanography* 26.4 (2011).

Keigwin, Lloyd D., and Scott J. Lehman. "Deep circulation change linked to Heinrich event 1 and Younger Dryas in a middepth North Atlantic core." *Paleoceanography* 9.2 (1994): 185-194.

Kleiven, Helga Kikki Flesche, et al. "Reduced North Atlantic deep water coeval with the glacial Lake Agassiz freshwater outburst." *science* 319.5859 (2008): 60-64.

Lazier J.R.N. and Wright D.G. (1993) Annual velocity variations in the Labrador Current. J. Phys. Oceanogr. 23, 659-678.

E Böhm, J Lippold, M Gutjahr, M Frank, P Blaser, B Antz, J Fohlmeister (2015) Strong and deep Atlantic meridional overturning circulation during the last glacial cycle, ...Nature 517 (7532), 73-76

Nesje, Atle, et al. "Holocene glacier fluctuations of Flatebreen and winter-precipitation changes in the Jostedalsbreen region, western Norvay, based on glaciolacustrine sediment records." *The Holocene* 11.3 (2001): 267-280.

Mao, L., D.J.W. Piper, F. Saint-Ange, J.T. Andrewsa, M. Kienast (2014), Provenance of sediment in the Labrador Current: a record of hinterland glaciation over the past 125ka, Journal of Quaternary Science, 29, 650-660.

Meland, M.Y., E. Jansen , H. Elderfield (2005), Constraints on SST estimates for the northern North Atlantic/Nordic Seas during the LGM, Quaternary Science Reviews, 24, 835-852.

Murton, Julian B., et al. "Identification of Younger Dryas outburst flood path from Lake Agassiz to the Arctic Ocean." *Nature* 464.7289 (2010): 740-743.

Müller, Peter J., et al. "Calibration of the alkenone paleotemperature index U 37 K′ based on core-tops from the eastern South Atlantic and the global ocean (60 N-60 S)." *Geochimica et Cosmochimica Acta* 62.10 (1998): 1757-1772.

Pflaumann, U., et al. "Glacial North Atlantic: Sea-surface conditions reconstructed by GLAMAP 2000." *Paleoceanography* 18.3 (2003).

Prahl, F.G., S.G. Wakeham (1987), Calibration of unsaturation patterns in long chain ketone compositions for paleotemperature assessments, Nature, 330, 367-369.

Rosell-Melé, Antoni, et al. "Biomarker evidence for "Heinrich" events." *Geochimica et Cosmochimica Acta* 61.8 (1997): 1671-1678.

Rosell-Melé, Antoni, and Pau Comes. "Evidence for a Warm Last Glacial Maximum in the Nordic Seas or an example of shortcomings in UK 37′ and UK 37 to estimate low sea surface temperature?." *Paleoceanography* 14.6 (1999): 770-776.

Sachs, J.P. (2007), Cooling of Northwest Atlantic slope waters during the Holocene, Geophysical Research Letters, 34, L03609, doi:10.1029/2006GL028495.

Sicre, M.-A., K. Weckström, M.-S. Seidenkrantz, A. Kujipers, M. Benetti, G. Masse, U. Ezat, S. Schmidt, I. Bouloubassi, J. Olse, M. Khodri, J. Mignot (2014), Labrador current variability over the last 2000 years, Earth and Planetary Science Letters, 400, 26-32.

Veiga-Pires, C. C., and C. Hillaire-Marcel. "U and Th isotope constraints on the duration of Heinrich events H0-H4 in the southeastern Labrador Sea." *Paleoceanography* 14.2 (1999): 187-199.

Weaver, A. J., Bitz, C. M., Fanning, A. M. & Holland, M. Thermohaline circulation: High latitude phenomena and the difference between the Paci®c and Atlantic. Annu. Rev. Earth Planet. Sci. 27, 231± 285 (1999).

D'Andrea, William J., and Yongsong Huang. "Long chain alkenones in Greenland lake sediments: Low δ 13 C values and exceptional abundance." *Organic Geochemistry* 36.9 (2005): 1234-1241.

World Ocean Atlas, (2013). www.nodc.noaa.gov

Yashayaev I. and Clark A. (2006) Recent warming of the Labrador Sea. AZMP Bulletin PMZA 5:12-20.

Yashayaev I., Dickson R.R. (2008) Transformation and fate of overflows in the northern North Atlantic, in Arctic-Subarctic Ocean Fluxes: Defining the Role of the Northern Seas in Climate, edited by R.R. Dickson, J. Meincke and P. Rhines, Chapter Arctic-Subarctic Ocean Fluxes 505-526, Springer, New York.

Yashayaev I., Loder J.W. (2016) Recurrent Replenishment of Labrador Sea Water and Associated Decadal-Scale Variability. Journal of Geophysical Research - Oceans, Accepted manuscript, DOI: 10.1002/2016JC012046

de Vernal A. et al., 2001. Dinoflagellate cyst assemblages as tracers of sea-surface conditions in the northern North Atlantic, Arctic and sub-Arctic seas: the new 'n=677' data base and its application for quantitative paleoceanographic reconstruction. Journal of Quaternary Science, 16, 681-698.

de Vernal A., Rosell-Mele A., Kucera M., Hillaire-Marcel C., Eynaud F., Weinelt M., Dokken T., Kageyama M., 2006. Comparing proxies for the reconstruction of LGM sea-surface conditions in the northern North Atlantic. Quaternary Science Review, 25, 2820-2834.

Hemming S.R., 2004. Heinrich events: Massive Late Pleistocene detritus layers of the North Atlantic and their Global Climate imprint. Rev. Geophys., 42, RG1005, doi:10.1029/2003RG000128

Kirby M.E. and Andrews J.T., 1999. Mid-Wisconsin Laurentide Ice Sheet growth and decay: Implications for Heinrich events 3 and 4. Paleoceanography, 14 (2), 211-223.

Meland M.Y., Jansen E., Elderfield H., 2005. Constraints on SST estimates for the northern North Atlantic/Nordic Seas during the LGM. Quaternary Science Reviews, 24, 835-852.

Pflaumann U., Sarnthein M., Chapman M., d'Abreu L., Funnell B., Huels M., Kiefer T., Maslin M., Schulz H., Swallow J., van Kreveld S., Vautravers M., Vogelsang E., Weinalt M., 2003. Glacial North Atlantic: Sea-surface conditions reconstructed by GLAMAP 2000. Paleoceanography, 18, 1065, doi:10.1029/2002PA000774.

Rosell-Mele A. and Comes P., 1999. Evidence for a warm Last Glacial Maximum in the Nordic seas or an example of shortcomings in $U_{37}^{K'}$ and $U_{37}^{K}$ to estimate low sea surface temperature? Paleoceanography, 14 (6), 770-776.

Rosell-Mele A., Carter J., Eglinton G., 1994. Survey of distributions of long-chain alkenones and alkyl alkenonates in marine surface sediments from the north east Atlantic, 1994. Org. Geochem, 22, 501-509.

Rosell-Mele A., Weinelt M., Koc N., Jansen E., Sarnthein M., 1998. Variability of the Arctic front during the last climatic cycle. Application of a novel molecular proxy. Terra Nova, 10, 86-89.

Sachs J.P., 2007. Cooling of Northwest Atlantic slope waters during the Holocene. Geophysical research letters, 34, L03609, doi:1001029/2006GL028495.

Sicre M.-A., Weckström K., Seidenkrantz M.-S., Kujpers A., Benetti M., Masse G., Ezat U., Schmidt S., Bouloubassi I., Olsen J., Khodri M., Mignot J., 2014. Earth and Planetary Science Letters, 400, 26-32, doi:10.1016/j.epsl.2014.05.016.

Villanueva J., Grimalt J.O., Cortijo E., Vidal L., and Labeyrie L., 1997. A biomarker approach to the organic matter deposited in the North Atlantic during the last climatic cycle. Geochimica et Cosmochimica Acta, vol. 61, no. 21, pp. 4633-4646.

Weaver P.P.E., Chapman M.R., Eglinton G., Zhao M., Rutledge D., Read G., 1999. Combined coccolith, foraminiferal, and biomarker reconstruction of paleoceanographic conditions over the past 120 kyr in the northern North Atlantic (59°N, 23°W). Paleoceanography, 14, 3, 336-349.

# CHAPTER 6

# CHANGES IN WATER MASS CIRCULATION AND WEATHERING INPUTS IN THE LABRADOR SEA OVER THE LAST 35 KYRS BASED ON ND-HF-PB ISOTOPE COMPOSITIONS OF MARINE SEDIMENTS.

to be submitted as: Filippova A., Frank M., Kienast M, Gutjahr M., Hathorne E., Hillaire-Marcel C., (2017) Changes in water mass circulation and weathering inputs in the Labrador Sea over the last 33 kyrs based on Nd-Hf-Pb isotope compositions of marine sediments.

## ABSTRACT.

The Labrador Sea is an important region for the Atlantic Ocean Meridional Circulation, as a deep water formation site and as a main contributor to the North Atlantic Deep Water. Variations in the processes of deep water mass formation in the past and at the present time have been a focus of many studies, however, more information is still needed to improve our understanding of the ongoing processes and their role and significance in global climate change. Here we present Hf-Nd-Pb radiogenic isotope compositions from four sediment down cores from the Labrador Sea in order to obtain crucial information about the deep water mass circulation patterns and weathering inputs that prevailed in the region in the past and compare it to the present day. The new data suggest earlier inception of the Denmark Strait Overflow Water around 12 ka and establishment of the Labrador Current at the similar time. The εNd and the εHf seawater signatures form a new array termed the Labrador Sea array, feature that is observed in the present day surface waters off the coast of Canada. As at the present time the intermediate waters in the Labrador over the past could have been under significant influence of Hf release from dissolution of clay particles or clay associated colloids. Presence of the Labrador Sea Water was detected around 5 ka, suggesting intensified convection in the region to a depth of 2600 m.

## 6.2 INTRODUCTION.

The ocean plays an important role in controlling regional and global climate. In many instances over the past fluctuations of the climate system were a results of changes in the ocean circulation, driven by meridional heat and fresh water transport (cf. Dickson et al., 1988; Dommenget and Latif, 2002; Gulev et al., 2001). One of the crucial components for climate modelling and improvement of forecasting global climate dynamics in the future is understanding the mechanisms controlling the global ocean variability, and regular observations of the integral parts of the ocean systems.

The Atlantic Meridional Overturning Circulation (AMOC), driven by the heat exchange between the atmosphere and the ocean and transport of heat from equatorial regions to high latitudes, is one of the factors controlling the global climate. Understanding the dynamics and variability of the AMOC is crucial for climate change predictions. Variations in the processes of deep water convection and water mass formation in the past and during the modern time have been a focus of many studies (Dickson and Brown, 1994; Vellinga and Wood, 2002; Hall et al., 2006; Chen et al., 2012; Trouet et al., 2012; McCarthy et al., 2014).

The Labrador Sea is one of the key regions contributing to the formation of North Atlantic Deep Water and changes in its hydrography have potential to influence the AMOC and global climate. The formation of deep waters in the area is defined by the inflow of waters from the Arctic, such as the West Greenland Current entering through the Denmark Strait and the Labrador Current entering through the Davis Strait. The Labrador Sea is bounded by the warm and saline inflow of the North Atlantic Current waters from the south, resulting in a counterclockwise surface flow in the Labrador Sea (Lazier and Wright, 1993). The annual accumulation of cold and fresh water and its injection into the deeper layers makes the Labrador Sea the freshest and coldest basin of the Subpolar North Atlantic (SPNA) (Yashayaev et al., 2015). Wind driven convection, promoted by strong winter cooling, leads to the formation of the Labrador Sea Water (LSW), which is being transported out of the Labrador Sea and is entrained in the North Atlantic Deep Water (NADW) (Yashayaev and Clark, 2006; Yashayaev and Loder, 2009). The North Atlantic Deep Water is formed by mixing of the LSW, the North East Atlantic Deep Water (NEADW), the Denmark Strait Overflow Water (DSOW), and the Iceland Scotland Overflow Water (ISOW). The ability to trace and understand processes of the deep water formation in the Labrador Sea is crucial for reliability of our future climate predictions. Regular annual monitoring cruises in the Labrador Sea provided good quality climate records over the last few decades (Yashayaev et al., 2008; Yashayaev et al., 2015). However, to be able fully understand the ongoing processes and their role and significance in global climate change, records of the past ocean circulation are necessary. By means of Hf-Nd-Pb radiogenic isotope compositions we are able to obtain crucial information on the deep water mass circulation patterns and weathering inputs in the Labrador Sea that prevailed in the region in the past and compare it to the present day.

Combined radiogenic Hf, Nd and Pb isotope compositions are a powerful tool to trace present and past ocean circulation and changes in weathering inputs (Bayon et al., 2006, 2009; Gutjahr et al., 2009; Godfrey et al., 2009; Rickli et al., 2009, 2010; Chen et al., 2012; Crocket et al., 2012; Stichel et al., 2012 a,b; Crocket et.al., 2013) but the exact mechanisms controlling their behavior and distribution in seawater, in particular those of Hf isotopes, are still not well constrained. Due to small differences in $^{143}Nd/^{144}Nd$ and $^{176}Hf/^{177}Hf$ ratios (four or fifth place after the decimal), Nd and Hf isotope ratios are expressed as εNd and εHf values:

$$\varepsilon Nd = \frac{\left(\frac{^{143}Nd}{^{144}Nd}sample\right) - \left(\frac{^{143}Nd}{^{144}Nd}CHUR\right)}{\frac{^{143}Nd}{^{144}Nd}CHUR} * 10000,$$

$$\varepsilon Hf = \frac{\left(\frac{^{176}Hf}{^{177}Hf}sample\right) - \left(\frac{^{176}Hf}{^{177}Hf}CHUR\right)}{\frac{^{176}Hf}{^{177}Hf}CHUR} * 10000,$$

where CHUR represents the present-day chondritic $^{143}Nd/^{144}Nd$ value of 0.512638 (Jacobssen and Wasserburg, 1980) and $^{176}Hf/^{177}Hf$ value of 0.282785 (Nowell et al., 1988; Bouvier et al., 2008).

The coherent behavior of Hf with Nd during the most magmatic processes resulted in a strong positive correlation of radiogenic Nd and Hf isotopes in most terrestrial rocks, which has been defined as a "mantle-crust array" or "terrestrial array" (Fig. 1, $\varepsilon Hf = 1.55 * \varepsilon Nd + 1.21$, Vervoort et al., 2011). However, Hf undergoes significant fractionation due to weathering and sediment transport (Dickin, 2005), resulting in the formation of the so called "seawater array", where for every given Nd a more radiogenic Hf is observed ($\varepsilon Hf = 0.62 * \varepsilon Nd + 7.38$, Albarède et al., 1998; Godfrey et al., 1997; David et al., 2001). Seawater array was explained by Hf fractionation during weathering caused by zircons and termed as a "zircon effect" (van de Flierdt et al., 2007) and in addition preferential release of radiogenic Hf from labile minerals with high Lu/Hf, such as apatite and sphene play an important role (Barford et al., 2003; Bayon et al., 2009; Godfrey et al., 2009; Chen et al., 2011). Lead isotope ratios do not display a strong correlation with Hf-Nd in continental rocks and oceanic basalts (Goldstein and Hemming, 2003). However, Pb is also fractioned during weathering and more radiogenic lead is preferentially released due to the radiation damage to the crystal lattice of the minerals during the radioactive decay of the parent isotopes ($^{235,238}U$, $^{232}Th$) which leaves daughter isotopes loosely bound in the minerals, causing their preferential mobilization at the grain boundaries (cf. Frank, 2002). As a consequence, radiogenic lead isotopes ($^{206}Pb$, $^{207}Pb$, $^{208}Pb$) are easier mobilized from rocks and minerals during weathering than nonradiogenic $^{204}Pb$. Thus, Pb isotope compositions of weathered solutions and dissolved Pb in seawater do not directly reflect the Pb isotope signature of the bulk source rocks (Blanckenburg and Nägler, 2001).

Studies carried out over the last decades in the Labrador Sea suggest that the DSOW inflow was not present until 8 - 6 ka based on $^{230}Th_{excess}$ data from a 6 m sequence raised from the Orphan Knoll by Veiga-Pires and Hillaire-Marcel (1998), which was later supported by records of the Nd-Pb isotope compositions of the clay fraction by Fagel et al. (2002, 2004). The inception of the inflow led to the formation of the DSOW, the densest and deepest water mass in the Labrador Sea as late as 6 - 5 ka (Bilodeau et al., 1994). The North East Atlantic Deep Water was not fully present in the Labrador Sea until 10 - 9 ka based on the stable oxygen and carbon isotope compositions of benthic foraminiferal assemblages (Bilodeau et al., 1994).

Here we present the first combined seawater Nd-Hf-Pb isotope composition data from four sediment down cores recovered from the Labrador Sea together with total dissolution data of the detrital fraction, which allow to trace the source origin of the sediments, supplied to the core locations. Additionally, several data points of Nd isotope composition of uncleaned foraminifera from each core have been obtained to test the reliability of the results and to see if the data reflect water mass signatures. In the light of the new data we revise the establishment times of different water masses present in the Labrador Sea and investigate the surface and deep water mass patterns in the Labrador Sea over the period of the last 35 kyrs.

## 6.3 MATERIALS AND METHODS.

### 6.3.1 MATERIALS

Core MD99-2227, hereafter called 2227 (58°5526 N, 48°2238 W) was recovered from the southwest Greenland Rise at the water depth of 3460 m by the research *vessel Marion Dufresne* in 1999 (Fig. 1). The total length of the core is 42.96 m. The focus of this study are the uppermost 6.5 m ( 0.75 to 20.32 ka), spanning the period of the Holocene, the Younger Dryas (YD), Heinrich Stadial 1 (HS1) and the inception of the last deglaciation. The age model fix points were published by Fagel et al. (2004) and were linearly interpolated. The core was sampled every 15 to 30 cm, depending on the availability of the material. A higher resolution of 10 cm was chosen around the 8.2 ka event, the YD and the HS1. At the beginning of the Holocene, the sedimentation rate increases from ~ 19 cm/kyr to 61 cm/kyr and then decreases again to 39 cm/kyr during the middle and the late Holocene.

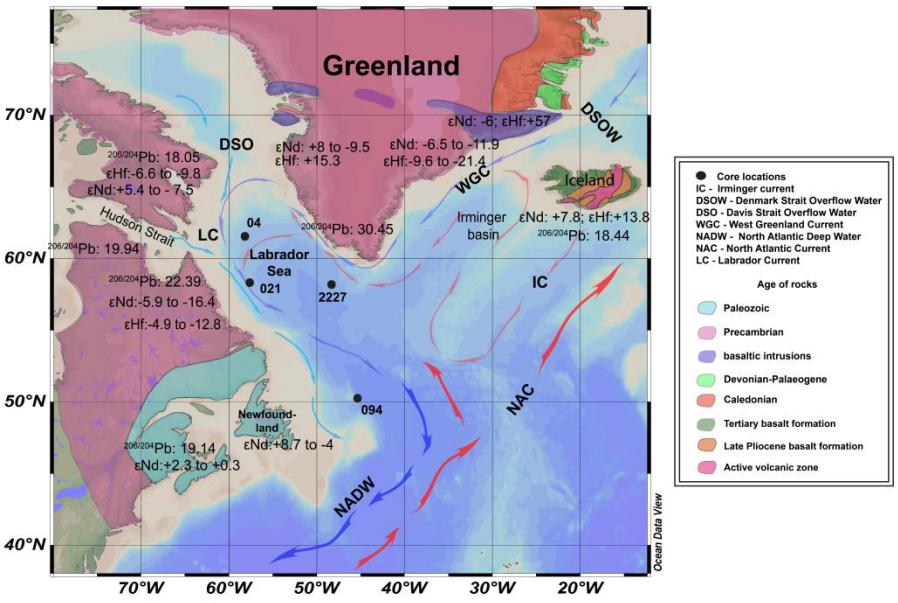

**Fig. 1** Map of the study area. Black dots represent core locations. Red arrows denote warm water currents, blue arrows cold water currents. Abbreviations stand for: Davis Strait Water (DSO), Denmark Strait Overflow Water (DSOW), Irminger Current (IC), North Atlantic Current (NAC), North Atlantic Deep Water (NADW), West Greenland Current (WGC). A schematic representation of the geology of the surrounding landmasses is shown and includes average εHf, εNd and $^{206/204}$Pb values of the rocks. For full ranges of the values, please refer to original publications (Welke et al., 1968; Gerasimovsky et al., 1975; Sun et al., 1975; Zindler et al., 1982; Brevart et al., 1986; Swinden et al., 1990; Elliott et al., 1991; Furman et al., 1992; Stern et al., 1994; Camire et al., 1995; Hards et al., 1995; Furman et al., 1995; Skulski et al., 1996; Hanan et al., 1997; Hardarson et al., 1997; La Fleche et al., 1998; Maclachlan et al., 1998; Nowell et al., 1998; Pe-Piper et al., 1998; Salter et al., 1998; Blichert-Toft et al., 1999; Minifie et al., 1999; Stecher et al., 1999; Chauvel et al., 200; Fitton et al., 2000; Hards et al., 2000; Kempton et al., 2000; Thirwall , 2000; Prestvik et al., 2001; Goodenough et al., 2002; Stracke et al., 2003; Thirwall et al., 2004; West et al., 2004; Kokfelt et al., 2006; Gaffney et al., 2007; Kitagawa et al., 2008; Tappe et al., 2008; Willbold et al., 2008; Peate et al., 2008; Kokfelt et al., 2009; Peate et al., 2009; Willbold et al., 2009; Hoffmann et al., 2010; Jackson et al., 2010; Peate et al., 2010; Chekolt et al., 2011; Kuritani et al., 2011; Koornneef et al., 2012; Szilas et al., 2012; Rizo et al., 2013; Shorttle et al., 2013; Manning et al., 2014 ).

Core HU08-029-0004, hereafter called 04 (61°2749 N, 58°0211 W) was obtained off the southern Baffin Island shelf in the northern Labrador Sea on board the Canadian Coast Guard (CCGS) research vessel *Hudson* in 2008, from a water depth of 2674 m (Fig. 1). The study covers the entire length of the core of 895 cm. The age model was previously published by Gibb et al. (2014). The sedimentation rate increases from values of ~ 27 cm/kyr prior to the LGM to higher sedimentation rates during the HS1 (44 cm/kyr) and the YD (102 cm/kyr). During the Holocene, the sedimentation rate gradually decreases to values as low as ~ 10 cm/kyr at the end of the Holocene.

Core HU84-030-021, hereafter called 021 (58°22600 N, 57°30.42 W) was collected from the continental slope of the western Labrador Sea from a water depth of 2853 m (Fig. 1). This study focuses on the upper 8 m. The age model was previously published by Hillaire-Marcel and de Vernal (1989) and was linearly interpolated between available AMS $^{14}$C ages. The sedimentation rate over the period from 27 to 17 ka was 27 - 28 cm/kyr. A slight increase is observed at the time of the YD reaching sedimentation rates around 39 cm/kyr, followed by a decrease to lower sedimentation rates of 16 cm/kyrs during the late Holocene.

Core HU91-045-094, hereafter called 094 (50°12.26 N, 45°41.14 W) was recovered from the western part of the Labrador Sea at Orphan Knoll, on board *CCGS Hudson* in 1991, from a depth of 3448 m. The total length of the core is 24 m, but this study focuses on the uppermost 4.5 m only. The age model is based on the previously published data by Hillaire-Marcel et al. (1994) and was linearly interpolated between available AMS $^{14}C$ ages. Lower sedimentation rates observed prior the LGM, the YD and the middle to the late Holocene range between 10 and 13 cm/kyr. High sedimentation rates between 35 and 39 cm/kyr were recorded from the LGM to the HS1.

In total between 22 and 32 samples per core were analyzed for seawater radiogenic Nd-Hf-Pb isotope compositions extracted from the ferromanganese coatings of marine sediments, complemented by 4 - 5 additional data points of Nd isotope compositions obtained from uncleaned foraminifera. In addition, 7 to 12 samples per core were analyzed for the Nd-Hf-Pb isotope compositions of the totally dissolved detrital fraction.

## 6.3.2 METHODS

### 6.3.2.1 SAMPLE PREPARATION AND MASS SPECTROMETRIC ANALYSIS

Neodymium, Hf and Pb isotope compositions were measured on samples from four cores following the procedure of Gutjahr et al. (2007) (Table A5, A6, A7). Briefly, 1.5 - 2 grams of freeze-dried sediment were leached with a solution of 10 % hydroxylamine mixed with 0.03 M EDTA for one hour. The resulted supernatant was dried down, dissolved in concentrated nitric acid, dried down again, and transferred to $Cl^-$ form by dissolution in concentrated HCl. Finally, samples were dried down and redissolved in loading solutions of 1 M HCl/0.05 M HF for cation exchange column chemistry to purify Nd and Hf and a mixture of 2 M HBr with 0.25 M $HNO_3$ and MQ for chromatographic purification of Pb, respectively. For Hf and Nd separation from the sample matrix a set of three columns was used: cation columns with AG 50W-X8 resin (200 - 400 dry mesh), columns loaded with Eichrom Ln-Spec resin with a bead size 50 - 100 µm for Nd purification and a third set of columns loaded with Eichrom Ln-Spec with a bead size 100 - 150 µm for Hf purification (Pin and Zalduegui, 1997; Münker et al., 2001). For Pb separation, only one set of columns filled with AG1-X8 resin, dry mesh 100 -200 µm was used (Manhes et al., 1978). Foraminifera cleaning followed the procedure of Tachikawa et al., (2014). Briefly, freeze-dried sediment samples were washed through a < 64 µm sieve and the remained fraction collected in a porcelain jar and dried down. All planktonic and benthic foraminiferal shells present in the samples were handpicked, crushed until all chambers were opened and subsequently cleaned with MQ and

ethanol. The remaining sample was then dissolved in 1 M acetic acid, dried down and redissolved in the loading solution for cation column chromatography following standard procedure (Pin and Zalduegui, 1997) The total dissolution procedure of the detrital fraction was modified from Burton et al., (2002). Briefly, 100 mg of freeze-dried sediment, after a second leaching step of 6.5 hours to completely remove any coatings, were subsequently treated with a combination of concentrated nitric, hydrochloric and hydrofluoric acids, refluxed and dried down. To dissolve all refractory minerals, including zircon, all samples were placed in metal jacket bombs in an oven at 200 °C for at least 4 - 5 days in a mixture of concentrated nitric and hydrofluoric acids. After complete dissolution the samples were dried down, treated with perchloric acid to remove remaining organic matter, dried down again and were redissolved in the loading solution for cation chromatography.

Neodymium isotope compositions of the foraminifera were measured on a Thermo Finnigan Neptune Plus MC-ICPMS at the Max Planck Research Group for Marine Isotope Geochemistry in Oldenburg, Germany. Neodymium, Hf and Pb isotope ratios of leachates and detrital fractions were carried out on the Nu Instruments MC-ICPMS at GEOMAR, Kiel. All measured Nd isotope compositions were corrected for instrumental mass bias to $^{146}Nd/^{144}Nd$ = 0.7219 applying an exponential mass fractionation law. All $^{143}Nd/^{144}Nd$ ratios were normalized to the accepted JNdi-1 standard value of 0.512115 (Tanaka et al., 2000). The external reproducibility of foraminifera data varied from 0.1 to 0.4 εNd units (2 S.D.), with an average value  0.31. The external reproducibility of the leachate data varied between 0.2 and 0.5 εNd units (2 S.D), with one exception of one run when it was 0.8 εNd units. The average long term reproducibility of the leachate measurements was  0.41 (2 S.D.) over the course of three years. The foraminifera blank was less than 89 pg and considered negligible. Blanks (n = 5) for leachates were less than 1270 pg and also considered negligible compared with the sizes of the samples (less than 1 % of the total amount of Nd in the samples).

Samples with Hf concentrations higher than 20 ppb were measured on the Nu Instruments MC-ICPMS at GEOMAR, Kiel, whereas those with concentrations lower than 20 ng/g were measured on the Thermo Finnigan Neptune Plus MC-ICP-MS at GEOMAR, Kiel. Measured Hf isotope compositions were corrected for instrumental mass bias to $^{179}Hf/^{177}Hf$ of 0.7325 applying an exponential mass fractionation law. All $^{176}Hf/^{177}Hf$ ratios were normalized to the accepted JMC475 standard value of 0.28216 (Nowell et al., 1998). External reproducibility of the Nu Instruments MC-ICPMS measurements varied between 0.3 and 0.7 (2 S.D.) with one exception during one run 1.8  (2 S.D.). Long-term external reproducibility was = 0.7 (2 S.D.) over the course of three years. Procedural blanks were less than 119 pg (n

= 4), with exception of one which was 5 ng and were considered negligible (less than 3 % of the total amount of Hf in the samples). On the Neptune Plus MC-ICPMS Hf samples were generally run at concentrations of 10 ppb, bracketed by a pair of JMC475 and Certipur standards after each three samples. The external reproducibility was 2 S.D. = 0.3 based on repeated measurements of the Certipur standards. All εHf values were corrected for Yb contribution using a calibration equation, based on repeated measurements of internal standards with different Yb concentrations, carried out by T. Chen.

Lead isotope composition measurements were carried on the Nu Instruments MC-ICPMS at GEOMAR, Kiel. All samples were run at concentrations of 50 ppb. All Pb ratios were normalized to the accepted values of NBS981 of 36.7219; 15.4963; 16.9405; 2.1677; 0.9147 for $^{208}Pb/^{204}Pb$, $^{207}Pb/^{204}Pb$, $^{206}Pb/^{204}Pb$, $^{208}Pb/^{206}Pb$ and $^{207}Pb/^{206}Pb$ ratios, respectively. Blanks were on average less than 1 ng (less than 1 %), with the exception of one single measurement yielding 28 ng (30 %), and were considered negligible.

With each batch of samples a reference material was analyzed (homogenized sediment sample). The 2 S.D reproducibility for εNd was ~ 0.3 (n = 4) and 2 S.D. (n = 4) for Pb was between 0.3 ($^{208}Pb/^{204}Pb$) and 0.1 ($^{206}Pb/^{204}Pb$). The Hf yield from all four reference material samples was zero, most likely due to high carbonate content. Additional duplicate samples (3 to 5 per core) were the same within the analytical error (for Nd, Hf and Pb).

## 6.4 RESULTS.

### 6.4.1 RELIABILITY OF THE SEAWATER DATA.

There are multiple ways to test the reliability of the extracted seawater data. The first approach to establish if the leachates represent the true seawater signal is to measure the εNd isotope composition of uncleaned foraminifera (Fig. 2 A). In this study only 2 to 5 samples in each core were selected for foraminiferal analysis for the entire core length due to the low abundance of foraminiferal shells. Most of the samples reflect the same values within error with only a few exceptions. In cores 2227, 04 and 094 some of the εNd signatures of uncleaned foraminifera are less radiogenic than the leachates, which could be explained by dolomite contamination, characterized by highly unradiogenic εNd values (Genna Patton, personal communication). Dolomite contamination could occur as a result of its incorporation in foraminiferal tests as microparticles during crystallization or by chemical exchange during early diagenesis (Cléroux et al., 2008, Marcott et al., 2011). In core 021 two samples of uncleaned foraminifera are more radiogenic than the leachates, which might be explained by dissolution of volcanic glass particles due to incomplete cleaning of the samples.

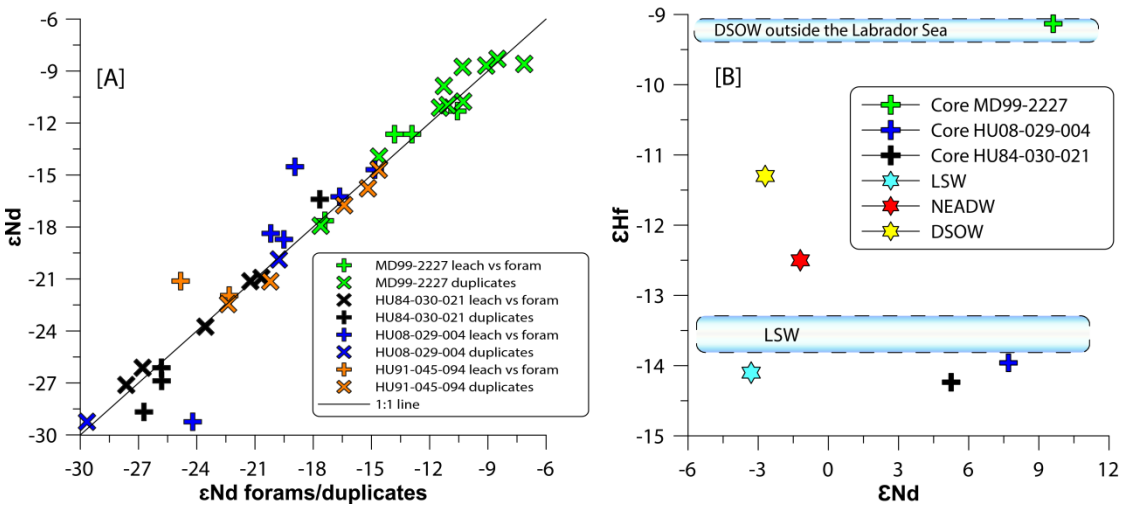


**Fig. 2** A. The εNd signatures of the leachates versus εNd signatures of uncleaned foraminifera for the same samples. Also shown is a comparison of the εNd signatures of the duplicate samples. The black line denotes the 1:1 relationship. B. The εHf versus εNd signatures of the youngest samples from each core. The εHf versus εNd signatures of LSW, NEADW, DSOW are also shown from Filippova et al (submitted). Horizontal blue bars denotes LSW and DSOW outside of the Labrador Sea (only εNd, Lacan and Jeandel, 2005). No εHf value is available for the youngest sample of core 094.

Additional information is provided by duplicate samples and reference material measured with each batch of samples. The major part of the duplicate data for εHf, εNd and Pb isotopes of the leachates and detrital material reproduce well within the error, with the exception of εHf analyses of two samples of core 094, which differ significantly and likely indicate incomplete homogenization of the samples. The εNd and Pb isotope signatures of the reference material (n = 4), analyzed with each batch of samples, are the same within the error bar.

The second option is to compare the modern day seawater values with the most recent samples, available in the study. As has been described in chapter 3 of this thesis, εNd and εHf signatures of the modern seawater masses present in the Labrador Sea were obtained during cruise on board of *CCGS Hudson* in study area in May 2013, which provides the basis for a calibration of the core tops. The youngest samples of the three sediment cores covering the last 2 kyrs show εNd values (-9.1 core 2227; -14 core 004; -14.2 core 021; -15.1 core 094) close to the modern seawater data in the range of the LSW ~ -14.1 (Filippova et al., submitted) and the DSOW outside the Labrador Sea -8.4 (Lacan and Jeandel, 2005) (Fig. 2 B). The locations of cores 021 and 04 are in the range of the modern LSW consistent with the water depths between 2600 and 2800 m. Core 094 for the sample of 2 kyrs is slightly less

radiogenic than the modern LSW in εNd. The near core top εNd value of core 2227 reflects a signature close to the modern DSOW outside of the Labrador Sea before its advection into the Labrador Sea (εNd). The εHf signatures of the youngest sediment samples are more radiogenic than the modern LSW up to 9 - 15 εHf units (Fig. 2 B). This, however, does not necessarily mean, that εHf signatures do not reliably reflect the seawater signal. It could suggest that hafnium is more sensitive to the short term variability in the water mass circulation in the Labrador Sea, which was proposed by Filippova et al. (submitted).

Based on these results we conclude that the dataset produced here is reliable and can be used for further interpretation of the leachate and foraminiferal data in terms of seawater signatures.

### 6.4.2 ND ISOTOPE COMPOSITION

The Nd isotope composition of the four sedimentary records covers the last 28 - 33 kyr with one shorter record of only 20 kyrs (core 2227). The εNd signatures over the studied period range between -8.3 in core 2227 (~2.7 ka) and -30.5 in core 021 (~ 18 ka), with more radiogenic values in core 2227 and less radiogenic in cores 021 and 04 (Fig. 3). The beginning of the record in core 094 shows an increase of εNd signatures from εNd ~ -18.7 (~ 33 ka) to more radiogenic value of εNd ~ -15.8 over the period of 5 kyrs. Similar radiogenic excursion is observed in cores 04 (εNd ~ -18.7) and 021 (εNd ~ -28.9), where εNd signature increases by around 2 εNd units over the period of 3 kyrs (from 30 to 27 kyrs). No reflection of the HS3 (~31 ka) is found in any of the data. At the time of the HS2 a drastic decrease of εNd towards less radiogenic values is observed in two cores 04 (εNd ~ -29.2) and 094 (εNd ~ -24.3), followed by a radiogenic excursion shortly afterwards of more than 10 εNd units. At the same time the HS2 is reflected in core 021 Nd by only a slight decrease of 2 to 3 εNd units (εNd =-29.8). Highly unradiogenic signatures, however, stay a persistent feature at this location all the way till the time of the HS1. During the LGM highly unradiogenic signal is recorded only in core 021 (εNd = -30.6), whereas in cores 2227, 04 and 094 more radiogenic εNd signatures were recorded, ranging between -14 and -18. The Heinrich Stadial 1 similarly to the HS2 is marked by a decrease in εNd signatures in three cores (2227, 04 and 094), with a more pronounced negative excursion in core 04 up to -27, and less in core 2227 εNd of -17.9. After the HS1 a prominent radiogenic excursion is observed in cores 2227 up to the beginning of the Holocene and in core 04, over the period between 16 and 12 kyrs. Interestingly, in core 2227 εNd signature reaches radiogenic values of -9.9 already at ~12 ka, which is only slightly less radiogenic than the present day DSOW or the ISOW. Gradual increase in radiogenic

signal is observed in core 021, where εNd signature slowly gets more radiogenic after the HS1, reaching -20.3 at the beginning of the Holocene. The εNd signatures in core 094 do not recover after the HS1 and stay relatively constant and unradiogenic (between -18 and -22) till the beginning of the Holocene. During the period of the "Mystery Interval" (17.5 and 14.5) two short term unradiogenic events are recorded in core 021, around 15.3 ka and 13.9 ka, with a decrease of 3 to 4 εNd units. The YD cold interval seems to be recorded only in one core 04 in our study, with a slight decrease of ~ 2 εNd units (εNd = -14.8 at 12.7 ka). However, in core 2227 during the YD, where no leachate samples are available, εNd signatures of uncleaned foraminifera also suggest a decrease towards unradiogenic values of around -14. At the beginning of the Holocene εNd signatures in the Labrador Sea are more radiogenic on the eastern side, ranging between -9.9 (at 10.8 ka) in core 2227 and -15.4 (at 10.8 ka) in core 04 and less radiogenic on the western side of -21.3 on average in cores 021 and 094 ( at 10.1 and 10.4 ka). In genera,l the overall radiogenic excursion over the Holocene is recorded in all four cores, with some short term negative events. Around the time of the 8.2 ka event a 2 εNd units decrease was recorded in cores 2227 and 04, where εNd signatures reach values of -12.6 and -18.5, respectively. A 5 εNd units decrease is recorded in core 021 around 6 ka. In core 094 during the late Holocene εNd signal decreases starting from 3.5 ka (εNd = -11.3), reaching -15.1 around 1.5 ka. The youngest samples εNd signatures are getting less radiogenic moving around the Labrador Sea, following the flow path of the main water currents, with radiogenic signature of -9.1 off the southern tip of Greenland and less radiogenic signature on the way out of the Labrador Sea in core 094 (εNd = -15.1). In cores 04 and 021 the εNd signatures of the youngest samples reach the present day εNd signature of the LSW, while core 2227 expresses signature close to the present day εNd signature of the DSOW and the ISOW.

The detrital εNd record follows similar trends as the εNd signatures of the leachates. Such events as the HS2 and the HS1 are recorded by pronounced shifts towards more unradiogenic values in cores ( 2227, 04 and 094), while core 021 is under the influence of highly unradiogenic source (between -27 and -28) till the beginning of the Holocene. In general the detrital εNd signatures are getting more radiogenic in cores 2227 and 021 over the Holocene, while in cores 04 and 094 the signal appears to be relatively unchanged since the beginning of the Holocene.

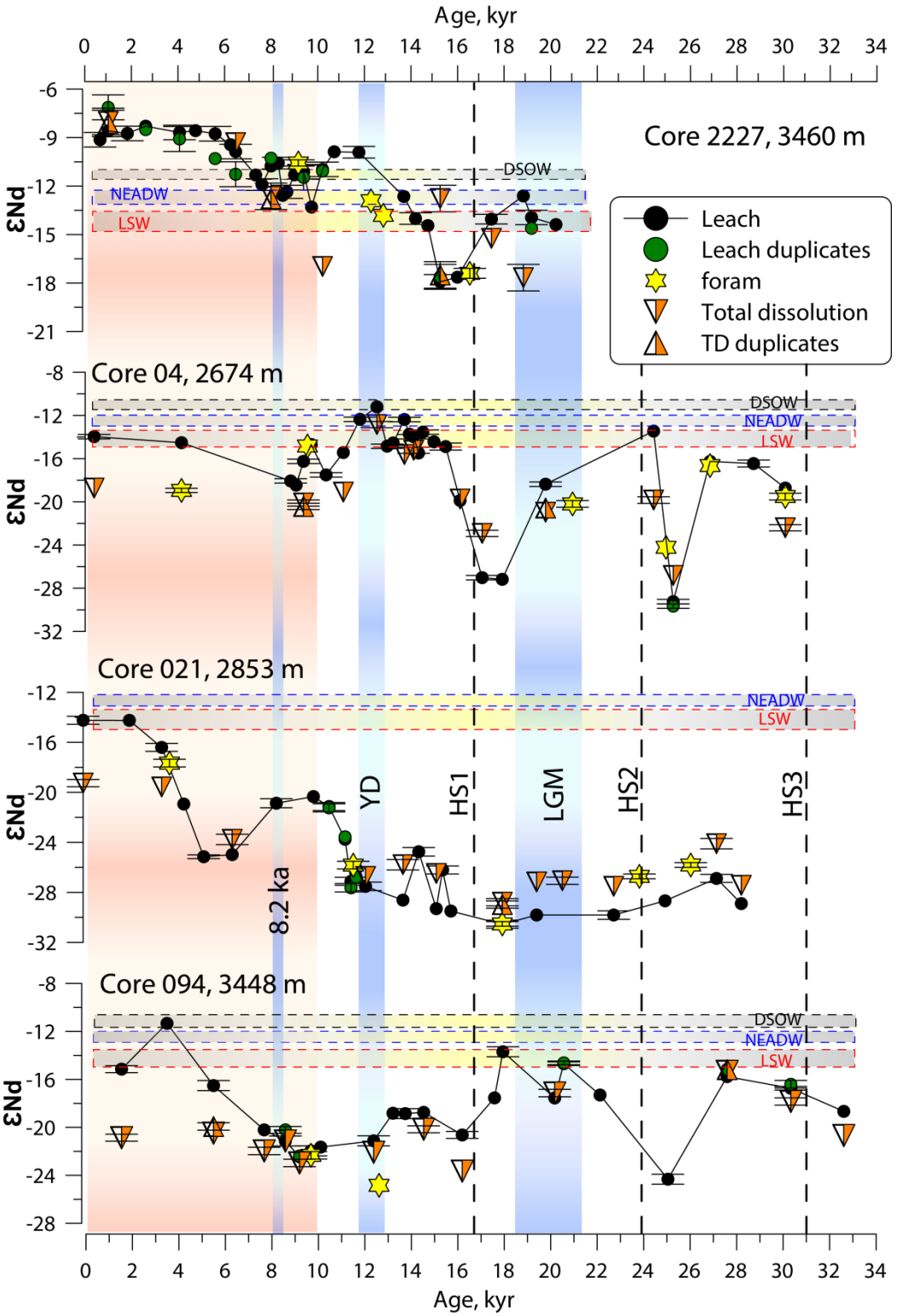


**Fig. 3** The εNd signatures of seawater extracted from ferromanganese coatings (black circles) and of the detrital fraction (orange triangles) of the four sediment cores of this study. Uncleaned foraminifera (yellow stars), duplicate leachates (green circles), totally dissolved detrital fraction duplicates (upside-down triangles) are also shown. Vertical bars denote times of major events: Heinrich Stadial 3 (HS3, Hemming, 2004), Heinrich Stadial 2 (HS2, Hemming, 2004), Last Glacial Maximum (LGM, Pflaumann et al., 2000), Heinrich Stadial 1

(HS1, Hemming, 2004), Younger Drays (YD, Rasmussen et al., 2006), 8.2 ka event (Hoffmann et al., 2012). The red vertical bar denotes the Holocene. Horizontal bars denote εNd signatures of the present day seawater in the Labrador Sea (LSW, NEADW, DSOW, Filippova et al., submitted).

### 6.4.3 Hafnium isotope composition.

The εHf signatures of the leachates in general over the studied period express lower variability, than εNd, however more pronounced excursions towards unradiogenic values are recorded during such events as the Heinrich Stadials and the YD. Overall εHf signatures range between +10.7 (at 1.9 ka) in core 2227 and -34.8 (at 16.2 ka) in core 094 (Fig. 4).

Similar trends are observed in εHf signatures as for εNd. The radiogenic excursion between 33 and 27 ka recorded in εNd is noticeable only in core 021, where values get more radiogenic from -22.5 to -15.6 over a period of less than 2 kyrs. The Heinrich Stadial 2 is reflected by negative excursion of εHf in all cores, the most prominent decrease, however, is observed in core 021 of almost 10 εHf units (εHf = -25.7). Similar to εNd signatures of the leachates εHf signal stays highly unradiogenic in core 021 all the way till the YD. During the LGM radiogenic signatures are observed in cores 2227 and 04 between +9. and + 4.3 and less radiogenic in core 094 of -3.9, while in core 021 highly unradiogenic values are recorded (-25.1). Highly pronounced unradiogenic excursions are recorded in core 094 during the time of the HS1 and the YD cold interval (~ -34 and ~ -29, respectively), and to less extent in cores 2227 (+2.1, HS1 and +4.8, YD), core 04 (-0.6, HS1) and core 021 (-21, YD). Over the period of the Holocene the record in general similarly to εNd expresses gradual radiogenic excursion in three cores (04 and 021), no record for the Holocene is available at the moment. Relatively constant values are observed in core 2227 showing a close range of values between +7.7 (8.7 ka) and +10.7 (1.9 ka). An unradiogenic event is observed in core 021 (5.2 ka), with εHf value of -7.5. The youngest samples reach close range of εHf values between +9.6 (2227) and +5.3 (094). The same trend as in εNd data is seen here, where εHf values are getting less radiogenic moving around the Labrador Sea. As for detrital εNd detrital εHf signature seem to decrease during such events as the Heinrich Stadials and the YD, seen in core 04 (HS1, YD), core 021 (YD) and 094 (at 15 ka). The εHf values of the core 021 so no significant change over the period between the HS2 and the YD, expressing highly unradiogenic values around -36. Over the Holocene in core 2227 (-7) and 021 (-24) the detrital εHf signature gets more radiogenic, while in core 094 on the opposite is less radiogenic (-24). Core 04 expresses in overall higher variability in the detrital εHf signatures.

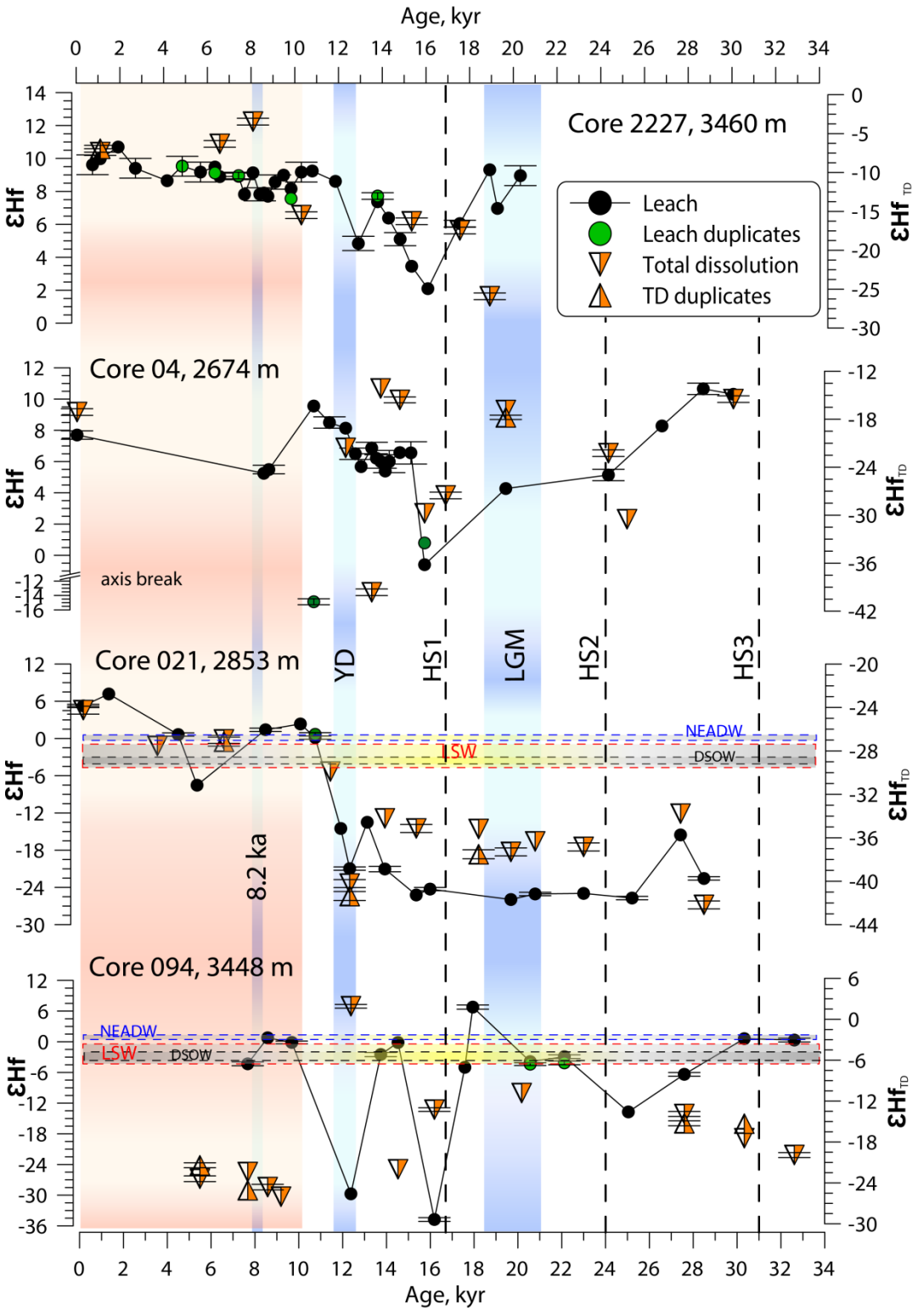


**Fig. 4** The seawater εHf signature extracted from the ferromanganese coatings (black circles) and detrital fraction (orange triangles) of the four sediment cores of this study. Duplicates of the leachates (green circles) of the totally dissolved detrital fraction (upside-down triangles) are also shown. Vertical bars denote times of major events: Heinrich Stadial 3 (HS3, Hemming, 2004), Heinrich Stadial 2 (HS2, Hemming, 2004), Last Glacial Maximum

(LGM, Pflaumann et al., 2000), Heinrich Stadial 1 (HS1, Hemming, 2004), Younger Drays (YD, Rasmussen et al., 2006), 8.2 ka event (Hoffmann et al., 2012). The red vertical bar denotes the Holocene. Horizontal bars denote εHf signatures of the present day seawater in the Labrador Sea (LSW, NEADW, DSOW, Filippova et al., submitted).

### 6.4.4 LEAD ISOTOPE COMPOSITION

Lead isotope data follow similar to Nd and Hf patterns. Such events as the Heinrich Stadials, the YD are reflected by positive excursions towards radiogenic values in all cores, although not all of the events are recorded in each core. The Heinrich Stadial 2 was recorded in cores 04 ($^{206/204}$Pb = 21.33) and core 094 ($^{206/204}$Pb = 20.17) (Fig. 5). Similar values are observed in these cores during the HS1, accompanied by radiogenic increase in core 2227 ($^{206/204}$Pb = 19.38). Similarly to Nd and Hf isotope records, $^{206/204}$Pb signature in core 021 is more radiogenic, than in other cores and stays relatively unchanged till the YD cold interval. During the LGM cores 2227, 04 and 094 show close range of $^{206/204}$Pb values between 19.55 (04) and 19.2 (094). A pronounce radiogenic excursion is seen in core 094 during the YD cold interval, where $^{206/204}$Pb reaches 20.77. An overall gradual decrease towards less radiogenic values is observed over the Holocene in all cores. Our core resolution did not capture the 8.2 ka event, however, a decrease prior 8 ka is observed in core 021 and after in core 2227. An increase started around 8 ka in core 021 is followed by a radiogenic peak around 5.2 ka with $^{206/204}$Pb ~ 20.84. The youngest samples show close range of values between 19.07 (04) and 19.53 (094), with less radiogenic values on the eastern side of the Labrador Sea and more radiogenic out of the Labrador Sea. The detrital $^{206/204}$Pb signatures do not express as much variability over the studied period as Nd and Hf. In core 094 no significant changes observed, with slightly more radiogenic signatures prior the HS1, followed by relatively constant signatures afterwards. In cores 2227 and 021 relatively constant $^{206/204}$Pb signatures are observed prior the Holocene, with a slight unradiogenic excursion in core 021 at the time of the YD, and more radiogenic signatures in both cores over the Holocene. Higher variability is seen in core 04, with negative excursions in $^{206/204}$Pb detrital signatures, associated with the Heinrich Stadials and the YD. The youngest samples in cores 04, 021 and 094 express close range of values between 17.40 (04) and 17.74 (094), while in core 2227 $^{206/204}$Pb signature is more radiogenic $^{206/204}$Pb ~18.57.

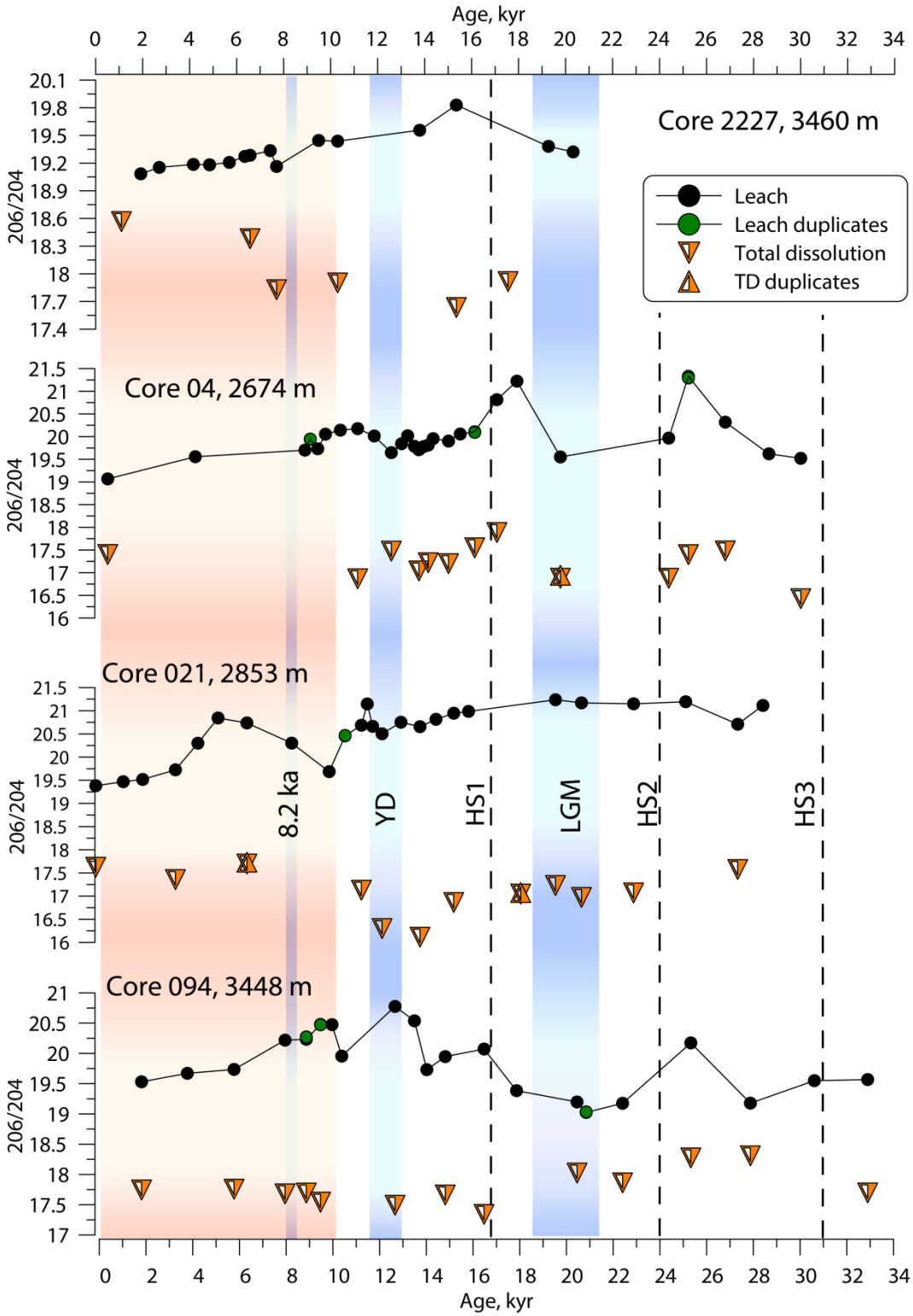


**Fig. 5** Seawater $^{206}Pb/^{204}Pb$ extracted from the ferromanganese coatings (black circles) and $^{206}Pb/^{204}Pb$ of the detrital fraction (orange triangles) of the sediments of the study. Duplicates of the leachates (green circles) and of the totally dissolved detrital fraction (upside-down triangles) are also shown. Vertical bars denote times of major events: Heinrich Stadial 3 (HS3, Hemming, 2004), Heinrich Stadial 2 (HS2, Hemming, 2004), Last Glacial Maximum (LGM, Pflaumann et al., 2000), Heinrich Stadial 1 (HS1, Hemming, 2004), Younger Drays

(YD, Rasmussen et al., 2006), 8.2 ka event (Hoffmann et al., 2012). The red vertical bar denotes the Holocene. Seawater $^{207}Pb/^{204}Pb$, $^{208}Pb/^{204}Pb$, $^{208}Pb/^{206}Pb$ are presented in Appendix. Error bars are smaller than symbol size.

## 6.5 DISCUSSION.

### 6.5.1 CHANGES OF THE SEAWATER RADIOGENIC ISOTOPE COMPOSITIONS OVER TIME.

#### 6.5.1.1 33 TO 27 KA.

The period from 33 ka to 27 ka is covered by the records of all cores with the exception of core 2227, which only covers the past 20 kyr. In core 021, located on the western side of the Labrador Sea both εNd and εHf signatures are highly unradiogenic during that period of time, feature that is persistent in εNd and εHf signatures all the way till the YD (Fig. 3, 4). In contrast, two records from cores 094 and 04 show relatively radiogenic εNd values during this period and essentially identical εNd values (Fig. 3). The εHf signatures in these two cores are, however, significantly different +0.5 for core 094 between 33 and 30 ka and between +10.3 and +8.3 for core 04 over the period between 30 and 27 ka, which decreases over this period of time (Fig. 4). Radiogenic εNd values in cores 04 and 094 may reflect the enhanced advection of Southern Source Waters (SCW), characterized by a radiogenic εNd signatures of -10 to -11 (Gutjahr et al., 2008; 2014; Lippold et al., 2015). Their presence was recorded prior to the LGM of the Blake Ridge (Gutjahr et al., 2008; 2014; Lippold et al., 2015). However, in the present study the location of the cores significantly further north and in the Labrador Sea (cores 04 and 021) makes it unlikely that they were reached by SCW to any significant extent. Additionally, cores 04 and 021 are shallower than the expected depth of SCW (2500 to 3000 m, Gutjahr and Lippold, 2011). Core 094 is deeper (> 3400 m) and on the way out of the Labrador Sea, where SCW potentially could have reached (Fig. 1). The detrital fraction data show that the radiogenic εNd excursion of the leachates was accompanied by a similar radiogenic excursion of the detrital εNd fraction coincident with radiogenic excursion in the detrital εHf data as well (Fig. 3, 4). Observed radiogenic excursion of εNd signature of the leachates could be explained by a reduction in the supply of the unradiogenic end member during the mixing of the water masses in the Labrador Sea. Over this period until the inception of deglaciation, North America was covered by the massive Laurentide ice sheet (LIS) (Dyke and Prest, 1987). Its presence stretched all the way over the western margin of the Labrador Sea (Dyke et al., 2002), which could have completely shut down or restricted input of highly unradiogenic waters coming

from the Hudson Bay and the Baffin Bay. This scenario (absence of unradiogenic end-member) is supported by similar signatures of εNd in cores 04 and 094 between 25 - 33 kyrs and similar change of around 6 εNd units in both cores. Highly unradiogenic εNd (between -28 to -30) and εHf (between -21 to -25) signatures of the leachates all the way up to the YD seen in core 021 can be explained by ablating ice sheet, which may have facilitated the release of unradiogenic Hf from zircon grains due to reworking by the ice sheet. This was also observed by Gutjahr et al., (2014) for the down core record from the Blake Ridge. This suggests that core 021 until the YD was under the influence of the melting LIS, and εNd and εHf signatures of the leachates rather reflect the signal of the retreating ice sheet and/or of glacial weathering inputs, than a water mass mixing signal. An accompanying positive excursion of the detrital εNd and εHf signals suggest an increased influence of waters coming from the area around the Iceland, bringing more radiogenic detrital material (Fig. 1). No εHf data of the leachates for the deeper core from the Blake Ridge (prior to the LGM) are available from the previous publication of Gutjahr et al. (2014) for comparison.

The overall trend observed over this time period in the western Labrador Sea is also consistent with increased input from the Arctic through the Denmark Strait. We see more radiogenic values in εNd of the leachates (core 04 and 094) together with more radiogenic detrital input (εNd and εHf in cores 021 and 094), which would be consistent with the radiogenic signal of the Icelandic basalts (Fig. 1). At the same time less radiogenic values of εHf are also consistent with the Arctic inflow, as quite unradiogenic values were recorded off the southern tip of Greenland (Filippova et al., submitted), suggesting influence of the IW or the WGC. Inputs from the Baffin Bay or the Hudson Strait are rather unlikely, as we would expect much more unradiogenic εNd values, given that water from the Baffin Bay is highly unradiogenic in its εNd (Piepgras and Wasserburg, 1988). This is also consistent with detrital data from core 021, where highly unradiogenic values were replaced by a more positive trend, followed by return to the same values during the HS2 and at the time of the LGM.

Lead isotope record of the leachates shows similar trends in two cores 021 and 094, where a pronounced negative excursion is recorded in all three isotopes ratios. This trend is in agreement with the data from Foster and Vance, (2006) and Gutjahr et al., (2009), that record a decrease towards less radiogenic values prior the LGM and the HS2 in two ferromanganese crusts from New England Seamount and Blake Ridge, respectively. Core 04 shows, however, a positive excursion in $^{206/204}$Pb and $^{208/204}$Pb ratios, with an exception of $^{207/204}$Pb, for which a decrease towards less radiogenic Pb values is recorded (Fig. 5). Although core 021 recorded a negative excursion in all three Pb isotopes ratios, the absolute difference was much smaller,

than in cores 04 and 094. This observation, together with highly unradiogenic values of εNd and εHf in core 021, makes the assumption of a strong LIS influence and glacial weathering even more likely. As glacial erosion would provide extensive quantities (Bell and Laine, 1985) of freshly weathered rocks and it would lead to preferential release of highly radiogenic lead (Harlavan et al., 1998; Foster and Vance, 2006). Looking at the detrital record over the period of 25 to 33 kyrs, we see a clear positive excursion in core 04 in all three Pb isotopes ratios, and a slight increase in $^{206}Pb/^{204}Pb$ in core 094. This is consistent with increased input from around Iceland, characterized by highly radiogenic $^{206}Pb/^{204}Pb$ values (Fig. 1).

#### 6.5.1.2 HEINRICH STADIALS 2 AND 1.

No reflection of the HS3 is seen in our data. However, the HS2 and the HS1 are marked by negative excursion towards less radiogenic values in both εNd and εHf of the leachates and detrital fraction in all cores, although not in every core both events are recorded (Fig. 3 and 4). Although both events seem to have a common source and one mechanism (Hemming, 2004), some differences could be observed in recorded signals of εNd and εHf signatures between the cores. Cores 021 and 04 εNd signatures, unlike εHf signatures of the leachates, seem to record a close range of values during both events (εNd between -27 and -28.6 during the HS1), similar to a uniform value of ~ -28 during HS2 in the same cores. Cores 2227 and 094, on the other hand, show more radiogenic εNd signals (εNd ~ -18 and ~ -20, respectively) during the HS1 in comparison to the signal recorded during the HS2 in core 094 (εNd ~ -24). Whereas εHf signatures show a much broader range of values during both events, from +5.1 (core 04) to -25.7 (core 021) during the HS2 and between -34.8 (core 094) and +2.1 (core 2227) during the HS1. The εHf signature of the leachates opposite to εNd shows a clear, pronounced decrease of more than 30 εHf units in core 094, accompanied by a decrease in detrital fraction as well up to -22. Such strong decrease of εHf signature of the leachates during HS1 is recorded only in core 094. However, the fact that in core 021 εHf signatures of the detrital fraction are highly unradiogenic (> -35) and core 04 experiences negative excursions in the detrital εHf signatures during both events (εHf ~ -30) suggests that a higher resolution is necessary to capture these events in all cores possibly due to short residence time of Hf in such semi-enclosed basin as the Labrador Sea (Filippova et al., submitted).

In general, highly unradiogenic εNd and εHf signatures of the detrital fraction are consistent with weathering signal of old rocks Proterozoic and Archean in age surrounding North Atlantic (Hemming, 2004). It is known that water masses affected by such weathering inputs have highly unradiogenic εNd signatures like in the Baffin Bay, where εNd is ~ -26

(Stordal and Wasserburg, 1986) or along the coast of the Labrador Sea, where surface waters have εNd signatures of ~ -26 (Filippova et al., submitted).

Radiogenic excursion to the pre-stadial values on the order of the modern day LSW (εNd ~ -14.1, Filippova et al., submitted) after decrease towards unradiogenic values associated with the HS2 and the HS1 recorded in εNd signature of the leachates in core 04 and leachates in core 094 may (only after HS1) suggest intensified convection in the region that promoted the formation of the LSW. The possible mechanism, although for the period of the Holocene, was proposed by Thornalley et al (2009), based on the link between the NAC salinity and the Subpolar Gyre dynamics, caused by fresh water inputs. Whether or not the same mechanism was operating during the time preceding the Holocene, needs further inquiry. However, this statement holds only if the LSW signature remained unchanged over the studied period. On the other hand, it could suggest an increasing water input from Greenland Iceland Scotland Seas (GIS), bringing waters with radiogenic εNd signal formed due to basalt weathering around Iceland or Greenland (Fig. 1). This would be consistent with an increase towards more radiogenic εHf values of the detrital fraction in core 04 and modern day seawater εHf signature of the LSW or the DSOW (Filippova et al., submitted) observed in core 094 right after the HS2 (Fig. 3). These both assumptions are, however, not mutually exclusive, as the latter could be a result of the proposed by Thornalley et al. (2009) mechanism.

Pronounced radiogenic peaks in all three Pb isotope ratios for core 04 and 094, and to a lesser extent in core 021 during both events the HS2 and the HS1, are consistent with input of freshly weathered glacial material, which due to incongruent weathering of lead would preferentially release a more radiogenic fraction (Gutjahr et al., 2009; Vance et al., 2009; Kurzweil et al., 2010; Crocket et al., 2012, 2013). An additional source of radiogenic lead could be Fe-Mn oxyhydroxide-bound Pb, released from the pre-formed Fe-Mn oxides hosted on terrestrial IRD, which has been reported previously by Kurzweil et al., (2010) for the sediments supplied to the Laurentian Fan. Gutjahr et al., (2014) suggested the same mechanism to explain the radiogenic peak in εHf during the HS1, which accompanied a positive excursion in Pb in their data from the Blake Ridge. Here, however, we don't observed an increase towards more radiogenic values during the HS2 or the HS1 in εHf data.

#### 6.5.1.3 LGM.

During the LGM two different trends are observed in the data. On the one hand, cores 094 and 2227 follow the same patterns in that εNd signature of the leachates became more

radiogenic reaching present day εNd values of the DSOW in the Labrador Sea in core 2227 and present day LSW in core 094 (Filippova et al., submitted). The εHf signatures in both cores behave coherently as well, reaching similar values by the end of the LGM of +6.8 for core 094 and +8.7 for core 2227. In addition, the detrital fraction of core 2227 shows an increase towards more radiogenic εNd and εHf values between 20 and 17 ka, and thus similar to εNd and εHf signatures of the detrital fraction in core 094. Core 04 on the other hand, starts to resemble highly unradiogenic εNd signatures from core 021, which is not surprising as it is located in close proximity and at similar depth as core 021 and suggests an increased influence of unradiogenic inputs coming from the ablating ice sheet. This may suggest strengthening of the inflow from the GIS seas due to restricted inflow of the Arctic waters into the Baffin Bay and out into the Labrador Sea through the Davis Strait.

This assumption is also consistent with lead isotope data, whereby core 04 expresses more radiogenic values, while in cores 094 and 2227 lead isotope ratios are less radiogenic and closely resemble each other (Fig. 4, 5, 6).

#### 6.5.1.4 MYSTERY INTERVAL AND YOUNGER DRYAS.

The end of the HS1 is highlighted by a gradual increase towards more radiogenic seawater εNd and εHf values in all cores, together with positive εNd and εHf of the detrital fraction in cores 04 and 094. There are two sources of highly radiogenic Hf and Nd in the area, which are Iceland basalts and Western Greenland (Fig. 1). However, the fact that $^{206/204}$Pb isotope signature is marked by rather a decrease in both leachates and detrital in all cores (Fig. 5) suggests that at least lead signal came from location other than Greenland, that is characterized by highly radiogenic signatures. This potentially reflects input of highly radiogenic waters coming through the Denmark Strait (DSOW), that by coming into contact with Icelandic basalts acquire highly radiogenic εNd (Lacan and Jeandel, 2005) and potentially highly radiogenic εHf and unradiogenic lead isotope signatures (Fig. 1). This would be consistent with εNd signatures of the leachates in cores 2227 and 04 on the order of the present day NEADW in the Labrador Sea (-12.5 , Filippova et al., submitted) and similar signatures of the detrital εNd (~ -15 by the YD) and εHf of the leachates. Less radiogenic εNd signal of the leachates in cores 021 and 094 on the other hand in comparison to cores 04 and 2227 (8 to 11 εNd units) may be a result of increased influence of the retreating LIS. Williams et al. (2012) proposed that enhanced seasonality in the region resulted in stadial summers, that were sufficiently enough to allow the LIS melt, waters of which would potentially have highly unradiogenic εNd and εHf values. These waters influence would be

seen only in cores 021 and 094 due to their marginal position, which is also supported by radiogenic peaks in $^{206/204}$Pb data recorded only in cores 021 and 094 at the time of the YD. In addition fresh water input into the Labrador Sea could have preconditioned the North Atlantic for AMOC changes via the Gulf Stream System (Thornalley et al., 2009; Otto-Blienser et al., 2010).

The YD period itself in our record was marked only by negative excursion towards less radiogenic values in εHf of the leachates in cores 2227, 021 and 094 (Fig. 4), while εNd signatures of the leachates show a decrease not more than 2 εNd units in one core 094. However, unradiogenic excursion observed after the YD in εNd signatures of the leachates in cores 2227, 04 and 094 together with decrease in detrital εNd signal in cores 2227 and 04 would be consistent with AMOC reduction, and decreased influence of waters coming through the Denmark Strait. Short range of unradiogenic εNd (between -19 and -23) and εHf (between -27 and -22) signatures of the detrital fraction suggests the establishment of the alongshore Labrador Current starting already around 12 ka. Relatively stable $^{206/204}$Pb signal (between 17.54 and 17.76) of the detrital fraction in core 021 over the last 14 kyrs suggests even earlier presence of the LC.

#### 6.5.1.5 HOLOCENE.

The beginning of the Holocene is characterized by a gradual increase of the strength of radiogenic signal recorded in all four cores both in εNd and εHf of the leachates accompanied by a unradiogenic excursion in lead isotope data. As mentioned above, the main source of highly radiogenic Nd are the DSOW and the ISOW, which are the most likely explanation for more radiogenic signatures in all cores even prior the YD. However, it has been previously suggested, that the DSOW inflow did not start until around 8 ka (Fagel et al., 2002). Based on our data from core 2227, however, there are evidence that this inflow initiated to its full strength already at around 12 ka. The seawater εNd signature reached -9.9 and then remained similar throughout the middle to the late Holocene with three unradiogenic events centered around 9.8 ka, 8.6 ka and 7.7 ka ranging between -13.3 to -11.9. This seawater signature (-9.9) is in good agreement with the modern day signature of the DSOW and the ISOW (Lacan and Jeandel, 2005). Additionally, the εNd signature of the detrital fraction shows an increase towards more radiogenic values already around 10 ka supporting an earlier initiation of the DSOW. The seawater εHf signature of core 2227 also showed a close range of values starting from 12 ka ranging between +7.7 and +10.7. Considering the position of the core in the flow path of the WGC and the DSOW, these data offer strong argument for an earlier inception of

the inflow coming through the Denmark Strait. The unradiogenic events recorded at 9.8 ka, 8.6 ka and 7.7 ka in the εNd data of core 2227 were also recorded in core 04 at 10 ka and 8.8 ka and could be reflecting changes in strength of the AMOC associated with fresh water input during the YD and the 8.2 ka event.

The dramatic outbreak of the glacial lake during the Holocene, or the 8.2 kyr event is recorded in the data, however, not in all cores. The εNd signal of the leachates suggests a 2 to 4 εNd unit drop in all cores except 094, where no unradiogenic signal was detected. The εHf signal of the leachates in core 094, in contrast, shows a decrease right after the 8 ka. In core 2227 on the other hand no reflection of the freshwater input is recorded in the εHf signal of the leachates. The strongest signal is seen in cores 021 and 04, which would be consistent with the flood path through the Hudson Strait. The εNd and εHf signatures of the detrital fraction do not reflect a significant change in the source. The overall unradiogenic εNd signatures are consistent with the input from old terrains and the unradiogenic excursion in εHf could be attained due to delayed inputs of the products of glacial weathering of zircon grains.

The presence of the LSW in cores 021 and 04 was not recorded until 5 ka based on the seawater εNd signal, suggesting also that during the late Holocene convection in the region was much more intensive and formation of the LSW reached up to 2600 m, which is deeper than today. This is plausible as prior to 1994 during the cold state of the Labrador Sea, the LSW was detected at depths of up to 2400 m (Yashayaev and Clark, 2006; Yashayaev et al., 2008). The εHf signal of the leachates is, however, much more radiogenic than the modern day signature of the LSW. This could be a result of decadal variability of εHf signature, proposed by Filippova et al., (submitted) due to incongruent weathering of Hf and differences in time it takes for the signal to travel within different water masses in the Labrador Sea (Yashayaev et al., 2008). Interestingly in core 094 the modern day DSOW εNd signature was attained around 3 ka and εHf signature already around 7 ka (Fig. 3, 4). However, the presence of the DSOW at core site 094 was followed by a significant drop in εNd towards less radiogenic LSW-like values. Considering the depth of the core, it is unlikely that the LSW could propagate that deep, which would require a significant decrease in sea surface temperatures (SST), to promote such strong convection. The alkenone unsaturation ratio recorded a drop of SST in two out of four cores at that time (Filippova et al., chapter 5 to be submitted). This unradiogenic event is consistent with 2.7 cooling event recorded in numerous records in the North Atlantic (Alley et al., 1999; Andrews and Giraudeau, 2003; Bakke et al., 2008). As no change is recorded at that time in core 2227, which is located in the flow path

of the WGC and the DSOW, the source of the change might be elsewhere. The absence of changes in the detrital signal could suggest alteration of the mixing rates. In that case, one of the possible unradiogenic sources could be the Labrador Current, which might have increased its inflow at that time. However, no data to support that claim are available. The other possibility would be the intrusion of unradiogenic waters through the Gulf of St. Lawrence. Oppo et al. (2003) connected this 2.7 ka event with surface cooling and subsequent possible slowdown of the AMOC. Any of these assumptions, however, needs to be supported by additional data.

To be able more fully interpret Hf isotope signatures, however, more data on the present day seawater masses signatures are necessary, especially constraining the εHf signal of the water masses coming from the Arctic.

### 6.5.2 ISOTOPE SIGNATURE OF THE TOTALLY DISSOLVED DETRITAL FRACTION.

#### 6.5.2.1 SEAWATER ARRAY.

Hafnium and Nd behave similarly during the most magmatic processes, which results in a strong positive correlation of radiogenic Nd and Hf isotopes in most terrestrial rocks, which has been defined as a "mantle-crust array" or "terrestrial array" (Fig. 6, $\varepsilon Hf = 1.55 * \varepsilon Nd + 1.21$, Vervoort et al., 2011). Studies based on the ferromanganese crusts and nodules showed that seawater forms a distinct and well defined correlation between Hf and Nd isotopes as well. However, for every given value of εNd a more radiogenic value of εHf than expected from the bulk rock composition is observed. This trend, which deviates from the "terrestrial array", is referred to as the "seawater array" ($\varepsilon Hf = 0.62 * \varepsilon Nd + 7.38$, Albarède et al., 1998; Godfrey et al., 1997; David et al., 2001).

Plotting the new data on the εHf versus εNd diagram we see a significant scattering of the data between the seawater and terrestrial arrays for both leachates and totally dissolved detrital fractions. The detrital fraction of core 021 and partially of core 04 falls closely along the terrestrial array suggesting that the source of sedimentary input was located in close proximity, consistent with the input from surrounding landmasses through the Hudson Bay and the Baffin Bay. The other part of the detrital data for cores 04, 094 and 2227 fall closer to clay array, suggesting that more finer sediment fraction reached these cores location, consistent with the sources outside of the Labrador Sea, such as GIS seas. The leachate data for each core plot well above the detrital fraction, suggesting that if the influence of the weathering inputs was present, it was rather small. In addition, the signal of the terrestrial

inputs coming from Canadian terrains is most likely highly unradiogenic in εHf on the order of -10 (Filippova et al., submitted). The position of core 021 leachates data close to the clay array suggests that this core location could have been controlled by Hf release from the dissolution of clay particles or clay associated colloids, which strikingly resembles the modern day situation observed for the intermediate waters in the Labrador Sea (Filippova et al., submitted).

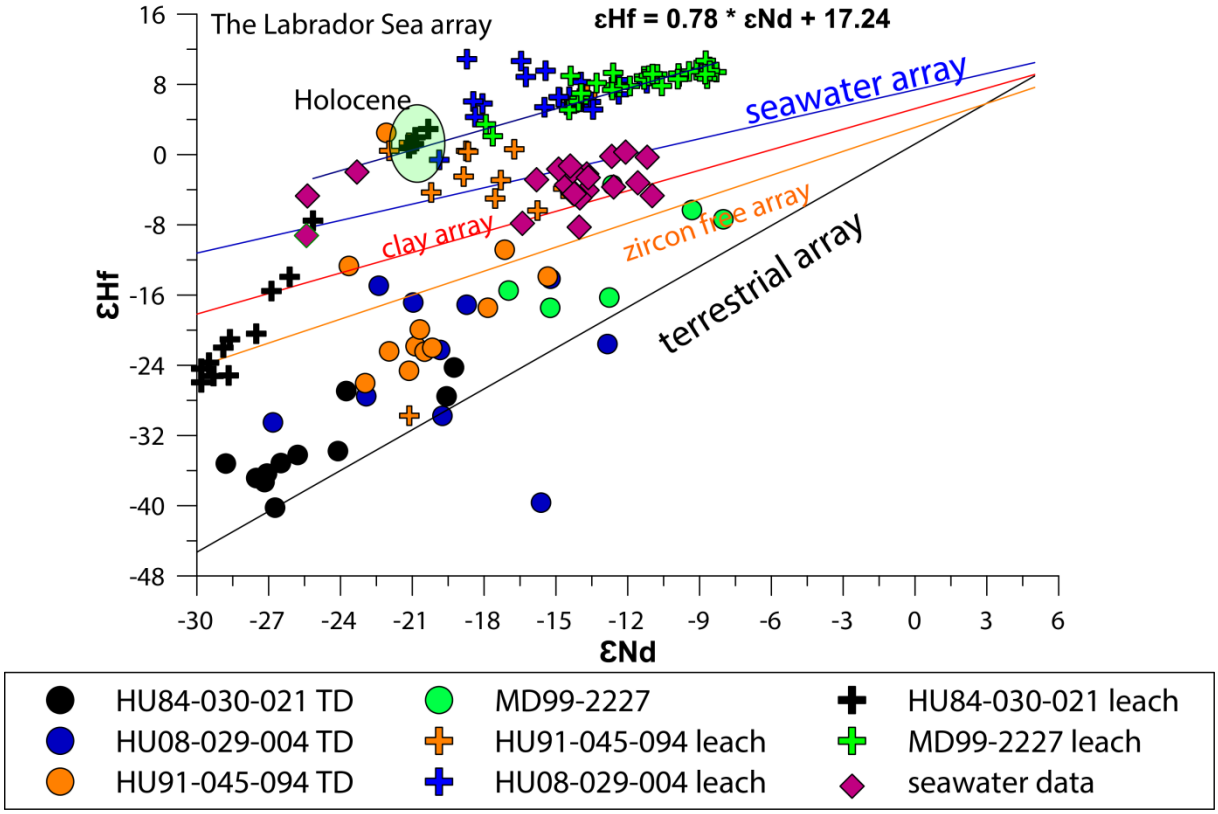


**Fig. 6** εHf versus εNd of the seawater (leachates, crosses) and totally dissolved detrital fraction data (circles). Data of the present day seawater samples are shown in filled diamonds. On the plot are also shown: terrestrial array (Vervoort et al., 2011); seawater array (Albarède et al., 1998; Godfrey et al., 1997; David et al., 2001); clay array (Bayon et al., 2016); zircon free sediment array (Bayon et al., 2009). A new Labrador Sea array, formed based on the new data from this study is also shown.

A fact worth mentioning is how the data plot above the seawater array, forming its own obvious trend (εHf = 0.78 * εNd + 17.24), for all the data from cores 2227 and 04, and the data from core 021 representing the Holocene. Core 094 samples are closer to the seawater array and more scattered around it, which is consistent with this core location being essentially outside of the Labrador Sea. More than that, three modern day seawater samples collected of the coast of Canada in May 2013 (Filippova et al., submitted) fall on this new

array, suggesting that this feature was not strictly persistent over the Holocene but is also detectable in the present day Labrador Sea. Such a trend may represent a particular rock type present in the Labrador Sea or in its surroundings from which the weathered signal is acquired by surface waters. The precise origin of the Labrador Sea array is yet to be identified, for which more seawater Hf data, especially from river waters around the Labrador Sea are needed.

### 6.5.2.2 DETRITAL DATA: SOURCE PROVENANCE.

The combination of different isotope systems offers a better understanding of the source provenance of the sediments studied here. Addition of Hf isotopes to the widely used pair of Nd and Pb isotopes helps to improve the deciphering of the sedimentary inputs and ease the distinction between different time periods or events.

The analysis of the detrital fraction from four sedimentary records presented in this study reveal differences between their sources based on the isotopic signatures of Pb, Nd and Hf (Fig. 7). The εNd versus Pb isotope plot suggests different sources of inputs for all cores for the most of the record. Looking at the εNd versus $^{206}Pb/^{204}Pb$ we can see that core 021 was under the influence of the distinct source all the time until the beginning of the Holocene, which agrees well with the seawater signatures, which shows a highly unradiogenic εNd, εHf and $^{206}Pb/^{204}Pb$ signatures prior 10 kyrs. Combining $^{206}Pb/^{204}Pb$ with εHf allows to define additional distinct events in the signature of the detrital fraction, such the HS2 and the HS1 and time period before the LGM.

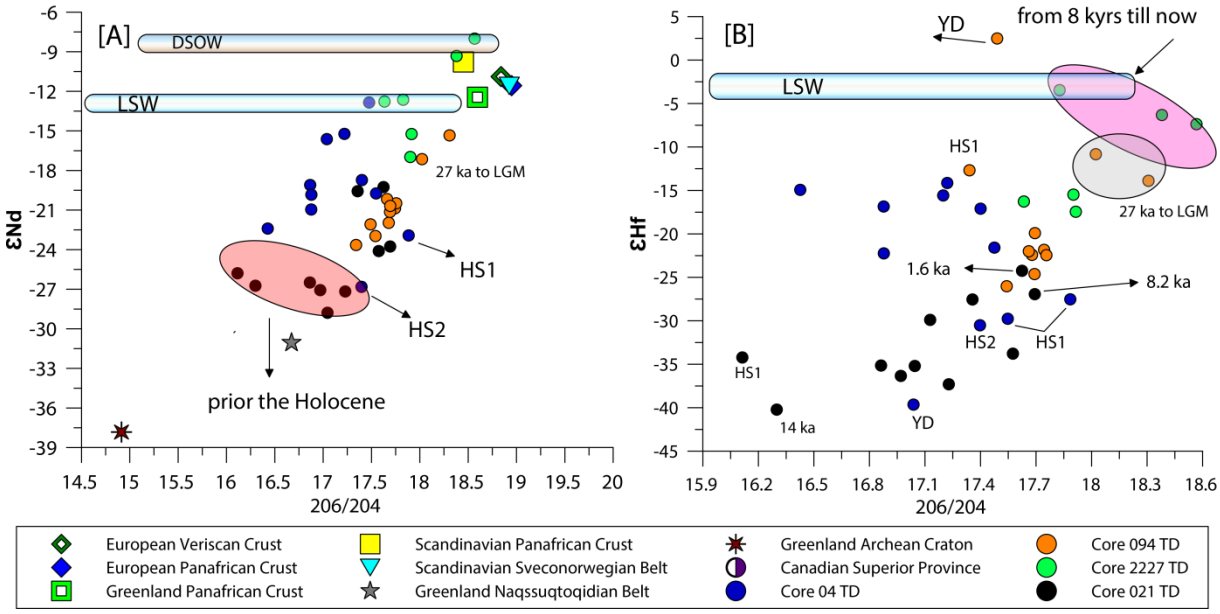


**Fig. 7** Nd, Hf and Pb isotopic systematics of the four studied sediment cores. Potential source areas are shown. Full reference list is shown in Fagel et al. (2002). Horizontal bars

denote the LSW and the DSOW outside of the Labrador Sea signatures from (Lacan and Jeandel, 2005; Filippova et al., submitted).

Core 04, interestingly, plots separately from core 021, despite of their locations close to each other and similar depths (Fig. 7). They have similar lead isotope composition, however, εNd is more radiogenic in core 04, where with the beginning of the Holocene these two cores have similar εNd signatures, but core 021 has more radiogenic $^{206}Pb/^{204}Pb$. This suggests that core 021 gain most of its inputs prior the Holocene from the old Canadian terrains, coming through the Hudson Bay, while core 04 received inputs from the western side of Greenland (Fig. 1). During the Holocene core 021 expresses more radiogenic εNd signatures on the order as in core 04, however, $^{206}Pb/^{204}Pb$ signal becomes more radiogenic, which could reflect the input of material into the LC from the western coast of the Labrador Sea previously covered by the LIS. The εHf data show that over the course of study core 04 location was under the influence of different sources, similar to other cores locations at different times, which probably reflects reestablishment of the water mass circulation after such events like the HS2 and the HS1, the YD or the 8.2 ka event. Based on both εNd and εHf versus Pb isotopes plots we could see a distinct signatures of both the HS2 and the HS1 in core 04, 021 and 094 (Fig. 7). The Heinrich Stadial 2 from core 04 plots close to the data of core 021, for the time prior the Holocene, supporting the assumption that core 021 was under the influence of the same or similar source that provided material during the Heinrich Stadial 2. The Heinrich Stadial 1 on the other hand, plots close to core 021 data during the Holocene. This suggests that the HS1 and the HS2 may have had different sources or they were delivered through different routes (Mackenzie versus Mississippi), which resulted in the difference of εNd signature of those two events. In addition, core 021 location shifted to another more radiogenic source after the inception of deglaciation. It also suggests, that core 094 and 021 (during the Holocene) were and are under the influence of the sediments coming from a common source. On the other hand, εHf versus $^{206}Pb/^{204}Pb$ indicates a clear distinction between cores 094 and 021, with similar source for core 021 as for core 094 only at the time of the 8.2 ka event and during the late Holocene. Core 094 though based on εHf data plots closely together with core 2227, before it changed to a distinct detrital signature around 8 ka till present, which is the time of the suggested DSOW inception consistent with radiogenic εHf and εNd, and more radiogenic $^{206}Pb/^{204}Pb$. This is also seen on the εNd versus $^{206}Pb/^{204}Pb$ plot, where core 2227 falls well above other data, highlighting its distinction from other sites during the middle to the late Holocene.

The available data on potential sources are limited due to the lack of studies on combined Hf, Nd and Pb isotopes, however, it gives us some rough ideas on the origin of the introduced sediment material. The available data from Fagel et al. (2002) suggest that core 2227 was mainly under the influence of the European sources together with potential inputs coming from Greenland. However, some publications show highly radiogenic $^{206}Pb/^{204}Pb$ signal from the southern Greenland, suggesting that if any input from Greenland was present it might have been limited or $^{206}Pb/^{204}Pb$ signatures significantly differ over different parts of Greenland (Fig. 1 and references for the figure). The input from the Icelandic basalts would be consistent with recorded in core 2227 after 8 ka εNd, εHf and $^{206}Pb/^{204}Pb$ isotope signatures. Core 021 plots closer to Greenland sources represented by Archean rocks. The unradiogenic $^{206}Pb/^{204}Pb$ signature to core 021 location might have been delivered from the area near the Hudson Strait. Core 094 and 04 are positioned somewhere in the middle between these two end members, suggesting active mixing between them. Over the studied period the sources change towards more european origin in all cores as reflected by a shift towards more radiogenic εNd and Pb values, which most likely is a reflection of the DSOW inception.

## 6.6 CONCLUSIONS.

The Hf-Nd-Pb isotope records obtained from four sediment cores provide new information on the climatic and oceanographic evolution in the Labrador Sea over the last 33 kyrs. The overall trends observed in the data coincident with major events such as the Heinrich Stadial 2 and the Heinrich Stadial 1, the Last Glacial Maximium, the Younger Dryas and the Lake Agassiz outburst at 8.2 ka for which negative excursions towards less radiogenic values of εNd and εHf for both leachates and detrital are observed. The Pb isotope record follows similar trends, opposite in sign, with pronounced radiogenic peaks during the same events, reflecting the effects of incongruent weathering due to glacial conditions.

The new data provide new constraints on the establishment of different water masses in the Labrador Sea. The inception of the Denmark Strait Overflow Water may have already started earlier than previously thought at ~ 12 ka, which is supported by εNd and εHf data of the leachates and detrital fraction of core 2227. The εHf and εNd signatures of the detrital fraction in cores 094 and 021 suggest the establishment of the alongshore Labrador current around 12 ka.

During the Holocene the presence of the Labrador Sea Water was recorded around 5 ka in cores 04 and 021, suggesting that convection and formation of the LSW in the studied region was more intense, reaching up to 2600 m which is deeper than at the present day.

The detrital radiogenic isotope data of core 021 show that prior the Holocene, this core location could have been controlled by Hf release from the dissolution of clay particles or clay associated colloids, which strikingly resembles the modern day situation observed for the intermediate waters in the Labrador Sea. The modern circulation patterns in the Labrador Sea may not have been established until 8 ka, which is earlier than postulated before based on core 2227 detrital isotope signatures.

The leachate data from cores 2227, 04 and 094 form its own new array above the seawater array in εNd versus εHf space. More than that, three modern day seawater samples collected of the coast of Canada fall on this new array, suggesting that this feature was not strictly persistent over the Holocene but is also detectable in the present day Labrador Sea. This trend could reflect a particular rock type present in the Labrador Sea or in its surroundings from which the weathered signal is acquired by surface waters.

The source provenance analysis suggests that all four cores were under the influence of sources of European, Greenland, Icelandic origin together with input from around the Hudson Strait.

Overall the new data demonstrate, how a combination of multiple proxies and different isotope systems can improve our understanding of the water mass processes in the Labrador Sea and provide new crucial information.

## ACKNOWLEDGEMENTS.

A. Filippova was supported by a PhD fellowship of the Helmholtz Research School on Ocean System Science and Technology HOSST (www.hosst.org) at GEOMAR Helmholtz Centre for Ocean Research Kiel (VH-KO-601) and Kiel University. We also would like to thank Tianyu Chen, Veit Dausmann, Jutta Heinze, Georgi Laukert, Anne Osborne, and Moritz Zieringer for their help in the laboratory.

## REFERENCE LIST.

Albarède F., Simonetti A., Vervoort J.D., Blichert-Toft J., Abouchami W. (1998) A Hf-Nd isotopic correlation in ferromanganese nodules. Geophys. Res. Lett. 25 (20), 3895-3898.

Andersen T. ; Age And Petrogenesis Of The Qassiarsuk Carbonatite-Alkaline Silicate Volcanic Complex In The Gardar Rift, South Greenland ; Mineral. Mag. 61 [1997] 499-513

Barrat, Jean-Louis, and Jean-Francois Joanny. "Theory of polyelectrolyte solutions." *Advances in chemical physics* 94 (1996): 1-66.

Barfod G.H., Otero O., Albarède F. (2003) Phosphate Lu-Hf geochronology. Chemical Geology 200, 241-253.

Bayon, Germain, et al. "Determination of rare earth elements, Sc, Y, Zr, Ba, Hf and Th in geological samples by ICP-MS after Tm addition and alkaline fusion." *Geostandards and Geoanalytical Research* 33.1 (2009): 51-62.

Bayon G., Burton K.W., Soulet G., Vigier N., Dennielou B., Etoubleau J., Ponzevera E., German C.R., Nesbitt R.W. (2009) Hf and Nd isotopes in marine sediments: constraints on global silicate weathering. Earth Planet. Sci. Lett. 277, 318-326.

Bayon G., Skonieczny C., Delvigne C., Toucanne S., Bermell S., Ponzevera E., André L. (2016) Environmental Hf–Nd isotopic decoupling in World river clays. Earth and Planetary Science Letters 438, 25-36.

Bell, Michael, and E. P. Laine. "Erosion of the Laurentide region of North America by glacial and glaciofluvial processes." *Quaternary Research* 23.2 (1985): 154-174.

Bilodeau, G., Vernal, A.d., Hillaire-Marcel, C., 1994. Benthic foraminiferal assemblages in Labrador Sea sediments: relations with deep-water mass changes since deglaciation. Canadian Journal of Earth Sciences 31, 128-138.Blichert-Toft J., Arndt N. T. (1999) Hf isotope compositions of komatiites. Earth Planet. Sci. Lett. 171, 439-451, doi: 10.1016/S0012-821x(99)00151-X

Brevart O., Dupre R., Allegre C.-J. ; Lead-Lead Age Of Komatiitic Lavas And Limitations On The Structure And Evolution Of The Precambrian Mantle ; Earth Planet. Sci. Lett. 77 [1986] 293-302

Burton, K. W. and Vance, D. (2000) Glacial-interglacial variations in the neodymium isotope composition of seawater in the Bay of Bengal recorded by planktonic foraminifera. *Earth and Planetary Science Letters* **176**, 425-441.

Chauvel C., Hemond C. ; Melting Of A Complete Selection Of Recyclewd Oceanic Crust: Trace Element And Pb Isotopic Evidence From Iceland ; Geochemistry Geophysics Geosystems 1 [2000]

Chekol T. A., Kobayashi K., Yokoyama Tetsuya, Sakaguchi C., Nakamura E. (2011) Timescales Of Magma Differentiation From Basalt To Andesite Beneath Hekla Volcano, Iceland: Constraints From U-Series Disequilibria In Lavas From The Last Quarter-Millennium Flows. Geochim. Cosmochim. Acta, 75 , 256-283

Chen T.Y., Ling H.F., Frank M., Zhao K.D., Jiang S.Y. (2011) Zircon effect alone insufficient to generate seawater Nd-Hf isotope relationships. $G^3$ 12, 5, Q05003, doi:10.1029/2010GC003363, ISSN:1525-2027.

Crocket, K.C., Foster, G.L., Vance, D., Richards, D.A., Tranter, M., 2013. A Pb isotope tracer of ocean-ice sheet interaction: the record from the NE Atlantic during the Last Glacial/Interglacial cycle. Quaternary Science Reviews 82, 133-144.

David K., Frank M., O'Nions R.K., Belshaw N.S., Arden J.W., Hein J.R. (2001) The Hf isotope composition of global seawater and the evolution of Hf isotopes in the deep Pacific Ocean from Fe-Mn crusts. Chem. Geol. 178, 23-42.

Dyke, Arthur S., and Victor K. Prest. "Late Wisconsinan and Holocene history of the Laurentide ice sheet." *Géographie physique et Quaternaire* 41.2 (1987): 237-263.

Dyke, A. S., et al. "The Laurentide and Innuitian ice sheets during the last glacial maximum." *Quaternary Science Reviews* 21.1 (2002): 9-31.

Elliott T. R., Hawkesworth C. J., Grönvold K. ; Dynamic Melting Of The Icelandic Plume ; Nature 351 [1991] 201-206

Fagel N., Innocent C., Ariepy C., Hillaire-Marcel C., 2002. Sources of Labrador Sea sediments since the Last Glacial Maximum inferred from Nd-Pb isotopes. Geochim. Cosmichim. Acta, 66, 2569-2581.

Fagel N., Hillaire-Marcel C., Humbelt M., Brasseur R., Weis D., Stevenson R., 2004. Nd and Pb isotope signatures of the clay-size fraction of Labrador Sea sediments during the Holocene: Implications for the inception of the modern deep circulation pattern. Paleoceanography, 9, doi:10.1029/2003PA000993

Fitton J. G., Larsen L. M., Saunders A. D., Hardarson B. S., Kempton P. D.J. (2000) Paleogene continental to oceanic magmatism on the SE Greenland continental margin at 63° N: a review of the results of ocean drilling program legs 152 And 163. Petrol. 41, 951-966, doi: 10.1093/petrology/41.7.951

Frank M. (2002) Radiogenic isotopes: Tracers of past ocean circulation and erosional input. Reviews of Geophys. 40, 1001, 1001, 10.1029/2000RG000094

Foster, Gavin L., and Derek Vance. "Negligible glacial–interglacial variation in continental chemical weathering rates." *Nature* 444.7121 (2006): 918-921.

Furman T., Frey F. A., Park Kye-Hun ; Chemical Constraints On The Petrogenesis Of Mildly Alkaline Lavas From Vestmannaeyjar, Iceland: The Eldfell (1973) And Surtsey (1963-1967) Eruptions ; Contrib. Mineral. Petrol. 109 [1991] 19-37

Furman T., Frey F. A., Meyer P. S. ; Petrogenesis Of Evolved Basalts And Rhyolites At Austurhorn, Southeastern Iceland: The Role Of Fractional Crystallization ; J. Petrol. 33 [1992] 1405-1445

Gaffney A. M., Blichert-Toft J., Nelson B. K., Bizzarro M., Rosing M. T., Albarede F. (2007) Constraints on source-forming processes of West Greenland kimberlites inferred from Hf-Nd isotope systematics. Geochim. Cosmochim. Acta 71, 2820-2836, doi: 10.1016/j.gca.2007.03.009

Gerasimovsky V. I., Laktionova N. V., Kovalenker V. G. (1975) Vanadium, Chromium, Nickel Cobalt And Copper In Iceland Lavas ; Geochem. Int., 12 (4), 160-171

Gibb, Olivia T., et al. "Diachronous evolution of sea surface conditions in the Labrador Sea and Baffin Bay since the last deglaciation." *The Holocene* 25.12 (2015): 1882-1897.

Godfrey L.V., Lee D.C., Sangrey W.F., Halliday A.N., Salters V.J.M., Hein J.R. and White W.M. (1997) The Hf isotopic composition of ferromanganese nodules and crusts and hydrothermal manganese deposits: implications for seawater Hf. Earth Planet. Sci. Lett. 151 (1-2), 91-105.

Godfrey L.V., Zimmermann B., Lee D.C., King R.L., Vervoort J.D., Sherrell R.M., Halliday A.N. (2009) Hafnium and neodymium isotope variations in NE Atlantic seawater. Geochem. Geophys. Geosys. 10, Q08015. http://dx.doi.org/10.1029/2009gc002508.

Goodenough K. M., Upton B. G. J., Ellam R. M. J.(2002) Long-term memory of subduction processes in the lithospheric mantle: evidence from the geochemistry of basic dykes in the Gardar Province of south Greenland. Geol. Soc. London 159, 705-714, doi: 10.1144/0016-764901-154

Gutjahr, M., Frank, M., Stirling, C. H., Klemm, V., van de Flierdt, T., and Halliday, A. N., 2007. Reliable extraction of a deepwater trace metal isotope signal from Fe-Mn oxyhydroxide coatings of marine sediments. Chemical Geology 242, 351-370.

Gutjahr, M., Frank, M., Stirling, C. H., Keigwin, L. D., and Halliday, A. N., 2008. Tracing the Nd isotope evolution of North Atlantic deep and intermediate waters in the Western North Atlantic since the Last Glacial Maximum from Blake Ridge sediments. Earth and Planetary Science Letters 266, 61-77.

Gutjahr, M., Frank, M., Halliday, A.N., Keigwin, L.D., 2009. Retreat of the Laurentide ice sheet tracked by the isotopic composition of Pb in western North Atlantic seawater during termination 1. Earth and Planetary Science Letters 286, 546-555.

Gutjahr, M., Frank, M., Lippold, J., Halliday, A.N., 2014. Peak Last Glacial weathering intensity on the North American continent recorded by the authigenic Hf isotope composition of North Atlantic deep-sea sediments. Quaternary Science Reviews 99, 97-111.

Gutjahr, M., Lippold, J., 2011. Early arrival of Southern Source Water in the deep North Atlantic prior to Heinrich event 2. Paleoceanography 26.Hanan B. B., Schilling J.- G. ; The Dynamic Evolution Of The Iseland Mantle Plume: The Lead Isotope Perspective ; Earth Planet. Sci. Lett. 151 [1997] 43-60

Hards V. L., Kempton P. D., Thompson R. N., Greenwood P. B. ; The Magmatic Evolution Of The Snaefell Volcanic Centre: An Example Of Volcanism During Incipient Rifting In Iceland ; J. Volcanol. Geotherm. Res. 99 [2000] 97-121

Hards V. L., Kempton P. D., Thompson R. N. ; The Heterogeneous Iceland Plume: New Insights From The Alkaline Basalts Of The Snaefell Volcanic Center ; J. Geol. Soc. London 152 [1995] 1003-1009

Hardarson B. S., Fitton J. G., Ellam R. M., Pringle M. S. ; Rift Relocation - A Geochemical And Geochronological Investigation Of A Paleo-Rift In Northwest Iceland ; Earth Planet. Sci. Lett. 153 [1997] 181-196

Harlavan, Y., Erel, Y., and Blum, Y.D., 1998, Systematic changes in lead isotopic composition with soil age in glacial granitic terrains: Geochimica et Cosmochimica Acta, v. 62, p. 33–46, doi:10.1016/S0016-7037(97)00328-1

Hillaire-Marcel, C., de Vernal, A., Bilodeau, G., Wu, G., 1994. Isotope stratigraphy, sedimentation rates and paleoceanographic changes inthe Labrador Sea. Canadian Journa lof Earth Sciences 31, 63–89.

Hoffmann J. E., Münker C., Polat A., König S., Mezger K., Rosing M. T. (2010) Highly Depleted Hadean Mantle Reservoirs In The Sources Of Early Archean Arc-Like Rocks, Isua Supracrustal Belt, Southern West Greenland. Geochim. Cosmochim. Acta 74, 7236-7260, doi: 10.1016/j.gca.2010.09.027

Jackson m. G., Carlson R. W., Kurz M. D., Kempton P. D., Francis D. M., Blusztajn J. (2010) Evidence for the survival of the oldest terrestrial mantle reservoir ; Nature 466, 853-856, doi: 10.1038/NATURE09287

Kempton P. D., Fitton J. G., Saunders A. D., Nowell G. M., Taylor R. N., Hardarson B. S., Pearson D. G. ; The Iceland Plume In Space And Time: A Sr-Nd-Pb-Hf Study Of The North Atlantic Rifted Margin ; Earth Planet. Sci. Lett. 177 [2000] 255-271

Kitagawa H., Kobayashi K., Makishima A., Nakamura E. (2008) Multiple Pulses Of The Mantle Plume: Evidence From Tertiary Icelandic Lavas. J. Petrol., 49, 1365-1396

Kokfelt T. F., Hoernle K. A., Lundstrom C. C., Hauff F., Van Den Bogaard P. ; Time-Scales For Magmatic Differentiation At The Snaefellsjökull Central Volcano, Western Iceland: Constraints From U-Th-Pa-Ra Disequilibria In Post-Glacial Lavas ; Geochim. Cosmochim. Acta 73 [2009] 1120-1144

Kokfelt T. F., Hoernle K. A., Hauff F., Fiebig J., Werner R., Garbe-Schönberg D. ; Combined Trace Element And Pb-Nd-Sr-O Isotope Evidence For Recycled Oceanic Crust (Upper And Lower) In The Iceland Mantle Plume ; J. Petrol. 47 [2006] 1705-1749

Koornneef J. M., Stracke A., Bourdon B., Meier M. A., Jochum K. P., Stoll B., Grönvold K. (2012) Melting Of A Two-Component Source Beneath Iceland. J. Petrol., 53, 127-157

Kuritani T., Yokoyama Tetsuya, Kitagawa H., Kobayashi K., Nakamura E. ; Geochemical Evolution Of Historical Lavas From Askja Volcano, Iceland: Implications For Mechanisms And Timescales Of Magmatic Differentiation ; Geochim. Cosmochim. Acta 75 [2011] 570-587

Kurzweil, F., Gutjahr, M., Vance, D., Keigwin, L., 2010. Authigenic Pb isotopes from the Laurentian Fan: Changes in chemical weathering and patterns of North American freshwater runoff during the last deglaciation. Earth and Planetary Science Letters 299, 458-465.

La Fleche M. R., Camire G. E., Jenner G. A. (1998) Geochemistry of post-arcadian, carboniferous continental intraplate basalts from the Maritimes Basin, Magdalenen Islands, Quebec, Canada. Chem. Geol. 148, 115-136, doi: 10.1016/S0009-2541(98)00002-3

Lacan F. and Jeandel C. (2005) Acquisition of the neodymium isotopic composition of the North Atlantic Deep Water. $G^3$, 6, 12, Q12008, doi:10.1029/2005GC000956, ISSN:1525-2027.

Lazier J.R.N. and Wright D.G. (1993) Annual velocity variations in the Labrador Current. J. Phys. Oceanogr. 23, 659-678.

Le Fèvre, B. and Pin, C. (2002), Determination of Zr, Hf, Th and U by Isotope Dilution and Inductively Coupled Plasma-Quadrupole Mass Spectrometry After Concomitant Separation Using Extraction Chromatography. Geostandards Newsletter, 26: 161–170. doi:10.1111/j.1751-908X.2002.tb00884.x

E Böhm, J Lippold, M Gutjahr, M Frank, P Blaser, B Antz, J Fohlmeister (2015) Strong and deep Atlantic meridional overturning circulation during the last glacial cycle, ...Nature 517 (7532), 73-76

Maclachlan K., Dunning G. R. (1998) 235-258 U-Pb ages and tectonomagmatic relationships of Early Ordovician Low-Ti Tholeiites, Boninites and related plutonic rocks in Central Newfoundland, Canada. Contrib. Mineral. Petrol. 133

Maclachlan K., Dunning G. R. Can. J. (1998) U-Pb ages and tectono-magmatic evolution of Middle Ordovician volcanic rocks of the Wild Bight Group, Newfoundland, Appalachians Earth Sci. 35, 998-1017, doi: 10.1139/cjes-35-9-998

Manhes, G., Minster, J. F. and Allegre, C. J. (1978) Comparative uranium-thorium-lead and rubidium-strontium study ofthe saint severin amphoterite: consequences for early solar system chronology. Earth Planet. Sci. Lett. 39, 14–24

Manning C. J., Thirlwall M. F. (2014) Isotopic Evidence For Interaction Between Öraefajökull Mantle And The Eastern Rift Zone, Iceland. Contrib. Mineral. Petrol., 167 (959)

Minifie M. J., Kerr A. C., Ernst R. E., Hastie A. R., Ciborowski T. J. R., Desharnais G., Millar I. L. (2013) The Northern and Southern sections of the Western ca. 1880 Ma Circum-Superior Large Igneous Province, North America: The Pickle Crow Dyke Connection? Lithos 174, 217-235, doi: 10.1016/j.lithos.2012.03.017

Münker C., Weyer S., Scherer S., Mezger K. (2001) Separation of high field strength elements (Nb, Ta, Zr, Hf) and Lu from rock samples for MC-ICPMS measurements. Geochem. Geophys. Geosys. 2, 12, doi:10.1029/2001GC000183.

Nowell G.M., Kempton P.D., Noble S.R., Fitton J.G., Saunders A.D., Mahoney J.J., Taylor R.N. (1998) High precision Hf isotope measurements of MORB and OIB by thermal ionization mass spectrometry: insights into the depleted mantle. Chem. Geol. 149, 211-233. doi: 10.1016/S0009-2541(98)00036-9

Öhlander B., Ingri J., Land M., and Schöberg H. (2000) Change of Sm-Nd isotope composition during weathering of till. Geochim. Cosmochim Acta 64, 813-820.

Oppo, D. W., McManus, J. F. & Cullen, J. L. Deepwater variability in the Holoceneepoch. Nature 422, 277–278 (2003

Patchett P.J., White W.M., Feldman H., Kielinczuk S., Hofmann A.W. (1984) Hafnium Rare-Earth element fractionation in the sedimentary system and crystal recycling into the earth's mantle. Earth Planet. Sci. Lett. 69, 365-378.

Peate D. W., Breddam K., Baker J. A., Kurz M. D., Barker A. K., Prestvik T., Grassineau N., Skovgaard A. C. (2010) Compositional Characteristics And Spatial Distribution Of Enriched Icelandic Mantle Components. J. Petrol., 51, 1447-1475

Peate D. W., Baker J. A., Jakobsson S. P., Waight T. E., Kent A. J. R., Grassineau N., Skovgaard A. C. ; Historic Magmatism On The Reykjanes Peninsula, Iceland: A Snap-Shot Of Melt Generation At A Ridge Segment ; Contrib. Mineral. Petrol. 157 [2009] 359-382

Pe-Piper G., Piper D. J. W. ; Geochemical Evolution Of Devonian-Carboniferous Igneous Rocks Of The Magdalen Basin, Eastern Canada: Pb- And Nd-Isotope Evidence For Mantle And Lower Crustal Sources ; Can. J. Earth Sci. 35 [1998] 201-221

Piepgras D.J. and Wasserburg G.J. (1987) Rare-earth element transport in the western North Atlantic inferred from Nd isotopic observations. Geochim. Cosmochim. Acta 51, 1257-1271, doi:10.1016/j.epsl.2006.11.027.

Pin C., Zalduegui J.S. (1997) Sequential separation of light rare-earth elements, thorium and uranium by miniaturized extraction chromatography: application to isotopic analyses of silicate rocks. Anal. Chem. Acta 339, 79-89

Prestvik T., Goldberg S., Karlsson H. R., Grönvold K. ; Anomalous Strontium And Lead Isotope Signatures In The Off-Rift Öraefajökull Central Volcano In South-East Iceland: Evidence For Enriched Endmember(S) Of The Icelandic Mantle Plume? ; Earth Planet. Sci. Lett. 190 [2001] 211-220

Salters V. J. M., White W. M. (1998) Hf Isotope Constraints On Mantle Evolution ; Chem. Geol., 145, 447-460

Shorttle O., Maclennan J., Piotrowski A. M. ; Geochemical Provincialism In The Iceland Plume ; Geochim. Cosmochim. Acta 122 [2013] 363-397

Stecher O., Carlson R. W., Gunnarsson B. ; Torfajökull: A Radiogenic End-Member Of The Iceland Pb-Isotopic Array ; Earth Planet. Sci. Lett. 165 [1999] 117-127

Skulski T., Percival J. A. (1996) Allochthonous 2.78 Ga Oceanic Plateau Slivers In A 2.72 Ga Continental Arc Sequence; Vizien Greenstone Belt, Northeastern Superior Province, Canada. Lithos 37, 163-179, doi: 10.1016/0024-4937(95)00035-6

Skulski T., Percival J. A. (1996) Allochthonous 2.78 Ga Oceanic Plateau Slivers In A 2.72 Ga Continental Arc Sequence; Vizien Greenstone Belt, Northeastern Superior Province, Canada. Lithos 37, 163-179, doi: 10.1016/0024-4937(95)00035-6

Stordal M.C. and Wasserburg G.J. (1986) Neodymium isotopic study of Baffin Bay water sources of REE from very old terranes. Earth Planet. Sci. Lett. 77, 259-272.

Stracke A., Zindler A., Salters V. J. M., Mckenzie D. M., Blichert-Toft J., Albarede F., Grönvold K. (2003) Theistareykir Revisited ; Geochemistry Geophysics Geosystems,

Sun Shen-Su, Tatsumoto M., Schilling J.- G. ; Mantle Plume Mixing Along The Reykjanes Ridge Axis: Lead Isotope Evidence ; Science 190 [1975] 143-147

Sun Shen-Su, Jahn B.-M. ; Lead And Strontium Isotopes In Post-Glacial Basalts From Iceland ; Nature 255 [1975] 527-530

Swinden H. S., Jenner G. A., Fryer B. J., Hertogen J., Roddick J. C. (1990) Petrogenesis and paleotectonic history of the Wild Bight Group, an ordovician rifted island arc in Central Newfoundland. Contrib. Mineral. Petrol. 105, 219-241, doi: 10.1007/BF00678987

Szilas K., Hoffmann J. E., Schersten A., Rosing M. T., Windley B. F., Kokfelt T. F., Keulen N., Van Hinsberg V., Naeraa T., Frei R., Münker C. (2012) Complex calc-alkaline volcanism recorded in mesoarchaean supracrustal belts north of Frederikshab Isblink, Southern West Greenland: implications for subduction zone processes in the early Earth. Prec. Research 208-211, 90-123, doi: 10.1016/j.precamres.2012.03.013

Szilas K., Hoffmann J. E., Schersten A., Kokfelt T. F., Münker C.(2013) Archaean andesite petrogenesis: insights from the Graedefjord Supracrustal Belt, Southern West Greenland. Prec. Research 236, 1-15, doi: 10.1016/j.precamres.2013.07.013

Tanaka T., Togashi S., Kamioka H., Amakawa H., Kagami H., Hamamoto T., Yuhura M., Orihashi, Y., Yoneda, S., Shimizu, H., Kunimaru, T., Takahashi, K., Yanagi, T., Nakano, T., Fujimaki, H., Shinjo, R., Asahara, Y., Tanimizu, M., Dragusanu, C. (2000) JNdi-1: a neodymium isotopic reference in consistency with LaJolla neodymium. Chem. Geol. 168 (3–4), 279–281.

Tappe S., Foley S. F., Kjarsgaard B. A., Romer R. L., Heaman L. M., Stracke A., Jenner G. A. (2008) Between carbonatite and lamproite-diamondiferous torngat ultramafic lamprophyres formed by carbonate-fluxed melting of cratonic marid-type metasomes. Geochim. Cosmochim. Acta 72, 3258-3286, doi: 10.1016/j.gca.2008.03.008

Tachikawa, K., A. M. Piotrowski, and G. Bayon (2014), Neodymium associated with foraminiferal carbonate as a recorder of seawater isotopic signatures, Quat. Sci. Rev.,88,1–13.

Thirlwall M. F., Gee M. A. M., Taylor R. N., Murton B. J. ; Mantle Components In Iceland And Adjacent Ridges Investigated Using Double Spike Pb Isotopic Ratios ; Geochim. Cosmochim. Acta 68 [2004] 361-386

Thirlwall M. F. ; Inter-Laboratory And Other Errors In Pb Isotope Anlyses Investigated Using A 207pb-204pb Double Spike ; Chem. Geol. 163 [2000] 299-322

D. Vance, D.A.H. Teagle and G.L. Foster (2009) Variable Quaternary chemical weathering rates and imbalances in marine geochemical budgets, Nature 458, 493 496

Veiga-Pires, C. C., *and* C. Hillaire-Marcel *(*1999*)*, U and Th isotope constraints on the duration of Heinrich events H0-H4 in the southeastern Labrador Sea, Paleoceanography, 14*(*2*)*, 187–199, *doi:*10.1029/1998PA900003.

Vervoort J.D., Plank T., Prytulak J. (2011) The Hf-Nd isotopic composition of marine sediments. Geochim. et Cosmocim. Acta 75, 20, 5903-5926, doi:10.1016/j.gca.2011.07.046.

von Blanckenburg, F. and Nägler, T. F., 2001. Weathering versus circulation-controlled changes in radiogenic isotope tracer composition of the Labrador Sea and North Atlantic Deep Water. Paleoceanography 16, 424-434.

West D. P.; Jr., Coish R. A., Tomascak P. B. (2004) Tectonic setting and regional correlation of ordovician metavolcanic rocks of the Casco Bay Group, Maine: evidence from trace element and isotope geochemistry. Geol. Mag. 141, 125-140, doi: 10.1017/S0016756803008562

Willbold M., Hegner E., Stracke A., Rocholl A. ; Continental Geochemical Signatures In Dacites From Iceland And Implications For Models Of Early Archaean Crust Formation ; Earth Planet. Sci. Lett. 279 [2009] 44-52

Welke H. J., Moorbath S., Cumming G. L., Sigurdsson H. ; Lead Isotope Studies On Igneous Rocks From Iceland ; Earth Planet. Sci. Lett. 4 [1968] 221-231

Yashayaev I. and Clark A. (2006) Recent warming of the Labrador Sea. AZMP Bulletin PMZA 5:12-20.

Yashayaev I., Dickson R.R. (2008) Transformation and fate of overflows in the northern North Atlantic, in Arctic-Subarctic Ocean Fluxes: Defining the Role of the Northern Seas in Climate, edited by R.R. Dickson, J. Meincke and P. Rhines, Chapter Arctic-Subarctic Ocean Fluxes 505-526, Springer, New York.

Zindler A., Komatiites (Arndt, N. T.,E. G. Nisbet, E. G.) (1982) Nd And Sr isotopic studies of komatiites and related rocks, Allen & Unwin, 399-420

## SUMMARY.

The Labrador Sea is one of the important regions for deep water formation in the North Atlantic and one of the main contributors of fresh water to North Atlantic Deep Water. Studies carried out in this region help to understand the mechanisms controlling the thermohaline circulation and to learn more about key aspects of climate-ocean interactions. The overall goal of my PhD project was to provide new insights into the mechanisms and processes that are driving surface and deep water formation in the Labrador Sea, and apply this knowledge in paleoclimate studies to better understand the climate of the past in order to be able to predict future climate changes.

The focus of this thesis were two major components of the water mass circulation in the Labrador Sea: surface water currents and intermediate and deep waters.

Alkenone paleothermometry was applied to track the variability of the surface waters based on sea surface temperatures. Although its robustness as a temperature proxy in high latitude regions has been questioned, it is shown in **Chapter 4** that it can be used reliably for sea surface temperature reconstructions in most parts of the western North Atlantic if a set of conditions are met, such as appropriate age control of the sediment samples and low risk of pre-formed alkenone input. One of the new findings in this study was the importance of the proximity to those areas of the ocean characterized by steep gradients and frontal systems. The new results showed that most of the samples with high temperature offsets between 5 and 10 °C from the western North Atlantic region are located in areas of particularly steep temperature gradients, which was especially true for regions with overall low sea surface temperatures. This suggests that in strongly temperature stratified waters or highly dynamic

ocean environments the mean World Ocean Atlas temperature fields might not capture the highly dynamic sea surface temperature variability, thereby introducing a bias. In addition, lateral transport has the potential to introduce allochthonous alkenones in regions characterized by steep sea surface temperature gradients. As pointed out previously and consistent with the new results, local sea surface temperature increase due to water restratification as a consequence of freshwater inputs can be a source of significant warm bias in such regions as the Nordic Seas.

In **Chapter 5** a detailed paleoceanographic study was carried out on four sediment cores providing information on sea surface temperature variations in the Labrador Sea over the last 35 kyrs. The records prior to the Holocene were only partially preserved in all cores, partly expressed negative $U_{37}^{K}$ values, and were thus considered unreliable in view of the resulting negative sea surface temperatures. The Holocene proxy signatures, however, have been well preserved over the last 10 kyrs and showed that the Holocene was a period of unstable climate in the western North Atlantic that has been characterized by multiple temperature fluctuations, likely due to increased cold water inputs from the Arctic or fresh water inputs such as during 8.2 ka event.

The second part of this PhD project focused on intermediate and deep waters.

The study described in **Chapter 3** shows that all water masses present today in the Labrador Sea have distinct radiogenic hafnium and neodymium isotope signatures. One of the main findings was a better distinction of Irminger water and shallow and deep Labrador Sea Water based on hafnium isotope compositions, rather than on those of neodymium. The current study also shows that the Labrador Sea Water in 2013 was formed up to a depth of about 1500 m. This was shallower than before and consistent with warming of the Labrador Sea and weakening of the winter convection. The εHf signature of the main water masses in the Labrador Sea was most likely mainly controlled by weathering inputs from the surrounding terrains. It was concluded that hafnium has a shorter oceanic residence time than previously assumed, which, however, due to missing information on the continental input fluxes could not be supported by a detailed mass balance calculations. Higher variability of εHf over εNd in our study was interpreted as a possible reflection of decadal changes in the production of the Labrador Sea Water. The new data allowed to conclude that although tracing of large scale ocean mixing processes may not be possible based on Hf isotopes, there is clearly prospect for their application in other restricted basins with similar geological and hydrographic settings.

**Chapter 6** was based on radiogenic hafnium-neodymium-lead isotope records obtained from the same sediment cores as in chapter 5 over the last 35 kyrs. The data showed distinct unradiogenic signatures during periods such as Heinrich Stadial 1 and 2, the Last Glacial Maximum and the Younger Drays, as well as during the 8.2 ka event. One of the main findings of this study was an earlier inception of the Denmark Strait Overflow Water around 12 ka, supported by εNd and εHf data of the leachates and detrital fraction of core 2227. The εHf and εNd signatures of the detrital fraction in cores 094 and 021 suggest the establishment of the alongshore Labrador current around 12 ka. Hafnium and neodymium isotope signatures during particular periods of the Holocene showed that convection in the region may have been more intense and formation of the Labrador Sea Water was deeper than today reaching 2600 m depth. An interesting observation was a distinct array above the seawater array formed by sediment samples from the Labrador Sea on an εHf-εNd plot.

Overall, the new data demonstrate that a combination of multiple proxies and different isotope systems can improve our understanding of the water mass processes in the region and can provide new crucial information.

## OUTLOOK

Over the last three years of my work on the current PhD project I encountered several questions that were beyond the scope of this project but still are clearly of importance for further proxy development and should be answered in the nearest future.

For alkenone paleothermometry, the exact mechanisms controlling the alkenone distributions and unsaturation ratios is not yet resolved. It is crucial for the improvement of proxy applications for paleoreconstructions to define the main factors of alkenone production and the mechanisms behind it. The alkenone sea surface temperature proxy would benefit from improved understanding of E. huxleyi relationship to cold temperatures and the exact effect cold temperatures have on the alkenone production. Do short-term temperature drops result in preferential degradation of already produced alkenones for metabolic purposes? What drives the non-linear behavior of alkenone distributions in cold temperatures?

The paleoreconstructions carried out on the sediment cores raised the question of the exact tetra alkenone origin and their relation to the occurrence of icebergs or to salinity changes, as in some of the samples high tetra alkenone abundances are coincident with events such as Heinrich stadials, the LGM, or the Younger Dryas.

The study of the present day hafnium and neodymium signatures of different water masses in the Labrador Sea again raised the question of the correct oceanic hafnium residence

time in seawater. Although the data obtained in our study strongly suggest a short residence time of hafnium in the Labrador Sea, this needs to be supported by mass balance calculations. The calculations are, however, highly speculative until hafnium fluxes and inputs from river waters and other continental sources will be better constrained based on direct measurements of river waters and the exchange of hafnium with the marginal sediments.

Finally, more studies on hafnium behavior in seawater are necessary. In which form is hafnium mainly present in seawater? Is there any truly dissolved hafnium in seawater? In what form is hafnium delivered to the ocean within river waters? Resolving these questions would help to better understand the marine behavior of hafnium and its isotopic composition and to improve its application as a proxy for water mass mixing and weathering inputs.

# APPENDIX

## CHAPTER 4

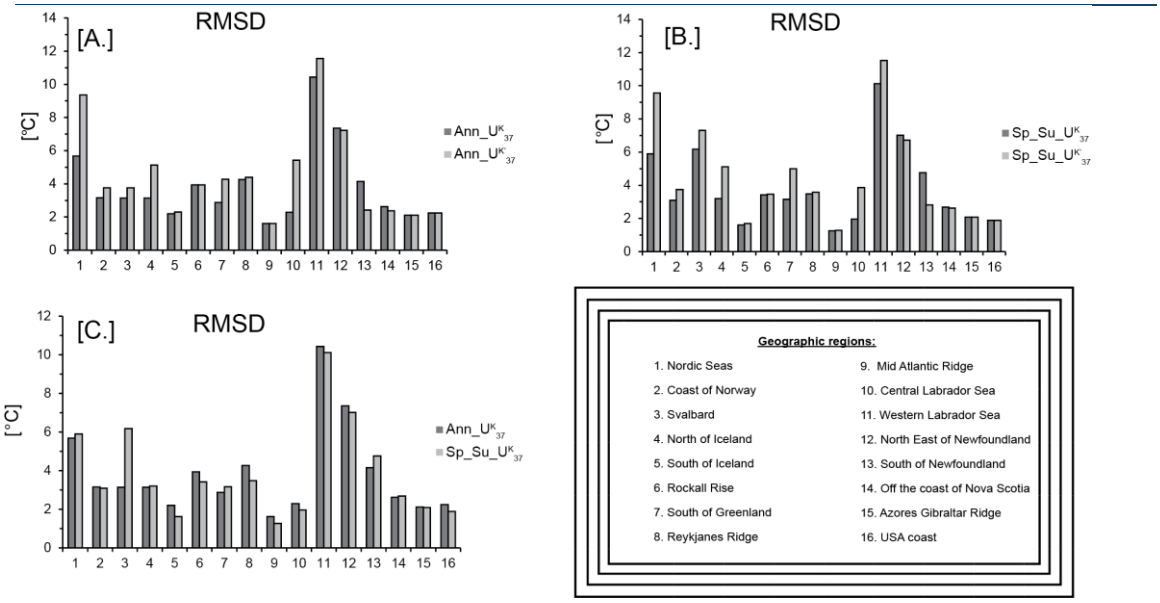


**Figure A1** Comparison of RMSD values for A. Annual SST_ $U^{K}_{37}$ with Annual SST_ $U^{K`}_{37}$ B. Sp_Su SST_ $U^{K}_{37}$ with Sp_Su SST_ $U^{K`}_{37}$ C. Annual SST_ $U^{K}_{37}$ with Sp_Su SST_ $U^{K}_{37}$.

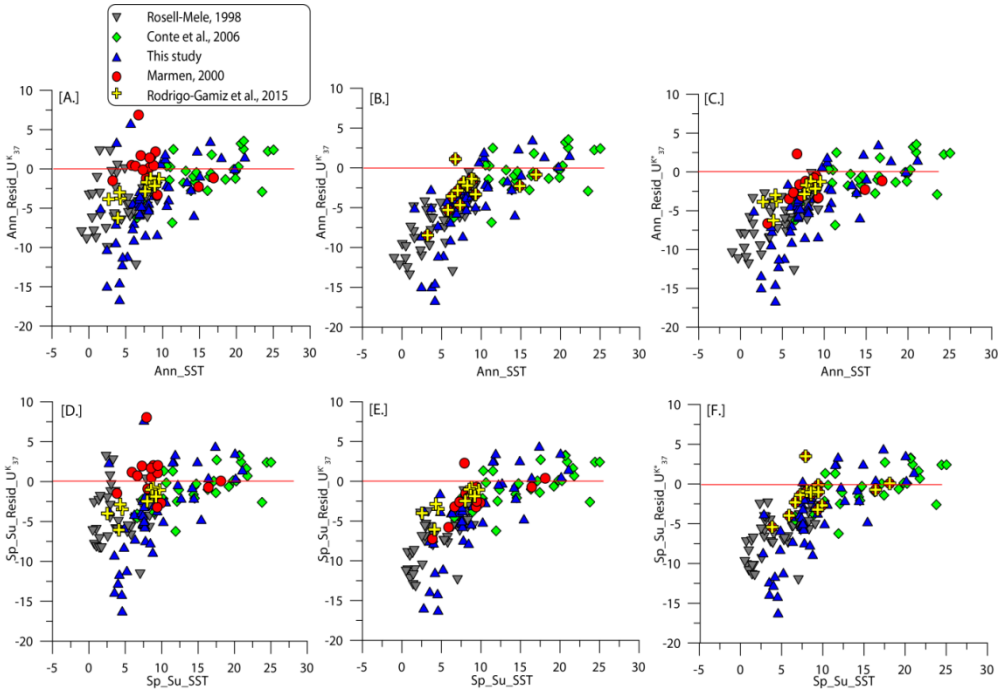


**Figure A2** A. Annual SST vs Ann_ $U^{K}_{37}$_Residuals, B. Annual SST vs Ann_ $U^{K`}_{37}$_Residuals, C. Annual SST vs Ann_ $U^{K*}_{37}$_Resdiuals, D. Spring Summer SST vs Sp_Su_ $U^{K}_{37}$_Residuals, E. Spring Summer SST vs Sp_Su_ $U^{K`}_{37}$_Residuals, F. Spring Summer SST vs Sp_Su_ $U^{K*}_{37}$_Resdiuals. Color and symbols denote different laboratories.

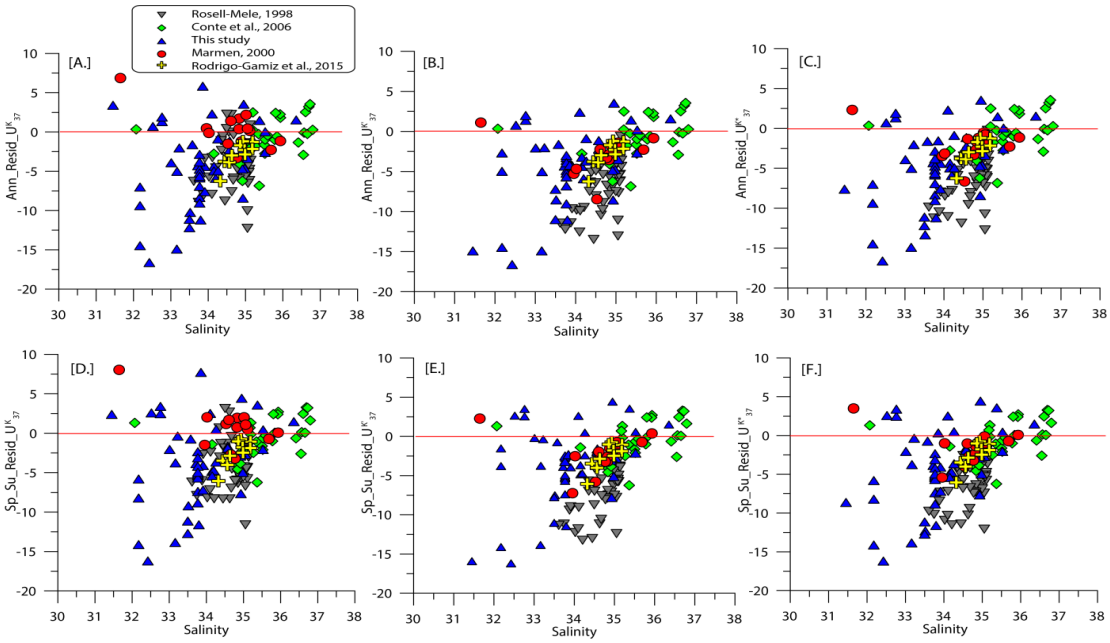


**Figure A3** A. Salinity vs Ann_ $U^{K}_{37}$_Residuals, B. Salinity vs Ann_ $U^{K`}_{37}$_Residuals, C. Salinity vs Ann_ $U^{K*}_{37}$_Resdiuals, D. Salinity vs Sp_Su_ $U^{K}_{37}$_Residuals, E. Salinity vs Sp_Su_ $U^{K`}_{37}$_Residuals, F. Salinity vs Sp_Su_ $U^{K*}_{37}$_Resdiuals. Color and symbols denote different laboratories.

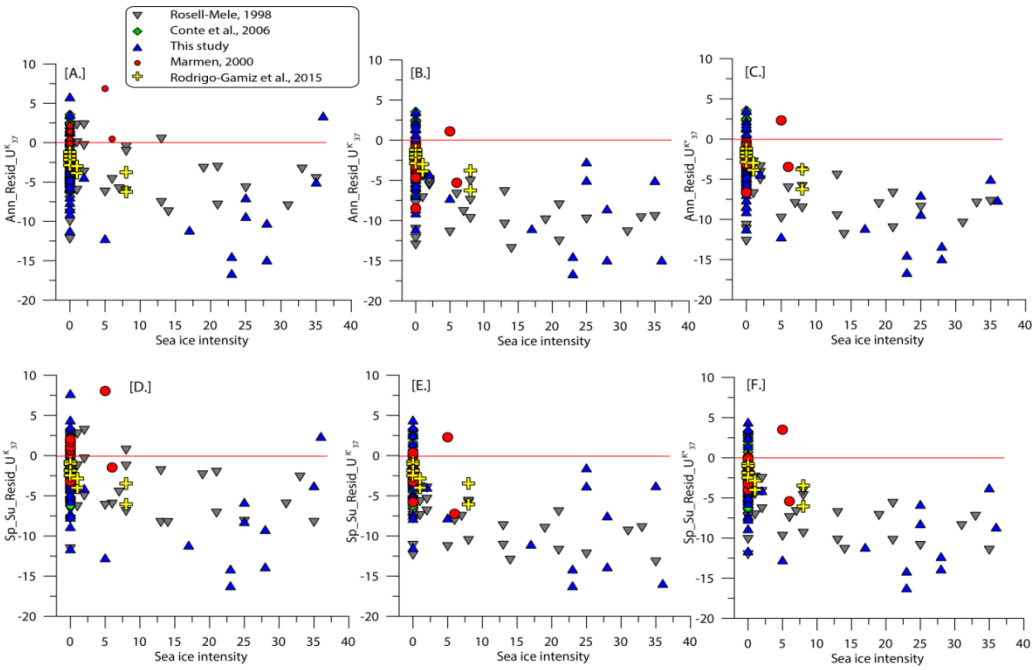


**Figure A4** A. Sea ice intensity vs Ann_ $U^{K}_{37}$_Residuals, B. Sea ice intensity vs Ann_ $U^{K`}_{37}$_Residuals, C. Sea ice intensity vs Ann_ $U^{K*}_{37}$_Resdiuals, D. Sea ice intensity vs Sp_Su_ $U^{K}_{37}$_Residuals, E. Sea ice intensity vs Sp_Su_ $U^{K`}_{37}$_Residuals, F. Sea ice intensity vs Sp_Su_ $U^{K*}_{37}$_Resdiuals. Color and symbols denote different laboratories.

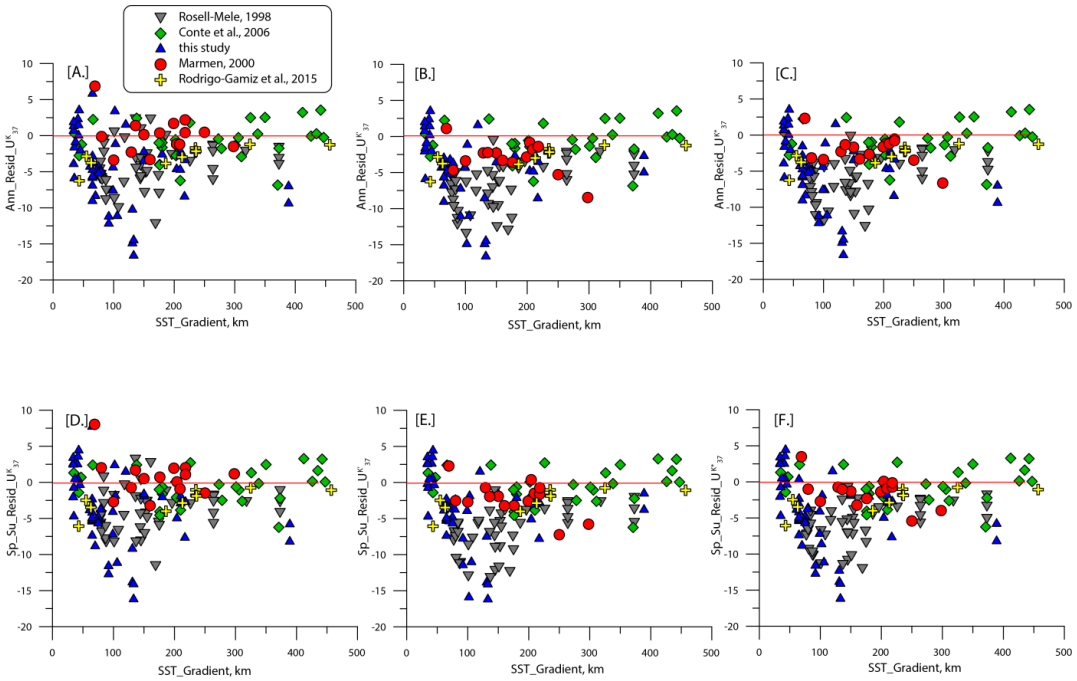


**Figure A5** All residuals versus SST_Gradient shown in km for different laboratories for A. Ann_Resid_ $U^{K}_{37}$ B. Ann_Resid_ $U^{K`}_{37}$ C. Ann_Resid_ $U^{K*}_{37}$ D. Sp_Su_Resid_ $U^{K}_{37}$ E. Sp_Su_Resid_ $U^{K`}_{37}$ F. Sp_Su_Resid_ $U^{K*}_{37}$

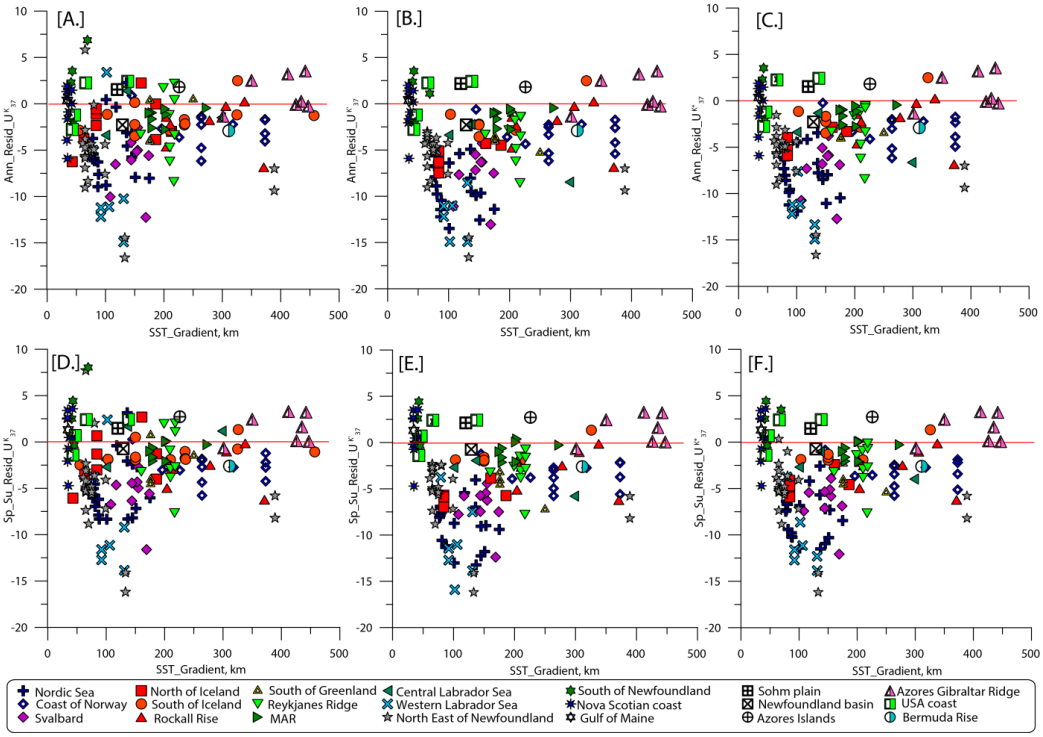


**Figure A6** All residuals versus SST_Gradient shown in km for different geographical regions for A. Ann_Resid_ $U^{K}_{37}$ B. Ann_Resid_ $U^{K`}_{37}$ C. Ann_Resid_ $U^{K*}_{37}$ D. Sp_Su_Resid_ $U^{K}_{37}$ E. Sp_Su_Resid_ $U^{K`}_{37}$ F. Sp_Su_Resid_ $U^{K*}_{37}$

| Sample code | Latitude | Longitude | Annual Temp. WOA, T [°C] | Spring Summer Temp. WOA, T [°C] | Salinity, [‰] | Sea ice intensity, [times/in 35 yr] | UK37 | UK'37 | UK*37 | *Second run UK'37 | *Third run UK'37 |
|---|---|---|---|---|---|---|---|---|---|---|---|
| 99036_035 | 40° 13' 11 N | 61° 21' 35 W | 19.76 | 20.15 | 35.53 | 0 | 0.695 | 0.695 | 0.695 | | |
| 2004_024_033 | 49° 32' 59 N | 46° 51' 0 W | 8.12 | 7.66 | 34.16 | 0 | 0.456 | 0.456 | 0.456 | | |
| 98039_009 | 41° 26' 23 N | 54° 46' 48 W | 16.47 | 17.38 | 34.95 | 0 | 0.471 | 0.471 | 0.471 | | |
| 2009_061_0124 | 48° 43' 11 N | 45° 8' 24 W | 6.11 | 7.61 | 33.77 | 0 | 0.474 | 0.474 | 0.474 | 0.401 | 0.519 |
| 2000_036_030 | 42° 21' 0 N | 62° 1' 48 W | 10.82 | 12.68 | 33.01 | 0 | 0.469 | 0.469 | 0.530 | 0.469 | |
| 2004_024_052 | 49° 23' 24 N | 48° 10' 47 W | 5.94 | 6.24 | 33.91 | 2 | 0.385 | 0.385 | 0.385 | 0.398 | |
| 2009_061_0121 | 48° 24' 35 N | 44° 46' 12 W | 6.77 | 7.21 | 33.73 | 0 | 0.409 | 0.409 | 0.409 | | |
| 98039_010 | 42° 20' 24 N | 54° 42' 36 W | 14.69 | 14.91 | 34.10 | 0 | 0.453 | 0.453 | 0.453 | 0.439 | |
| 91020_014 | 41° 47' 23 N | 62° 20' 24 W | 13.31 | 14.20 | 33.58 | 0 | 0.537 | 0.537 | 0.537 | | |
| 2009_061_0117 | 48° 38' 59 N | 45° 10' 12 W | 6.88 | 7.41 | 33.77 | 0 | 0.393 | 0.393 | 0.464 | 0.393 | |
| 2004_030_003 | 42° 49' 47 N | 62° 2' 59 W | 9.74 | 11.62 | 32.52 | 0 | 0.342 | 0.342 | 0.342 | 0.303 | |
| 2010_020_0059 | 49° 8' 24 N | 51° 21' 0 W | 4.16 | 4.58 | 32.43 | 23 | 0.730 | 0.730 | 0.730 | | |
| 9102_0008 | 41° 28' 11 N | 62° 0' 54 W | 14.25 | 15.44 | 34.20 | 0 | 0.709 | 0.709 | 0.709 | | |
| 96029_069 | 43° 4' 12 N | 55° 49' 47 W | 10.54 | 12.22 | 33.23 | 0 | 0.459 | 0.459 | 0.459 | | |
| 2010_020_0058 | 48° 52' 48 N | 51° 51' 35 W | 3.66 | 4.83 | 32.18 | 25 | 0.254 | 0.254 | 0.474 | 0.254 | |
| 99036_052 | 42° 44' 24 N | 62° 7' 11 W | 10.36 | 11.52 | 32.76 | 0 | 0.342 | 0.342 | 0.342 | 0.321 | |
| 2004_024_032 | 49° 30' 35 N | 46° 52' 11 W | 8.12 | 7.67 | 34.16 | 0 | 0.418 | 0.418 | 0.476 | 0.418 | |
| 99036_055 | 42° 38' 24 N | 62° 7' 1 W | 10.36 | 11.87 | 32.76 | 0 | 0.306 | 0.306 | 0.323 | 0.306 | |
| 91020_012 | 41° 16' 12 N | 61° 48' 43 W | 15.05 | 16.42 | 34.26 | 0 | 0.570 | 0.570 | 0.570 | | |
| 2006_040_0057 | 57° 34' 47 N | 58° 55' 12 W | 2.46 | 3.50 | 33.52 | 28 | 0.194 | 0.407 | 0.566 | 0.407 | |
| 2009_061_0119 | 48° 36' 35 N | 45° 6' 35 W | 6.88 | 7.41 | 33.77 | 0 | 0.379 | 0.379 | 0.427 | 0.379 | |
| 99036_037 | 40° 15' 35 N | 61° 11' 23 W | 17.97 | 20.08 | 35.38 | 0 | 0.583 | 0.583 | 0.589 | 0.583 | |
| 98039_005 | 38° 45' 0 N | 49° 53' 59 W | 21.15 | 21.09 | 36.36 | 0 | 0.668 | 0.668 | 0.691 | 0.668 | |
| 2004_024_041 | 50° 12' 0 N | 45° 40' 47 W | 8.08 | 9.38 | 34.27 | 0 | 0.433 | 0.433 | 0.474 | 0.433 | |
| hu91_045_071 | 58° 33' 36 N | 28° 26' 24 W | 8.79 | 9.46 | 35.06 | 0 | 0.445 | 0.445 | 0.445 | 0.441 | |
| hu91045_005 | 54° 25' 12 N | 56° 15' 35 W | 3.76 | 2.76 | 31.45 | 36 | 0.056 | 0.659 | 0.420 | | |

| | | | | | | | | | | |
|---|---|---|---|---|---|---|---|---|---|---|
| hu91045_014 | 54° 27' 0 N | 53° 25' 47 W | 1.59 | 2.85 | 33.17 | 35 | 0.262 | 0.262 | 0.262 | |
| 2005_033b_052 | 54° 56' 23 N | 51° 24' 35 W | 5.24 | 5.22 | 33.50 | 17 | 0.584 | 0.584 | 0.584 | |
| 2006_040_0004 | 54° 51' 0 N | 52° 37' 48 W | 4.54 | 4.00 | 33.50 | 5 | 0.432 | 0.432 | 0.596 | 0.432 |
| 2006_040_0057 | 57° 34' 47 N | 58° 53' 59 W | 2.46 | 3.52 | 33.16 | 28 | 0.617 | 0.617 | 0.617 | |
| 2009_061_0129 | 48° 31' 44 N | 45° 8' 52 W | 6.88 | 7.41 | 33.77 | 0 | 0.459 | 0.459 | 0.459 | |
| 2001_043_001 | 49° 30' 3 N | 45° 15' 35 W | 9.27 | 8.77 | 33.77 | 0 | 0.625 | 0.625 | 0.625 | 0.511 |
| 2006_040_0003 | 54° 47' 42 N | 52° 19' 16 W | 4.58 | 4.19 | 33.80 | 0 | 0.565 | 0.565 | 0.565 | 0.541 |
| 2004_024_033 | 49° 32' 23 N | 46° 51' 7 W | 8.12 | 7.67 | 33.77 | 0 | 0.484 | 0.484 | 0.484 | |
| 2009_061_0114 | 49° 56' 27.6" | 45° 3' 10 W | 6.11 | 7.77 | 33.77 | 0 | 0.544 | 0.544 | 0.544 | |
| 2010_020_0059 | 49° 8' 24" | 51° 21' 10 W | 4.16 | 4.52 | 32.18 | 23 | 0.659 | 0.659 | 0.659 | |
| 2010_020_0058 | 48° 53' 2.4" | 51° 23' 9 W | 3.66 | 4.86 | 32.18 | 25 | 0.396 | 0.396 | 0.396 | 0.329 |
| 2004_024_050 | 49° 25' 29 N | 48° 10' 44 W | 5.94 | 6.34 | 33.91 | 0 | 0.491 | 0.491 | 0.491 | 0.383 |
| 2009_061_0124 | 48° 43' 15 N | 45° 8' 31 W | 6.88 | 7.58 | 33.77 | 0 | 0.458 | 0.458 | 0.458 | |
| 2009_61_129 | 48° 31' 48 N | 45° 8' 59 W | 6.88 | 7.39 | 33.77 | 0 | 0.365 | 0.365 | 0.365 | |
| 2009_61_124 | 48° 43' 11 N | 45° 8' 24 W | 6.88 | 7.58 | 33.77 | 0 | 0.397 | 0.397 | 0.397 | |
| 2009_061_113 | 48° 55' 12 N | 45° 11' 23 W | 5.67 | 7.56 | 33.85 | 0 | 0.039 | 0.373 | 0.282 | |
| GIK17050-1 | 55° 28' 11 N | 27° 52' 58 W | 10.57 | 10.22 | 34.98 | 0 | 0.545 | 0.545 | 0.545 | |
| GIK17049-6 | 55° 12' 0 N | 26° 43' 11 W | 10.84 | 10.56 | 34.93 | 0 | 0.476 | 0.476 | 0.476 | |
| GIK17055-1 | 48° 12' 36 N | 27° 3' 21 W | 13.86 | 14.41 | 35.52 | 0 | 0.587 | 0.587 | 0.587 | |
| GIK23523-3 | 62° 15' 3 N | 30° 13' 14 W | 7.32 | 8.26 | 34.58 | 0 | 0.380 | 0.380 | 0.380 | |
| GIK23528-3 | 63° 9' 50 N | 28° 50' 29 W | 6.92 | 8.46 | 34.58 | 0 | 0.387 | 0.387 | 0.387 | |
| GIK23522-2 | 63° 45' 43 N | 28° 39' 31 W | 7.98 | 8.58 | 34.58 | 0 | 0.381 | 0.381 | 0.381 | |
| GIK23519-5 | 64° 47' 50 N | 29° 35' 44 W | 8.43 | 7.70 | 34.58 | 0 | 0.360 | 0.360 | 0.360 | |
| GIK17052-4 | 56° 25' 54 N | 56° 25' 55 W | 7.68 | 8.44 | 34.93 | 0 | 0.575 | 0.575 | 0.575 | |
| GIK17051-2 | 56° 9' 43 N | 31° 59' 23 W | 7.14 | 8.95 | 34.92 | 0 | 0.435 | 0.435 | 0.435 | |

* concentrations of tetra alkenone in the second and third run

were zero

**Table A1** New data sample information: position, annual and spring-summer temperatures, salinity and alkenone unsaturation indices.

| Author | Geographical region | total number of samples | | Ann_SST WOA, 2013 | | | Sp_Su_SST WOA, 2013 | | | Ann_SST, Levitus, 1994 (Rosell-Mele, 1998) Ann_SST WOA, 2009 (Rodrigo-Gamiz et al., 2015) | | | Sp_Su_SST WOA, 2009 | | |
|---|---|---|---|---|---|---|---|---|---|---|---|---|---|---|---|
| | | | | $U^{K}_{37}$ | $U^{K'}_{37}$ | $U^{K*}_{37}$ | $U^{K}_{37}$ | $U^{K'}_{37}$ | $U^{K*}_{37}$ | $U^{K}_{37}$ | $U^{K'}_{37}$ | $U^{K*}_{37}$ | $U^{K}_{37}$ | $U^{K'}_{37}$ | $U^{K*}_{37}$ |
| Rosell-Mele, 1998 | Nordic Seas | 46 | $r^2$ | 0.39 | 0.1 | 0.2 | 0.45 | 0.1 | 0.25 | 0.35 | 0.05 | 0.16 | n/a | n/a | n/a |
| | | | 2sdev | 6.1 | 6.38 | 5.8 | 5.7 | 5.85 | 5.32 | 6.31 | 6.34 | 5.86 | n/a | n/a | n/a |
| | | | RMSD | 7.6 | 7.5 | 7.5 | 8.12 | 8.22 | 8.15 | 9.76 | 9.67 | 9.7 | n/a | n/a | n/a |
| | | | SEM | 0.46 | 0.47 | 0.4 | 0.44 | 0.46 | 0.42 | 0.47 | 0.47 | 0.43 | n/a | n/a | n/a |
| Marmen, 2000 | Labrador Sea, South of Iceland, Reykjanes ridge, Central Atlantic | 15 | $r^2$ | 0.75 | 0.59 | 0.7 | 0.7 | 0.61 | 0.69 | n/a | n/a | n/a | n/a | n/a | n/a |
| | | | 2sdev | 5.07 | 4.4 | 3.9 | 5.26 | 4.56 | 4.06 | n/a | n/a | n/a | n/a | n/a | n/a |
| | | | RMSD | 2.44 | 3.55 | 2.8 | 2.63 | 3.11 | 2.42 | n/a | n/a | n/a | n/a | n/a | n/a |
| | | | SEM | 0.65 | 0.57 | 0.5 | 0.68 | 0.59 | 0.52 | n/a | n/a | n/a | n/a | n/a | n/a |
| Conte et al., 2006 | South of Iceland, Central Atlantic, Reykjanes ridge, Off the coast of USA, Off the coast of Africa | 30 | $r^2$ | 0.77 | 0.77 | 0.8 | 0.82 | 0.82 | 0.82 | n/a | n/a | n/a | n/a | n/a | n/a |
| | | | 2sdev | 5.13 | 5.13 | 5.1 | 4.85 | 4.85 | 4.85 | n/a | n/a | n/a | n/a | n/a | n/a |
| | | | RMSD | 2.63 | 2.63 | 2.6 | 2.44 | 2.44 | 2.44 | n/a | n/a | n/a | n/a | n/a | n/a |
| | | | SEM | 0.47 | 0.47 | 0.5 | 0.44 | 0.44 | 0.44 | n/a | n/a | n/a | n/a | n/a | n/a |
| This study | South of Iceland, Reykjanes ridge, Labrador Sea, North and South off Newfoundland, Off the coast of Nova Scotia, Central Atlantic | 51 | $r^2$ | 0.13 | 0.09 | 0.1 | 0.11 | 0.05 | 0.07 | n/a | n/a | n/a | n/a | n/a | n/a |
| | | | 2sdev | 9.4 | 9.7 | 9.2 | 9 | 10 | 10 | n/a | n/a | n/a | n/a | n/a | n/a |
| | | | RMSD | 6.6 | 6.7 | 6.7 | 6.3 | 6.5 | 6.4 | n/a | n/a | n/a | n/a | n/a | n/a |
| | | | SEM | 0.68 | 0.66 | 0.6 | 0.71 | 0.7 | 0.7 | n/a | n/a | n/a | n/a | n/a | n/a |
| Rodrigo-Gamiz et al., | North and South of Iceland | 10 | $r^2$ | | 0.66 | | | 0.66 | | | 0.69/0.9* | | | 0.64/0.91* | |

| | | | | | | | |
|---|---|---|---|---|---|---|---|
| 2015 | | **2sdev** | 3.04 | 3.3 | 2.8/1.9* | 2.4/1.4* | |
| | | **RMSD** | 3.18 | 3 | 3.1/2.6* | 1.16/0.7* | |
| | | **SEM** | 0.48 | 0.51 | 0.44/0.3* | 0.39/0.2* | |

*one value was removed

**Table A2** Separate analysis of each data set

| | **Geographical region** | **total number of samples** | | **Ann_SST WOA 2013** | | | **Sp_Su_SST WOA, 2013** | | | Author |
|---|---|---|---|---|---|---|---|---|---|---|
| | | | | $U^{K}_{37}$ | $U^{K'}_{37}$ | $U^{K*}_{37}$ | $U^{K}_{37}$ | $U^{K'}_{37}$ | $U^{K*}_{37}$ | |
| 1 | Nordic Seas | 20 | **$r^2$** | 0.17 | 0.1 | 0.12 | 0.1 | 0 | 0 | Rosell-Mele, 1998 |
| | | | **2sdev** | 6.06 | 5.02 | 4.84 | 6.2 | 5.08 | 4.85 | |
| | | | **RMSD** | 5.68 | 9.36 | 8.18 | 5.9 | 9.56 | 8.37 | |
| | | | **SEM** | 0.95 | 0.79 | 0.76 | 0.98 | 0.8 | 0.77 | |
| 2 | Coast of Norway | 13 | **$r^2$** | 0.2 | 0.11 | 0.13 | 0.22 | 0.35 | 0.31 | Rosell-Mele,1998; Conte et al., 2006 |
| | | | **2sdev** | 4.34 | 5.85 | 4.9 | 3.01 | 2.7 | 2.74 | |
| | | | **RMSD** | 3.15 | 3.76 | 3.54 | 3.09 | 3.74 | 3.52 | |
| | | | **SEM** | 0.49 | 0.45 | 0.45 | 0.42 | 3.78 | 0.38 | |
| 3 | Svalbard | 9 | **$r^2$** | 0 | 0 | 0 | 0 | 0 | 0 | Rosell-Mele, 1998 |
| | | | **2sdev** | 4.34 | 5.86 | 4.9 | 5.02 | 4.63 | 4.69 | |
| | | | **RMSD** | 3.14 | 3.76 | 3.55 | 6.18 | 7.31 | 6.93 | |
| | | | **SEM** | 0.49 | 0.45 | 0.45 | 0.84 | 0.77 | 0.78 | |
| | Svalbard | 6(3 outliers removed, with high residuals) | **$r^2$** | 0.37 | 0.27 | 0.33 | 0.5 | 0.86 | 0.81 | Rosell-Mele, 1998 |
| | | | **2sdev** | 2.89 | 2.64 | 2.68 | 2.48 | 2.41 | 2.39 | |
| | | | **RMSD** | 5.19 | 6.51 | 6.1 | 4.8 | 6.16 | 5.73 | |
| | | | **SEM** | 0.6 | 0.7 | 0.67 | 0.41 | 0.4 | 0.39 | |
| 4 | North of Iceland | 9 | **$r^2$** | 0.29 | 0.1 | 0.23 | 0.3 | 0 | 0.14 | Rosell-Mele, |

| | | | | | | | | | | |
|---|---|---|---|---|---|---|---|---|---|---|
| | | | **2sdev** | 5.02 | 2.92 | 2.5 | 5.2 | 2.83 | 4.39 | 1998;Rodrigo- |
| | | | **RMSD** | 3.14 | 5.13 | 4.4 | 3.2 | 5.12 | 2.47 | Gamiz et al., 2015 |
| | | | **SEM** | 0.84 | 0.49 | 0.42 | 0.86 | 0.47 | 0.41 | |
| | | | **$r^2$** | 0 | 0.15 | 0.12 | 0 | 0 | 0 | Conte et al., 2006; Marmen, 2000; Rodrigo-Gamiz et al., 2015; this study |
| 5 | South of Iceland | 12 | **2sdev** | 3.2 | 3.05 | 3.01 | 2.23 | 1.98 | 1.95 | |
| | | | **RMSD** | 2.2 | 2.3 | 2.23 | 1.61 | 1.7 | 1.65 | |
| | | | **SEM** | 0.46 | 0.44 | 0.44 | 0.33 | 0.29 | 0.28 | |
| | | | **$r^2$** | 0 | 0 | 0 | 0.18 | 0.13 | 0.1 | |
| 6 | Rockall Rise | 7 | **2sdev** | 5 | 5.05 | 5 | 4.25 | 4.3 | 4.26 | Conte et al., 2006; this study |
| | | | **RMSD** | 3.93 | 3.93 | 3.35 | 3.42 | 3.46 | 3.42 | |
| | | | **SEM** | 0.95 | 0.95 | 0.95 | 0.8 | 0.81 | 0.8 | |
| | | | **$r^2$** | 0.46 | 0.43 | 0.46 | 0.45 | 0.43 | 0.45 | |
| | Rockall Rise | 5(2 outliers removed) | **2sdev** | 2.01 | 2.16 | 2.01 | 2.07 | 2.14 | 2.08 | Conte et al., 2006; this study |
| | | | **RMSD** | 1.48 | 1.48 | 1.44 | 1.91 | 1.95 | 1.91 | |
| | | | **SEM** | 0.39 | 0.41 | 0.39 | 0.39 | 0.4 | 0.39 | |
| | | | **$r^2$** | - | - | - | - | - | - | |
| 7 | South of Greenland | 4 | **2sdev** | 5.14 | 1.47 | 1.3 | 4.5 | 3.47 | 2.63 | Conte et al., 2006; Marmen, 2000 |
| | | | **RMSD** | 2.87 | 4.28 | 3.59 | 3.16 | 5 | 4.24 | |
| | | | **SEM** | 1.29 | 0.37 | 0.33 | 1.23 | 0.86 | 0.66 | |
| | | | **$r^2$** | 0 | 0 | 0 | 0.17 | 0.17 | 0.17 | Conte et al., 2006; Marmen, 2000; this study |
| 8 | Reykjanes Ridge | 9 | **2sdev** | 7.25 | 4.81 | 5.38 | 6.34 | 4.08 | 4.57 | |
| | | | **RMSD** | 4.26 | 4.4 | 4.21 | 3.48 | 3.58 | 3.38 | |
| | | | **SEM** | 1.21 | 0.8 | 0.9 | 1.06 | 0.68 | 0.76 | |
| 9 | MAR | 8 | **$r^2$** | 0.82 | 0.77 | 0.82 | 0.64 | 0.58 | 0.64 | Conte et al., 2006; |

| | | | | | | | | | | |
|---|---|---|---|---|---|---|---|---|---|---|
| | | | **2sdev** | 1.76 | 1.83 | 1.76 | 1.79 | 1.92 | 1.79 | Marmen, 2000; this study |
| | | | **RMSD** | 1.61 | 1.61 | 1.62 | 1.26 | 1.28 | 1.26 | |
| | | | **SEM** | 0.31 | 0.32 | 0.31 | 0.32 | 0.34 | 0.32 | |
| 10 | Central Labrador | 3 | **$r^2$** | - | - | - | - | - | - | Marmen, 2000 |
| | | | **2sdev** | 4.82 | 6.63 | 5.37 | 4.79 | 4.08 | 2.94 | |
| | | | **RMSD** | 2.29 | 5.42 | 4.38 | 1.96 | 3.86 | 2.84 | |
| | | | **SEM** | 1.39 | 1.91 | 1.55 | 1.38 | 1.18 | 0.85 | |
| 11 | Western Labrador | 7 | **$r^2$** | 0.11 | 0.45 | 0.28 | 0.55 | 0.1 | 0.43 | this study |
| | | | **2sdev** | 12.24 | 7.01 | 6.79 | 1.68 | 8.17 | 6.83 | |
| | | | **RMSD** | 10.43 | 11.55 | 11.22 | 10.12 | 11.53 | 11.03 | |
| | | | **SEM** | 2.31 | 1.33 | 1.29 | 2.21 | 1.54 | 1.29 | |
| 12 | North East of Newfoundland | 22 | **$r^2$** | 0.19 | 0.24 | 0.24 | 0.18 | 0.3 | 0.26 | Marmen, 2000; this study |
| | | | **2sdev** | 8.91 | 7.03 | 7.13 | 9.46 | 7.23 | 7.47 | |
| | | | **RMSD** | 7.35 | 7.23 | 7.29 | 7.01 | 6.72 | 6.81 | |
| | | | **SEM** | 0.95 | 0.75 | 0.76 | 1 | 0.77 | 0.79 | |
| 13 | South of Newfoundland | 4 | **$r^2$** | - | - | - | - | - | - | Marmen, 2000; this study |
| | | | **2sdev** | 7.36 | 4.8 | 4.88 | 7.04 | 3.95 | 4.14 | |
| | | | **RMSD** | 4.15 | 2.42 | 2.61 | 4.76 | 2.82 | 3.09 | |
| | | | **SEM** | 1.84 | 1.2 | 1.22 | 1.76 | 0.99 | 1.04 | |
| 14 | Off the coast of Nova Scotia | 9 | **$r^2$** | 0.65 | 0.71 | 0.65 | 0.62 | 0.67 | 0.62 | this study |
| | | | **2sdev** | 5.3 | 4.93 | 5.3 | 5.53 | 5.25 | 5.54 | |
| | | | **RMSD** | 2.62 | 2.38 | 2.62 | 2.68 | 2.62 | 2.68 | |
| | | | **SEM** | 0.8 | 0.82 | 0.8 | 0.92 | 0.88 | 0.92 | |
| 15 | Azores Gibraltar Ridge | 7 | **$r^2$** | 0.67 | 0.67 | 0.67 | 0.37 | 0.37 | 0.37 | Conte et al., 2006 |
| | | | **2sdev** | 3.85 | 3.85 | 3.85 | 3.22 | 3.22 | 3.22 | |
| | | | **RMSD** | 2.11 | 2.11 | 2.11 | 2.08 | 2.08 | 2.08 | |

| | | | | | | | | | | |
|---|---|---|---|---|---|---|---|---|---|---|
| | | | **SEM** | 0.73 | 0.73 | 0.73 | 0.61 | 0.61 | 0.61 | |
| | | | **$r^2$** | - | - | - | - | - | - | |
| 16 | USA coast | 4 | **2sdev** | 5.16 | 5.16 | 5.16 | 3.63 | 3.63 | 3.63 | Conte et al., 2006 |
| | | | **RMSD** | 2.24 | 2.24 | 2.24 | 1.88 | 1.88 | 1.88 | |
| | | | **SEM** | 1.29 | 1.29 | 1.29 | 0.91 | 0.91 | 0.91 | |

**Table A3** Analysis of the data set by geographical regions

## CHAPTER 5

| Core Name | Latitude [N] | Longitude [W] | Depth [cm] | Age [kyr] | Area c34:4 | Area c37:3 | Area c37:2 | Total conc. [ng/g] | % tetra | UK37 | UK'37 | UK*37 | UK37-SST | UK'37-SST | UK*37-SST |
|---|---|---|---|---|---|---|---|---|---|---|---|---|---|---|---|
| | | | 15 | 1.10 | **n/a** | 7.7 | 10.2 | 2060 | 0 | 0.57 | 0.57 | 0.57 | 15.93 | 15.93 | 15.93 |
| | | | 69 | 2.71 | 5.2 | 37.6 | 23.3 | 4308 | 20 | 0.27 | 0.38 | 0.35 | 6.96 | 10.26 | 9.35 |
| | | | 125 | 4.16 | **n/a** | 18.4 | 12.6 | 4277 | 22 | 0.41 | 0.41 | 0.41 | 10.98 | 10.98 | 10.98 |
| | | | 189 | 5.69 | 5.9 | 25.6 | 20.2 | 8372 | 23 | 0.28 | 0.44 | 0.39 | 7.05 | 12.03 | 10.51 |
| | | | 239 | 6.57 | 7.8 | 37.1 | 28.9 | 5964 | 21 | 0.29 | 0.44 | 0.39 | 7.33 | 11.94 | 10.53 |
| | | | 299 | 7.70 | 17.1 | 27.6 | 20.2 | 4458 | 30 | 0.05 | 0.42 | 0.31 | 0.11 | 11.47 | 8.10 |
| | | | 319 | 8.09 | 8.5 | 9.7 | 6.6 | 5327 | 34 | -0.08 | 0.40 | 0.27 | -3.65 | 10.94 | 6.73 |
| | | | 335 | 8.40 | 7.8 | 24.9 | 21.0 | 6479 | 25 | 0.25 | 0.46 | 0.39 | 6.12 | 12.53 | 10.52 |
| **MD99-2227** | **58°55.26 N** | **048°22.38 W** | 341 | 8.51 | 21.4 | 48.4 | 35.9 | 5973 | 25 | 0.14 | 0.43 | 0.34 | 2.82 | 11.57 | 8.96 |
| | | | 345 | 8.59 | 18.4 | 30.3 | 22.5 | 5551 | 29 | 0.06 | 0.43 | 0.32 | 0.41 | 11.58 | 8.24 |
| | | | 399 | 9.49 | 15.7 | 41.6 | 34.4 | 5764 | 24 | 0.20 | 0.45 | 0.38 | 4.85 | 12.38 | 10.03 |
| | | | 449 | 10.30 | 10.6 | 22.5 | 17.8 | 4583 | 28 | 0.14 | 0.44 | 0.35 | 2.95 | 12.05 | 9.26 |

| | | | | | | | | | | | | | | |
|---|---|---|---|---|---|---|---|---|---|---|---|---|---|---|
| | | | 459 | 10.80 | 6.3 | 38.1 | 24.6 | 3590 | 21 | 0.27 | 0.39 | 0.36 | 6.70 | 10.56 | 9.47 |
| | | | 469 | 11.33 | 11.4 | 32.3 | 23.2 | 3489 | 25 | 0.18 | 0.42 | 0.35 | 4.01 | 11.33 | 9.18 |
| | | | 479 | 11.86 | 11.7 | 10 | 18.3 | 2476 | 35 | 0.17 | 0.65 | 0.46 | 3.67 | 18.26 | 12.53 |
| | | | 499 | 12.91 | 8.6 | 16 | 14.7 | 3800 | 29 | 0.16 | 0.48 | 0.37 | 3.37 | 13.18 | 10.00 |
| | | | 545 | 15.35 | 5.7 | 5.2 | 8.3 | 2315 | | | | **low** | **concentration** | | |
| | | | 559 | 16.09 | 10.5 | 17.9 | 16.4 | 2595 | 29 | 0.13 | 0.48 | 0.37 | 2.66 | 13.16 | 9.76 |
| | | | 569 | 16.62 | 31.9 | 40.4 | 35.2 | 3686 | 31 | 0.03 | 0.47 | 0.33 | -0.40 | 12.78 | 8.59 |
| | | | 619 | 19.27 | n/a | n/a | n/a | | | | | | | | |
| | | | 639 | 20.32 | n/a | n/a | n/a | | | | | | | | |
| | | | 1 | 0.10 | n/a | 11.5 | 12.2 | 1187 | 0 | 0.51 | 0.51 | 0.51 | 14.27 | 14.27 | 14.27 |
| | | | 14 | 1.40 | n/a | 26.2 | 18.2 | 1457 | 0 | 0.41 | 0.41 | 0.41 | 11.09 | 11.09 | 11.09 |
| | | | 29 | 3.85 | n/a | 22.9 | 15 | 1346 | 0 | 0.40 | 0.40 | 0.40 | 10.66 | 10.66 | 10.66 |
| | | | 45 | 6.08 | 14.3 | 39.1 | 33.8 | 1900 | 17 | 0.22 | 0.46 | 0.39 | 5.44 | 12.72 | 10.41 |
| | | | 67 | 8.54 | n/a | 32.4 | 24.4 | 1682 | 0 | 0.43 | 0.43 | 0.43 | 11.68 | 11.68 | 11.68 |
| | | | 69 | 8.61 | n/a | 18 | 15.3 | 1205 | 0 | 0.46 | 0.46 | 0.46 | 12.59 | 12.59 | 12.59 |
| | | | 74 | 8.77 | 6.7 | 40.1 | 34.2 | 2163 | 19 | 0.34 | 0.46 | 0.42 | 8.95 | 12.62 | 11.46 |
| | | | 79 | 8.93 | 8.5 | 44.8 | 35.9 | 1743 | 19 | 0.31 | 0.44 | 0.40 | 7.97 | 12.15 | 10.86 |
| | | | 84 | 9.09 | 13.8 | 41.6 | 34.5 | 1832 | 23 | 0.23 | 0.45 | 0.38 | 5.64 | 12.40 | 10.30 |
| **HU08-029-004** | **61°2749** | **58°0211** | 89 | 9.26 | 16.7 | 62.9 | 47.3 | 2212 | 20 | 0.24 | 0.43 | 0.37 | 5.97 | 11.67 | 9.96 |
| | | | 94 | 9.42 | 21.9 | 86.4 | 73.9 | 4189 | 17 | 0.29 | 0.46 | 0.41 | 7.32 | 12.64 | 10.96 |
| | | | 101 | 9.61 | 17.1 | 63.2 | 38.4 | 1400 | 21 | 0.18 | 0.38 | 0.32 | 4.10 | 10.12 | 8.47 |
| | | | 115 | 10.06 | 20.2 | 75.8 | 61.2 | 2786 | 19 | 0.26 | 0.45 | 0.39 | 6.57 | 12.20 | 10.46 |
| | | | 130 | 10.47 | 23.5 | 85.9 | 70.9 | 2975 | 18 | 0.26 | 0.45 | 0.39 | 6.63 | 12.37 | 10.58 |
| | | | 144 | 10.80 | 10.7 | 58.2 | 42.7 | 1903 | 18 | 0.29 | 0.42 | 0.38 | 7.36 | 11.49 | 10.26 |
| | | | 159 | 11.16 | n/a | n/a | n/a | | | | | | | | |
| | | | 174 | 11.51 | 14.4 | 28.9 | 22.5 | 1476 | 27 | 0.12 | 0.44 | 0.34 | 2.40 | 11.93 | 9.03 |

| | | | | | | | | | | | | |
|---|---|---|---|---|---|---|---|---|---|---|---|---|
| 189 | 11.87 | 22.5 | 29.1 | 5.7 | 3309 | 36 | -0.29 | 0.16 | 0.10 | -10.22 | 3.63 | 1.68 |
| 205 | 12.24 | 15.8 | 17.9 | 16 | 4143 | 33 | 0.00 | 0.47 | 0.32 | -1.21 | 12.97 | 8.42 |
| 219 | 12.54 | n/a | 7.8 | 5.3 | 1577 | 0 | 0.40 | 0.40 | 0.40 | 10.93 | 10.93 | 10.93 |
| 229 | 12.68 | 5.2 | 8.8 | n/a | 1624 | | | | **low concentration** | | | |
| 239 | 12.82 | 13.5 | 7.7 | 5.1 | 2609 | 39 | -0.32 | 0.40 | 0.19 | -11.01 | 10.74 | 4.54 |
| 242 | 12.86 | n/a | n/a | n/a | | | | | | | | |
| 250 | 12.94 | 9 | 8.4 | 5.3 | 3868 | 35 | -0.16 | 0.39 | 0.23 | -6.27 | 10.39 | 5.74 |
| 252 | 12.96 | n/a | n/a | n/a | | | | | | | | |
| 259 | 13.03 | 18.3 | 21.8 | 9.4 | 4176 | 35 | -0.18 | 0.30 | 0.19 | -6.78 | 7.80 | 4.42 |
| 267 | 13.11 | 16.3 | 18.7 | 9.9 | 4097 | 35 | -0.14 | 0.35 | 0.22 | -5.65 | 9.16 | 5.35 |
| 279 | 13.23 | 15.5 | 17.3 | 9.7 | 3841 | 35 | -0.14 | 0.36 | 0.23 | -5.47 | 9.55 | 5.58 |
| 289 | 13.33 | 22.7 | 29.7 | 14 | 5949 | 34 | -0.13 | 0.32 | 0.21 | -5.30 | 8.37 | 5.06 |
| 299 | 13.42 | 24.7 | 32.4 | 14.2 | 4731 | 34 | -0.15 | 0.30 | 0.20 | -5.80 | 7.90 | 4.70 |
| 309 | 13.52 | 32.1 | 30.3 | 17.6 | 4141 | 37 | -0.18 | 0.37 | 0.22 | -6.83 | 9.80 | 5.33 |
| 320 | 13.63 | 25.3 | 18.6 | 10.9 | 3664 | 39 | -0.26 | 0.37 | 0.20 | -9.30 | 9.86 | 4.69 |
| 330 | 13.73 | 16.5 | 12.2 | 7.5 | 3017 | 38 | -0.25 | 0.38 | 0.21 | -8.87 | 10.20 | 4.94 |
| 339 | 13.82 | 24.3 | 19.4 | 9.8 | 4830 | 39 | -0.27 | 0.34 | 0.18 | -9.55 | 8.84 | 4.22 |
| 349 | 13.91 | 28.8 | 27.6 | 16.1 | 4532 | 37 | -0.18 | 0.37 | 0.22 | -6.64 | 9.83 | 5.40 |
| 361 | 14.03 | 24.3 | 21.8 | 12.9 | 2859 | 37 | -0.19 | 0.37 | 0.22 | -7.19 | 9.93 | 5.29 |
| 369 | 14.11 | 21.1 | 22.8 | 11.7 | 2661 | 36 | -0.17 | 0.34 | 0.21 | -6.46 | 8.94 | 5.04 |
| 379 | 14.21 | 24.4 | 21 | 11.5 | 2615 | 38 | -0.23 | 0.35 | 0.20 | -8.20 | 9.39 | 4.79 |
| 401 | 14.46 | 17.8 | 8.9 | 7.8 | 3005 | 40 | -0.29 | 0.47 | 0.23 | -10.12 | 12.82 | 5.52 |
| 419 | 14.69 | 16.9 | 18.3 | 13.2 | 1949 | 33 | -0.08 | 0.42 | 0.27 | -3.65 | 11.37 | 6.93 |
| 439 | 14.94 | 17.7 | 18.9 | 15.4 | 2933 | 34 | -0.04 | 0.45 | 0.30 | -2.67 | 12.27 | 7.64 |
| 458 | 15.19 | 19.1 | 24.3 | 25.4 | 2846 | 34 | 0.09 | 0.51 | 0.37 | 1.44 | 14.15 | 9.85 |
| 499 | 15.81 | n/a | n/a | n/a | | | | | | | | |

| | | | | | | | | | | | | |
|---|---|---|---|---|---|---|---|---|---|---|---|---|
| 518 | 16.24 | n/a | 8.7 | n/a | 1264 | | | | **low concentration** | | | |
| 541 | 16.76 | n/a | n/a | n/a | | | | | | | | |
| 559 | 17.17 | 5 | 5.8 | 8.6 | 2071 | 32 | 0.19 | 0.60 | 0.44 | 4.29 | 16.76 | 12.10 |
| 579 | 17.62 | n/a | **8.9** | n/a | 779 | | | | | | | |
| 599 | 18.32 | n/a | 6.5 | 8.1 | 2273 | 0 | 0.55 | 0.55 | 0.55 | 15.48 | 15.48 | 15.48 |
| 619 | 19.48 | 7.3 | 6.6 | 6.8 | 4182 | 34 | -0.02 | 0.51 | 0.33 | -2.07 | 14.04 | 8.62 |
| 639 | 20.64 | 19.9 | 26.2 | 17 | 2345 | 32 | -0.05 | 0.39 | 0.27 | -2.73 | 10.59 | 6.83 |
| 660 | 21.86 | 5.8 | n/a | n/a | 991 | | | | **low concentration** | | | |
| 679 | 22.96 | 26.2 | 19.3 | 12 | 3067 | 39 | -0.25 | 0.38 | 0.21 | -8.82 | 10.28 | 4.99 |
| 699 | 24.12 | 17.5 | 9.9 | 6.8 | 2715 | 40 | -0.31 | 0.41 | 0.20 | -10.81 | 11.01 | 4.69 |
| 719 | 24.65 | n/a | n/a | n/a | | | | | | | | |
| 739 | 24.96 | n/a | n/a | n/a | | | | | | | | |
| 759 | 25.27 | n/a | n/a | 5.8 | 627 | | | | **low concentration** | | | |
| 778 | 26.54 | n/a | n/a | n/a | | | | | | | | |
| 800 | 28.41 | 23.2 | 15 | 13.4 | 2508 | 56 | -0.19 | 0.47 | 0.26 | -7.09 | 12.96 | 6.54 |
| 816 | 29.77 | n/a | n/a | n/a | 902 | | | | | | | |
| 1 | 0.04 | n/a | 32.6 | 20.5 | 3118 | 0 | 0.39 | 0.39 | 0.39 | 10.37 | 10.37 | 10.37 |
| 13 | 0.49 | 23.1 | 72.9 | 49.7 | 5432 | 21 | 0.18 | 0.41 | 0.34 | 4.20 | 10.95 | 9.00 |
| 32 | 1.21 | 12.7 | 62.1 | 36.8 | 5016 | 19 | 0.22 | 0.37 | 0.33 | 5.21 | 9.94 | 8.66 |
| 44 | 1.66 | n/a | 53 | 29.9 | 3309 | 0 | 0.36 | 0.36 | 0.36 | 9.60 | 9.60 | 9.60 |
| 54 | 2.04 | n/a | 30.3 | 24.2 | 2301 | 0 | 0.44 | 0.44 | 0.44 | 12.12 | 12.12 | 12.12 |
| 73 | 2.75 | n/a | 49.8 | 34.4 | 3524 | 0 | 0.41 | 0.41 | 0.41 | 11.05 | 11.05 | 11.05 |
| 91 | 3.43 | n/a | 64.5 | 50.3 | 3675 | 0 | 0.44 | 0.44 | 0.44 | 11.94 | 11.94 | 11.94 |
| 100 | 3.77 | n/a | 37.7 | 29 | 3323 | 0 | 0.43 | 0.43 | 0.43 | 11.84 | 11.84 | 11.84 |
| 110 | 4.39 | n/a | 38.9 | 30.6 | 2355 | 0 | 0.44 | 0.44 | 0.44 | 12.01 | 12.01 | 12.01 |
| 122 | 5.12 | 13.3 | 21.5 | 15.3 | 3344 | 30 | 0.04 | 0.42 | 0.31 | -0.12 | 11.27 | 7.92 |

| | | | | | | | | | | | | | | | |
|---|---|---|---|---|---|---|---|---|---|---|---|---|---|---|---|
| **HU84-030-021** | **58°22600** | **57°30.42** | 124 | 5.25 | 11.2 | 17.1 | 10.5 | 2138 | 32 | -0.02 | 0.38 | 0.27 | -1.88 | 10.19 | 6.87 |
| | | | 131 | 5.68 | 16.2 | 28 | 18.2 | 2272 | 30 | 0.03 | 0.39 | 0.29 | -0.36 | 10.60 | 7.51 |
| | | | 144 | 6.48 | 14.4 | 19.2 | 14.6 | 3996 | 32 | 0.00 | 0.43 | 0.30 | -1.21 | 11.76 | 7.85 |
| | | | 156 | 7.21 | 14.5 | 29.2 | 22.3 | 3846 | 27 | 0.12 | 0.43 | 0.34 | 2.25 | 11.79 | 8.91 |
| | | | 175 | 8.38 | 10.8 | 37.7 | 27.4 | 4940 | 23 | 0.22 | 0.42 | 0.36 | 5.29 | 11.42 | 9.61 |
| | | | 191 | 9.37 | 16.6 | 45.6 | 33.5 | 5379 | 24 | 0.18 | 0.42 | 0.35 | 4.02 | 11.50 | 9.27 |
| | | | 201 | 9.98 | 10.5 | 36.1 | 26.8 | 4656 | 23 | 0.22 | 0.43 | 0.37 | 5.40 | 11.58 | 9.73 |
| | | | 208 | 10.41 | 15.5 | 48.8 | 35.8 | 4701 | 22 | 0.20 | 0.42 | 0.36 | 4.81 | 11.49 | 9.50 |
| | | | 212 | 10.66 | 9.9 | 25.2 | 20.3 | 5097 | 26 | 0.19 | 0.45 | 0.37 | 4.36 | 12.19 | 9.77 |
| | | | 217 | 10.97 | 14 | 20 | 15.1 | 4373 | 31 | 0.02 | 0.43 | 0.31 | -0.65 | 11.70 | 7.99 |
| | | | 228 | 11.35 | 19.7 | 47.5 | 35.8 | 4245 | 24 | 0.16 | 0.43 | 0.35 | 3.40 | 11.69 | 9.20 |
| | | | 233 | 11.48 | 8.1 | 10.9 | 8.9 | 2922 | 32 | 0.03 | 0.45 | 0.32 | -0.46 | 12.29 | 8.33 |
| | | | 238 | 11.60 | n/a | n/a | n/a | | | | | | | | |
| | | | 247 | 11.83 | n/a | n/a | n/a | | | | | | | | |
| | | | 263 | 12.23 | n/a | n/a | n/a | | | | | | | | |
| | | | 279 | 12.64 | 6.6 | 7.2 | 0 | 1328 | | | | | | | |
| | | | 295 | 13.04 | 9 | 5.7 | 5.1 | 1565 | 36 | -0.20 | 0.47 | 0.26 | -7.30 | 12.98 | 6.47 |
| | | | 309 | 13.40 | 9.6 | 6.6 | 5.7 | 1902 | 36 | -0.18 | 0.46 | 0.26 | -6.73 | 12.71 | 6.55 |
| | | | 327 | 13.85 | 5 | n/a | n/a | 699 | | | | **low concentration** | | | |
| | | | 339 | 14.15 | n/a | n/a | n/a | 0 | | | | | | | |
| | | | 354 | 14.53 | 21.2 | 54.7 | 31.9 | 3108 | 25 | 0.10 | 0.37 | 0.30 | 1.67 | 9.83 | 7.63 |
| | | | 363 | 14.76 | 8.1 | 16.4 | 10.1 | 2923 | 30 | 0.06 | 0.38 | 0.29 | 0.42 | 10.22 | 7.51 |
| | | | 384 | 15.29 | 14 | 8.8 | 5.9 | 2306 | 38 | -0.28 | 0.40 | 0.21 | -9.89 | 10.83 | 4.90 |
| | | | 399 | 15.67 | n/a | n/a | n/a | | | | | | | | |
| | | | 409 | 15.92 | 5.2 | n/a | n/a | 1140 | | | | **low concentration** | | | |
| | | | 479 | 18.14 | 49.5 | 39.3 | 3.2 | 1767 | 46 | -0.50 | 0.08 | 0.03 | -16.58 | 0.95 | -0.28 |

| | | | | | | | | | | | | | | |
|---|---|---|---|---|---|---|---|---|---|---|---|---|---|---|
| | | | 550 | 20.77 | 9.5 | 20.8 | 13.3 | 519 | 29 | 0.09 | 0.39 | 0.31 | 1.31 | 10.49 | 7.91 |
| | | | 580 | 21.88 | 7.9 | 11.1 | 11.4 | 1377 | 31 | 0.12 | 0.51 | 0.38 | 2.16 | 14.02 | 10.03 |
| | | | 610 | 22.99 | 8.1 | 18.6 | 5.8 | 1113 | 30 | -0.07 | 0.24 | 0.18 | -3.48 | 5.87 | 4.07 |
| | | | 639 | 24.06 | 5.7 | 15 | 11.4 | 1083 | 28 | 0.18 | 0.43 | 0.36 | 4.05 | 11.75 | 9.43 |
| | | | 669 | 25.17 | 18.5 | 33.7 | 34.2 | 1529 | 26 | 0.18 | 0.50 | 0.40 | 4.17 | 13.93 | 10.66 |
| | | | 699 | 26.28 | n/a | 6.9 | n/a | 671 | | | | | | | |
| | | | 730 | 27.42 | n/a | 13.2 | 13.3 | 1253 | 0 | 0.50 | 0.50 | 0.50 | 13.88 | 13.88 | 13.88 |
| | | | 758 | 28.46 | 8.5 | 16.7 | 19.8 | 1146 | 27 | 0.25 | 0.54 | 0.44 | 6.28 | 15.11 | 12.00 |
| | | | 3 | 1.53 | 6.3 | 46 | 32.6 | 4642 | 18 | 0.31 | 0.41 | 0.38 | 8.05 | 11.24 | 10.30 |
| | | | 17 | 2.63 | n/a | 57.3 | 42.5 | 5405 | 0 | 0.43 | 0.43 | 0.43 | 11.57 | 11.57 | 11.57 |
| | | | 28 | 3.49 | 5.4 | 23.8 | 19.1 | 4988 | 24 | 0.28 | 0.45 | 0.40 | 7.26 | 12.16 | 10.65 |
| | | | 45 | 4.83 | n/a | 28.4 | 20.4 | 3925 | 0 | 0.42 | 0.42 | 0.42 | 11.33 | 11.33 | 11.33 |
| | | | 59 | 5.49 | n/a | 21.6 | 18 | 2720 | 0 | 0.45 | 0.45 | 0.45 | 12.44 | 12.44 | 12.44 |
| | | | 74 | 6.96 | n/a | 34.2 | 27.8 | 2575 | 0 | 0.45 | 0.45 | 0.45 | 12.25 | 12.25 | 12.25 |
| | | | 89 | 7.67 | n/a | 13.2 | 12 | 2716 | 0 | 0.48 | 0.48 | 0.48 | 13.10 | 13.10 | 13.10 |
| | | | 101 | 8.24 | n/a | 12 | 12.3 | 2502 | 0 | 0.51 | 0.51 | 0.51 | 14.01 | 14.01 | 14.01 |
| | | | 108 | 8.58 | 7.8 | 30.5 | 31.5 | 3811 | 22 | 0.34 | 0.51 | 0.45 | 8.96 | 14.06 | 12.34 |
| | | | 117 | 9.00 | 5.4 | 23.6 | 23.8 | 4738 | 23 | 0.35 | 0.50 | 0.45 | 9.23 | 13.88 | 12.33 |
| **HU91-045-94** | **50°12.26** | **45°41.14** | 121 | 9.19 | 8.2 | 39.5 | 35.9 | 3447 | 20 | 0.33 | 0.48 | 0.43 | 8.71 | 13.09 | 11.68 |
| | | | 126 | 9.57 | 7.2 | 23.3 | 20.5 | 1213 | 25 | 0.26 | 0.47 | 0.40 | 6.57 | 12.85 | 10.85 |
| | | | 129 | 9.68 | 14.4 | 32.2 | 35.1 | 7070 | 8 | 0.25 | 0.52 | 0.43 | 6.34 | 14.47 | 11.69 |
| | | | 135 | 9.91 | 6.6 | 38.5 | 37.3 | 2501 | 19 | 0.37 | 0.49 | 0.45 | 9.96 | 13.58 | 12.38 |
| | | | 140 | 10.10 | 8.3 | 50.8 | 46.9 | 2646 | 17 | 0.36 | 0.48 | 0.44 | 9.70 | 13.21 | 12.07 |
| | | | 155 | 11.17 | 5.8 | 38.7 | 37.3 | 2307 | 18 | 0.39 | 0.49 | 0.46 | 10.34 | 13.54 | 12.48 |
| | | | 171 | 12.38 | n/a | 7.8 | 7.9 | 1002 | | | | **low concentration** | | | |
| | | | 174 | 12.61 | n/a | n/a | n/a | | | | | | | | |

| | | | | | | | | | | | | |
|---|---|---|---|---|---|---|---|---|---|---|---|---|
| 182 | 13.21 | 11.1 | 15.8 | 20.6 | 1795 | 29 | 0.20 | 0.57 | 0.43 | 4.73 | 15.82 | 11.81 |
| 187 | 13.59 | n/a | n/a | n/a | | | | | | | | |
| 189 | 13.74 | n/a | 5.7 | 6.6 | 821 | | | | **low concentration** | | | |
| 194 | 14.34 | n/a | 5.1 | 6 | 1053 | | | | **low concentration** | | | |
| 199 | 14.53 | 5.7 | 13.3 | 17 | 1531 | 27 | 0.31 | 0.56 | 0.47 | 8.18 | 15.67 | 12.98 |
| 215 | 15.80 | n/a | n/a | n/a | | | | | | | | |
| 230 | 16.19 | n/a | n/a | n/a | | | | | | | | |
| 244 | 16.55 | n/a | n/a | n/a | | | | | | | | |
| 262 | 17.58 | n/a | 6.1 | n/a | 790 | | | | **low concentration** | | | |
| 276 | 17.94 | n/a | n/a | n/a | | | | | | | | |
| 294 | 20.17 | n/a | 6.4 | n/a | 486 | | | | **low concentration** | | | |
| 308 | 20.56 | 14.8 | 15.3 | 10.5 | 2130 | 35 | -0.11 | 0.41 | 0.26 | -4.54 | 11.00 | 6.50 |
| 324 | 21.01 | 11.8 | 20.8 | 13.5 | 1792 | 30 | 0.04 | 0.39 | 0.29 | -0.22 | 10.59 | 7.54 |
| 339 | 22.12 | 7.2 | 9.4 | 7.4 | 871 | 32 | 0.01 | 0.44 | 0.31 | -1.08 | 12.01 | 8.01 |
| 354 | 23.49 | 9.1 | 8.7 | 7.1 | 761 | 34 | -0.08 | 0.45 | 0.29 | -3.77 | 12.28 | 7.31 |
| 371 | 25.04 | n/a | n/a | n/a | | | | | | | | |
| 385 | 26.32 | n/a | n/a | n/a | | | | | | | | |
| 399 | 27.59 | 42.6 | 43.8 | 35.5 | 4931 | 34 | -0.06 | 0.45 | 0.29 | -3.10 | 12.23 | 7.49 |
| 414 | 28.96 | n/a | n/a | n/a | | | | | | | | |
| 429 | 30.33 | n/a | 6.8 | 9.2 | 1198 | | 0.58 | 0.58 | 0.58 | 16.09 | 16.09 | 16.09 |
| 445 | 31.79 | n/a | 10.5 | 11.9 | 1117 | | 0.53 | 0.53 | 0.53 | 14.77 | 14.77 | 14.77 |
| 454 | 32.61 | 5.1 | 10.1 | 11 | 1570 | 29 | 0.23 | 0.52 | 0.42 | 5.49 | 14.46 | 11.39 |

**Table A4** Core locations and names. Addionally peak areas are shown, total concentration of alkenones, and alkenone derived SST.

| Core Name | Latitude [N] | Longitude [W] | Depth [cm] | Interpolated Age [kyr] | εNd | External error 2 S.D. | Duplicate samples | External error 2 S.D. | TD εNd | External error 2 S.D. | TD Duplicate samples | External error 2 S.D. |
|---|---|---|---|---|---|---|---|---|---|---|---|---|
| | | | 1.5 | 0.75 | -9.13 | 0.45 | | | | | | |
| | | | 15 | 1.10 | -8.59 | 0.45 | -7.13 | 0.77 | -8.00 | 0.82 | -8.13 | 0.82 |
| | | | 46 | 1.92 | -8.75 | 0.45 | | | | | | |
| | | | 69 | 2.71 | -8.30 | 0.45 | -8.51 | 0.77 | | | | |
| | | | 125 | 4.16 | -8.68 | 0.45 | -9.09 | 0.77 | | | | |
| | | | 156 | 4.85 | -8.57 | 0.45 | | | | | | |
| | | | 189 | 5.69 | -8.76 | 0.45 | -10.30 | 0.77 | | | | |
| | | | 224 | 6.35 | -9.44 | 0.45 | | | | | | |
| | | | 239 | 6.57 | -9.87 | 0.45 | -11.27 | 0.77 | -9.32 | 0.82 | | |
| | | | 285 | 7.43 | -11.32 | 0.45 | | | | | | |
| | | | 299 | 7.70 | -11.91 | 0.36 | | | | | | |
| | | | 319 | 8.09 | -10.76 | 0.45 | -10.28 | 0.77 | -12.64 | 0.82 | -12.78 | 0.82 |
| | | | 335 | 8.40 | -10.58 | 0.36 | | | | | | |
| **MD99-2227, 3460 m** | **58°55.26** | **048°22.38** | 345 | 8.59 | -12.58 | 0.36 | | | | | | |
| | | | 355 | 8.77 | -12.36 | 0.40 | | | | | | |
| | | | 375 | 9.10 | -11.31 | 0.36 | | | | | | |
| | | | 399 | 9.49 | -11.11 | 0.45 | -11.47 | 0.77 | | | | |
| | | | 419 | 9.83 | -13.30 | 0.36 | | | | | | |
| | | | 449 | 10.30 | -10.97 | 0.45 | -11.07 | 0.77 | -16.98 | 0.82 | | |

| | | | | | | | | | |
|---|---|---|---|---|---|---|---|---|---|
| | 459 | 10.80 | -9.88 | 0.36 | | | | | |
| | 479 | 11.86 | -9.91 | 0.36 | | | | | |
| | 515 | 13.79 | -12.64 | 0.45 | | | | | |
| | 525 | 14.29 | -14.01 | 0.36 | | | | | |
| | 535 | 14.82 | -14.44 | 0.36 | | | | | |
| | 545 | 15.35 | -17.93 | 0.45 | -17.62 | 0.77 | -12.77 | 0.82 | -17.50 | 0.82 |
| | 559 | 16.09 | -17.64 | 0.36 | | | | | |
| | 585 | 17.55 | -14.05 | 0.30 | | | -15.24 | 0.82 | | |
| | 612 | 18.92 | -12.61 | 0.30 | | | -17.67 | 0.82 | | |
| | 619 | 19.27 | -13.94 | 0.45 | -14.62 | 0.77 | | | | |
| | 639 | 20.32 | -14.38 | 0.45 | | | | | | |
| | 1 | 0.10 | -13.96 | 0.21 | | | -18.73 | 0.29 | | |
| | 29 | 3.85 | -14.52 | 0.21 | | | | | | |
| | 67 | 8.54 | -18.07 | 0.21 | | | | | | |
| | 74 | 8.77 | -18.45 | 0.15 | | | | | | |
| | 84 | 9.09 | -16.25 | 0.21 | | | -20.11 | 0.29 | -20.42 | 0.29 |
| | 94 | 9.42 | -14.69 | 0.21 | | | | | | |
| | 115 | 10.06 | -17.51 | 0.21 | | | | | | |
| | 144 | 10.80 | -15.43 | 0.21 | | | | | | |
| | 174 | 11.51 | -12.36 | 0.21 | | | | | | |
| | 205 | 12.24 | -11.21 | 0.21 | | | -12.85 | 0.29 | | |
| | 229 | 12.68 | -14.85 | 0.21 | | | | | | |
| **HU08-029-004, 2674 m** | 250 | 12.94 | -14.55 | 0.21 | | | | | | |

| | | | | | | | | | | |
|---|---|---|---|---|---|---|---|---|---|---|
| **61°2749** | **58°0211** | 299 | 13.42 | -12.38 | 0.21 | | | -15.62 | 0.31 | |
| | | 320 | 13.63 | -13.73 | 0.15 | | | | | |
| | | 339 | 13.82 | -13.97 | 0.21 | | | -15.23 | 0.29 | |
| | | 361 | 14.03 | -15.48 | 0.21 | | | | | |
| | | 379 | 14.21 | -13.54 | 0.21 | | | | | |
| | | 419 | 14.69 | -14.44 | 0.21 | | | | | |
| | | 458 | 15.19 | -14.88 | 0.32 | | | | | |
| | | 499 | 15.81 | -19.87 | 0.32 | -19.77 | 0.21 | -19.74 | 0.29 | |
| | | 541 | 16.76 | -27.02 | 0.21 | | | -22.92 | 0.29 | |
| | | 579 | 17.62 | -27.17 | 0.15 | | | | | |
| | | 619 | 19.48 | -18.37 | 0.21 | | | -20.96 | 0.29 | -20.57 | 0.31 |
| | | 699 | 24.12 | -13.45 | 0.21 | | | -19.84 | 0.31 | |
| | | 739 | 24.96 | -29.24 | 0.21 | -29.66 | 0.21 | -26.82 | 0.29 | |
| | | 778 | 26.54 | -16.26 | 0.15 | | | | | |
| | | 800 | 28.41 | -16.45 | 0.32 | | | | | |
| | | 816 | 29.77 | -18.72 | 0.21 | | | -22.40 | 0.29 | |
| | | 1 | 0.04 | -14.24 | 0.32 | 0.00 | 0.00 | -19.26 | 0.29 | 0.00 | 0.00 |
| | | 54 | 2.04 | -14.24 | 0.36 | 0.00 | 0.00 | 0.00 | 0.00 | 0.00 | 0.00 |
| | | 91 | 3.43 | -16.40 | 0.32 | 0.00 | 0.00 | -19.57 | 0.42 | 0.00 | 0.00 |
| | | 110 | 4.39 | -20.93 | 0.32 | -20.67 | 0.34 | 0.00 | 0.00 | 0.00 | 0.00 |
| | | 124 | 5.25 | -25.15 | 0.15 | 0.00 | 0.00 | 0.00 | 0.00 | 0.00 | 0.00 |
| | | 144 | 6.48 | -24.98 | 0.32 | 0.00 | 0.00 | -23.76 | 0.42 | -23.95 | 0.42 |
| | | 175 | 8.38 | -20.87 | 0.36 | 0.00 | 0.00 | 0.00 | 0.00 | 0.00 | 0.00 |

| | | | | | | | | | | | | |
|---|---|---|---|---|---|---|---|---|---|---|---|---|
| **HU84-030-021, 2853 m** | **58°22600** | **57°30.42** | 201 | 9.98 | -20.34 | 0.32 | 0.00 | 0.00 | 0.00 | 0.00 | 0.00 | 0.00 |
| | | | 212 | 10.66 | -21.13 | 0.32 | -21.24 | 0.32 | 0.00 | 0.00 | 0.00 | 0.00 |
| | | | 228 | 11.35 | -23.75 | 0.42 | -23.55 | 0.34 | 0.00 | 0.00 | 0.00 | 0.00 |
| | | | 238 | 11.60 | -27.11 | 0.32 | -27.63 | 0.34 | 0.00 | 0.00 | 0.00 | 0.00 |
| | | | 247 | 11.83 | -26.12 | 0.32 | -26.79 | 0.32 | 0.00 | 0.00 | 0.00 | 0.00 |
| | | | 263 | 12.23 | -27.52 | 0.34 | 0.00 | 0.00 | -26.73 | 0.42 | 0.00 | 0.00 |
| | | | 327 | 13.85 | -28.61 | 0.34 | 0.00 | 0.00 | -25.79 | 0.42 | 0.00 | 0.00 |
| | | | 354 | 14.53 | -24.75 | 0.34 | 0.00 | 0.00 | 0.00 | 0.00 | 0.00 | 0.00 |
| | | | 384 | 15.29 | -29.30 | 0.32 | 0.00 | 0.00 | -26.49 | 0.42 | 0.00 | 0.00 |
| | | | 395 | 15.56 | -26.21 | 0.32 | 0.00 | 0.00 | 0.00 | 0.00 | 0.00 | 0.00 |
| | | | 409 | 15.92 | -29.49 | 0.15 | 0.00 | 0.00 | 0.00 | 0.00 | 0.00 | 0.00 |
| | | | 479 | 18.14 | -30.55 | 0.32 | 0.00 | 0.00 | -28.79 | 0.29 | -28.98 | 0.29 |
| | | | 519 | 19.62 | -29.81 | 0.34 | 0.00 | 0.00 | -27.17 | 0.42 | 0.00 | 0.00 |
| | | | 549 | 20.73 | 0.00 | 0.00 | 0.00 | 0.00 | -27.07 | 0.29 | 0.00 | 0.00 |
| | | | 609 | 22.95 | -29.81 | 0.34 | 0.00 | 0.00 | -27.52 | 0.42 | 0.00 | 0.00 |
| | | | 669 | 25.17 | -28.67 | 0.34 | 0.00 | 0.00 | 0.00 | 0.00 | 0.00 | 0.00 |
| | | | 729 | 27.39 | -26.88 | 0.32 | 0.00 | 0.00 | -24.11 | 0.42 | 0.00 | 0.00 |
| | | | 758 | 28.46 | -28.90 | 0.34 | 0.00 | 0.00 | -27.43 | 0.29 | 0.00 | 0.00 |
| | | | 3 | 1.53 | -15.15 | 0.29 | | | -20.86 | 0.29 | | |
| | | | 28 | 3.49 | -11.33 | 0.15 | | | | | | |
| | | | 59 | 5.49 | -16.52 | 0.42 | | | -20.49 | 0.31 | -19.93 | 0.31 |
| | | | 89 | 7.67 | -20.21 | 0.15 | | | -21.97 | 0.31 | | |
| | | | 108 | 8.58 | -21.14 | 0.42 | -20.21 | 0.29 | -21.14 | 0.31 | | |

| | | | | | | | | | | | | |
|---|---|---|---|---|---|---|---|---|---|---|---|---|
| | | | 121 | 9.19 | -22.45 | 0.42 | -22.39 | 0.42 | -22.97 | 0.31 | | |
| | | | 129 | 9.68 | -21.96 | 0.42 | | | | | | |
| | | | 140 | 10.10 | -21.65 | 0.32 | | | | | | |
| **HU91-045-94, 3448 m** | **50°12.26** | **45°41.14** | 171 | 12.38 | -21.12 | 0.42 | | | -22.09 | 0.31 | | |
| | | | 182 | 13.21 | -18.82 | 0.32 | | | | | | |
| | | | 189 | 13.74 | -18.85 | 0.42 | | | | | | |
| | | | 199 | 14.53 | -18.75 | 0.42 | | | -20.16 | 0.29 | | |
| | | | 230 | 16.19 | -20.63 | 0.29 | | | -23.65 | 0.31 | | |
| | | | 262 | 17.58 | -17.54 | 0.29 | | | | | | |
| | | | 276 | 17.94 | -13.70 | 0.42 | | | | | | |
| | | | 294 | 20.17 | -17.55 | 0.29 | | | -17.14 | 0.31 | | |
| | | | 308 | 20.56 | -14.69 | 0.15 | -14.62 | 0.15 | | | | |
| | | | 339 | 22.12 | -17.30 | 0.42 | | | 18.00 | 0.31 | | |
| | | | 371 | 25.04 | -24.32 | 0.42 | | | | | | |
| | | | 399 | 27.59 | -15.77 | 0.42 | -15.18 | 0.31 | -15.34 | 0.31 | -15.19 | 0.31 |
| | | | 429 | 30.33 | -16.74 | 0.15 | -16.41 | 0.32 | -17.84 | 0.31 | | |
| | | | 454 | 32.61 | -18.67 | 0.42 | | | -20.68 | 0.31 | | |

**Table A5** Neodymium isotope composition from four sediment cores. Data shown for ferromanganese coatings of authigenic fraction, detrital fraction.

| Core Name | Latitude [N] | Longitude [W] | Depth [cm] | Interpolated Age [kyr] | εHf | External error 2 S.D. | Duplicate | External error 2 S.D. | TD εHf | External error 2 S.D. | TD Duplicate | External error 2 S.D. |
|---|---|---|---|---|---|---|---|---|---|---|---|---|
| | | | 1.5 | 0.75 | 9.62 | 0.60 | | | | | | |
| | | | 15 | 1.10 | 9.98 | 0.60 | | | -7.38 | 0.43 | -6.94 | 0.43 |
| | | | 46 | 1.92 | 10.70 | 0.20 | | | | | | |
| | | | 69 | 2.71 | 9.41 | 0.60 | | | | | | |
| | | | 125 | 4.16 | 8.65 | 0.60 | | | | | | |
| | | | 156 | 4.85 | 9.54 | 0.20 | 9.53 | 0.60 | | | | |
| | | | 189 | 5.69 | 9.17 | 0.60 | | | | | | |
| | | | 224 | 6.35 | 9.48 | 0.20 | 9.12 | 0.20 | | | | |
| | | | 239 | 6.57 | 8.90 | 0.60 | | | -6.32 | 0.43 | | |
| | | | 285 | 7.43 | 8.91 | 0.20 | 8.96 | 0.20 | | | | |
| | | | 299 | 7.70 | 7.82 | 0.43 | | | | | | |
| | | | 319 | 8.09 | 9.13 | 0.60 | | | -3.46 | 0.43 | | |
| | | | 335 | 8.40 | 7.82 | 0.40 | | | | | | |
| **MD99-2227, 3460 m** | **58°55.26** | **048°22.38** | 345 | 8.59 | 7.90 | 0.43 | | | | | | |
| | | | 355 | 8.77 | 7.71 | 0.40 | | | | | | |
| | | | 375 | 9.10 | 8.57 | 0.43 | | | | | | |
| | | | 399 | 9.49 | 8.99 | 0.60 | | | | | | |
| | | | 419 | 9.83 | 8.16 | 0.40 | 7.56 | 0.43 | | | | |
| | | | 449 | 10.30 | 9.17 | 0.60 | | | -15.49 | 0.43 | | |

| | | | | | | | | | |
|---|---|---|---|---|---|---|---|---|---|
| | | | 459 | 10.80 | 9.24 | 0.40 | | | |
| | | | 479 | 11.86 | 8.61 | 0.40 | | | |
| | | | 515 | 13.79 | 4.84 | 0.43 | | | |
| | | | 525 | 14.29 | 7.37 | 0.20 | 7.72 | 0.20 | |
| | | | 535 | 14.82 | 6.38 | 0.40 | | | |
| | | | 545 | 15.35 | 5.10 | 0.40 | | | |
| | | | 559 | 16.09 | 3.45 | 0.60 | | -16.28 | 0.43 |
| | | | 585 | 17.55 | 2.10 | 0.43 | | | |
| | | | 612 | 18.92 | 6.05 | 0.20 | | -17.46 | 0.43 |
| | | | 619 | 19.27 | 8.74 | 0.50 | | -25.91 | 0.43 |
| | | | 639 | 20.32 | 6.97 | 0.60 | | | |
| | | | 1 | 0.10 | 7.70 | 0.27 | | -17.10 | 0.41 |
| | | | 29 | 3.85 | | | | | |
| | | | 67 | 8.54 | 5.25 | 0.27 | | | |
| | | | 74 | 8.77 | 5.49 | 0.27 | | | |
| | | | 84 | 9.09 | | | | | |
| | | | 94 | 9.42 | | | | | |
| | | | 115 | 10.06 | | | | | |
| | | | 144 | 10.80 | 9.55 | 0.71 | -14.87 | 0.41 | |
| | | | 174 | 11.51 | 8.50 | 0.36 | | | |
| **HU08-029-004, 2674 m** | **61°2749** | **58°0211** | 205 | 12.24 | 8.14 | 0.71 | | -21.58 | 0.41 |
| | | | 229 | 12.68 | 6.50 | 0.36 | | | |
| | | | 250 | 12.94 | 5.68 | 0.36 | | | |

| | | | | | | | | | |
|---|---|---|---|---|---|---|---|---|---|
| 299 | 13.42 | 6.87 | 0.36 | | | -39.64 | 0.41 | | |
| 320 | 13.63 | 6.21 | 0.36 | | | | | | |
| 339 | 13.82 | 6.01 | 0.43 | | | -14.14 | 0.41 | | |
| 361 | 14.03 | 5.39 | 0.40 | | | | | | |
| 379 | 14.21 | 6.00 | 0.71 | | | | | | |
| 419 | 14.69 | 6.57 | 0.40 | | | -15.58 | 0.36 | | |
| 458 | 15.19 | 6.56 | 0.71 | | | | | | |
| 499 | 15.81 | -0.60 | 0.71 | 0.79 | 0.36 | -29.77 | 0.36 | | |
| 541 | 16.76 | | | | | -27.53 | 0.41 | | |
| 579 | 17.62 | | | | | | | | |
| 619 | 19.48 | 4.27 | 0.71 | | | -16.85 | 0.41 | -17.76 | 0.27 |
| 699 | 24.12 | 5.14 | 0.36 | | | -22.24 | 0.41 | | |
| 739 | 24.96 | | | | | -30.51 | 0.41 | | |
| 778 | 26.54 | 8.28 | 0.27 | | | | | | |
| 800 | 28.41 | 10.66 | 0.36 | | | | | | |
| 816 | 29.77 | 10.31 | 0.27 | | | -15.49 | 0.41 | | |
| 1 | 0.04 | 5.25 | 0.27 | | | -24.25 | 0.37 | | |
| 54 | 2.04 | | | | | | | | |
| 91 | 3.43 | | | | | -27.54 | | | |
| 110 | 4.39 | 0.64 | 0.27 | | | | | | |
| 124 | 5.25 | -7.53 | 0.27 | | | | | | |
| 144 | 6.48 | | | | | -26.94 | | -27.15 | 0.41 |
| 175 | 8.38 | 1.40 | 0.27 | | | | | | |

| | | | | | | | | | | | | |
|---|---|---|---|---|---|---|---|---|---|---|---|---|
| **HU84-030-021, 2853 m** | **58°22600** | **57°30.42** | 201 | 9.98 | 2.34 | 0.27 | | | | | | |
| | | | 212 | 10.66 | 0.15 | 0.27 | 0.67 | 0.27 | | | | |
| | | | 228 | 11.35 | | | | | -29.90 | | | |
| | | | 238 | 11.60 | | | | | | | | |
| | | | 247 | 11.83 | | | | | | | | |
| | | | 263 | 12.23 | -14.50 | 0.27 | | | | | | |
| | | | 327 | 13.85 | -20.97 | 0.27 | | | -40.22 | | -41.36 | 0.41 |
| | | | 354 | 14.53 | -13.50 | 0.43 | | | | | | |
| | | | 384 | 15.29 | -21.04 | 0.43 | | | -34.22 | | | |
| | | | 395 | 15.56 | | | | | | | | |
| | | | 409 | 15.92 | -25.22 | 0.43 | | | -35.14 | | | |
| | | | 479 | 18.14 | | | | | | | | |
| | | | 519 | 19.62 | -24.27 | 0.27 | | | | | | |
| | | | 549 | 20.73 | | | | | -35.19 | | -37.52 | 0.41 |
| | | | 609 | 22.95 | -25.95 | 0.43 | | | -37.30 | | | |
| | | | 669 | 25.17 | -25.06 | 0.27 | | | -36.34 | | | |
| | | | 729 | 27.39 | -24.97 | 0.27 | | | -36.84 | | | |
| | | | 758 | 28.46 | -25.72 | 0.27 | | | | | | |
| | | | 3 | 1.53 | 0.00 | 0.00 | | | -21.84 | 0.41 | | |
| | | | 28 | 3.49 | 0.00 | 0.00 | | | | | | |
| | | | 59 | 5.49 | 0.00 | 0.00 | | | -23.39 | 0.41 | -21.42 | 0.36 |
| | | | 89 | 7.67 | -4.31 | 0.36 | | | -22.42 | 0.41 | -25.07 | 0.41 |
| | | | 108 | 8.58 | 0.78 | 0.27 | | | -24.62 | 0.41 | | |

| | | | | | | | | | | | | |
|---|---|---|---|---|---|---|---|---|---|---|---|---|
| | | | 121 | 9.19 | 0.00 | 0.00 | | | -26.03 | 0.36 | | |
| | | | 129 | 9.68 | -0.13 | 0.27 | | | | | | |
| | | | 140 | 10.10 | 0.00 | 0.00 | | | | | | |
| | | | 171 | 12.38 | -29.74 | 0.36 | | | 1.91 | 0.27 | | |
| **HU91-045-94, 3448 m** | **50°12.26** | **45°41.14** | 182 | 13.21 | 0.00 | 0.00 | | | | | | |
| | | | 189 | 13.74 | -2.50 | 0.41 | | | | | | |
| | | | 199 | 14.53 | -0.14 | 0.27 | | | -22.00 | 0.36 | | |
| | | | 230 | 16.19 | -34.76 | 0.36 | | | -13.25 | 0.27 | | |
| | | | 262 | 17.58 | -5.00 | 0.36 | | | | | | |
| | | | 276 | 17.94 | 6.78 | 0.41 | | | | | | |
| | | | 294 | 20.17 | 0.00 | 0.00 | | | -10.83 | 0.41 | | |
| | | | 308 | 20.56 | -3.89 | 0.43 | -4.38 | 0.27 | | | | |
| | | | 339 | 22.12 | -2.91 | 0.37 | -4.13 | 0.37 | | | | |
| | | | 371 | 25.04 | -13.72 | 0.27 | | | | | | |
| | | | 399 | 27.59 | -6.37 | 0.36 | | | -13.89 | 0.36 | -15.26 | 0.36 |
| | | | 429 | 30.33 | 0.61 | 0.43 | | | -17.44 | 0.41 | -15.30 | 0.36 |
| | | | 454 | 32.61 | 0.32 | 0.37 | | | -19.91 | 0.36 | | |

**Table A6** Hafnium isotope composition from four sediment cores. Data shown for ferromanganese coatings of authigenic fraction, detrital fraction

| Core Name | Latitude [N] | Longitude [W] | Depth [cm] | Interpolated Age [kyr] | 208/207Pb | 207/204Pb | 206/204Pb | 208/204Pb | 207/206Pb | TD 208/207Pb | TD 207/204Pb | 2 |
|---|---|---|---|---|---|---|---|---|---|---|---|---|
| | | | 46 | 1.92 | 39.25 | 15.64 | 19.08 | 2.06 | 0.82 | | | |
| | | | 69 | 2.71 | 39.36 | 15.66 | 19.15 | 2.06 | 0.82 | | | |
| | | | 125 | 4.16 | 39.43 | 15.66 | 19.19 | 2.05 | 0.82 | | | |
| | | | 156 | 4.85 | 39.40 | 15.66 | 19.18 | 2.05 | 0.82 | | | |
| | | | 189 | 5.69 | 39.45 | 15.66 | 19.21 | 2.05 | 0.82 | | | |
| | | | 224 | 6.35 | 39.57 | 15.67 | 19.27 | 2.05 | 0.81 | | | |
| | | | 239 | 6.57 | 39.61 | 15.67 | 19.28 | 2.05 | 0.81 | 38.75 | 15.47 | |
| MD99-2227, 3460 m | 58°55.26 | 048°22.38 | 285 | 7.43 | 39.83 | 15.66 | 19.34 | 2.06 | 0.81 | | | |
| | | | 319 | 7.70 | 40.13 | 15.62 | 19.16 | 2.09 | 0.82 | 38.74 | 15.41 | |
| | | | 399 | 9.49 | 39.83 | 15.66 | 19.45 | 2.05 | 0.81 | | | |
| | | | 449 | 10.30 | 39.78 | 15.66 | 19.44 | 2.05 | 0.81 | 38.38 | 15.59 | |
| | | | 515 | 13.79 | 39.89 | 15.67 | 19.56 | 2.04 | 0.80 | | | |
| | | | 545 | 15.35 | 40.31 | 15.70 | 19.83 | 2.03 | 0.79 | 37.86 | 15.55 | |
| | | | 619 | 19.27 | 39.78 | 15.64 | 19.38 | 2.05 | 0.81 | | | |
| | | | 639 | 20.32 | 39.84 | 15.62 | 19.32 | 2.06 | 0.81 | | | |
| | | | 1 | 0.10 | 39.33 | 15.64 | 19.07 | 2.06 | 0.82 | | | |
| | | | 29 | 3.85 | 39.98 | 15.66 | 19.56 | 2.04 | 0.80 | | | |
| | | | 67 | 8.54 | 40.25 | 15.67 | 19.70 | 2.04 | 0.80 | | | |
| | | | 74 | 8.77 | 40.56 | 15.68 | 19.94 | 2.03 | 0.79 | | | |
| | | | 84 | 9.09 | 40.24 | 15.67 | 19.73 | 2.04 | 0.79 | | | |
| | | | 94 | 9.42 | 40.62 | 15.69 | 20.05 | 2.03 | 0.78 | | | |
| | | | 115 | 10.06 | 40.56 | 15.69 | 20.14 | 2.01 | 0.78 | | | |
| | | | 144 | 10.80 | 40.42 | 15.69 | 20.18 | 2.00 | 0.78 | 36.40 | 14.95 | |
| | | | 174 | 11.51 | 40.38 | 15.71 | 20.01 | 2.02 | 0.78 | 37.66 | 15.29 | |
| | | | 205 | 12.24 | 39.96 | 15.67 | 19.65 | 2.03 | 0.80 | | | |

| | | | | | | | | | | | |
|---|---|---|---|---|---|---|---|---|---|---|---|
| | | | 229 | 12.68 | 40.42 | 15.64 | 19.84 | 2.04 | 0.79 | | |
| | | | 250 | 12.94 | 40.47 | 15.69 | 20.02 | 2.02 | 0.78 | | |
| HU08-029-004, 2674 m | 61°274 N | 58°0211 | 279 | 13.23 | 40.12 | 15.65 | 19.79 | 2.03 | 0.79 | | |
| | | | 299 | 13.42 | 40.01 | 15.66 | 19.71 | 2.03 | 0.79 | 37.19 | 15.15 |
| | | | 320 | 13.63 | 40.07 | 15.66 | 19.78 | 2.03 | 0.79 | | |
| | | | 339 | 13.82 | 40.08 | 15.67 | 19.81 | 2.02 | 0.79 | 37.36 | 15.21 |
| | | | 361 | 14.03 | 40.29 | 15.69 | 19.95 | 2.02 | 0.79 | | |
| | | | 419 | 14.69 | 40.06 | 15.68 | 19.90 | 2.01 | 0.79 | 37.93 | 15.12 |
| | | | 458 | 15.19 | 40.22 | 15.70 | 20.06 | 2.01 | 0.78 | | |
| | | | 499 | 15.81 | 40.59 | 15.73 | 20.11 | 2.02 | 0.78 | 38.00 | 15.38 |
| | | | 541 | 16.76 | 41.61 | 15.82 | 20.81 | 2.00 | 0.76 | 38.67 | 15.44 |
| | | | 579 | 17.62 | 41.98 | 15.88 | 21.22 | 1.98 | 0.75 | | |
| | | | 619 | 19.48 | 40.44 | 15.62 | 19.55 | 2.07 | 0.80 | 37.14 | 15.08 |
| | | | 699 | 24.12 | 40.38 | 15.66 | 19.97 | 2.02 | 0.78 | 37.13 | 15.04 |
| | | | 739 | 24.96 | 42.53 | 15.91 | 21.33 | 1.99 | 0.75 | 38.54 | 15.39 |
| | | | 778 | 26.54 | 40.14 | 15.72 | 20.32 | 1.98 | 0.77 | 38.60 | 15.36 |
| | | | 800 | 28.41 | 40.94 | 15.60 | 19.62 | 2.09 | 0.79 | | |
| | | | 816 | 29.77 | 40.79 | 15.58 | 19.52 | 2.09 | 0.80 | 37.09 | 15.09 |
| | | | 1 | 0.04 | 39.33 | 15.67 | 19.38 | 2.05 | 0.81 | 37.92 | 15.33 |
| | | | 32 | 1.21 | 39.98 | 15.67 | 19.47 | 2.05 | 0.80 | | |
| | | | 54 | 2.04 | 40.25 | 15.67 | 19.52 | 2.05 | 0.80 | | |
| | | | 91 | 3.43 | 40.56 | 15.70 | 19.73 | 2.04 | 0.80 | 37.82 | 15.28 |
| | | | 110 | 4.39 | 40.24 | 15.75 | 20.30 | 2.02 | 0.78 | | |
| | | | 124 | 5.25 | 40.62 | 15.83 | 20.84 | 2.01 | 0.76 | | |
| | | | 144 | 6.48 | 40.56 | 15.82 | 20.74 | 2.01 | 0.76 | 38.54 | 15.37 |
| HU84-030-021, 2853 m | 58°22600 | 57°30.42 | 175 | 8.38 | 40.42 | 15.72 | 20.30 | 2.02 | 0.77 | | |
| | | | 201 | 9.98 | 40.38 | 15.65 | 19.69 | 2.04 | 0.80 | | |
| | | | 212 | 10.66 | 39.96 | 15.74 | 20.46 | 2.02 | 0.77 | | |
| | | | 228 | 11.35 | 40.42 | 15.78 | 20.69 | 2.01 | 0.76 | 37.63 | 15.25 |
| | | | 238 | 11.60 | 40.47 | 15.84 | 21.15 | 2.01 | 0.75 | | |

| | | | | | | | | | | |
|---|---|---|---|---|---|---|---|---|---|---|
| | | | 247 | 11.83 | 40.12 | 15.81 | 20.66 | 2.01 | 0.77 | | |
| | | | 263 | 12.23 | 40.01 | 15.73 | 20.50 | 2.06 | 0.77 | 36.73 | 15.20 |
| | | | 295 | 13.04 | 40.07 | 15.73 | 20.75 | 2.02 | 0.76 | | |
| | | | 327 | 13.85 | 40.08 | 15.77 | 20.66 | 2.03 | 0.76 | 36.30 | 15.11 |
| | | | 354 | 14.53 | 40.29 | 15.74 | 20.82 | 2.00 | 0.76 | | |
| | | | 384 | 15.29 | 40.06 | 15.81 | 20.95 | 2.01 | 0.75 | 37.65 | 15.25 |
| | | | 409 | 15.92 | 40.22 | 15.82 | 20.99 | 2.01 | 0.75 | | |
| | | | 519 | 19.62 | 40.59 | 15.88 | 21.24 | 2.00 | 0.75 | 38.38 | 15.33 |
| | | | 549 | 20.73 | 41.61 | 15.86 | 21.17 | 2.00 | 0.75 | 38.10 | 15.30 |
| | | | 609 | 22.95 | 41.98 | 15.85 | 21.15 | 2.01 | 0.75 | 38.26 | 15.30 |
| | | | 669 | 25.17 | 40.44 | 15.88 | 21.19 | 2.00 | 0.75 | | |
| | | | 729 | 27.39 | 40.38 | 15.78 | 20.71 | 2.01 | 0.76 | 38.31 | 15.36 |
| | | | 758 | 28.46 | 42.53 | 15.85 | 21.11 | 2.00 | 0.75 | | |
| | | | 3 | 1.53 | 40.00 | 15.69 | 19.53 | 2.05 | 0.80 | 38.23 | 15.37 |
| | | | 28 | 3.49 | 40.15 | 15.69 | 19.67 | 2.04 | 0.80 | | |
| | | | 59 | 5.49 | 40.27 | 15.71 | 19.74 | 2.04 | 0.80 | 38.25 | 15.41 |
| | | | 89 | 7.67 | 40.95 | 15.77 | 20.22 | 2.03 | 0.78 | 38.25 | 15.38 |
| | | | 108 | 8.58 | 41.13 | 15.76 | 20.23 | 2.03 | 0.78 | 38.42 | 15.38 |
| | | | 121 | 9.19 | 41.34 | 15.79 | 20.48 | 2.02 | 0.77 | 38.27 | 15.36 |
| | | | 129 | 9.68 | 41.22 | 15.77 | 20.48 | 2.01 | 0.77 | | |
| | | | 140 | 10.1 | 40.54 | 15.65 | 19.96 | 2.04 | 0.79 | | |
| | | | 171 | 12.38 | 41.30 | 15.81 | 20.78 | 1.99 | 0.76 | 37.94 | 15.37 |
| HU91-045-94, 3448 m | 50°12.26 | 45°41.14 | 182 | 13.21 | 41.08 | 15.78 | 20.54 | 2.00 | 0.77 | | |
| | | | 189 | 13.74 | 40.24 | 15.68 | 19.73 | 2.04 | 0.79 | | |
| | | | 199 | 14.53 | 40.50 | 15.69 | 19.95 | 2.03 | 0.79 | 38.24 | 15.37 |
| | | | 230 | 16.19 | 40.70 | 15.74 | 20.07 | 2.03 | 0.78 | 38.03 | 15.39 |
| | | | 262 | 17.58 | 39.72 | 15.65 | 19.38 | 2.05 | 0.81 | | |
| | | | 294 | 20.17 | 39.51 | 15.64 | 19.20 | 2.06 | 0.81 | 38.27 | 15.43 |
| | | | 308 | 20.56 | 39.19 | 15.64 | 19.03 | 2.06 | 0.82 | | |
| | | | 339 | 22.12 | 39.50 | 15.65 | 19.17 | 2.06 | 0.82 | 36.82 | 14.86 |

| | | | | | | | | | |
|---|---|---|---|---|---|---|---|---|---|
| | 371 | 25.04 | 40.95 | 15.76 | 20.17 | 2.03 | 0.78 | 38.52 | 15.49 |
| | 399 | 27.59 | 39.41 | 15.65 | 19.18 | 2.06 | 0.82 | 38.59 | 15.50 |
| | 429 | 30.33 | 40.03 | 15.67 | 19.55 | 2.05 | 0.80 | | |
| | 454 | 32.61 | 40.37 | 15.66 | 19.57 | 2.06 | 0.80 | 38.51 | 15.37 |

**Table A7.**Lead isotope composition from four sediment cores. Data shown for ferromanganese coatings of authigenic fraction, detrital fraction

| Core Name | Latitude [N] | Longitude [W] | Depth [cm] | Interpolated Age [kyr] | εNd | External error 2 S.D. |
|---|---|---|---|---|---|---|
| MD99-2227, 3460 m | 58°55.26 | 048°22.38 | 385 | 9.26 | -10.57 | 0.19 |
| | | | 489 | 12.38 | -12.91 | 0.19 |
| | | | 499 | 12.91 | -13.81 | 0.00 |
| | | | 525 | 14.29 | -14.01 | 0.36 |
| | | | 569 | 16.62 | -17.40 | 0.31 |
| | | | 29 | 3.85 | -18.94 | 0.19 |
| | | | 89 | 9.26 | -14.83 | 0.19 |
| HU08-029-004, 2674 m | 61°2749 | 58°0211 | 639 | 20.64 | -20.19 | 0.31 |
| | | | 719 | 24.65 | -24.21 | 0.19 |
| | | | 778 | 26.54 | -16.64 | 0.19 |
| HU84-030-021, 2853 m | 58°22600 , | 57°30.42 | 99.5 | 3.77 | -17.66 | 0.31 |
| | | | 242 | 11.70499495 | -25.82 | 0.31 |
| | | | 479 | 18.14230769 | -30.52 | 0.19 |
| | | | 639 | 24.05946746 | -26.72 | 0.19 |
| | | | 699 | 26.27840237 | -25.81 | 0.19 |
| HU91-045-94, 3448 m | 50°12.26 | 45°41.14 | 174 | 12.61 | -24.83 | 0.31 |

**Table A8** Neodymium isotope composition of uncleaned foraminifera from four sediment cores.

# ACKNOWLEDGEMENTS.

I would like to thank Martin and Markus for their support, guidance, and encouragement during my study in Kiel and visit stay in Halifax.

For help in the lab I would like to thank Jutta, Chris, Ed and others who maintain the Nu plasma, Moritz, Anne, Zhimian, Tianyu, Mario, Daniel, Janett, Kristin, Georgi, Veit and others for all their assistance in the lab and/or helpful discussions during my study here. The list goes on… Special additional thanks to Georgi who helped me with the German Abstract of this thesis.

I would like to thank Claire for helping me with the lab during my stay in Halifax and answering all my questions. I would like to thank HOSST for the opportunity to become a part of something big.

I would like to thank Nastya and Sasha for supporting me during my stay in Kiel and for being my friends, also Ira, Ira, Katya.

I would like to thank my family, my mother for patience, my sister for support.

I would like to thank my husband for being there for me and encouraging me to not give up. And my son for making me wake up every morning and for giving a new meaning to my life.

Thank you to everyone…

# CURRICULUM VITAE

***Filippova Alexandra***

*E-mail:*afilippova@geomar.de

*Born:* January 23, 1987

*Nationality:* Russian

## Education

- *Geomar Helmholtz Centre for Ocean Research in Kiel, PhD student* — **Nov 2012-Feb 2015**

- *St. Petersburg State University – University of Hamburg*
  **Master** of Ecology with specialization in "Applied Polar and Marine Sciences" (MSc program for "Applied Polar and Marine Sciences (POMOR)" — **Sep 2009-Oct 2011**

- *Christian-Albrechts-Universität zu Kiel*
  Student of MSc program "Marine Geosciences" for one semester (40 credit points out 180) — **Oct 2010-Jan 2011**

- *St. Petersburg State University*
  Faculty of Geography and Geoecology, Department of Geoecology and Nature Management
  **Specialist** in Geoecology and Nature Management — **Sep 2004-Jun 2009**

- Senior Secondary (Full) School № 278 with advanced study of German and English Languages, St. Petersburg, Russia
  Average result – 5 (out of 5) — **Sep 1994-Jun 2004**

## Scientific publications

- Filippova A., Kienast M., Frank M., Schneider, R., 2016. Alkenone paleothermometry in the North Atlantic: A review and synthesis of surface

sediment data and calibrations. Geochemistry, Geophysics, Geosystems, 17 (4), 1370-1382, DOI: 10.1002/2015GC006106.

- Filippova A., Frank M., Kienast M., Rickli J., Hathorne E., Yashayaev I.M., Pahnke, K. (2016) Water mass circulation and weathering inputs in the Labrador Sea based on coupled Hf-Nd isotope compositions and rare earth element distributions. Submitted to Geochimica et Cosmochimica Acta.

**Conferences.**

- AGU 2013, San Francisco. Poster presentation: Changes of the deep circulation and erosional inputs into the Labrador Sea over the Late Quaternary.
- GAC MAC, Montreal, 2015. Alkenone paleothermometry in the NW Atlantic: A review and synthesis of surface sediment data and calibrations. Poster presentation.
- Goldschmidt conference, Prague, 2015. Water mass formation in the Labrador Sea based on coupled Hf-Nd isotope compositions and REE distributions. Oral presentation